Nano-scale Ionic Cross-links in Polymers
Controlled Synthesis, Morphology and Mechanical Properties

Cover: Simplified pictorial representation of the ionic cross-links in random ionomers (background of the cover), and time resolved 2D-Small angle X-ray scattering images of the polyester ionomer at different temperatures (front cover).

An electronic version of this thesis is available in PDF-format on the website of the Eindhoven University of Technology.

Nano-scale Ionic Cross-links in Polymers

Controlled Synthesis, Morphology and Mechanical Properties

PROEFSCHRIFT

ter verkrijging van de graad van doctor aan de
Technische Universiteit Eindhoven, op gezag van de
Rector Magnifucus, prof.dr. R.A. van Santen, voor een
commissie aangewezen door het College voor
Promoties in het openbaar te verdedigen
op maandag 15 december 2003 om 16.00 uur

door

Sreepadaraj Karanam

geboren te Anantapur, India

Dit proefschrift is goedgekeurd door de promotoren:

prof.dr. P.J. Lemstra
en
prof.dr. C. Bailly

Copromotor:
dr.ir. J.G.P. Goossens

|| Sri Lakshmi Chennakesava Swamy Prasanam ||

The path from dreams to success does exist. May you have the vision to find it, the courage to get on to it, and the perseverance to follow it. Wishing you a great journey.

> *— Late Dr. Kalpana Chawla,The first Indian woman astronaut and one of the crew member of Space Shuttle Columbia.*

Dedicated to my parents and family

Contents

Summary

Ionomers are a class of synthetic polymers which contain up to 15 mol % of ionic groups along a nonionic polymer backbone. Ionic groups are introduced by neutralization of acid groups present in the polymer. The difference in polarity between the polar ionic groups and nonpolar polymer backbone results in the aggregation of the ionic groups in the polymer matrix. Thus, ionic groups tend to microphase separate and form ion-rich domains or ionic aggregates, often referred to as multiplets, with sizes in the range of nanometers. These ionic aggregates act as ionic cross-links and enhance several properties, such as modulus, gloss, hardness, viscosity, and melt strength. The thermal sensitivity of the ionic cross-links compared to the conventional covalent cross-links can be used to develop e.g. new resins with thermoreversible cross-link properties for in-mold coating applications. In-mold coating integrates the molding and coating of a plastic product in one single step. The advantages of in-mold coating over conventional coating are no solvent emission, high application efficiency, and low energy consumption curing conditions.

The objective of this research is to establish the structure–morphology–property relationships of ionomers. The focus has been on controlled synthesis, morphological characterization and thermoreversible nature of ionic cross-links by varying a) the architecture (block ionomers vs. random vs. telechelic) of the backbone, b) molecular weight and polydispersity index (PDI), c) ionic content, and d) type of counterion. Poly(methyl methacrylate) (PMMA) and polyesters were selected as polymer backbone materials for ionomer synthesis because of their well-established properties and proven performance in the coating industry. PMMA ionomers with well-defined polymer architectures were prepared via "controlled" and free radical polymerization (FRP).

For practical and economic reasons, an efficient synthetic procedure based on atom transfer radical polymerization (ATRP) was developed to prepare well-defined PMMA block ionomers using readily available and easily removable metal catalysts and initiators. In the synthetic strategy *tert*-butyl methacrylate (tBMA) was used as the precursor for the methacrylic acid comonomer to overcome the acid group sensitivity of the ATRP catalyst system. Di- and triblock copolymers of MMA and tBMA were prepared with defined molecular weight and low PDI at various compositions of tBMA. The existence of block copolymer structure and the influence of the ATRP reaction conditions on the final block copolymer structure such as chemical composition distribution were proved by Normal Phase Gradient Polymer Elution Chromatography (NP-GPEC). The GPEC technique turned out to be very successful and is a powerful complementary technique

to Size Exclusion Chromatography (SEC) in the analysis of block copolymers, especially with a short second block length. Trifluoroacetic acid was used in the selective hydrolysis of the PtBMA block to obtain the methacrylic acid based blocks, which were neutralized in solution by ethanolic potassium hydroxide resulting in the well-defined PMMA block ionomers (and ionic counterparts with an ionic content of more than 15 mol %).

The successful synthesis and molecular characterization put a basis for understanding the morphology of the PMMA block copolymers. Small Angle X-ray Scattering (SAXS) and differential scanning calorimetry were used to reveal the morphology of these materials. A single SAXS peak was observed in di- and triblock precursors and the ionic counterparts indicating a clear microphase separation but the absence of highly ordered structures. A wide range of interdomain spacings (characteristic Bragg distance, d_B, 10-30 nm) was achieved in the precursors and in the ionic counterparts by simply controlling the total degree of polymerization of the block copolymer. These results illustrate the use of ATRP as a precision polymerization technique to synthesize block copolymers with controlled architectures and desired nano-scale microdomain sizes. Finally, the time resolved SAXS results of the diblock ionomer revealed that the thermal stability of the ionic aggregate in the block ionomer is a strong function of block copolymer composition. At the same ionic block length, the block ionomer with a long nonionic block length forms an ionic aggregate with a low aggregate number compared to the ionomer with a short nonionic block. As a result, a weak ionic aggregate is formed, which reorganizes at high temperatures. These results reveal the potential of controlling and regulating the characteristics of ionic aggregates in the block ionomers.

PMMA random ionomers were used to investigate the influence of ionic cross-links, which act as additional cross-links and enhance the network density, on improving the mechanical properties of PMMA, since the increase in network density with ionic cross-linking is more effective in random than in block ionomers. PMMA random ionomers with potassium as counterion [P(MMA-*co*-K$^+$MA)] were synthesized by copolymerization of methyl methacrylate with methacrylic acid at different acid contents and subsequent neutralization of the acid copolymers. SAXS and dynamic mechanical thermal analysis confirmed the formation of ionic multiplets with a broad range of intermultiplet distances indicating the effect of polymer architecture on the ionomer morphology. The observed morphological results were discussed in terms of the well-established Eisenberg, Hird, and Moore (EHM model) multiplet-cluster model.

The results of simultaneous time resolved SAXS and tensile testing on thin films of PMMA and the corresponding potassium ionomers indicated that crazing was suppressed in ionomers compared to PMMA due to ionic cross-links, which increase the effective network density and the craze initiation stress, but reduce the maximum draw ratio. This might be indicative for an increase in the fracture resistance of the ionomers. The molecular weight and degree of neutralization of the acid precursor are two important factors, which determine balance between the mechanical properties and processing of the ionomers. The results of the uniaxial compression testing of PMMA with low (made by ATRP) and high (made by FRP) PDI indicated that at same number average molecular weight the strain hardening modulus (G_r) is higher for the low PDI material. This is due to dilution of the effective network density because of the low molecular weight material present in the high PDI PMMA. These results demonstrate the importance of controlling molecular parameters such as PDI and M_n and their influence on intrinsic properties such as G_r of the polymers. The results of the mechanical properties of the random ionomers and PMMA show that using ionomer cross-links in combination with a low polydispersity index is a potential method to enhance mechanical properties of glassy polymers without losing melt processability.

Telechelic polyester ionomers with a high thermal stability of the backbone and low strength of the ionic aggregates (due to the architecture) were used to demonstrate the thermoreversible nature of the ionic cross-links. The results of SAXS and FTIR spectroscopy revealed the presence of a critical ion content above which a clear microphase separation occurs. High temperature FTIR spectroscopy and rheology measurements indicated that the thermal stability of the ionic aggregates and the viscosity are a strong function of the counterion used in neutralization. Further, SAXS and dynamic viscosity results indicated the presence of order-disorder transition temperature (T_i) for ionic multiplets. These results signify the potential of polyester ionomers as resins for injection molding applications, viscosity modifiers and additives. However, polyesters with higher molecular weight than that of investigated in this study are needed to achieve good mechanical properties and yet retain the thermoreversible character of the resins. Finally, the approach taken in this research increases the fundamental understanding of relationship between architecture, morphology and properties of ionomers.

Chapter 1

General Introduction

1.1 Polymers as materials

Polymers form a group of materials consisting of long chain molecules containing a large number of repetition of structural or building units, called monomers, joined by the same type of linkage.[1] The type of linkage to join monomers can be either covalent, ionic or hydrogen bonding; covalent linkage is the most dominant linkage present in polymers. The monomer units can arrange in a different fashion to give different material properties. The chemical reaction by which polymers are formed from monomers is known as polymerization. Polymers in the natural world have been around since the beginning and are referred to as biopolymers. Life itself stores its parameters and other essential components in a polymer database called DNA, a biopolymer. Mother Nature deploys proteins (polymers of amino acids; Nature's building blocks or monomers) as enzymes, which regulate all of the fine biochemical reactions taking place in our body, maintaining a delicate equilibrium. Starch, cellulose, and natural rubber are examples of some of the biopolymers, which possess characteristics of polymeric materials.

Synthetic polymers have been studied since 1832. The word plastic, derived from the Greek 'plassein' meaning 'to shape', is the most common and popular name for synthetic polymers.[2] At the very start of the previous century (1907), Baekeland in Ghent, Belgium synthesized the first fully synthetic polymer known as Bakelite. Bakelite's hardness and high heat resistance made it an excellent choice for an electrical insulator. Today, we have a vast number of synthetic polymers, such as polyethylene, polypropylene, polyamide, polyester and polycarbonate, which play an increasingly important role in all aspects of human life.[3] It is very evident that synthetic polymers are emerging as one of the important materials of choice.[4] Polymers already have a vast range of applications that exceed applications of any other class of materials. Current applications extend from bulk materials, adhesives, coatings, foams, and packaging materials to textile and industrial fibers, composites, electronic, biomedical, and optical devices. Polymer applications have been developed in such diverse areas as conduction and storage of electricity, heat and light, molecular based information storage and processing, molecular composites, unique separation membranes,

revolutionary forms of food processing and packaging, health, housing, and transportation.[2] Polymer science, the science of making and manipulating long chain molecules, is a highly interesting field independent of whether these molecules are of synthetic or natural origin. Furthermore, by combining the principles of biotechnology and nanotechnology[5] one can further explore the intrinsic possibilities of polymers ranging from the focus on ultimate mechanical performance in 1-D, 2-D or 3-D(imensions), via structuring polymer molecules in devices (displays, plastic electronics and solar cells) to mimicking Nature in tissue engineering and other advanced biomedical applications.[6]

1.2 Ionomers

Ionomers constitute a class of synthetic polymers, which contain up to 15 mol % of ionic groups along a nonionic polymer backbone.[7] Ionic groups are introduced by the neutralization of the corresponding acid groups present in the polymer. The difference in polarity between the polar ionic groups and nonpolar polymer backbone results in the aggregation of the ionic groups in the polymer matrix. Thus, ionic groups tend to microphase separate and form ion-rich domains or ionic aggregates referred to as multiplets with sizes in the range of few nanometers. These ionic aggregates act as ionic cross-links and enhance several properties, such as modulus, gloss, hardness, glass transition temperature, viscosity, and melt strength.[8,9] Ionomers usually contain neutralized sulfonic or carboxylic acid groups. It is well known that sulfonated ionomers associate much stronger than the carboxylated analogues.[10] This makes it very difficult or even impossible to process sufonated ionomers. An additional disadvantage of sulfonated ionomers is that they have to be fully neutralized in order to avoid thermal degradation at elevated temperatures.[7] However, carboxylated ionomers can be processed at elevated temperatures and partial neutralization of carboxylated groups results in stable ionomers.

Considerable research has been carried out on understanding the structure–property relationships of random ionomers for which the ionic groups are randomly distributed along the polymer backbone.[7-9] It is now well established that the physical, mechanical, and viscoelastic properties of ionomers are strongly dependent on the morphology of the ionomers. Several parameters such as the architecture of the backbone, flexibility of the backbone, dielectric constant of the polymer matrix, ionic content, degree of neutralization, chemical nature of the ionic groups, and the presence of plasticizers determine the morphology in ionomers.[11] The architecture of the ionomer is one of the most important parameters that determine the morphology. By controlling the

location of the ionic functionality on the polymer chain, a range of ionomers with large variation in architectures, such as random ionomers, telechelic ionomers,[12] segmented ionomers,[13] and block ionomers,[10-15] can be synthesized. Most commercial ionomers, such as poly(ethylene-*co*-methacrylic acid) copolymers, which are partially neutralized with sodium or zinc (hydr)oxides (commonly known as Surlyn®) and sulfonated poly(tetrafluoroethylene) (commonly known as Nafion®), are random ionomers in which the ionic functionalities are randomly distributed along the polymer backbone.[7]

Several models have been proposed to describe the morphology and the structure–property relationships of the random ionomers during the last 25 years.[16-19] Though the model by Eisenberg, Hird, and Moore (EHM model) seems to be the most accepted for random ionomers, a general consensus on the correct model of the ionomer morphology structure and properties is lacking.[11] According to the EHM model,[11] several ion pairs aggregate due to electrostatic interactions to form multiplets in the nonpolar matrix. The multiplet sizes are 6–8 Å (a few ion pairs) (See Figure 1.1). The formation of multiplets depends on the competition between electrostatic interactions among ion pairs and the elastic forces of the polymer chains to which the ionic groups are attached. The mobility of the polymer segments immediately surrounding the multiplet is reduced relative to that of the bulk material and is called restricted mobility layer. The sizes of the multiplet including the reduced mobility layer are close to 30 Å in diameter and are expected to be too small to manifest their own T_g. A single multiplet will essentially act as a cross-link point. With increasing ion content, the number density of the multiplets increases leading to overlapping of the restricted mobility regions around the multiplets. These overlapping regions are referred to as clusters. At a particular ion content, the sizes of the clusters exceed the threshold size for independent phase behavior (50–100 Å) at which point they exhibit their own T_g. Then, the ionomer exhibits two T_g's, one for the nonpolar matrix and the second one for the clusters. Figure 1.2 shows the pictorial representation of the cluster formation at various ion contents. It is important to realize that the particular model to be selected for describing the ionomer morphology is very much system dependent.

Block ionomers are basically block copolymers with at least one ionic block.[10-15] It is well known that block copolymers tend to microphase separate into self-assembled ordered structures with nanoscale periodicities, because of the immiscibility between the dissimilar blocks. Hexagonal close packed (hex) cylinders, body centered cubic (bcc) spheres, lamellar structures and more complex phases have been observed in amorphous block copolymers.[20-22] The resulting microdomains are responsible for the special properties of these materials. Macrophase separation is

prevented by the covalent bonds between the blocks. Several parameters determine whether microphase separation occurs and which ordered structure is formed. Among these parameters are the block copolymer composition and the degree of incompatibility between the blocks, given by the product χN, where χ is the Flory-Huggins interaction parameter and N is the degree of polymerization.[20] As an example, the phase diagram of a polystyrene-polyisoprene diblock[23] copolymer is given in Figure 1.3.
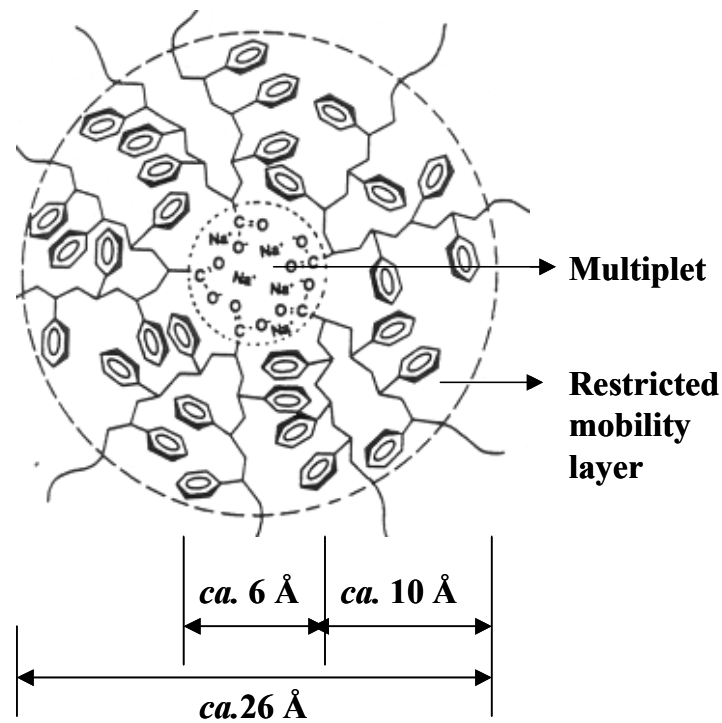
Figure 1.1: *Pictorial representation of multiplet formation in polystyrene ionomer. Sodium carboxylate is the ionic group.*

Compared to random ionomers, the morphology of ionomer block copolymers containing both non-ionic and ionic blocks is less studied.[24] Introduction of ionic groups into block copolymers is a complicating factor because it causes two competing effects that may affect the morphology.[25,26] First, when one of the blocks contains ionic groups, the degree of incompatibility between the blocks is increased drastically and therefore the thermodynamic driving force for phase separation is much larger. So even for very small block lengths, phase separation can occur. Secondly, because aggregation of ionic groups may occur, polymer chains get anchored in ionic domains, leading to a reduction in chain mobility. However, chain mobility is necessary for the

phase separation and the introduction of ionic groups will therefore result in a morphology, which is kinetically trapped and usually non-equilibrium (thermodynamically unstable) structures are formed. The result of these two counteracting effects is not yet completely understood. The phase separation will be less perfect, leading to a somewhat disturbed structure.[25,27]
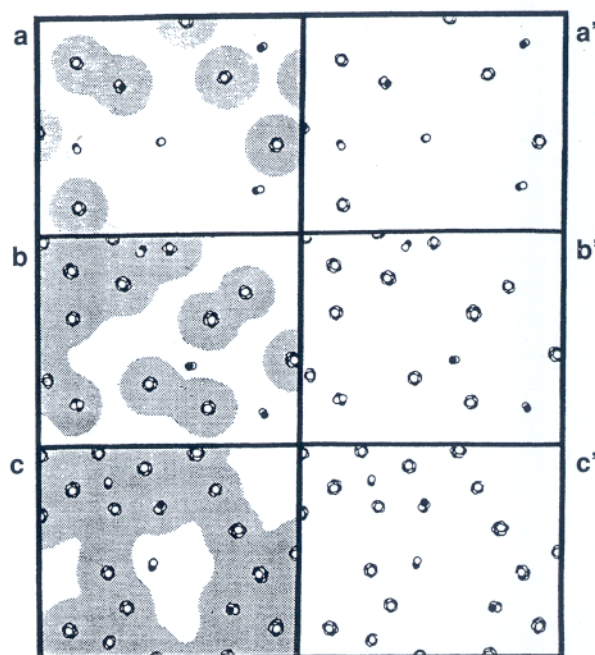
Figure 1.2: *Representation of the morphologies of random ionomers at (a) low ion content, (b) intermediate ion content, and (c) high ion content. The shaded areas indicate regions of restricted mobility. a'–c', the spatical arragement of multiplets considering only electron density factors without regard to chain mobility. Reprinted from Eisenberg et al.[11]*

Interest in the ionomer field is growing because of their wide range of applications such as packaging, membranes, bulk plastic materials (golf balls, bowling pins, and bumper guards), coatings, adhesives, imaging systems, and magnetic recording mediums.[7-9] Ionomers offer a wide range of challenges and opportunities both to industrial and academic researchers. The industrial interest is, in part, because ionic interactions permit control of the physical properties of polymers, even at low ion concentrations as mentioned earlier. An even more important reason for industrial interest is the use of ionomers as additives in composites, as tie coats between two dissimilar polymer layers, in miscibility enhancement, and in the modification of mechanical properties in general and rheological properties in particular.[7]

From the academic point of view, the relationship between the chemical structure, the morphology, and the physical properties of the materials is of primary interest. Understanding the

nature of aggregates has been a goal of two decades of phenomenological research, as has been the relation between morphology and physical properties.
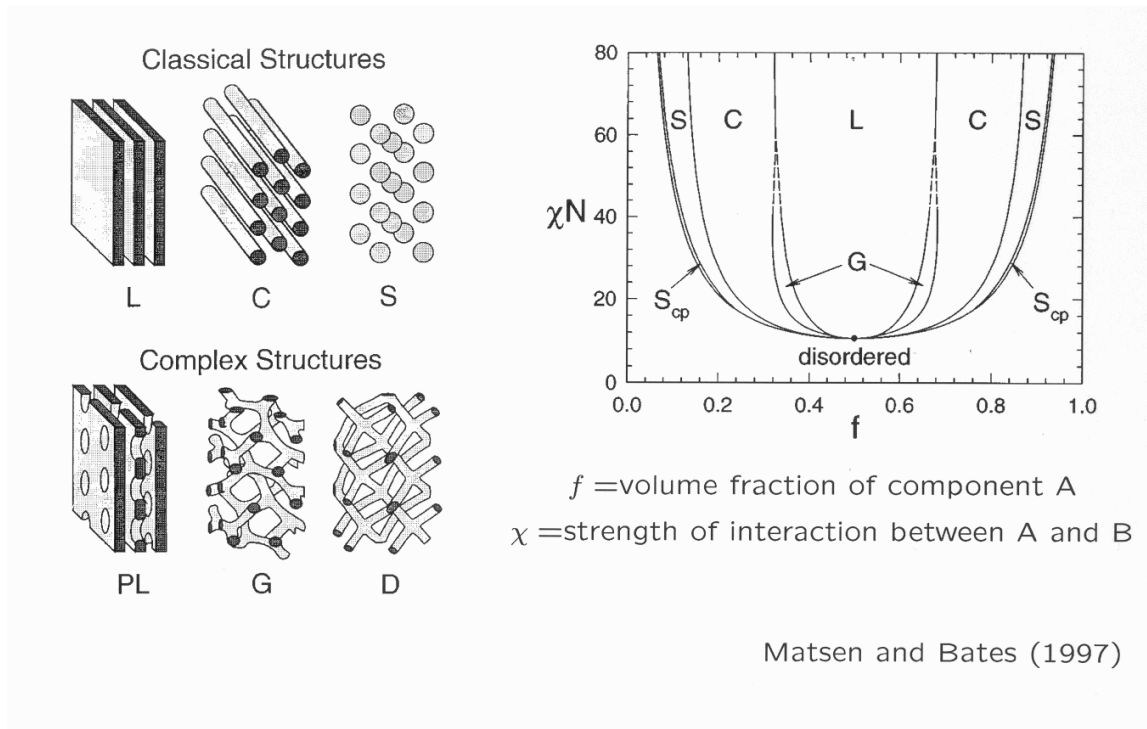
Figure 1.3: *Phase diagram for a PS-PI diblock copolymer.[23]*

1.3 Coatings: Paints and Lacquers

A lot of plastic products are coated and finished after production, either for aesthetic or for functional reasons.[28,29] Coatings can be present in many forms and can be applied to the plastic substrate using various techniques (which of course depend on the physical state of the paint). Most decorative paints used for plastic coatings are solvent-based paints or water-based latices. These can be applied to the substrate making use of brushes, paint rollers or spray guns including electrostatic spraying. Next to that, powders can be used as coating material; they are sprayed onto the substrate and form a uniform layer after a heat treatment. Commonly used coating application techniques (based on spraying) are accompanied by several problems,[28] such as a low application efficiency, solvent emission, contaminations, and energy consuming curing conditions. Moreover, the emission of volatile organic components (VOC) from solvent-based paints has raised many environmental and health issues in the last two decades. To circumvent this problem, new and strict legislations

have been passed and paint manufacturers are forced to seriously reduce the VOC fraction of paints or to develop new environmental friendly coating systems/techniques. As a result, coating manufactures and producers are involved in developing new coating systems, which contain less solvent, such as high-solids, water-based paints or new kinds of powder-based coatings.[30]

1.4 Finishing in mold (FINIMOL)

In-mold coating or decoration (IMC/IMD) techniques integrate molding and coating of a plastic product in a single step, thereby eliminating the need of additional expensive and time consuming coating steps usually involved in the decoration of a plastic product.[31] Current approaches of in-mold coating are all based on a two-step molding/coating process resulting in relatively long cycle times.

The FINIMOL[32] (acronym for FINIshing in MOLd) project was started with the aim to solve the long molding-time problem of the in-mold coating while keeping the advantages of the in-mold coating. This can be achieved by developing a molding technology and coatings necessary for simultaneous molding of the coating material and the plastic part via 2-K injection molding. A schematic representation of the structure to be developed in the FINIMOL project is shown in Figure 1.4. The concept involves the formation of a plastic product with a core polymer, which essentially determines the structural properties of the plastic product, and a skin layer referred to as lacquer or paint, which determines the coating properties, such as UV or scratch resistance, and the appearance of the plastic product.

The characteristics of the coating resin to-be-used in the FINIMOL concept are (a) viscosity of the coating should be such that the coating is easily processable by extrusion and injection molding, (b) the glass transition temperature (T_g) should be above 50 ^{o}C for easy demolding after injection molding, and (c) the coating should have a post-mold curing mechanism to avoid premature curing during the molding step, e.g. curing initiated by the elevated temperatures that are usually present during the molding. Some useful methods of the post-mold curing are moisture or UV-initiated curing. However, disadvantages of the post-mold curing based on UV or moisture curing are (a) additional cost due to the extra post curing step, and (b) energy and time consumption during the post curing step, which largely increases the cycle time of the product.

Lacquer/ Paint
(UV, Scratch resistance)

Core polymer
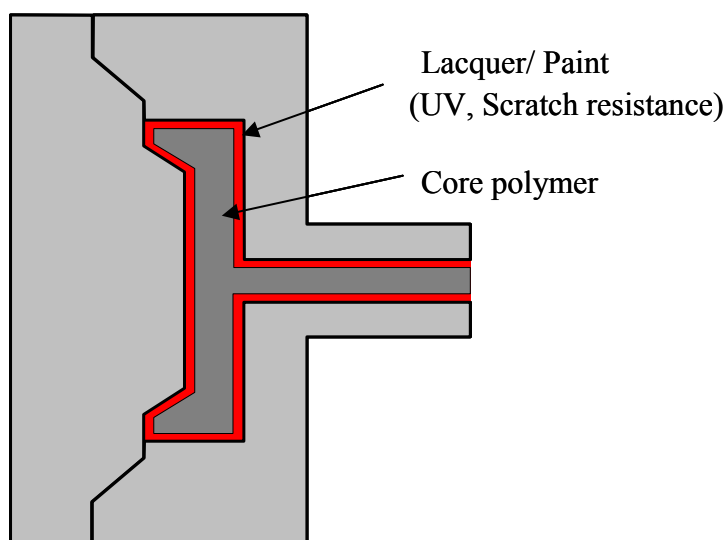
Figure 1.4: *Schematic representation of the structure of the plastic product to be developed in FINIMOL concept.*

1.5 Ionomers as coating materials for injection moldable paint in the FINIMOL concept

As mentioned earlier, ionic aggregates (multiplets) in ionomers can act as ionic cross-links and enhance several properties of the precursor polymers. Eisenberg[11,16] proposed that the formation of the ionic aggregates is a competition between the electrostatic interactions among the ions (cations and anions) that promote ionic aggregation and elastic forces that oppose ionic aggregation. In accordance with the rubber elasticity theory, the elastic forces increase with temperature, while the electrostatic interactions are less sensitive to temperature. The Eisenberg's[11] theory predicts the existence of a critical temperature for dissociation of the ionic aggregates at which the elastic forces exceed the magnitude of the electrostatic interactions. Upon increasing the temperature, the strength of the ionic aggregates becomes weaker and the material becomes processible. When the temperature decreases, the strong electrostatic interactions between the ionic groups and polarity differences between the matrix and ionic groups drive the formation of ionic cross-links (or ionic aggregates). Thus, in principle, the thermal sensitivity of the ionic cross-links in contradiction to covalent cross-links can be used to develop new resins with thermoreversible cross-link properties.

In this research a new approach was used, which combines the thermoreversible nature of ionomers and the FINIMOL concept to develop new injection moldable powder resins that can be

used in 2K-injection molding, film in-mold, and over-molding techniques. This approach has the following advantages: (a) elimination of post curing involved in conventional coatings, (b) compatible with the 2K- injection molding and over-molding techniques, since no curing mechanism is involved, and (c) possibility of having tunable viscoelastic properties by adjusting various structural features of the ionomers.

1.6 Objective and approach of current research

The main objective of this study is to investigate and establish the structure–morphology–property relationships of ionomers. For this purpose, it is necessary to study the influence of several parameters of the ionomers such as the chemical structure of the ionomer backbone, architecture of the ionomer, ionic content, degree of neutralization, and counterion on the morphology–mechanical–viscoelastic properties of the ionomers. In this research, apart from focusing on the thermoreversible nature of the ionomers, controlled synthesis and mechanical properties of the ionomers are also investigated. The approach taken in this research to achieve the above-mentioned objective is illustrated in Figure 1.5. Several synthetic parameters of the ionomers, such as the architecture of the ionomer, i.e., random *versus* block ionomers, ion content, degree of neutralization and counter ion were systematically varied to obtain ionomers with tailor-made architectures. As a result, ionomers with controlled morphological features, such as ion aggregate spacing, are obtained; these morphological features are characterized by small angle X-ray scattering[33] (SAXS). Furthermore, the observed structural and morphological features are related to the measured rheological and mechanical properties.

Poly(methyl methacrylate) (PMMA) and polyesters are chosen as suitable polymer backbone materials because of their well-established properties and proven performance in the coating industry.[28,29] Amorphous polyester ionomer precursors were obtained from DSM Resins. Carboxylic acid functionality is present at the chain ends.

1.7 Synthesis of ionomers

Free radical polymerization (FRP) is one of the most convenient ways to prepare polymers on a large industrial scale.[34] The advantages of the FRP technique over other polymerization techniques are its tolerance towards all kinds of impurities, such as stabilizers, trace amounts of oxygen and water, the moderate reaction temperatures, and the multiple polymerization processes available, e.g. bulk, solution, precipitation or emulsion polymerization.[35] Some disadvantages related to the mechanism of FRP is the poor control over the molecular weight, molecular weight

distribution, polymer architecture (such as block, star and telechelic polymers) and the difficulty (or even impossibility) of preparing well-defined copolymers or polymers with a predetermined functionality.[36] Commercial random ionomers such as Surlyn and Nafion are prepared by FRP.[7]

Morphology   SAXS
Thermoreversibility
Ionic domain spacing

Chemical Composition	
Polymer Architecture	Ionic groups
Random	Acid content
Block	% Neutralization
Ionomers	Type of Cation

Thermal properties DSC,TGA

Rheological properties

Mechanical Properties
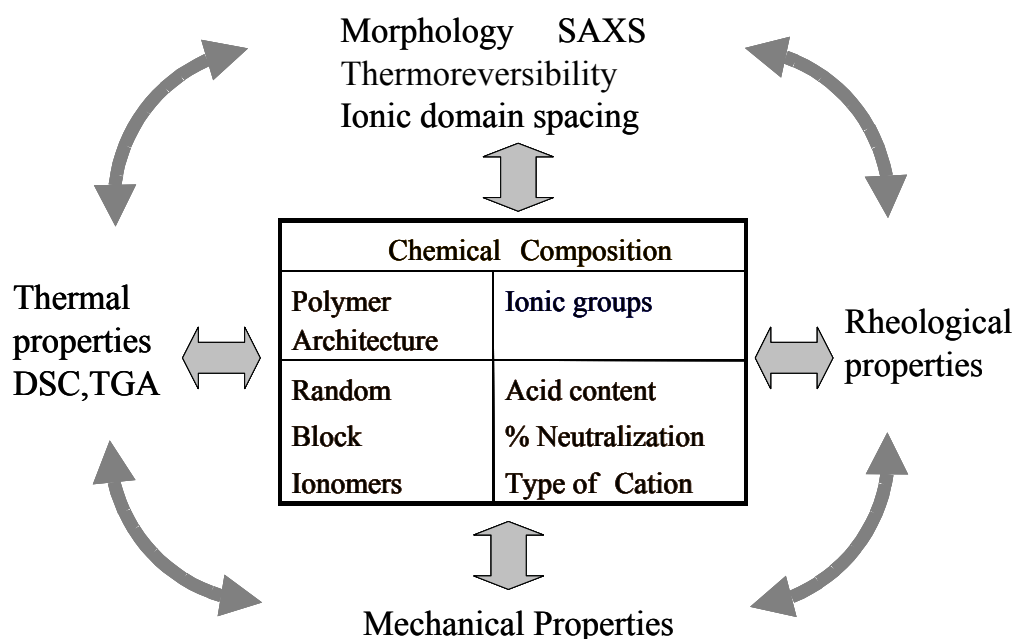
Figure 1.5: *Schematic representation of the approach taken in this research.*

Living polymerization methods can be used to synthesize polymers with a good control over M_n and architecture. Living ionic polymerization methods are extensively used for the synthesis of block copolymers.[37] However, the stringent conditions required for these polymerizations limit the range of monomers and functionalities that can be used.[38]

The recently developed controlled/living radical polymerization methods can provide a solution to these problems. With these polymerization methods, it is possible to synthesize polymers with a wide range of architectures with well-controlled M_n and a low polydispersity index (PDI) under less stringent conditions than for living ionic polymerization methods. The most studied controlled radical polymerization methods include atom transfer radical polymerization (ATRP),[39,40] reversible addition fragmentation chain transfer polymerization (RAFT)[41] and nitroxide mediated polymerization methods (NMP).[42,43] Out of these methods, ATRP seems to be

the most versatile,[44,45] being able to polymerize a wide range of monomers with well controlled M_n and in a wide range of well-defined structures.

1.7.1 Atom Transfer Radical Polymerization (ATRP)

ATRP, as well as other controlled radical polymerization methods, is based on an exchange between active and 'dormant' species.[44-47] In ATRP, a transition metal complex is utilized to induce halogen atom transfer between dormant (P_n–X) and active (P_n•) polymer chains (see Figure 1.6). For ATRP, the commonly used catalysts are copper halides (CuX, where X can be Cl or Br).

$$R-X + Cu(I)X / Ligand \xrightleftharpoons[k_{deact}]{k_{act}} R^{\cdot} + X-Cu(II)X / Ligand$$
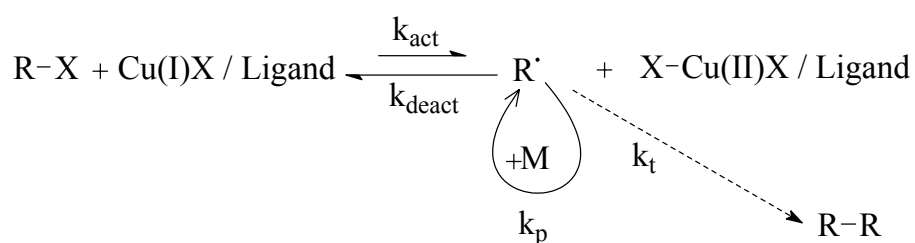
Figure 1.6: *Reaction scheme for ATRP.[19]*

Two requirements need to be fulfilled in order to achieve controlled conditions.[45] First, initiation has to be fast compared to propagation, such that all polymer chains start to grow at the same time. Secondly, the equilibrium between active and dormant chains has to be dynamic and favoring the dormant species, ensuring that only a low concentration of active species is present, thereby minimizing, but not excluding, termination reactions. The polymer chains can only grow by addition of monomer to the active chains. Thus, fast initiation and rapid exchange between dormant and active species accomplish a uniform growth of all chains, leading to a good control over M_n and low PDI. Because each monomer (at a given catalyst system) has its own specific equilibrium constant ($K_{eq} = k_{act}/k_{deact}$), optimal conditions for the polymerization can be quite different.[44] The parameters that can be adjusted include concentration, type of catalyst, ligand and initiator, the reaction temperature and the solvent. Therefore, understanding the role of each component is crucial in order to obtain well-defined polymers.

Block copolymers are usually synthesized by one of the following two ways.[44,45] The first method, referred to as one pot synthesis, involves addition of the second monomer to the reaction medium after nearly complete consumption of the first monomer. The disadvantage of this

approach is contamination of the second block with first monomer units. The second approach is a two-step procedure, known as macroinitiator approach, in which the first block is synthesized, isolated and purified. This block is then utilized as macroinitiator for the polymerization of the second monomer, leading to a diblock copolymer. When a bifunctional initiator is used for the synthesis of the macroinitiator, *ABA* triblock copolymers can be obtained.

The PMMA block ionomers investigated in this research are synthesized by ATRP utilizing the above-mentioned macroinitiator approach. The main disadvantage of ATRP is its sensitivity to the presence of carboxylic acid groups, which are essential functional groups for the synthesis of ionomers.[44,45] This disadvantage was overcome in this research by polymerizing protected monomers, followed by a deprotection step to generate acid groups. Another disadvantage of ATRP is the presence of the catalyst complex (copper ligand complex) after polymerization. This disadvantage is subdued to some extent by using a heterogeneous catalyst complex, which can be easily removed from the polymer solution by passing the polymer solution through a silica column. The synthetic scheme adapted in this research to obtain PMMA diblock ionomers is shown in Scheme 1.1. A similar strategy is used for triblock ionomers except that a difunctional initiator was used instead of a monofunctional initiator.

The synthetic strategy uses *tert*-butyl methacrylate (tBMA) as the precursor for the methacrylic acid (MAA) to overcome the acid group sensitivity of the ATRP catalyst system. The *tert*-butyl ester group can be selectively hydrolyzed to the corresponding acid under mild reaction conditions. The synthetic design (see Scheme 1.1) entails four basic steps: (1) the controlled synthesis of mono- and difunctional poly(methyl methacrylate) (PMMA) macroinitiators with defined molecular weight and a low polydispersity index (PDI), (2) the efficient initiation of tBMA by the PMMA macroinitiators resulting in poly(methyl methacrylate-*b*-*tert*-butyl methacrylate) (PMMA-*b*-PtBMA, diblock) and poly(*tert*-butyl methacrylate-*b*-methyl methacrylate-*b*-*tert*-butyl methacrylate) (PtBMA-*b*-PMMA-*b*-PtBMA, triblock) ester precursors, (3) the selective hydrolysis of the PtBMA block yielding the corresponding di- (PMMA-*b*-PMAA) and triblock (PMAA-*b*-PMMA-*b*-PMAA) acid precursors, and (4) solution neutralization of the acid precursors to the corresponding di- (PMMA-*b*-PK$^+$MA) and triblock (PK$^+$MA-*b*-PMMA-*b*-PK$^+$MA) ionomers. Figure 1.7 shows the ligands used in the ATRP of the MMA and tBMA.

Scheme 1.1 synthesis of PMMA diblock ionomers

Step 1 Synthesis of monofunctional macroinitiators.
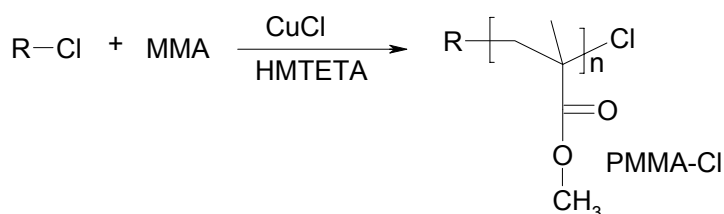
Step 2 Synthesis of MMA and tBMA diblock copolymer from PMMA macroinitiator.
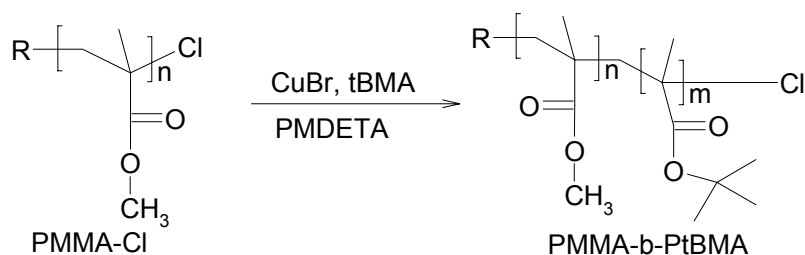
Step 3 Selective hydrolysis of PMMA-b-PtBMA to PMMA-b-PMAA.
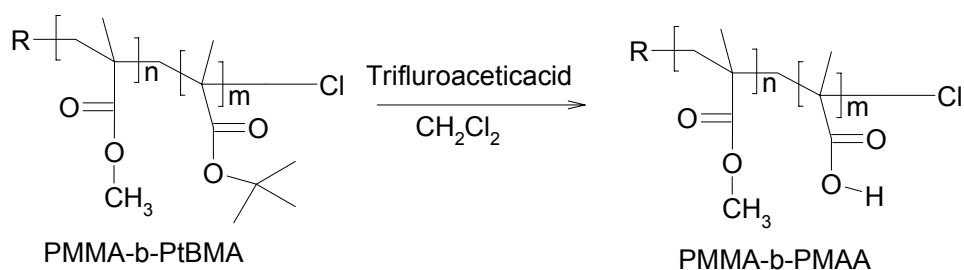
Step 4 Neutralization of PMMA-b-PMAA to diblock ionomer.
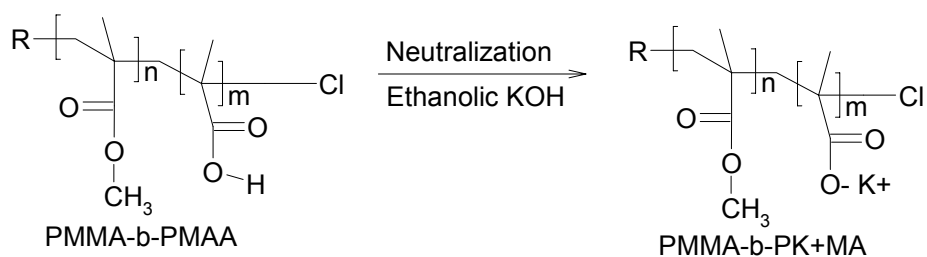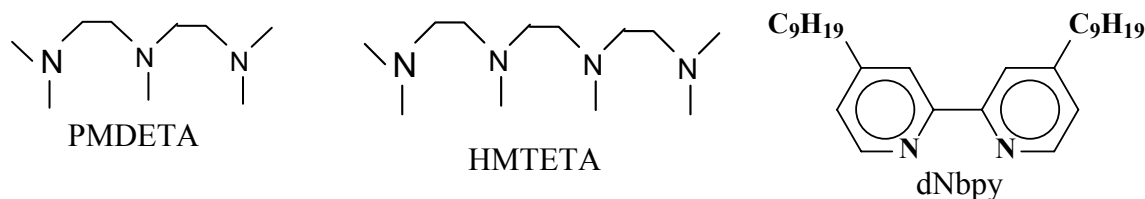
Figure 1.7: *Chemical structures of the ligands used in the atrom transfer radical polymerization; where PMDETA is N,N,N′,N″,N″-pentamethyldiethylenetriamine; HMTETA is N,N,N,N′,N‴,N‴-hexamethyltriethylenetetramine; dNbpy is 4,4′-di-5-nonyl-2, 2′-bipyridine.*

1.8 Outline of the thesis

The purpose of this study is to establish and understand the structure–property relationships of ionomers. For this purpose, ionomers with tailored architectures have to be synthesized.

Chapter 2 describes the atom transfer radical polymerization (ATRP) of *tert*-butyl methacrylate (tBMA) using a CuX/*N,N,N′,N″,N″*-pentamethyldiethylenetriamine (PMDETA) catalytic system with various initiators R–X (X = Br, Cl). Furthermore, details of the synthesis, chromatographic, and spectroscopic characterization of low molecular weight difunctional poly(methyl methacrylate) (PMMA) macroinitiators and the corresponding poly(tBMA-*b*-MMA-*b*-tBMA) triblock ester precursor copolymers with a range of tBMA compositions are presented.

Chapter 3 describes the results of the synthesis, chromatographic, and spectroscopic characterization of high molecular weight monofunctional PMMA macroinitiators and the corresponding poly(MMA-*b*-tBMA) diblock ester precursor copolymers with defined molecular weight and low polydispersity index (PDI). Details of the effect of molecular weight of the macroinitiator, nature of catalyst system (heterogeneous/homogeneous), and the amount of solvent on the degree of control achieved in the block copolymerization are also discussed.

The conversion of the ester precursors to the corresponding acid precursors by selective hydrolysis of the tBMA is a very important step in the synthesis of block ionomers. Trifluoroacetic acid was used as a catalyst for the selective hydrolysis of tBMA. In Chapter 4, results of synthesis and spectroscopic characterization of the selective hydrolysis of ester precursors to obtain acid precursors and subsequent neutralization of the acid precursors to the ionomers (and ionic counter parts with more than 15 mol % ionic groups) is presented. Small angle X-ray scattering (SAXS) was used to investigate the morphological features of the di- and triblock ester, acid precursors and

ionomers. The influence of polymer architecture, molecular weight and acid content on the morphological features of the block precursors and ionomers is described in this chapter.

Random PMMA and telechelic polyester ionomers are the focus of study in Chapter 5. The influence of molecular parameters such as molecular weight, acid content and type of counter ion on the formation and association of the ion aggregates is investigated. High temperature fourier transform infrared (FTIR) spectroscopy, dynamic mechanical thermal analysis (DMTA), and SAXS are used to elucidate the morphological features of the ionomers.

The influence of ionic cross-links on the mechanical properties of PMMA is investigated in Chapter 6. SAXS coupled with mechanical testing is used to study the deformation mechanisms of ionomers such as crazing and shear yielding. The results of influence of molecular weight, ion content and degree of neutralization on crazing are described. Furthermore, uniaxial compression testing is used to study the intrinsic deformation behavior of the PMMA. The effect of the polydispersity index on the intrinsic mechanical properties such as yield stress and strain hardening modulus are described.

Chapter 7 reports the results of the influence of temperature on the stability of ion aggregate in telechelic polyester random ionomers and PMMA-based diblock ionomers using time resolved small angle X-ray scattering (SAXS). Rheology experiments were also used to confirm the SAXS results in the case of polyester ionomers. The results of the influence of molecular parameters such as ion content, degeee of neutralization and counterion on the viscosity and storage modulus of the polyester ionomers are presented. Further, the results of the block copolymer composition on the thermal stability of the block ionomer morphology are discussed.

1.9 References

(1)   Young, R. J. *Introduction to Polymers*, **1989**, Chapman and Hall, University Press, Cambride.

(2)   Fenichell, S. *Plastics: making of a synthetic century*, **1996**, Harper Business, New York.

(3)   Meikle, J. L. *American Plastic: a Cultural History* , **1995**, New Brunswick: Rutgers University Press.

(4)   Brewer, J. *Materials Science and Engineering*, www.mse.usue.edu.

(5)   Put, J. *European Polymer Federation, Special Issue*, **2001**, 23.

(6)   Lemstra, P. J. *European Polymer Federation, Special Issue*, **2001**, 5.

(7)   Eisenberg A.; Kim, J. S. *Introduction to Ionomers*, **1998**, John Wiley & Sons, Inc.

(8)   Tant, M.R.; Mauritz, K, A.; Wilkes, G. L. Eds. *Ionomers: Synthesis, Structure, Properties and Applications*, **1997**, Blackie Academic and Professional: London.

(9)   Schlick, S. *Ionomers: Characterization, Theory, and Applications*. **1996,** Ed.; CRC Press: Boca Raton, FL.

(10)   Venkateshwaran, L. N.; York, G. A.; Deporter, C. D.; McGrath, J. E.; Wilkes, G. L. *Polymer*, **1992**, 33, 2277.

(11)   Eisenberg, A.; Hird, B.; Moore, R. B. *Macromolecules*, **1990**, 23, 4098.

(12)   Jérôme, R.; Broze, G. *Rubb. Chem. Technol.*, **1985**, *58*, 223.

(13)   Feng, D.; Venkateshwaran, L.; Wilkes, G. L.; Stark, J. E.; Leir. C. M. *J. Appl. Polym. Sci.* **1989**, *37*, 1549.

(14)   Gauthier, S.; Esenberg, A. *Macromolecules*, **1987**, 20, 760.

(15)   Weiss, R. A.; Sen, A.; Pottic, L. A.; Willis, C. L. *Polymer*, **1991**, 32, 1867.

(16)   Eisenberg, A. *Macromolecules*, **1970**, 3, 147.

(17)   Marx, C. L.; Caulfield, D. F.; Cooper, S. L. *Macromolecules*, **1973**, 6, 3.

(18)   Yarusso, D. J.; Cooper, S. L. *Macromolecules*, **1983**, 16, 1871.

(19)   Kumar, S.; Pineri, M. *J. Poly. Sci., Polym. Phys. Ed.* **1986**, 24, 1767.

(20)   Leibler, L. *Macromolecules*, **1980**, 13, 1602.

(21)   Bates, F. S.; Fredrikson, G. H. *Annu. Rev. Phys. Chem.* **1990**, 40, 525.

(22)   Hamley, I. W. *The Physics of Block Copolymers*, **1998**, p.24, Oxford University Press.

(23)   Khadapur, A. K. *Macromolecules*, **1995**, 28, 8796.

(24)   Gouin, J.P.; Williams, C.E.; Eisenberg, A. *Macromolecules*, **1989**, *22*, 4573.

(25)   Mani, S.; Weiss, R. A.; Williams, C. E.; Hahn, S. F. *Macromolecules*, **1999**, 32, 3663.

(26)   Storey, R. F.; Baugh, D. W. *Polymer*, **2000**, 41, 3205.

(27)   Dubois, P.; Yu, Y.S.; Teyssié, P.; Jérôme, R. *Rubber chemistry and technology*, **1997**, 70, 714.

(28)   Paul, S. *Surface coatings: Science and Technology*, **1996**, Chichester, Wiley.

(29)   Zeno, W. W. Jr.; Jones, F.N.; Pappas, S. P. *Organic Coatings: Science and Technology*, **1994**, Wiley Inter Science.

(30)   Mapleston, P. *Modern Plastics*, **2001**, 2, 56.

(31)   Olmsted, B. A.; Davis, M. E. *Practical injection molding*, **2001**, Dekker, Basel.

(32)   FINIMOL project is a collaborative project between DSM, AKZO-NOBEL, Hartman, Eindhoven Univesity of Technology and Dutch Environmental agency Economy, Ecology and Technology (EET).

(33)   Glatter, O.; Kratky, O. *Small Angle X-ray Scattering*, Academic Press Inc. (London) LTD. **1982**, p.228.

(34)   Moad, G.; Solomon, D. H. *The Chemistry of Free Radical Polymerization,* **1995**, 1st ed.; Elsevier Science Ltd.: Oxford.

(35)   Otsu, T. J. *Polym. Sci., Part A Polym. Chem.* **2000**, 38, 2121.

(36)   Matyjaszewski, K. *Controlled Radical Polymerisation*, American Chemical Society, Washington DC, **1998**, Chapters 1 & 16.

(37)   Szwarc, M. *Nature*, **1956**, 178, 1168.

(38)   Haddleton, D. M.; Muir, A. V. G.; Richards, S. N. *In Macromolecular Design of Polymeric Materials*: Hatada, K.; Kitamyama, T.; Vogl, O. Eds. Marcel Dekker: New York, **1997**, 123.

(39)   Kato, M.; Kamigaito, M.; Sawamoto, M.; Higashimura, T. *Macromolecules*, **1995**, 28, 1721.

(40)   Wang, J.S.; Matyjaszweski, K. *Macromolecules*, **1995**, *28*, 7901.

(41)   Chiefari, J.Y.K.; Chong, Y.K; Ercole, F.; Krstina, J.; Le, T. P. T.; Mayadunne, T. R A.; Meijs, G.F.; Moad, G. *Macromolecules*, **1998**, 31, 5559.

(42)   Solomon, D. H.; Rizzardo, E.; Cacioli, P. *European Patent Application*, **1985**, 135 280 A2.

(43)   Georges, M. K.; Veregin, R. P. N.; Kazmaier, P. M.; Hamer, G. K. *Macromolecules*, **1993**, 26, 2987.

(44)   Matyjaszewski, K.; Xia, J. *Chemical Reviews*, **2001**, *101*, 2921.

(45)   Kamigaito, M.; Ando, T.; Sawamoto, M. *Chemical Reviews*, **2001**, *101,* 3689.

(46)   Coessens, V.; Pintauer, T.; Matyjaszewski, K. *Prog. Polym. Sci.* **2001**, 26, 337.

(47)   Qiu, J.; Charleux, B.; Matyjaszewski, K. *Prog. Polym. Sci.* **2001**, 26, 2083.

Chapter 2

"Controlled" Synthesis and Characterization of model Methyl methacrylate/*tert*-Butyl Methacrylate triblock copolymers via ATRP

ABSTRACT: The heterogeneous atom transfer radical polymerization (ATRP) of *tert*-butyl methacrylate (tBMA) using various initiators R–X (X = Br, Cl) and with CuX/*N,N,N',N'',N''*-pentamethyldiethylenetriamine (PMDETA) catalytic system was investigated. The importance of the structure of the initiator on the polymerization of tBMA was briefly examined. Polymerization of tBMA with ethyl 2-bromoisobutyrate resulted in uncontrolled polymerization due to slow initiation because of the low back strain effect and relatively high propagation rate constant of tBMA. Well-controlled polymers were obtained with *p*-toluenesulfonyl chloride and 2,2,2, -trichloroethanol initiators. This can be explained by the fast initiation coupled with the rapid establishment of the equilibrium between the active and dormant species in the polymerization. Poly(methyl methacrylate) macroinitiators were used to synthesize poly(tBMA-*b*-MMA-*b*-tBMA) triblock copolymers in a range of tBMA compositions. The use of a mixed halogen system in the block copolymer synthesis leads to fast initiation and fast deactivation resulting in controlled molecular weights and a low polydispersity index. Gradient polymer elution chromatography was used to confirm the block copolymer structure. The retention time of the block copolymer lies in between the retention times of the two homopolymers, indicating the existence of a (block) copolymer structure. This technique was successfully used to identify the influence of the ATRP reaction conditions on the final block copolymer structure.

2.1 Introduction

Considerable research has been carried out on understanding the structure–property relationships[1–3] of random ionomers for which the ionic groups are randomly distributed along the polymer backbone. Compared to crystalline ionomers amorphous ionomers are more suitable for

studying the effect of ionic interactions on the morphology and on structure–property relationships to avoid the complexities arising from the crystalline domains. Among the amorphous polymers, polystyrene ionomers are studied extensively,[4,5] while studies on poly(methyl methacrylate) (PMMA)[6] based ionomers appear less frequently. Only a few reports related to the study of block ionomers with a PMMA backbone were published.[7] McGrath and co-workers[7,8] reported on the synthesis and characterization of methacrylate block ionomers by using living anionic polymerization, where the ionomer block was prepared by the hydrolysis and subsequent neutralization of poly(*tert*-butyl methacrylate).

Several research groups[9,10] used *tert*-butyl acrylate (tBA) as a suitable monomer for introducing acrylic acid units in synthesizing block copolymers with various architectures. However, the corresponding methacrylate, i.e., *tert*-butyl methacrylate (tBMA), is rarely used to introduce methacrylic acid units by ATRP. Matyjaszewski[11] and co-workers were the first to report the polymerization of tBMA by ATRP using the CuCl/HMTETA (*N,N,N,N′,N‴,N‴-* hexamethyltriethylenetetramine*)* catalyst system with an ethyl 2-bromoisobutyrate initiator (EBriB). The polymerization was carried out at 90 ºC in 50 vol % anisole. The semilogarithmic plot of conversion *vs* time was nonlinear, but a high initiation efficiency was claimed for this system. Haddleton[12] systematically studied ATRP of sterically hindered methacrylates at 90 ºC in 50 vol % xylene using EBriB/CuBr/imine systems. The increased steric hindrance at the α-carbon of the side chain in the methacrylates apparently results in low rates of polymerization and high rates of termination. Especially in the case of tBMA uncontrolled molecular weight and a high PDI were reported. These results were explained on the basis of possible hydrolysis of the tBMA monomer to the acid, leading to catalyst poisoning. Recently, Hadjichristidis[13] reported the synthesis of graft copolymers of PtBMA on polystyrene by the CuBr/bipyridine catalyst system. In this case, the backbone was produced with a 2,2,6,6-tetramethylpiperidine-*N*-oxyl-mediated stable free-radical polymerization process from the copolymerization of styrene and *p*-(chloromethyl)styrene, but so far, block copolymerizations of tBMA with available methacrylic, acrylic, and styrenic monomers by ATRP have not been reported.

In this chapter, the importance of initiator selection, when a heterogeneous catalyst like PMDETA/CuX is employed in the controlled radical polymerization of tBMA is presented. The effect of the structure of the initiator and initiation mechanism on the control achieved in the polymerization is briefly discussed. Furthermore, the synthesis of well-defined difunctional (bromine end groups) PMMA macroinitiators and their block copolymerization with tBMA to

obtain triblock copolymers in various compositions with controlled molecular weight and a relatively low PDI using PMDETA/CuCl catalyst system is discussed. The absorbance ratio method was used to determine the composition of the block copolymers by FTIR spectroscopy. Results of the synthesis and characterization by spectroscopic and chromatographic techniques of block copolymers are presented. Gradient polymer elution chromatography (GPEC) is applied to characterize the block copolymers and to evaluate the effectiveness of block copolymerization reaction conditions during ATRP.

2.2 Experimental Section

2.2.1 Materials

Methyl methacrylate (Aldrich, 99%), *tert*-butyl methacrylate (Aldrich, 99%), toluene (Aldrich, 99%), dichloromethane (Biosolve, 99%), and methyl ethyl ketone (Aldrich, 99%) were vacuum distilled and stored at − 15 °C. Ethylene glycol (99%), *N,N,N′,N″,N″*-pentamethyldiethylenetriamine (99%), ethyl 2-bromoisobutyl bromide (99%), 2,2,2-trichloroethanol, butyl acetate (99%), triethylamine (99%), *p*-toluenesulfonyl chloride (97%), 2,2,2-trichloroethanol (98%) and silica (0.04–0.6 mm) were obtained from Aldrich and used without further purification. Cu^{I}Br (98%), and Cu^{I}Cl (98%) were obtained from Aldrich and purified as follows. Copper halides were stirred with glacial acetic acid for 24 h under a nitrogen atmosphere, later washed consecutively with glacial acetic acid, ethanol, and diethyl ether and dried at 40 ^{o}C for 3 days and stored under an argon atmosphere.

2.2.2 Analysis and Measurements

Determination of Conversion and Molecular Weight Distribution. The conversion of the monomer during the polymerization was determined by gas chromatography (GC) analysis. GC measurements were carried out on a Hewlett-Packard 5890 SII, equipped with an AT-Wax capillary column (30 m × 0.53 mm × 10 μm), using a HP 3393a integrator to obtain the chromatogram. Dilute polymer solutions in tetrahydrofuran (THF) were made in 1.5 mL crimp neck vials and measured using an autosampler. The injection temperature was 200 °C, and a 10 °C min$^{−1}$ heating ramp was used. SEC measurements were carried out using a Waters GPC equipped with a Waters 510 pump, a Waters 410 differential refractometer (40 °C), a Waters WISP 712 autoinjector (50 μL injection volume), a PL gel (5 μm particles) 50 × 7.5 mm guard column, and two PL gel mixed-C (5

μm particles) 300 × 7.5 mm columns (40 °C). Data acquisition and processing were performed using Waters Millennium 32 (v32) software. Tetrahydrofuran (THF, Biosolve, stabilized with BHT) was used as eluent at a flow rate of 1.0 mL/min, dilute polymer solutions of 2 mg/mL were made, and a 50 μL solution was injected for analysis. Calibration was done using polystyrene (PS) standards (Polymer Laboratories, 580–7.1 × 10^6 g mol^{-1}), and molecular weights are calculated using the universal calibration principle with Mark-Houwink parameters for PMMA[14] (PMMA: $K = 0.944 \times 10^{-4}$ dL g^{-1}, $a = 0.719$).

Spectroscopic Analysis. The FTIR spectra were recorded with a BioRad Excalibur 3000 series spectrometer. One hundred scans at a resolution of 4 cm^{-1} were signal-averaged, and the BioRad Merlin software was used to analyze the spectra. Samples were prepared by casting films from a dilute polymer solution on KBr pellets for FTIR measurements. These films were thin enough to be within the range where the Beer–Lambert[15] law can be applied. The carbonyl (C=O) stretch vibration in the two homopolymers PMMA and PtBMA are observed at 1732 and 1726 cm^{-1} respectively. In the block copolymer the separate carbonyl peaks were observed as one broad single peak. An absorbance ratio method[16] was used to estimate the chemical composition of the block copolymers. A1 and A2 are the absorbances of the band at 847 cm^{-1} (assigned to the skeletal vibration of *tert*-butoxy group in PtBMA homopolymer) and the carbonyl ester peak at 1730 cm^{-1} respectively. The ratio A1/A2 is proportional to the mole percentage of tBMA present in the block copolymer. A calibration curve was constructed to relate the ratio A1/A2 to the mole percentage of tBMA by preparing blends of PMMA and PtBMA of various known concentrations. The data can be fitted well with a linear relation (see Supporting Information at the end of Chapter 2). The validity of the calibration curve was verified by making blends with intermediate concentrations. FT-NMR spectra were recorded with a Varian 400 MHz spectrometer. NMR spectra were recorded in CDCl$_3$ at 25 °C. All chemical shifts are reported in ppm downfield from tetramethylsilane (TMS), used as the internal standard ($\delta = 0$ ppm).

GPEC Analysis. GPEC measurements were carried out on a Waters Alliance 2690 separation module with a Waters 2487 dual λ absorbance detector and a PL-EMD 960 ELSD detector (Nitrogen flow 5.0 mL/min, temperature 70 °C). A Zorbax Silica 5 μm column (4.6 mm × 150 mm, Dupont Chromatography) was used at 30 °C. A linear binary gradient starting from heptane (volume fraction, Φ = 1; 0 min nonsolvent for the polymers used in analysis) to THF (volume fraction, Φ = 1; 60 min good solvent for the polymers used in analysis) was used and is shown in

Table 2.1. The column was reset at the end of the gradient to initial conditions between 60 and 70 min. A gradient steepness, i.e., gradient change in fraction solvent per minute ($\Delta\Phi_{gradient}$) of 0.02 is applied. HPLC grade solvents obtained from BioSolve were used. A Varian 9010 solvent delivery system was used to maintain a stable flow rate of the eluents. Dilute polymer solutions were made in THF (10 mg/mL) and a sample of 25 μL was used for analysis. Data were acquired by Millenium 32 3.05 software.[17]

Table 2.1: *Linear Binary Gradient used for GPEC[a]*

step	time (min)	$\Phi_{heptane}$	Φ_{THF}	$\Delta\Phi g_{radient}$ (min^{-1})	flow (mL/min)
1	0	1	0	-	0.5
2	50	0	1	0.02	0.5
3	60	0	1	-	1.5
4	65	1	0	0.2	1.5
5	70	1	0	-	0.5

[a]The eluent compositions are given in volume fraction (Φ) and $\Delta\Phi g_{radient}$ steepness of   the applied step.

2.2.3 Synthetic Procedures

tBMA polymerization. A typical ATRP was carried out as follows. CuCl (0.082 g, 0.82 mmol), PMDETA (0.143 g, 0.82 mmol), and tBMA (5.014 g, 0.036 mol) were charged in a dry 50 mL three-neck round-bottom flask, and the flask was sealed with a rubber septum. The reaction mixture was bubbled with argon for 30 min to remove traces of oxygen. In a second, dry 25 mL three-neck round-bottom flask *p*TsCl (0.157 g, 0.82 mmol) and MEK (2.312 g, 0.03 mol) were charged, and the flask was sealed with a rubber septum. This initiator solution was also bubbled with argon for 30 min to remove traces of oxygen. Finally, the initiator solution was added via a degassed syringe to the monomer solution flask and immersed in an oil bath at 90 °C to start the polymerization. To study the kinetics of the polymerization, samples were drawn using a degassed syringe during the course of the reaction and diluted with THF. Part of the solution was used for gas chromatography (GC) to determine the monomer conversion, and the remaining part was used for SEC analysis. After completion of the reaction, THF (100 mL) was added to the flask, and a magnetic stirrer was used to dissolve the polymer. The resulting green (Cu^{II} complex) polymer solution was passed through a silica column (SiO$_2$) to remove the copper complex. The resulting colorless polymer

solution was concentrated by rotaevaporation, after which the polymer was collected and dried under vacuum for 3 days at 50 °C.

Synthesis of difunctional initiator. 1,2-Bis(bromoisobutyryloxy)ethane, a difunctional initiator, was synthesized in dichloromethane (DCM, 189 mL, 3.17 mol) through a coupling reaction of 2-bromoisobutyryl bromide (BIBB, 13.7 mL, 0.11 mol) with ethylene glycol (EG, 2.79 mL, 0.05 mol) in the presence of triethylamine (17.1 mL, 0.12 mol) at 0 °C under an argon atmosphere. Unreacted BIBB and EG were removed by sequential extraction with water, 1 M $NaHCO_3$, and a saturated NaCl solution. DCM was removed by rotaevaporation. The initiator was purified by dissolving in methanol at 50 °C and recrystallizing at −5 °C (this procedure was repeated at least three times) and characterized by ^{1}H NMR. Yield: 85%. ^{1}H NMR ($CDCl_3$): δ = 1.93 (6H, s), 4.43 (4H, s).

Synthesis of PMMA macroinitiators. To a dry 50 mL three-neck round-bottom flask CuBr (0.122 g, 0.83 mmol), $CuBr_2$ (when necessary), PMDETA (0.144 g, 0.83 mmol), and MMA (5.012 g, 0.05 mol) were charged and the flask was sealed with a rubber septum. The reaction mixture was bubbled with argon gas for 30 min to remove traces of oxygen. In a second dry 25 mL three-neck round-bottom flask difunctional initiator (0.299 g, 0.83 mmol) and toluene (1.823 g, 0.02 mol) were charged and the flask was sealed with a rubber septum. This initiator solution was also bubbled with argon for 30 min to remove traces of oxygen. Finally, the initiator solution was added via a degassed syringe to the monomer solution and immersed in an oil bath at 90 °C to start the polymerization. To study the kinetics of the polymerization, samples were drawn using a degassed syringe during the course of reaction and diluted with THF. Part of the solution was used for gas chromatography (GC) to determine the monomer conversion and the remaining part was used for SEC analysis. Polymer was purified as described in the tBMA homopolymerization section.

Synthesis of block copolymers. The halide exchange technique was used to synthesize the block copolymers. The procedure was the same as discussed in the previous section except that a macroinitiator (1.023 g, M_n = 6005, 0.16 mmol) and solvent (methyl ethyl ketone, 2.5 mL) were added to the flask initially. Once the macroinitiator was dissolved completely, the monomer (tBMA, 1.07 mL, 3.38 mmol) and PMDETA (0.022 g, 0.16 mmol) were added. The solution was bubbled with argon for 30 min and finally CuCl (0.023 g, 0.16 mmol) was added. The flask was immersed in an oil bath at 90 °C to start the polymerization. Samples were taken at regular intervals and analyzed for monomer conversion by GC. Polymer was purified as described above.

Nomenclature. The nomenclature used for the polymers can best be explained using examples. The designation MD6 refers to the difunctional poly(methyl methacrylate) macroinitiator with a

molecular weight of 6000. The notation BM6B refers to a triblock copolymer with PMMA middle block of molecular weight 6000 and PtBMA outer blocks synthesized by block copolymerization of MD6 with tBMA. Similarly, the designation MM4M refers to the chain extension of the MD4 macroinitiator with methyl methacrylate.

2.3 Results and Discussion

2.3.1 ATRP of *tert*-Butyl Methacrylate

Effect of Initiator. The CuBr or CuCl/PMDETA catalyst system was used in the homopolymerization of tBMA. The choice of the appropriate initiator/CuX (X = Cl, Br) system is a key parameter, when polymerizing monomers such as MMA with their high observed propagation rate constants ($k_p^{obs} = k_p K_{eq}$ according to the terminology defined by Matyjaszewski;[18] cf. Scheme 2.1) to avoid slow initiation (low observed initiation rate constant $k_i^{obs} = k_i K_{eq}^o$ compared to k_p^{obs}) and/or possible side reactions. This is more important when working with a highly active catalyst system like PMDETA/CuX ($K_{eq} \sim 10^{-7}$–10^{-6} for MMA with PMDETA/CuBr).

Scheme 2.1: *General scheme for Atom Transfer Radical Polymerization*

Initiation

$$R-X \;+\; Cu(I)Cl \;\underset{}{\overset{K_{eq}^o}{\rightleftharpoons}}\; R\cdot \;+\; Cu(II)X_2/L$$

$$R\cdot \;+\; monomer \;\xrightarrow{k_i}\; P_1\cdot$$

Propagation

$$P_n-X \;+\; Cu(I)Cl \;\underset{}{\overset{K_{eq}}{\rightleftharpoons}}\; P_n\cdot \;+\; Cu(II)X_2/L$$

$$P_n^{\cdot} \;+\; monomer \;\xrightarrow{k_p}\; P_{n+1}^{\cdot}$$

Termination

$$P_n^{\cdot} \;+\; P_m^{\cdot} \;\xrightarrow{k_{t,d}}\; P_n= \;+\; P_n^H$$

$$P_n^{\cdot} \;+\; P_m^{\cdot} \;\xrightarrow{k_{t,c}}\; P_{n+m}$$
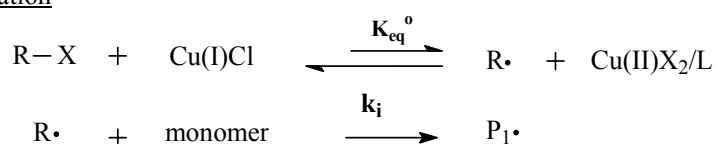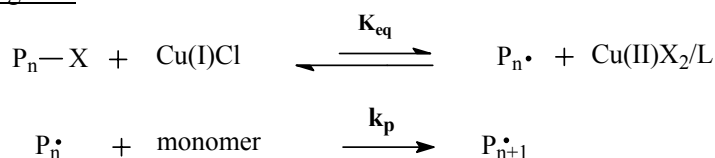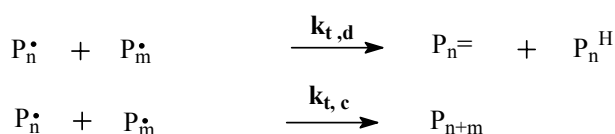
PMDETA was selected because (a) the catalyst complex is highly active, (b) easily available, (c) cost effective and (d) the catalyst complex can be easily separated from the polymer.[19] The three initiators used were EBriB, *p*-toluenesulfonyl chloride[20] (pTsCl), which is well-known as a universal initiator, and 2,2,2- trichloroethanol.[21] These three initiators were selected to study the effect of chlorine- and bromine-based initiation systems on the controlled polymerization of tBMA. EBriB has been used extensively in the polymerization of a variety of methacrylates.[22] Percec[20] and co-workers were the first to demonstrate the use of arenesulfonyl halides as universal initiators for heterogeneous and homogeneous metal-catalyzed living radical polymerization of styrene derivatives, methacrylates, and acrylates.

2.3.1.1 Polymerization with EbriB. Polymerizations of tBMA with the EBriB initiator and CuBr/PMDETA catalyst system in 30 vol % toluene at 90 ºC resulted in uncontrolled polymerization with a high polydispersity index (PDI ≈ 1.7, Table 2.2). The SEC traces of samples taken at regular time intervals during the polymerization showed a long tail towards the low molecular weight region, indicating that a large amount of radical termination occurred during the initial stages of the polymerization. The polymerization stopped after 30 min with no further increase in molecular weight.

Table 2.2: *ATRP of TBMA with the CuX (X = Br/Cl)/PMDETA catalyst system, initiated by three initiators in toluene at 90 ºC; [I]/[Cu]/[PMDETA] = 1:1:1.[a]*

Entry	Initiator	Catalyst	$[M]_o/[I]_o$	Solvent (%)	Reaction time (hr.)	Conv. (%)	M_n Exp.	M_n[b] theo.	PDI
1	EBriB	CuBr	42	30	5	40	4100	2600	1.65
2	EBriB	CuCl	42	50	6	60	5900	3600	1.50
3	PTsCl	CuCl	42	50	5	80	7000	4900	1.23
4	TCE	CuCl	42	50	5	70	6800	4300	1.22

[a]PMDETA = *N,N,N',N',N''*-pentamethyldiethylenetriamine, EBriB = ethyl 2-bromoisobutyrate, pTsCl = *p*-toluenesulfonyl chloride, TCE = 2,2,2, -trichloroethanol. [b]$M_{n,theo}$ = MW of initiator + ([M]/[I] × 142 × conversion).

The uncontrolled polymerization of tBMA from EBriB may be due to the following reasons. A successful ATRP initiating system requires the following two important parameters. First, the

initiation should be fast compared to propagation, and, secondly, it should minimize the probability of side reactions.[18] Thus, the apparent (observed) initiation rate constant ($k_i^{obs} = k_i K^o_{eq}$, Scheme 2.1) should be larger than the observed propagation rate constant, k_p^{obs} (i.e., $k_i K^o_{eq} \geq k_p K^{eq}$). It appears that for the EBriB/CuBr system, k_i^{obs} is much smaller than the observed propagation rate constant k_p^{obs}. This would result in slow and inefficient initiation with a significant portion of the initiator being lost due to termination reactions at the onset of the polymerization. Slow initiation coupled with the high equilibrium constant (K_{eq}) for methacrylates with the PMDETA/CuBr catalyst system would result in an uncontrolled polymerization. Slow initiation with the EBriB/CuBr/dNbpy initiator catalyst system in the polymerization of the MMA was reported earlier.[18] Although electronically similar to propagating species of methacrylates, EBriB is less active due to smaller back strain effect,[18] which apparently results in slow initiation of the tBMA polymerization.

Mixed halogen systems[23,24] (R–Br/CuCl) are used to increase the initiation rate constant in ATRP. A mixed halogen system results in faster initiation, slower propagation, and fast deactivation; as a consequence, the polymerization is more controlled. ATRP of MMA using a EBriB/CuCl[18] initiation system lead to a better molecular weight control and lower polydisperisty index than the EBriB/CuBr system. Polymerization of tBMA performed with an EBriB/CuCl/PMDETA mixed halogen system in 50 vol % toluene resulted in a continuous increase of molecular weight with conversion as opposed to the EBriB/CuBr system discussed above. The SEC traces of polymer samples taken at two reaction times are shown in Figure 2.1. Molecular weights increased with conversion but PDI was high and the low molecular weight tail is also present in the SEC traces. The use of a mixed halogen system increased the initiation rate; however, it was not sufficient to achieve a controlled polymerization. The slow initiation also affects the polydispersity index. PDI is inversely related to the concentration of Cu^{II} (see Eq 2.1) and the rate of deactivation. In successfully controlled radical polymerizations, the equilibrium between the dormant (polymeric halides) and active species (growing radicals, cf. Scheme 2.1) occurs rapidly and the contribution of termination reactions can be neglected. The ability to regulate the radical levels to low concentrations and thus suppress radical–radical termination via coupling or disproportionation is based on the fast establishment of the following inequality, i.e., $k_d[R^•][Cu(II)/L] >> k_t[R^•]^2$. If k_d or the Cu^{II} concentration is too low, the latter term $k_t[R^•]^2$ cannot be neglected and irreversible termination reactions will be significant, resulting in uncontrolled polymerization. This is possible because at the beginning of the polymerization the concentration of deactivator is built up until the rate of deactivation of the radical by Cu(II)/L is faster than the rate

of radical consumption by coupling or disproportionation. When initiation is slow and continuous, the equilibrium Cu^{II} concentration will be reached slowly, and consequently $k_t[R^\cdot]^2$ might be equal to or higher than $k_d[R^\cdot][Cu(II)/L]$. This may result in significant radical termination during the polymerization. Similar effects were reported in the polymerization of MMA[18] by the 1-PECl/CuCl initiation system, which is a poor initiating system for MMA polymerizations**.**
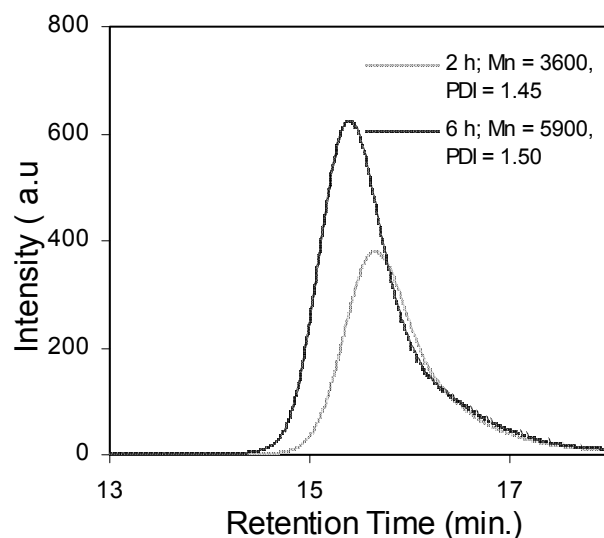
Figure 2.1: *GPC traces of PtBMA at two time intervals during the ATRP polymerization in toluene at 90 ^oC. [EBriB]$_0$ = [CuCl]$_0$ = [PMDETA]$_0$ = 0.07 M, [tBMA]$_0$ = 3.03 M.*

$$\frac{M_w}{M_n} = 1 + \frac{k_p[RX]_o}{k_d[X - M_t^{n+1}/L]}(\frac{2}{p} - 1) \qquad (2.1)$$

where k_p = propagation rate constant
$\quad k_d$ = deactivation rate constant
$\quad p$ = conversion

2.3.1.2 Polymerization with pTsCl. ATRP polymerizations of tBMA using pTsCl initiator and CuCl/PMDETA catalyst system were performed in 50 vol % toluene at 90 ºC. The molar ratio of initiator to catalyst to ligand is similar to the one used in the EBriB reaction and the polymerization results can be related to the structure of the initiator. A typical semilogarithmic kinetic plot of the homopolymerization of tBMA with *p*TsCl is shown in Figure 2.2. The kinetic plot of the

conversion *vs* time is close to linear up to 60% conversion, indicating that a constant number of growing polymer chains are present. The molecular weight increased linearly with conversion, and the PDI decreased progressively with conversion (See Figure 2.3) with a final polydispersity index of less than 1.25 (see Table 2.2). This is also evident from the SEC traces of polymer samples taken at regular intervals during the polymerization (Figure 2.3). The peak retention time progressively shifts towards lower values. The SEC peak is symmetrical with no tailing in the low molecular weight region. These results show that pTsCl successfully initiates the controlled polymerization of tBMA.
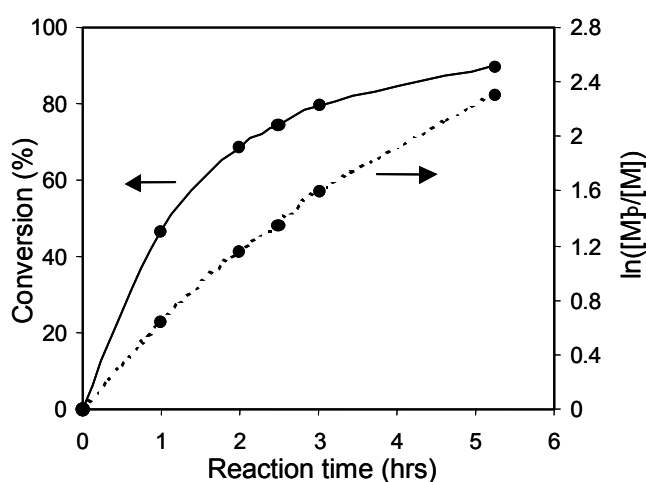
Figure 2.2: *Plots of ln([M]$_0$/[M]) vs reaction time and monomer conversion vs reaction time for the ATRP of tBMA in toluene at 90 ^{o}C. [pTsCl]$_0$ = [CuCl]$_0$ = [PMDETA]$_0$ = 0.07 M, [tBMA]$_0$ = 3.03 M.*

The observed differences in the polymerization behavior may be due to differences in the initiation mechanism[25] involved in the two types of initiators. Percec[26] and co-workers proposed the initiation mechanism for sulfonyl halide initiators in metal catalyzed radical polymerization. The propagation and reversible termination steps are identical for sulfonyl and alkyl halides. The first difference is that the metal-catalyzed reduction of the arylsulfonyl halide to the corresponding sulfonyl radical is faster than that of corresponding alkyl radical. This may, therefore, facilitate a higher rate of initiation than propagation. In this case, all of the initiator is consumed before significant propagation occurs. The second difference is that the sulfonyl radicals formed from sulfonyl halides are more stable and form sulfonyloxy and/or sulfinyl[26]radicals through a reversible combination process. This stabilization is believed to be due to sulfinyl radicals that do not initiate

or dimerize. Therefore, pTsCl results in a fast initiation, which establishes a fast equilibrium between the dormant and active species, thus leading to a controlled polymerization. This is clearly reflected in the narrow MWDs of the poly(tBMA) initiated by pTsCl, indicating that all of the chains are initiated simultaneously during the initiation stage of the polymerization. Trichloroethanol (TCE) was also used as an initiator for polymerization of tBMA with CuCl/PMDETA catalyst system to further verify the importance of fast initiation in controlled polymerization of tBMA. Destarac[21] showed that using TCE as initiator resulted in a fast and nearly quantitative initiation of MMA using a CuCl/bpy catalyst system. Polymerization of tBMA using a TCE/CuCl/PMDETA initiator catalyst system led to a low PDI and controlled molecular weight (entry 4, Table 2.2).
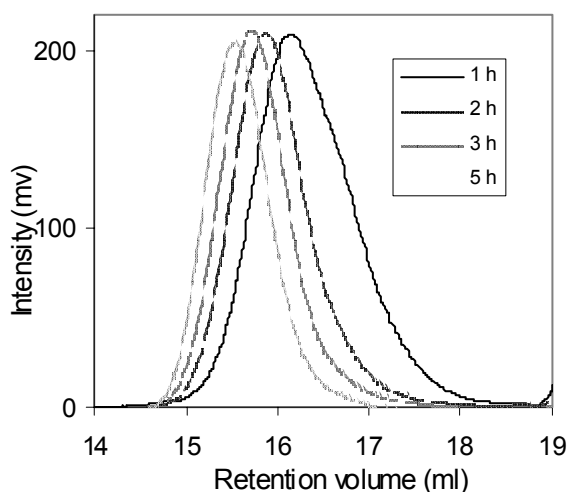
Figure 2.3: *GPC traces of PtBMA polymerized in toluene at 90 ºC at various reaction time intervals illustrating the growth of PtBMA chain length: 1 h (M_n = 2900, PDI = 1.39); 2 h (M_n = 4200, PDI = 1.28); 3 h (M_n = 5600, PDI = 1.23); 5 h (M_n = 7000, PDI = 1.21); $[p\text{-}TsCl]_0$ = $[CuCl]_0$ = $[PMDETA]_0$ = 0.07 M, $[tBMA]_0$ = 3.05 M.*

2.3.2 Synthesis of Block Copolymers

The synthetic strategy to prepare model triblock (A-B-A) ionomer precursors is given in first two steps of Scheme 1.1 (See Chapter 1). The scheme involves two steps: (1) synthesis of living difunctional PMMA macroinitiators with well-controlled molecular weight and PDI and (2) copolymerization with tBMA to obtain triblock copolymers. The most important aspect of these

polymerizations is that the selected reaction conditions result in living PMMA macroinitiators, which successfully initiate tBMA polymerization leading to block copolymers with controlled molecular weight and low PDI.

2.3.2.1 Difunctional PMMA macroinitiators. MMA was polymerized in toluene with a difunctional initiator, CuBr and PMDETA catalyst system at 90 ^{o}C via ATRP in 30 vol % toluene solution. The choice of bromine initiator was due to the easy synthetic accessibility of the difunctional bromine initiator by a simple coupling reaction between ethylene glycol and 2-bromo isobutyryl bromide (BIBB). The kinetic plots of $ln([M]_o/[M])$ *vs* reaction time (t) and monomer conversion versus reaction time for the ATRP of MMA using this system are shown in Figure 2.4. The plot is linear up to 80% conversion, indicating that the number of propagating species is constant during polymerization. It is necessary to stop the reaction around 90% conversion to maintain a high chain-end functionality. Table 2.3 summarizes the results of the macroinitiator synthesis. Fast polymerizations and a good correlation between the theoretical (from conversion measurements) and experimental (from SEC analysis) molecular weight indicates a high initiation efficiency. PDI was between 1.2 and 1.3 under these heterogeneous catalyst[27] conditions due to the low solubility of Cu^{II} species (deactivator in ATRP equilibrium). For low molecular weight PMMA macroinitiators (coded as MD4 and MD2), polymerizations were done in 50 vol % toluene to decrease the initiator and catalyst concentration. This will reduce the high initial radical concentration, thereby suppressing excessive termination reactions.
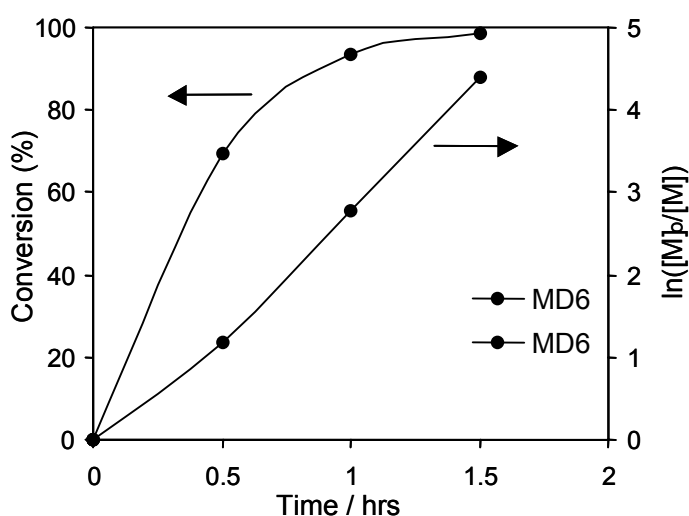
Figure 2.4: *Plots of ln([M]$_0$/[M]) vs reaction time and monomer conversion vs time for the ATRP of MMA in toluene at 90 ^{o}C. [Initiator]$_0$ = [CuBr]$_0$ = [PMDETA]$_0$ = 0.107 M, [MMA]$_0$ = 6.443 M.*

Table 2.3: *ATRP of MMA initiated by the difunctional initiator catalyzed by the CuBr/PMDETA system: the preparation of difunctional macroinitiators.*

Experiment	M:I:Cu:L	Reaction Time (min.)	Conversion (%)	Theoretical M_n^a	Experimental M_n^b		
					M_n	M_w	PDI
MD15	150:1:1:1	170	94	14500	15900	20500	1.25
MD8	80:1:1:1	140	85	7200	8000	10100	1.27
MD6	60:1:1:1	125	95	6200	6000	7800	1.25
MD4^c	40:1:1:1	100	88	3800	4100	5500	1.31
MD2^c	20:1:1:1	110	80	2050	2600	3500	1.32

$^a M_W$ initiator $+ 100$ ($[MMA]_0/[I]_0 \times$ conversion). ^{b}From SEC analysis in THF using universal calibration for PMMA with PS standards. ^{c}additional Toluene and Cu(II) are added to dilute the radical concentration.

2.3.2.2 ATRP Initiated by PMMA Macroinitiators

Chain Extension with MMA. The prepared polymers were used as macroinitiators for block copolymerizations. The resulting molecular weights and polydispersities are summarized in Table 2.4. The halogen exchange technique[23] was used for all polymerizations to improve the macroinitiator efficiency. Recent studies have used Cu^I chloride complexed with simple linear amine ligands in conjunction with bromine-terminated macroinitiators to successfully prepare several block copolymers.[23] This is due to the fact that the Br group initially provides a fast initiation, but the replacement of the bromine atom at the chain end by chlorine shortly after the polymerization is started suppresses undesirable secondary reactions by decreasing the radical concentration, while the initiation remains fast compared to propagation. Methyl ethyl ketone was used as solvent to increase the solubility of the Cu^{II} complex (deactivator) to obtain a low PDI. The living character of the polymerization is demonstrated by chain extension of MD4 by MMA (entry MM4M in Table 2.4). Figure 2.5a shows the SEC traces of MD4 and the chain extended macroinitiator MM4M. The clear shift of the SEC peak of MM4M to shorter retention times and the absence of a tail or shoulder at higher retention times show that the efficiency of the macroinitiator is high, which is characteristic for a living polymerization. The theoretical molecular weight matches well with the experimental molecular weight.

Table 2.4: *Summary of ATR block copolymerizations of TBMA initiated by PMMA macroinitiators catalysed by CuCl/PMDETA[a] in methyl ethyl ketone. (temperature of the reaction = 90 °C; Macroinitiator: MEK = 1: 2 (Weight Ratio)).*

Experiment	Macroinitiator	Molecular Weight (PDI)	DP[c] of second block [Reaction time(min), Conversion(%)]	Theoretical M_n[d] of block PMMA/PtBMA	Experimental M_n[e] of PMMA/PtBMA	MW's from GPC		Mole % of tBMA from FTIR
						M_n	PDI	
MM4M	MD4	4100 (1.31)	30 [120, 85]	3000 (PMMA)	2700	6800	1.28	NA
BM6B[b]	MD6	6000 (1.25)	28 [180, 72]	1800 (PtBMA)	2200	8200	1.20	21.3
BM8B	MD8	8000 (1.27)	28 [150, 73]	2400 (PtBMA)	2700	10700	1.31	23.0
BM15B	MD15	15900 (1.25)	28 [240, 80]	3090 (PtBMA)	3100	19000	1.35	16.2
BM7B	MD7	7300 (1.25)	42 [180, 56]	3370 (PtBMA)	4300	11600	1.35	28.2
BM2B	MD2	2600 (1.32)	28 [120,74]	3100 (PtBMA)	3400	6000	1.39	52

[a] I : Cu(I)Cl : PMDETA = 1 :1 : 1. [b] Where B is PtBMA and M is PMMA. [c] DP is targetted degree of polymerisation of the second block PMMA or PtBMA. [d] (Monomer MW)([M]o/[I]o × conversion). [e] From SEC analysis in THF using universal calibration for PMMA with PS standards.

Copolymerization with tBMA. Copolymerizations with *tert*-butyl methacrylate were performed to obtain triblock copolymers with a range of molecular weights (Table 2.4). Low molecular weight tBMA blocks were targeted since ionomers with a high mole percentage of ionic groups are difficult to process due to strong ionic interactions.[1] Figure 2.5b shows the SEC traces of MD6 and the triblock copolymer BM6B. The SEC traces are unimodal and nearly symmetrical and there is very little tailing to lower molecular weights in the block copolymer trace, which could have been indicative of un-reacted macroinitiator. The large overlap of the SEC peaks is due to the lower targeted molecular weight of the tBMA block. The measured molecular weights are not absolute molecular weights, since the hydrodynamic volume of the block copolymer may differ considerably from the corresponding PMMA macroinitiators in THF. However, there is a relatively good agreement between the theoretical molecular weights and experimental molecular weight values as measured by SEC with universal calibration curve for PMMA (Mark–Houwink–Sakurada constants[14] for PMMA: K = 9.4 × 10^{-4} dL g^{-1}, a = 0.719) based on linear PS standards. The polymerization was stopped before 100% conversion of monomer to avoid side reactions. The block copolymers were purified, dried, and analyzed by ^{1}H-NMR to verify incorporation of the tBMA monomer. A relevant part of the NMR spectra of a macroinitiator and a block copolymer are shown in Figure 2.6. The presence of the peak at 1.4 ppm confirms the incorporation of the *tert*-butyl group in the block copolymers. The α-methyl protons are observed at 0.8–1.2 ppm and

methylene protons from the backbone are seen at 1.7–3.1 ppm. The sharp peak at 1.62 ppm is due to water present in the deuterated chloroform.
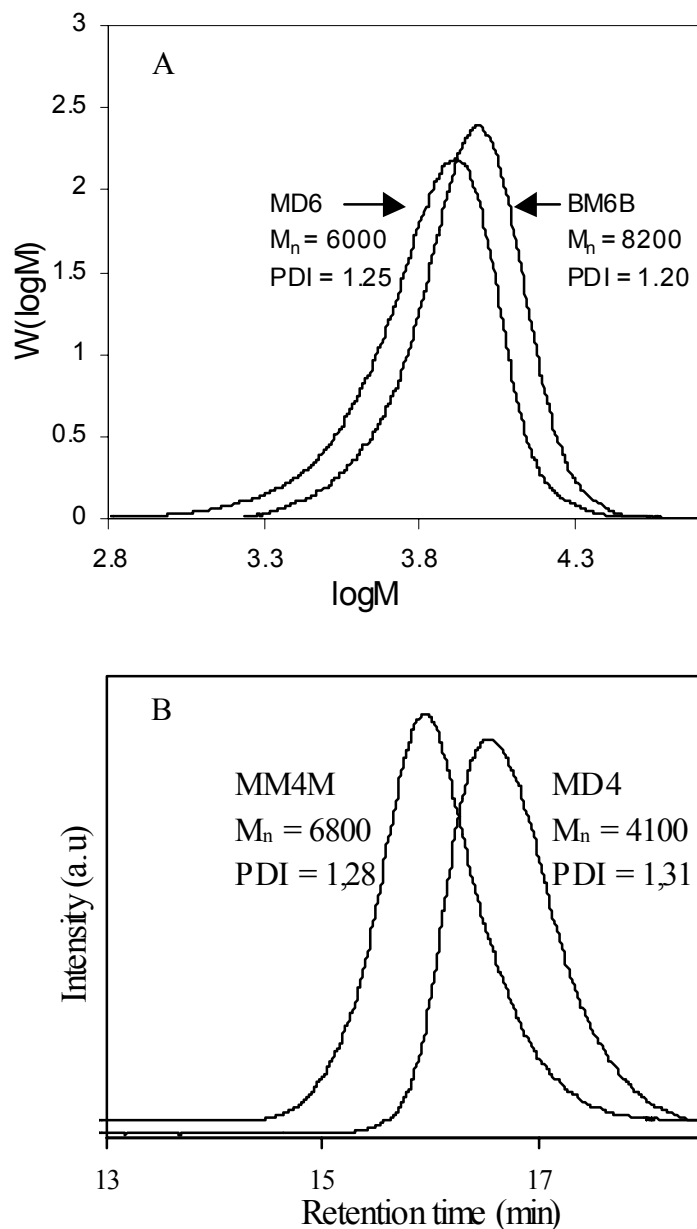
Figure 2.5: *SEC traces of (A) macroinitiator MD4 (difunctional PMMA macroinitiator; M_n = 4100, PDI = 1.31) and MM4M (chain extended PMMA using MD4 as macroinitiator; M_n = 6800, PDI = 1.28). [PMMA-Br]$_0$ = [CuCl]$_0$ = [PMDETA]$_0$ = 0.124 mol/L; [MMA]$_0$ = 3.71 mol/L and (B) SEC traces of macroinitiator MD6 (difunctional PMMA macroinitiator; M_n = 6000, PDI = 1.25) and block copolymer BM6B (triblock with PMMA middle block of molecular weight 6000 and PtBMA outer blocks; M_n = 8200, PDI = 1.20). [PMMA–Br]$_0$ = [CuCl]$_0$ = [PMDETA]$_0$ = 0.04 × 10^{-2} mol/L; [tBMA]$_0$ = 0.946 mol/L.*
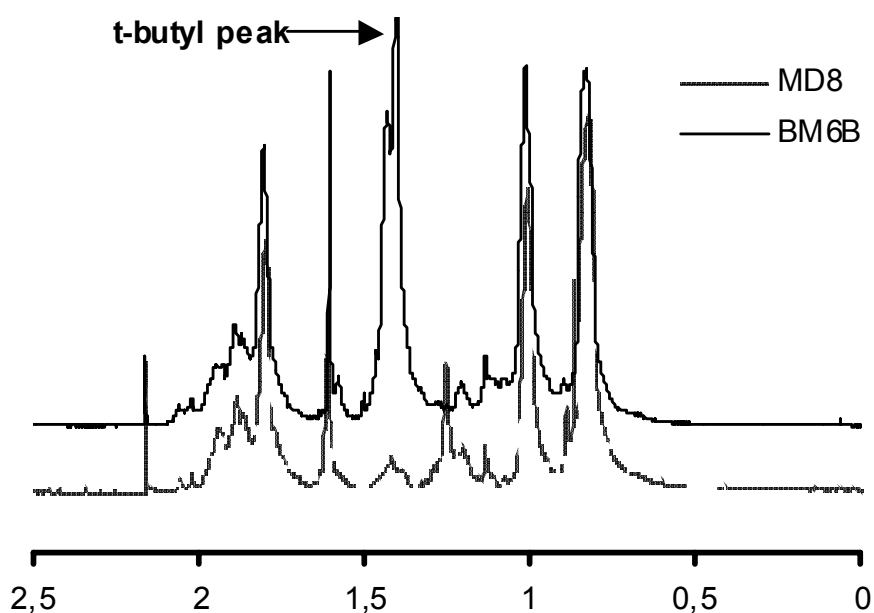
Figure 2.6: *Partial NMR spectra of macroinitiator MD8 (difunctional PMMA macroinitiator with M_n = 8000) and block copolymer BM8B (triblock with PMMA middle block of molecular weight 8000 and PtBMA outer blocks).*

2.3.3 Chemical Composition of Block Copolymers

FTIR Analysis. NMR spectra cannot be used to determine the composition of the block copolymers because of the very similar backbone structure of the polymers, which leads to overlap of the signals, especially in the *tert*-butyl group region. Therefore, the chemical composition of the block copolymers was determined by FTIR spectroscopy. Horace[28] reported on the characteristic infrared absorptions of the *tert*-butoxy group present in various organic molecules. The spectrum can be divided into four spectral regions, i.e., 720–770 cm^{-1}, 820–920 cm^{-1}, 1000–1040 cm^{-1} and 1155–1200 cm^{-1}. The 820–920 cm^{-1} absorptions originate from the skeletal vibration of the *tert*-butoxy group.[28] The absorption at 847 cm^{-1} can be assigned to the above-mentioned skeletal vibration in the FTIR spectrum of PtBMA. Since this band is well-resolved and separated in the block copolymer spectrum, we used this peak to estimate mole percentage of the tBMA in the block copolymer. Table 2.4 lists the mole percentage of tBMA for the various block copolymers.

2.3.4 GPEC Analysis of Block Copolymers.

Characterization techniques such as NMR and IR can give information about the overall chemical composition of copolymers, but cannot distinguish between a polymer blend and a copolymer with the same overall chemical composition. On the other hand, SEC can give an indication of the existence of block copolymer by measuring the increase of the hydrodynamic volume of the copolymer vs. the hydrodynamic volume of the macroinitiator. However, SEC cannot be used as a direct proof for the existence, purity and for the determination of the chemical composition distribution (CCD) of the block copolymer. High-performance liquid chromatography (HPLC)[29] is an established technique for selective separation and characterization of block and random copolymers. Separation of polymers in HPLC is based on a combination of adsorption/partitioning, precipitation/redissolution, and exclusion effects. Since the contribution of these separate mechanisms can be different in each specific case, it is preferred to use the name gradient polymer elution chromatography[30] (GPEC is a registered trademark of Waters Chromatography). In GPEC, separation of polymers is based on differences in column interactions, as is the case in isocratic chromatography, but also on precipitation and redissolution mechanisms as the eluent composition changes gradually in time. Application of GPEC therefore, provides the possibility to separate polymeric compounds according to molar mass, chemical composition, and chain(-end) functionality. For example, GPEC recently has been applied to characterize random and block copolymers.[31] In the current study, we used normal phase GPEC with THF and *n*-heptane as eluents. The gradient used is shown in Table 2.1. The retention times under these chromatographic conditions for a number of PMMA and PtBMA samples prepared via ATRP are shown in Figure 2.7. The following conclusions are drawn from Figure 2.7. The molecular weight (M_n) dependency of PMMA on the retention time ranges from 38 min (M_n = 2500) to 44 min (M_n = 18000). The large dependence of retention time on molecular weight may result in broad peaks for PMMAs with this gradient. Similarly, the molecular weight (M_n) dependency of PtBMA on the retention time ranges from 24 min (M_n = 4000) to 26 min (M_n = 60000). The two homopolymers are well separated at all molecular weights and a retention time difference of 15 min indicates that the selectivity of the gradient selected is high. PtBMA with its bulky nonpolar ester group elutes first compared to the methyl group of PMMA. The retention time increases with molecular weight and becomes independent of the molecular weight at a certain critical molecular weight that is characteristic for each homopolymer. Although the two homopolymers have different molar mass dependencies, the block copolymer can be separated from the homopolymer. Figure 2.7 shows that when the

retention time is less than 38.5 min PMMA molecules will not elute at this retention time unless the segments are chemically linked to PtBMA as in a (block) copolymer. A difference in the chemical composition of the copolymer leads to a change in retention time of the copolymer, which can be used to establish the block copolymer structure.
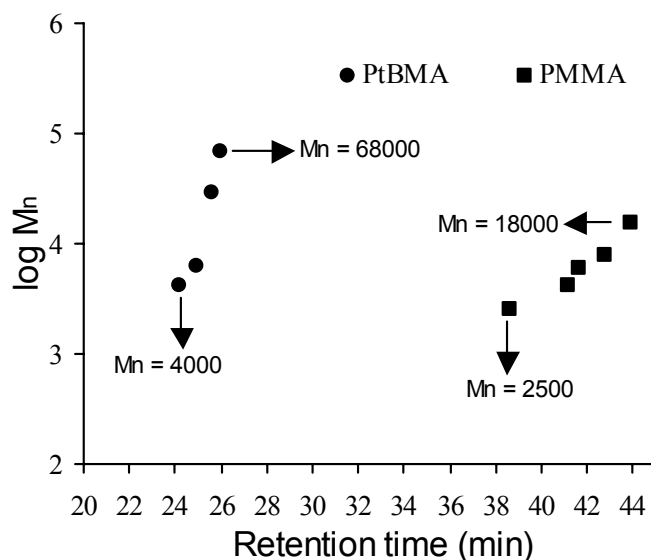
Figure 2.7: *The molar mass dependence of poly(tert-butyl methacryalte) (PtBMA, ●, 4000, 6300, 30200, 68000 g/mol) and poly(methyl methacrylate) (PMMA, ■, 2500, 4300, 6000, 8000, 18000 g/mol) homopolymers on the retention time in the GPEC under heptane–THF (2%/min) gradient on a silica column.*

2.3.4.1 Analysis of Block Copolymers. GPEC traces of BM2B, MD2, BM6B, and MD6 are shown Figure 2.8a and 2.8b. The presence of the block copolymer peak in between the peaks of two homopolymers is a clear evidence for the block copolymer formation. The retention time of the block copolymer compared to the macroinitiator is lowered and shifted toward the PtBMA homopolymer even though the molecular weight of the block copolymer is higher. The difference in the elution behavior is a direct indication of the chemical composition difference between the macroinitiator and the block copolymer. The sensitivity of the GPEC technique is evident from the elution behavior of BM6B and MD6 in SEC, and GPEC respectively (Figures 2.5b and 2.8b). In GPEC, the peaks from the block copolymer and the macroinitiator are well-resolved. The relative shift in the retention time of the block copolymer compared to the corresponding macroinitiator is dependent on the chemical composition (mole percentage of tBMA) of the block copolymer.
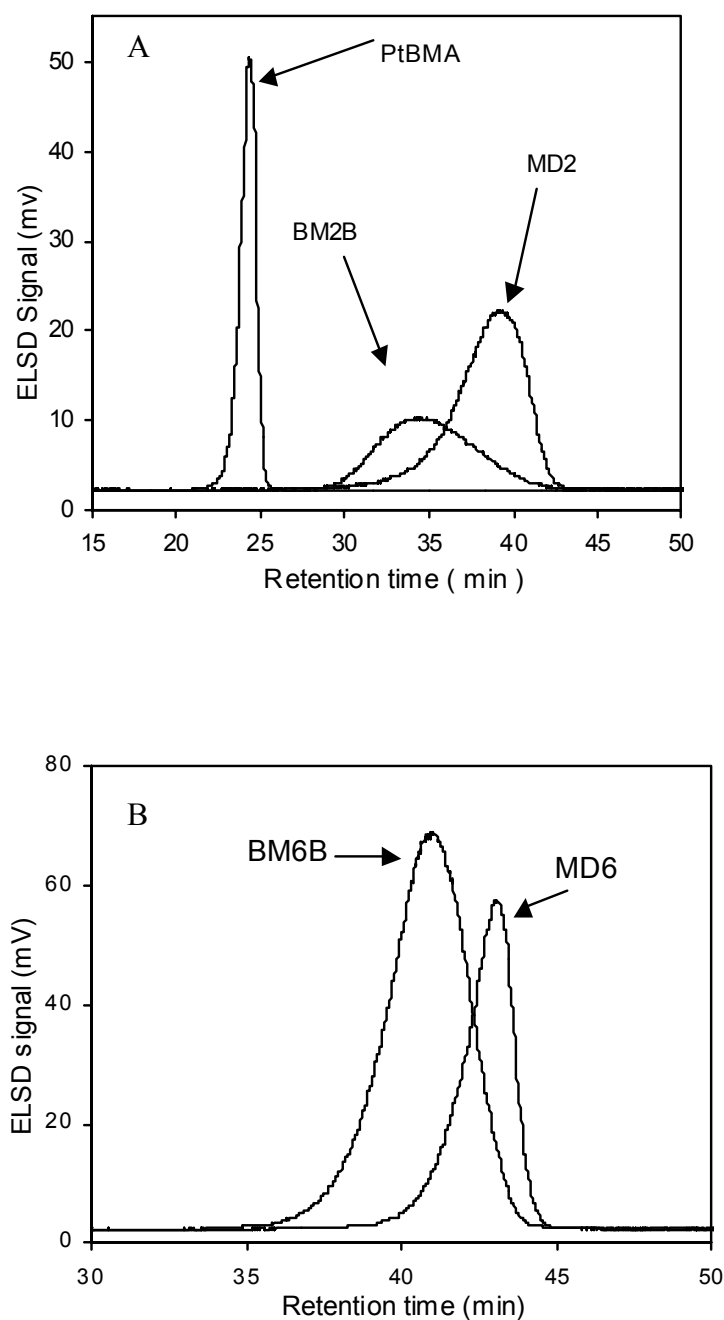
Figure 2.8: *GPEC traces of (A) macroinitiator MD2 (difunctional PMMA macroinitiator with M_n = 2600) and block copolymer BM2B (triblock with PMMA middle block of molecular weight 2600 and PtBMA outer blocks) and (B) macroinitiator MD6 (difunctional PMMA macroinitiator with M_n = 6000) and block copolymer BM6B (triblock with PMMA middle block of molecular weight 6000 and PtBMA outer blocks) using heptane–THF (2%/min) gradient on a silica column.*

2.3.4.2 Effect of Block Copolymer Reaction Conditions. There are two factors that govern the success of block copolymer synthesis using ATRP: chain-end functionality and cross-propagation efficiency.[32] Efficient cross-propagation depends on the relative reactivity ratios, propagation rate constants, and equilibrium constants of both macroinitiator and growing chains. When well–matched,[33] the molecular weights of the polymers will be predictable with low polydispersity indices. If the above conditions are not met, initiation will be slower than propagation, resulting in a nonuniform length of the PtBMA block and heterogeneities in the block copolymer. The halogen exchange technique, i.e., R–Br/CuCl, improves the cross-propagation efficiency, resulting in better control of the polymerization. The developed GPEC technique is very sensitive for this block length distribution, i.e., the distribution of the PtBMA block length in the copolymer. Figure 2.9 shows the GPEC traces of the macroinitiator and block copolymer synthesized by ATRP where no halogen exchange technique is used, i.e., CuBr is used as a catalyst rather than CuCl. Though the peak position is shifted toward a lower retention time, the bimodal, asymmetrical peak demonstrates that the polymerization is poorly controlled. SEC analysis gave a unimodal and symmetrical peak for this block copolymer (not shown here). For the first time we demonstrate qualitatively the use of the GPEC technique to study the influence of macroinitiator initiation on the block copolymer structure.
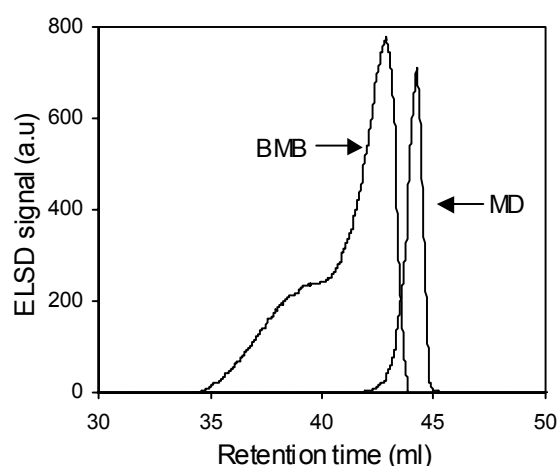
Figure 2.9: *GPEC traces of macroinitiator MD and block copolymer BMB (triblock with PMMA middle block and PtBMA outer blocks) using heptane–THF gradient (2%/min) on a silica column.*

2.4 Conclusions

The results of the heterogeneous atom transfer radical polymerization of tBMA indicate that the selection of the initiator is an important factor to obtain poly(tBMA) with well-defined molecular weights and low PDI. *p*-toluenesulfonyl chloride and trichloroethanol were efficient initiators due to higher initiation rates compared to the propagation rate. Dibromo-functionalized living PMMA macroinitiators synthesized using a CuBr/PMDETA catalyst system, successfully initiates the tBMA polymerization, resulting in triblock copolymers with controlled molecular weight and narrow molecular weight distribution. PMMA macroinitiators were more effective than the corresponding EBriB initiator in tBMA polymerization. The spectroscopic and chromatographic characterization of the copolymers reveal the effectiveness of the halogen exchange technique used in the block copolymer synthesis to achieve high macroinitiator efficiency. GPEC analysis of the block copolymers confirms the presence of the block copolymer structure and shows that the macroinitiator efficiency is high. The selectivity of the gradient in GPEC to PtBMA length in the block copolymer enables to measure the chemical composition distribution of the block copolymers. GPEC might be effectively used to study the influence of copolymerization reaction conditions on the resulting block copolymer structure. GPEC separation of block copolymers can be improved by optimizing gradient shape and steepness, resulting in quantitative analysis of the block copolymer. These precursor materials can be selectively hydrolyzed and neutralized with metal salts to obtain well-defined block ionomers.

2.5 References

(1)   Eisenberg A.; Kim, J. S. *Introduction to Ionomers*, **1998**, John Wiley & Sons, Inc.

(2)   Tant, M.R., Mauritz, K, A., Wilkes, G. L. *Ionomers: Synthesis, Structure, Properties and Applications*. **1997**, Eds., Blackie Academic and Professional: London.

(3)   Schlick, S. *Ionomers: Characterization, Theory, and Applications*. **1996**, Ed.; CRC Press: Boca Raton, FL.

(4)   Eisenberg, A.; Navratil, M. *Macromolecules*, **1974**, 7, 90.

(5)   Hara, M.; Jar, P.; Sauer, J. A. *Polymer*, **1991**, 32, 1622.

(6)   Ma, X.; Sauer, J. A.; Hara, M. *Macromolecules*, **1995**, 28, 3953.

(7)   Reporter, C. D.; Long, T. E.; McGrath, J. E. *Polym. Int.*, **1994**, 33, 205.

(8)   Venkateshwaran, L. N.; York, G. A.; De Porter, C. D.; Mc Grath, J. E.; Wilkes, G. L. *Polymer*, **1992**, 33, 2277.

(9)   Heise, A; Hedrick, J. L.; Frank C. W.; Miller R. D. *J. Am. Chem. Soc*, **1999**, 121, 8647.

(10)   Davis, K. A.; Matyjaszewski, K. *Macromolecules*, **2000**, 33, 4039.

(11)   Zhang, X.; Xia, J.; Matyajaszewski, K. *Polm. Prepr. (Am. Chem. Soc. , Div. Polym. Chem.*), **1999**, 40(2), 440.

(12)   Haddleton, D. M.; Crossman, M. C.; Dana, B. H.; Duncalf, D. J.; Heming, A. M.; Kukulji, D.; Shooter, A. J. *Macromolecules*, **1999**, 32, 2110.

(13)   Moschogianni, P.; Pispas, S.; Hadjichristidis, N. *J. Poly. Sci. Part A: Polym. Chem.* **2001**, 39, 650.

(14)   Beuermann, S.; Paquet, D. A., Jr.; Mc Minn, J. H.; Hutchinson, R. A.; *Macromolecules* **1996**, 29, 4206.

(15)   Coleman, M. M.; Painter, P.C. J. *Macromol. Sci., Rev. Macromol. Chem.* **1978**, C16, 1975.

(16)   Williams, H. L.; Han K. *J. Appl. Poly. Sci.* **1989**, 38, 73.

(17)   Staal, W. J.; PhD thesis; Eindhoven University of Technology, Eindhoven, The Netherlands, **1996**.

(18)   Matyjaszewski, K.; Wang, J. L.; Grimaud, T.; Shipp, D. A. *Macromolecules*, **1998**, 31, 1527.

(19)   Kroll, R.; Eschbaumer, C.; Schubert, U. S.; Buchmeister, M. R.; Wurst, K. *Macromol. Chem. Phys.* **2001**, 202, 645.

(20)   Percec, V.; Barboiu, B. *Macromolecules*, **1995**, 28, 7970.

(21)   Destarac, M.; Matyjaszewski, K.; Boutevin, B. *Macromol. Chem. Phys.* **2000**, 201, 265.

(22)   Coessens, V.; Pintauer, T.; Matyjaszewski, K. *Prog. Polym. Sci.* **2001**, 26, 337.

(23)   Matyjaszewski, K.; Shipp, D. A.; Wang, J. L.; Grimaud, T.; Patten, T. E. *Macromolecules* **1998**, 31, 6836.

(24)   Chambard, G.; Klumperman, B.; German, A. L. *Macromolecules*, **2000**, 33, 4417.

(25)   Percec, V.; Barboiu, B.; Kim, H, J. *J. Am. Chem. Soc.* **1998**, 120, 305.

(26)   Percec, V., Barboiu, B.; Bera K. T.; Sluis, M.; Grubbs, R. B.; Frechet, M. J. J. *J. Polym. Sci. Part A: Polym. Chem.* **2000**, 38, 4776.

(27)   Snijder, A.; Klumperman, B.; van der Linde, R. *Macromolecules*, **2002**, 35, 4785.

(28)   Ory, H. A. *Anal. Chem.*, **1960**, 32, 509.

(29)   Katz, E.; Eksteen, R.; Schoenmakers, P.; Miller, N. *Handbook of HPLC;* Marcel Dekker: New York*, **1979**.

(30)   Philipsen, H. J. A.; De Cooker, M. R.; Claessens, H. A.; Klumperman, B.; German, A.L. *J. Chromatogr. A*, **1997,** 761, 147.

(31)   Cools, P. J. C. H.; Maesen, F.; Klumperman, B.; van Herk, A. M.; German, A. L. *J. Chromatogr. A,* **1996**, 736, 125.

(32)   Robin S.; Gnanou Y. *Controlled radical polymerization: progress in ATRP, NMP and RAFT, vol. 768. Washington, DC: Am. Chem. Soc.,* **2000**, p.334.

(33)   Davis, K. A.; Matyjaszewski, K. *Macromolecules*, **2001**, 34, 2101.

2.6 Supporting Information
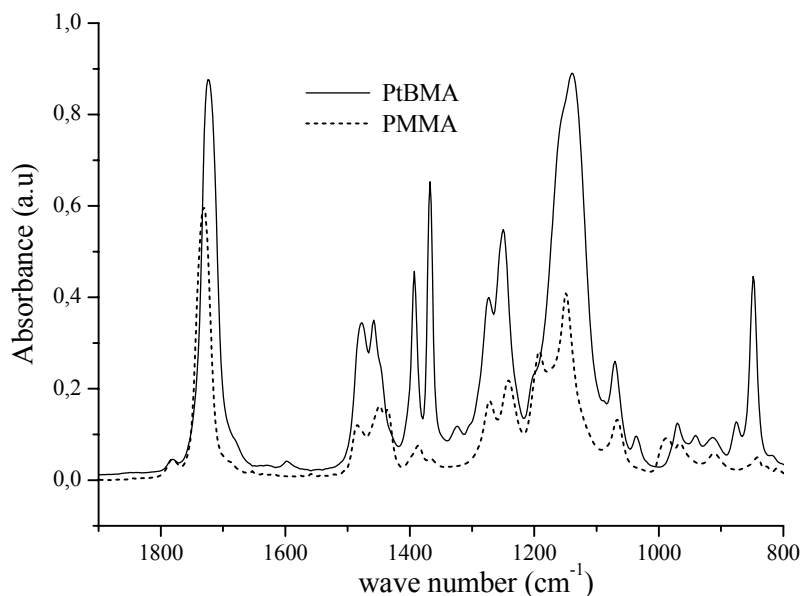
Figure 2.10: *FTIR spectra of selected regions of two homopolymers PMMA and PtBMA.*
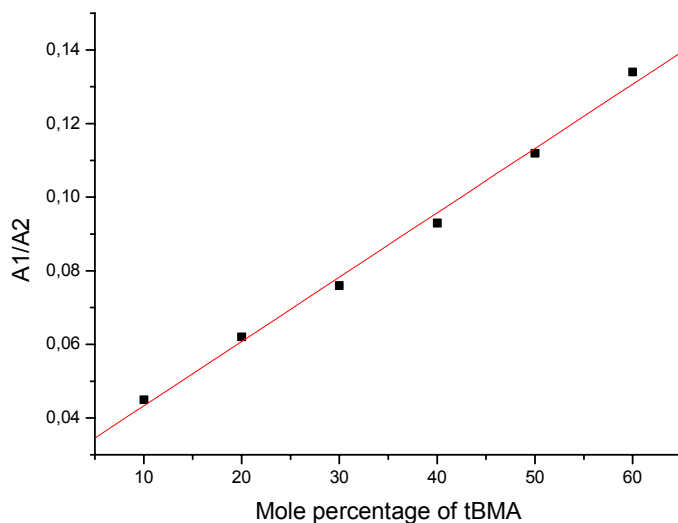
Figure 2.11: *Calibration curve for the quantitative estimation of percentage of tBMA content in the blockcopolymer. Where A1 and A2 are absorbances of the band at 847 cm^{-1} (assigned to the skeletal vibration of tert-butoxy group in PtBMA homopolymer) and the band at 1730 cm^{-1} (assigned to the carbonyl ester peaks of both PMMA and PtBMA).*
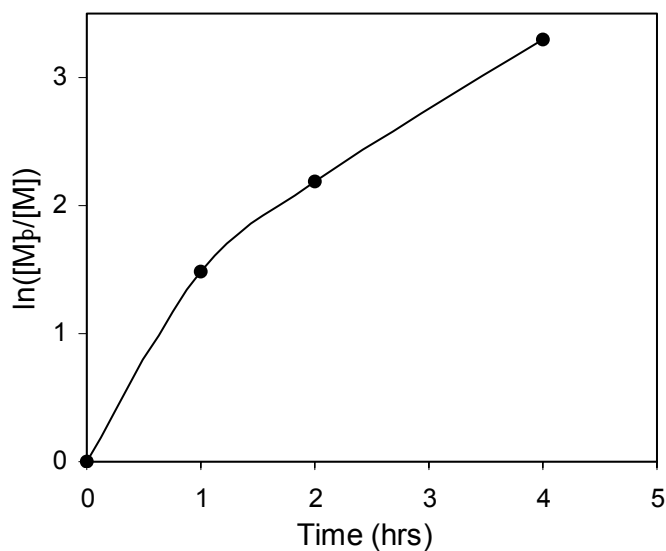
Figure 2.12: *Plot of ln([M]$_0$/[M]) versus reaction time for the ATRP of tBMA using PMMA-Br as the initiator and CuCl/PMDETA as the catalyst in MEK at 90 ^{o}C. [PMMA−Br]$_0$ = [CuCl]$_0$ = [PMDETA]$_0$ = 0.04 × 10^{-2} mol/L; [tBMA]$_0$ = 0.946 mol·L^{-1}*
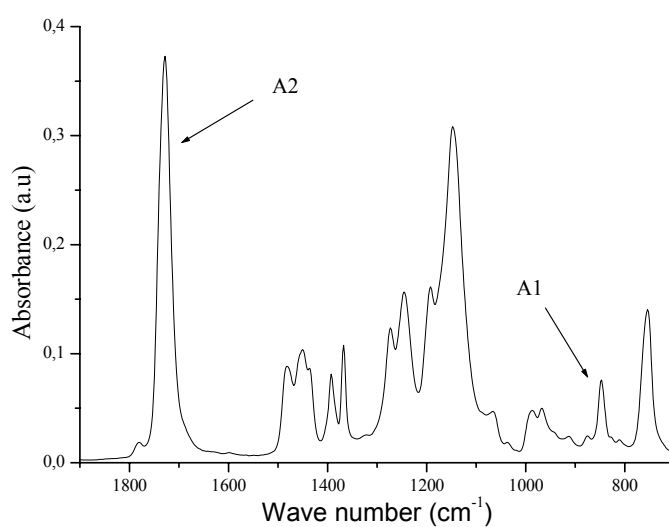
Figure 2.13: *FTIR spectra of selected regions of block copolymer BM6B (triblock with PMMA middle block of molecular weight 6000 and PtBMA outer blocks).*
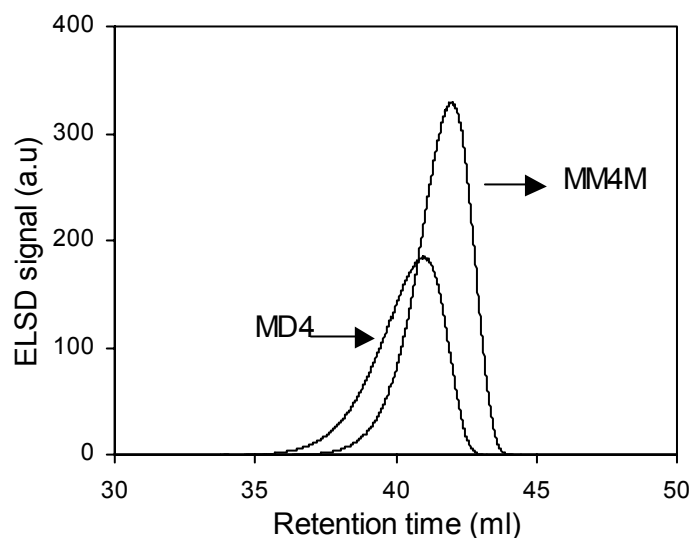
Figure 2.14: *GPEC traces of macroinitiator MD4 (difunctional PMMA macroinitiator with M_n = 4100) and MM4M (chain extension of the MD4 macroinitiator with methyl methacrylate) using heptane–THF gradient (see Table 2.1 experimental section) on a silica column*
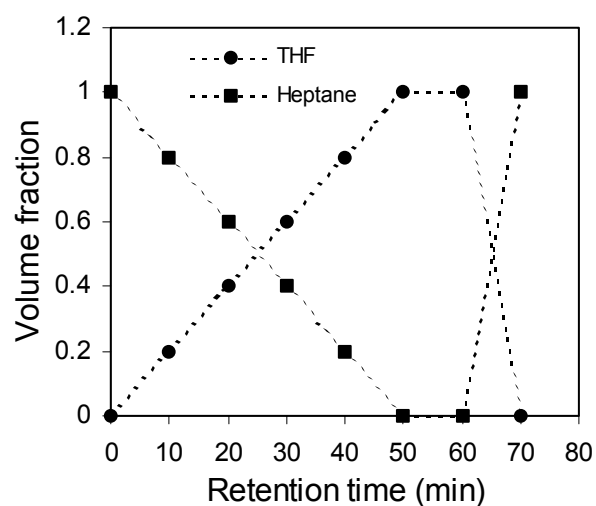
Figure 2.15: *Schematic plot of the gradient (heptane, THF) described in Table 2.1.*

Chapter 3

"Controlled" Synthesis and Characterization of High Molecular Weight Methyl Methacrylate/*tert*-Butyl Methacrylate Diblock copolymers via ATRP

ABSTRACT: Atom transfer radical polymerization (ATRP) of methyl methacrylate (MMA) with 2,2,2–trichloroethanol (TCE) as initiator and CuCl/*N,N,N,N',N''',N'''*-hexamethyltriethylenetetramine (HMTETA) as a catalyst system was investigated. Poly(methyl methacrylate) (PMMA) macroinitiators with defined molecular weight, a low polydispersity index (PDI) and a high end-group functionality were obtained. These PMMA macroinitiators successfully initiate block copolymerization of *tert*-butyl methacrylate (tBMA) resulting in poly(MMA-*b*-tBMA) diblock copolymers with low PDI for a range of tBMA block lengths. Gradient polymer elution chromatography (GPEC) was used to confirm the block copolymer structure. Furthermore, the effect of molecular weight of the macroinitiator, nature of catalyst system (heterogeneous/homogeneous), and the amount of solvent on the degree of control achieved in the block copolymerization was studied. The GPEC technique was successfully used to demonstrate the effect of the aforementioned parameters on the block copolymer structure. In particular, the use of a homogeneous catalyst system, CuBr/4,4'-di-5-nonyl-2, 2'-bipyridine (dNbpy), and a large ratio of methyl ethyl ketone (MEK) to PMMA macroinitiator lead to the synthesis of well controlled high molecular weight diblock copolymers. This can be explained by the complete solubility of the Cu(II) complex, the deactivating species in the ATRP mechanism, by the use of the dNbpy as a ligand and the polar solvent (MEK). The homogeneous catalyst condition leads to efficient activation/deactivation exchange reactions between the growing polymer chains and the dormant polymer chains resulting in well-controlled block copolymers.

3.1 Introduction

This chapter focuses on the synthesis and characterization of the high molecular weight poly(MMA-*b*-tBMA) diblock copolymers by ATRP. Hence it is worthwhile to review the relevant literature. As mentioned in the first chapter, block copolymers can be synthesized in two ways: one pot method and macroinitiator method. Several research groups[1-6] used ATRP successfully to synthesize block copolymers of methacrylates and acrylates involving these two methods. However, there are only limited reports in the literature concerning the synthesis of (meth)acrylic block copolymers from high molecular weight (meth)acrylic macroinitiators via ATRP. Jerome *et al.*[6] reported the ATRP synthesis of ABA triblock copolymers ($M_n \approx 90$ K, 140 K, and 156 K, from SEC measurements) of methyl methacrylate (MMA, A block) and *n*-butyl acrylate (BA, B block) using the homogeneous $NiBr_2(PPh_3)_2$ catalyst. MMA was polymerized with a bromine end-functionalized poly(n-butyl acrylate) (PBA−Br, $M_n \approx 60$ K, 105 K, from SEC measurements) macroinitiator. The mechanical and viscoelastic properties of these block copolymers were inferior to those of similar block copolymers synthesized by anionic polymerization. The origin of these differences in the properties was related to the polydispersity of the PMMA outer blocks (large diversity in the length of the PMMA outer blocks), arising from the slow initiation of MMA by the PBA−Br macroinitiator.

Matyjaszewski *et al.*[7] synthesized similar high molecular weight ($M_n \approx 90$ K, PDI < 1.35) ABA triblock copolymers utilizing the halogen exchange technique, which improved the cross-propagation between PBA macroinitiators and MMA resulting in better control of molecular weights and PDI. They reported the successful copper mediated homogeneous (CuCl/dNbpy catalyst) and heterogeneous (CuCl/HMTETA catalyst) ATRP polymerization of MMA with a high molecular weight PBA−Br ($M_n \approx 67$ K) macroinitiator. A lower PDI of the triblock copolymer was obtained with the homogeneous catalyst compared to the heterogeneous catalyst indicating that polymerization is better controlled under homogeneous catalyst conditions. Important conclusions of these studies were that (a) the use of a homogeneous catalyst system coupled with halogen exchange leads to well controlled high molecular weight *ABA* triblock copolymers of MMA and BA, (b) SEC analysis of the triblock copolymers can not provide a detailed chemical composition distribution of the block copolymers, particularly in this case of shorter PMMA outer blocks compared to the middle longer PBA block, and (c) the importance of the analysis of the accurate block copolymer structure, specifically in terms of differences in the chemical composition, and its

influence on the measured mechanical properties. So far, reports concerning the synthesis of high molecular weight PMMA macroinitiators and their successful initiation of *tert*-butyl methacrylate (tBMA) to obtain high molecular weight poly(MMA-*b*-tBMA) diblocks via ATRP have not been available. Moreover, the chemical composition analysis of such high molecular weight all-methacrylate *A-B* diblock copolymers with short '*B*' block lengths has not been reported.

This chapter presents results of the synthesis of highly chlorine-end functionalized poly(methyl methacrylate) (PMMA) macroinitiators with well defined molecular weight and a low polydispersity index (PDI) using a CuCl/HMTETA catalyst system and 2,2,2–trichloroethanol (TCE) as initiator. These PMMA macroinitiators successfully initiate block copolymerizations of *tert*-butyl methacrylate (tBMA) resulting in poly(MMA-*b*-tBMA) diblock copolymers with a low PDI for a range of tBMA block lengths. More specifically, low molecular weight tBMA blocks were targeted, since ionomers with a high mole percentage of ionic groups are difficult to process due to strong ionic interactions. Furthermore, the effect of molecular weight of the macroinitiator, nature of catalyst system (heterogeneous/homogeneous), and the amount of solvent on the degree of control achieved (PDI and the chemical composition of the final block copolymer) in the block copolymerization are presented. Gradient polymer elution chromatography (GPEC) was used to confirm the block copolymer structure.

3.2 Experimental Section

3.2.1 Materials

Methyl methacrylate (Aldrich, 99%), *tert*-butyl methacrylate (Aldrich, 99%), p-xylene, and methyl ethyl ketone (Aldrich, 99%) were vacuum distilled and stored at −15 °C. *N,N,N,N′,N‴,N‴*-hexamethyltriethylenetetramine (HMTETA), 2,2,2–trichloroethanol (98%), *N,N,N′,N″,N″*-pentamethyldiethylenetriamine (PMDETA), butyl acetate (99%), and silica (0.04–0.6 mm) were obtained from Aldrich and used without further purification. Cu^{I}Br (99%) and Cu^{I}Cl (99%) were obtained from Aldrich and purified as follows. Copper halides were stirred with glacial acetic acid for 24 h under a nitrogen atmosphere, washed consecutively with glacial acetic acid, ethanol, diethyl ether, dried at 40 °C for three days, and stored under an argon atmosphere.

3.2.2 Analysis and Measurements

Determination of Conversion and Molecular Weight Distribution. The conversion of the monomer during the polymerization was determined by gas chromatography (GC) analysis. GC measurements were carried out on a Hewlett-Packard 5890 SII, equipped with an AT-Wax capillary column (30 m × 0.53 mm × 10 μm), using a HP 3393a integrator to obtain the chromatogram. Dilute polymer solutions in tetrahydrofuran (THF) were made in 1.5 mL crimp neck vials and measured using an auto sampler. An injection volume of 3 μl was used. A temperature limit of 40–200 ^{o}C was used. The injection temperature was 200 °C and a 10 °C min^{-1} heating ramp was used. SEC measurements were carried out using a Waters GPC equipped with a Waters 510 pump, a Waters 410 differential refractometer (40 °C), a Waters WISP 712 autoinjector (50 μL injection volume), a PL gel (5 μm particles) 50 × 7.5 mm guard column, and two PL gel mixed-C (5 μm particles) 300 × 7.5 mm columns (40 °C). Data acquisition and processing were performed using the Waters Millennium 32 (v3.05) software. Tetrahydrofuran (THF, Biosolve, stabilized with butylated hydroxytoluene, BHT) was used as eluent at a flow rate of 1.0 mL/min, dilute polymer solution of 2 mg/mL were made, and injected for analysis. Calibration was done using polystyrene (PS) standards (Polymer Laboratories, 580–7.1 × 10^6 g mol^{-1}), and molecular weights are calculated using the universal calibration principle with Mark–Houwink parameters for PMMA[8] (PMMA: $K = 0.944 \times 10^{-4}$ dL g^{-1}, $a = 0.719$, PS: $K = 1.14 \times 10^{-4}$ dL g^{-1}, $a = 0.716$).

Spectroscopic Analysis. The FTIR spectra were recorded with a BioRad Excalibur 3000 series spectrometer. One hundred scans at a resolution of 4 cm^{-1} were signal-averaged and the BioRad Merlin software was used to analyze the spectra. Samples were prepared by casting films from a dilute polymer solution on KBr pellets for FTIR measurements. These films were thin enough to be within the range where the Beer–Lambert[9] law can be applied. The detailed FTIR procedure and analysis of the data were described in Chapter 2. FT-NMR spectra were recorded with a Varian 400 MHz spectrometer. NMR spectra were recorded in CDCl$_3$ at 25 ^{o}C. All chemical shifts are reported in ppm downfield from tetramethylsilane (TMS), used as an internal standard ($\delta = 0$ ppm).

GPEC Analysis. GPEC measurements were carried out on a Waters Alliance 2690 separation module with a Waters 2487 dual λ absorbance detector and a PL-EMD 960 ELSD detector (Nitrogen flow 5.0 mL/min, temperature 70 ^{o}C). A Zorbax silica 5 μm column (4.6 mm × 150 mm, Dupont Chromatography) was used at 30 ºC. A linear binary gradient starting from heptane (volume fraction, Φ = 1; 0 min; nonsolvent for the polymers used in analysis) to THF (volume

fraction, $\Phi = 1$; 60 min; good solvent for the polymers used in analysis) was used. The column was reset at the end of the gradient to initial conditions between 60 and 70 min. A gradient steepness, i.e., gradient change in fraction solvent per minute ($\Delta\Phi_{gradient}$), of 0.02 was applied. A detailed description of the gradient used is given in Chapter 2. HPLC grade solvents obtained from Biosolve were used. A Varian 9010 solvent delivery system was used to maintain a stable flow rate of the eluents. Dilute polymer solutions were made in THF (10 mg/mL), and a sample volume of 25 μL was used for analysis. Data were acquired and analyzed by the Millenium 32 3.05 software.[10]

MALDI-TOF-MS: Measurements were performed on a Voyager-DE STR (Applied Biosystems, Framingham, MA) instrument equipped with a 337 nm nitrogen laser. Positive-ion spectra were acquired in reflector mode. DCTB (trans-2-[3-(4-tert-butylphenyl)-2-methyl-2-propenylidene]malononitrile) was chosen as the matrix. Sodium trifluoracetate (Aldrich, 98%) was added as the cationic ionization agent. The matrix was dissolved in THF at a concentration of 40 mg/mL. Sodium trifluoracetate was added to THF at a concentration of 1 mg/mL. The dissolved polymer concentration in THF was approximately 1 mg/mL. For each spectrum 1000 laser shots were accumulated. In a typical MALDI experiment, the matrix, salt and polymer solutions were premixed in the ratio: 5 μL sample: 5 μL matrix: 0.5 μL Salt. Approximately 0.5 μL of the obtained mixture was hand spotted on the target plate.

3.2.3 Synthetic Procedures

Synthesis of PMMA Macroinitiators. CuCl (0.164 g, 1.66 mmol), CuBr$_2$ (0.011 g, 0.08 mmol), HMTETA (0.382 g, 1.66 mmol), *p*-xylene (22.031 g, 0.20 mol), and MMA (20.012 g, 0.2 mol) were charged to a dry 250 mL three-neck round-bottom flask, and the flask was sealed with a rubber septum. The reaction mixture was bubbled with argon gas for 30 min to remove traces of oxygen. In a second, dry 25 mL three-neck round-bottom flask, trichloroethanol (0.481 g, 3.32 mmol) and *p*-xylene (8.012 g, 0.07 mol) were charged, and the flask was sealed with a rubber septum. This initiator solution was also bubbled with argon for 30 min to remove traces of oxygen. Finally, the initiator solution was added via a degassed syringe to the monomer solution and immersed in an oil bath at 90 ^{o}C to start the polymerization. To study the kinetics of the polymerization, samples were taken using a degassed syringe during the course of reaction and diluted with THF. Part of the solution was used for gas chromatography (GC) to determine the monomer conversion, while the remaining part was used for SEC analysis. After completion of the reaction, THF (100 mL) was added to the flask and a magnetic stirrer was used to dissolve the

polymer. The resulting green (Cu^{II} complex) colored polymer solution was passed through a silica column (SiO$_2$) to remove the copper complex. The resulting colorless polymer solution was concentrated by rota-evaporation, after which the polymer was collected and dried under vacuum for 3 days at 50 ºC.

Synthesis of Block Copolymers. CuBr was used as catalyst for the block copolymer synthesis. The procedure was the same as discussed in the previous section except that a macroinitiator (8.056 g, M_n = 4200, 1.90 mmol) and solvent (methyl ethyl ketone, 6.02 mL) were added to the flask initially. Once the macroinitiator was completely dissolved, the monomer (tBMA, 13.429 g, 0.094 mol) was added. The solution was bubbled with argon for 30 min to remove traces of oxygen. In a second, dry 25 mL three-neck round-bottom flask, MEK (6.42 mL), PMDETA (0.332 g, 1.91 mmol) and CuBr (0.275 g, 1.91 mmol) were charged and the flask was sealed with a rubber septum. This catalyst solution was also bubbled with argon for 30 min to remove traces of oxygen. Finally, the catalyst solution was added via a degassed syringe to the monomer solution and immersed in an oil bath at 90 ºC to start the polymerization. Initial and final samples were taken and analyzed for monomer conversion by GC. The obtained block polymer was purified as described above.

3.3 Results and discussion

3.3.1 Monofunctional PMMA Macroinitiators

ATRP proceeds via the establishment of a dynamic equilibrium between the active and dormant species as shown in Scheme 2.1. The overall rate of polymerization and the level of control during the polymerization are influenced by several internal variables, such as initiator, catalyst, solvent, ligand, type of transferring halogen (X) and external variables, such as temperature.[11,12] The choice of the appropriate initiator/CuX (X = Cl, Br) system is a key parameter, when polymerizing monomers such as MMA with a high equilibrium constant ($K_{eq} \sim 10^{-7}$ to 10^{-6}), to reduce the termination process (second order with respect to the concentration of radicals) and to establish the dynamic equilibrium between the dormant and active species.[13] This is more important when working with a highly active catalyst system like HMTETA/CuCl. HMTETA was selected because (a) the catalyst complex is highly active, (b) easily available, (c) cost effective and (d) the catalyst complex can be easily separated from the polymer.[14] MMA was polymerized via ATRP in *p*-xylene with a CuCl and HMTETA catalyst system and trichloroethanol (TCE) as initiator at 90 ºC. Only half an equivalent of metal catalyst to initiator was used in solution polymerizations to reduce the radical concentration and the rate of the polymerization.

Previously, Destarac *et al.*[15] showed that the use of 2,2,2–trichloroethanol (TCE) resulted in a fast and nearly quantitative initiation of MMA with a CuCl/bpy catalyst system. TCE was chosen because it is a readily available and a fast and efficient initiator. Although three chloride atoms are present per molecule, it is suggested in literature that only one atom is viable for initiation.[15] The choice for a chloride functional initiator was based on the fact that the ATRP equilibrium constant (K_{eq} for CuCl/TCE/PMDETA = $3.9*10^{-8}$) is lower than for a bromide–based system.[11,12,16] The lower equilibrium constant may lead to a better controlled polymerization. Furthermore, the more stable chloride bond (R–Cl) may minimize termination reactions at high conversions compared to the less stable bromide bond (R–Br), thereby resulting in highly chlorine end-functionalized PMMA macroinitiators. Snijder *et al.*[16] showed by electron spin resonance spectroscopy measurements that the ceiling concentration (concentration above which $Cu^{II}Cl_2$ precipitates during the polymerization) of $Cu^{II}Cl_2$ (CuCl/TCE/PMDETA system) is higher than the ceiling concentration of $Cu^{II}Br_2$ (CuBr/ethyl-2-bromo-2-methylpropionate, EBMP/PMDETA system), which has a positive effect on the degree of control in the polymerization. A higher deactivator concentration minimizes the side reactions at high conversions resulting in polymers with a low polydispersity index. A clear homogeneous polymerization solution was observed under these polymerization conditions.

Table 3.1: *ATRP of MMA initiated by trichloroethanol and catalyzed by CuCl/HMDETA system: Synthesis of monofunctional macroinitiators.[a]*

Ex. No.	M:I	p–Xylene (Vol %)	Reaction Time (h)	Conversion (%)	Theoretical M_n[b]	Experimental M_n[c]	
						M_n	PDI
M1[d]	120:1	61	8	73	4500	4200	1.22
M2	200:1	52	9	88	9000	11600	1.14
M3	200:1	52	10	88	8900	12800	1.15
M4	300:1	52	10	93	14100	16700	1.14
M5	1000:1	45	16	81	40500	38600	1.20
M6	1500:1	45	18	71	53300	53200	1.17
M7	2000:1	35	19	64	64000	60900	1.18

[a]Ratio of initiator to catalyst to ligand is 1 to 0.5 to 0.5. [b]MW initiator + 100 ($[MMA]_0/[I]_0$ × conversion). [c]From SEC analysis in THF using universal calibration for PMMA with PS standards. [d]$Cu^{II}Cl_2$ added to minimize the radical termination.

Table 3.1 summarizes the results of the PMMA macroinitiator synthesis. A good correlation between the theoretical (from conversion measurements), and experimental (from SEC analysis) molecular weight indicates a high initiator efficiency at all molecular weights. PDI was between 1.1 and 1.2, which is comparable to a homogeneous ATRP[17] catalytic system based on CuBr/4,4′-di-5-nonyl-2,2′-bypyridine (dNbpy) in conjunction with p-toluenesulfonyl chloride. In the case of a low molecular weight macroinitiator (M1, Table 3.1), $Cu^{II}Cl_2$ was added to reduce the initial radical concentration due to the high initiator to monomer ratio. Less solvent, (*p*-xylene), was used in case of high molecular weight macroinitiators (M5-M7, Table 3.1) to increase the polymerization rate. All polymerizations were stopped around 90 % conversion to avoid side reactions at high conversion and to retain a high chlorine-end functionality.

3.3.2 Synthesis of Block Copolymers

The synthetic strategy to prepare diblock (A-B) ionomer precursors is given in Scheme 1.1 (See Chapter 1). The scheme involves two steps: (1) synthesis of living monofunctional PMMA macroinitiators with well-controlled molecular weight and PDI and (2) copolymerization with tBMA to obtain diblock copolymers. Low molecular weight tBMA blocks were targeted, since ionomers with a large fraction of ionic groups are difficult to process due to strong ionic interactions.[18] Table 3.2 summarizes the results of copolymerization of *tert*-butyl methacrylate with PMMA macroinitiators. Block copolymers with a wide range of molecular weights and compositions were synthesized.

3.3.2.1 Low Molecular Weight Diblocks. The CuBr/PMDETA heterogeneous catalyst system in conjunction with a polar solvent methyl ethyl ketone was used in the block copolymerization of tBMA with low molecular weight PMMA−Cl macroinitiators (M1 to M4, Table 3.2) to obtain the corresponding diblock copolymers (DB1 to DB4, Table 3.2). A 1:1 ratio of CuBr to PMDETA, and a macroinitiator to solvent weight ratio of 1:2 was sufficient to achieve short reaction times ($\approx$ 3 to 5 h) and low PDI polymers. It was shown in Chapter 2 that the use of a highly active catalyst system (CuBr/PMDETA) and a polar solvent results in a high cross-propagation efficiency. Polar solvents, such as ethylene or propylene carbonate,[19] acetone,[20] diphenyl ether,[21] 1,2-dimethoxybenzene,[21] and dimethylformamide[22] fully solubilize the CuBr/PMDETA catalyst. The increase in catalyst concentration available in solution compared to nonpolar solvent conditions, leads to faster polymerization rates and lower polydispersities (because of the corresponding higher

Cu(II) concentration). Moreover Chambard *et al.*[23] reported that besides its effect on catalyst solubility, the polar solvent also increases the activation rate constant k_{act} (Figure 1.6, See Chapter 1) of macroinitiator. The use of copper bromide instead of copper chloride as catalyst in the block copolymerization results in lower polydispersity index values. This is due to the better efficiency of bromide in the deactivation step, as also observed by Bengouh[24] in a series of studies on the inhibition of MMA polymerization in DMF.

Table 3.2: *Summary of ATR Block (DBx) copolymerizations of tBMA initiated by PMMA (Mx) macroinitiators and catalyzed by CuBr in Methyl ethyl ketone*

Ex.No	Macro-initiator	Molecular Weight (PDI)	DP[b] of second block [Reaction time (h), Conversion (%)]	[MEK]/[Macro Initiator]	Theoretical $M_n^{\,c}$ of block PtBMA	MW's from GPC[d]		Mole % of tBMA from FTIR
						M_n	PDI	
DB1[a]	M1	4200 (1.22)	50 [2, 85]	72	10200	12500 (12300)[e]	1.30 (1.15)	38
DB2	M2	11600 (1.14)	70 [3.5, 82]	160	19800	19450 (19800)	1.23 (1.09)	24
DB3	M3	12800 (1.15)	70 [3, 86]	180	21500	21400 (20600)	1.22 (1.10)	23
DB4	M4	16700 (1.14)	70 [5, 73]	280	24000	24100 (22300)	1.20 (1.10)	16
DB5	M5	38600 (1.20)	105 [5, 31]	1050	NA	45500	1.28	8
DB6	M6	53200 (1.17)	105 [3.5, 42]	1500	58300	59600	1.25	9
DB7	M6	53200 (1.17)	176 [3.5, NA]	1500	NA	62700	1.27	9
DB7-1	M7	60900 (1.18)	245 [10, NA]	5300	NA	69700	1.32	<1
DB7-2[f]	M7	60900 (1.18)	245 [20, NA]	5100	NA	66700	1.18	<1

Temperature of the reaction = 90 °C; [a]DB1 to DB7 with *N,N,N′,N″,N″* pentamethyldiethylenetriamine (PMDETA) ligand, [MI] : [CuBr] : [PMDETA] = 1:1:1. [b]DP is targeted degree of polymerization of the second block PtBMA. [c]MI + (monomer MW)([M]o/[I]o × conversion). [d]from SEC analysis in THF using universal calibration for PMMA with PS standards. [e] number average molecular weight (M_n) from MALDI-TOF analysis. [f]dinonyl bipyridine (dNbpy) as ligand, [MI] : [CuBr] : [dNbpy] = 1: 3: 9.

Figure 3.1A and 3.1B show the SEC traces of M1 (M_n = 4200, PDI = 1.22), diblock DB1 (M_n = 12500, PDI = 1.30), M3 (M_n = 12800, PDI = 1.15), and diblock DB3 *(M_n = 21500, PDI = 1.22),* respectively. The SEC traces are unimodal and symmetrical, except for M3 and there is hardly any tail towards lower molecular weights in the block copolymer trace, which could have been an indication of unreacted macroinitiator. The overlap of the SEC peaks is due to the lower targeted molecular weight of the tBMA block. The measured molecular weights from SEC are not absolute molecular weights, since the hydrodynamic volume of the block copolymer may differ

considerably from the corresponding PMMA macroinitiators in THF solution. However, there is a good agreement between the molecular weights measured from MALDI-TOF (which are absolute molecular weights, See Table 3.2) and the molecular weights measured by SEC (which are relative molecular weights) using the universal calibration curve for PMMA (Mark-Houwink-Sakurada constants[8] for PMMA: K = $9.4*10^{-4}$ dL g^{-1}, a = 0.719) based on linear PS standards. These results suggest that universal calibration curve for PMMA is also valid for the low molecular weight diblock copolymers investigated in this study. Polymerization was stopped before 100% conversion of monomer (tBMA) to avoid side reactions, which could lead to higher PDI. The block copolymers were purified, dried and analyzed by ^{1}H-NMR to verify the incorporation of the tBMA monomer. The presence of a clear and distinct peak at 1.4 ppm in the NMR spectra of the block copolymer confirmed the incorporation of the *t-butyl* group in the block copolymers.
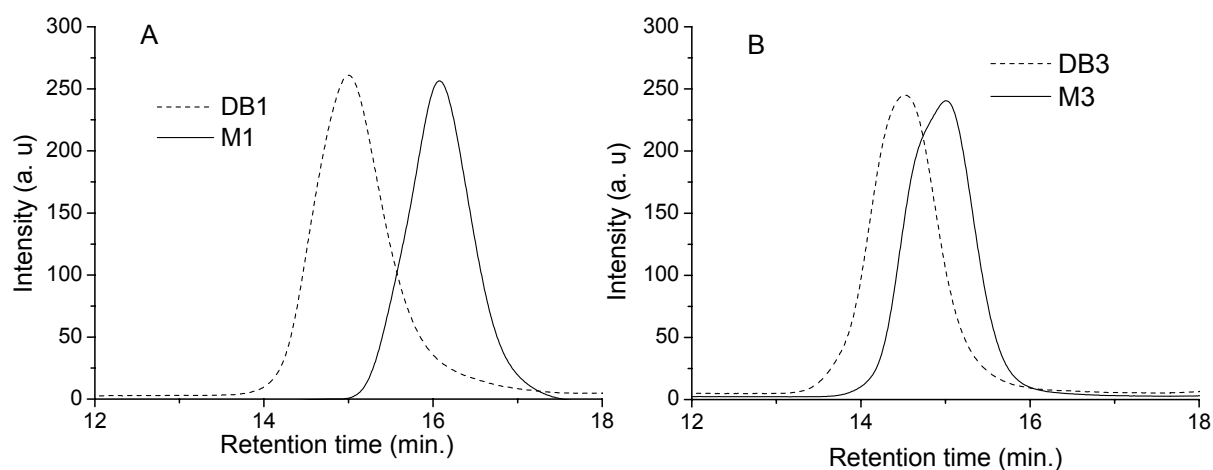
Figure 3.1: *SEC traces of (A) macroinitiator M1 (chlorine functional PMMA macroinitiator; M_n = 4200, PDI = 1.22) and DB1 (diblock copolymer of tBMA using M1 as macroinitiator; M_n = 12500, PDI = 1.30). [PMMA-Cl]$_0$ = [CuBr]$_0$ = [PMDETA]$_0$ = $6.85*10^{-2}$ mol/L; [tBMA]$_0$ = 3.38 mol/L. (B) macroinitiator M3 (chlorine functional PMMA macroinitiator; M_n = 12800, PDI = 1.15) and DB3 (diblock copolymer of tBMA using M3 as macroinitiator; M_n = 21500, PDI = 1.22). [PMMA-Cl]$_0$ = [CuBr]$_0$ = [PMDETA]$_0$ = $3.64*10^{-2}$ mol/L; [tBMA]$_0$ = 2.57 mol/L.*

3.3.2.2 High molecular weight diblocks. The CuBr/PMDETA catalyst system was also used for the polymerization of tBMA with high molecular weight PMMA macroinitiators (M5 to M7) resulting in corresponding high molecular weight block copolymers (DB5 to DB7). The ratio of the

catalyst to initiator was 1:1. The macroinitiator to solvent weight ratio was 1:2 as in the case of the low molecular weight diblock synthesis. The viscosity of the M5 macroinitiator solution was higher than the M1-M4 macroinitiator solutions at this weight ratio due to the higher molecular weight of M5. The reaction was stopped after nearly four hours, because it was not possible to keep the reaction mixture homogeneous with the magnetic stirrer as a result of the high viscosity of the solution. The results of the high molecular weight block copolymers are also summarized in Table 3.2. Figure 3.2 shows the SEC traces of macroinitiator (M5) and the resulting diblock copolymer (DB5). The SEC trace of the block copolymer is symmetrical, unimodal and shifted towards a lower retention time compared to the macroinitiator indicating the increase in molecular weight. However, due to the low targeted degree of polymerization (DP = 105) of the second block (PtBMA), there is only a small increase in the molecular weight of the block copolymer (DB5, M_n = 45500) compared to the macroinitiator (M5, M_n = 38600). This leads to large overlap of the two peaks in SEC providing no further information about the purity of the block copolymer. Similar SEC results were obtained with M6 and DB6. A low PDI was obtained in both cases. To further investigate the structure and purity of the block copolymers gradient polymer elution chromatography was used.
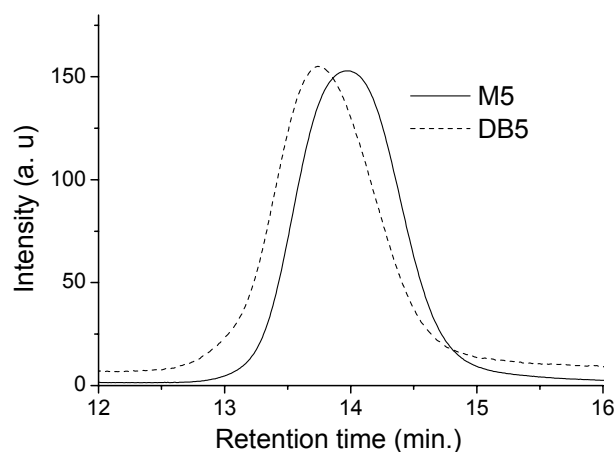
Figure 3.2: *SEC traces of macroinitiator M5 (chlorine functional PMMA macroinitiator; M_n = 38600, PDI = 1.20) and DB5 (diblock copolymer of tBMA using M5 as macroinitiator; M_n = 45500, PDI = 1.28). $[PMMA\text{-}Cl]_0 = [CuBr]_0 = [PMDETA]_0 = 8.83 \times 10^{-3}$ mol/L; $[tBMA]_0 = 0.933$ mol/L.*

3.3.3 GPEC Analysis of Block Copolymers

In the current study, the normal phase GPEC with THF and n-heptane as eluents was used to characterize the block copolymer structure. The gradient used and the details of the GPEC method were explained in depth in Chapter 2. The results from Chapter 2 indicated that the two homopolymers PMMA and PtBMA were well separated with retention time difference of 15 min at all molecular weights. PtBMA with its bulky non-polar ester group elutes first compared to PMMA with the methyl ester group. A difference in the chemical composition of the copolymer leads to a change in retention time of the copolymer, which can be used to establish the block copolymer structure.

The GPEC traces of M1, DB1 and M3, DB3 are shown in Figure 3.3A and 3.3B respectively. The retention time of DB1 is lower than that of the macroinitiator M1 and shifted clearly towards the PtBMA homopolymer. This shift in the peak position is a clear evidence for the block copolymer structure. The absence of tailing in the block copolymer peak clearly indicates the high efficiency of the PMMA macroinitiator in the polymerization of the tBMA. GPEC traces of the high molecular weight macroinitiator (M5) and block copolymer (DB5) are shown Figure 3.4. The retention time of the block copolymer is lower than that of M5 even though the molecular weight of the block copolymer is higher. The difference in elution behavior is a direct indication of the chemical composition difference between the macroinitiator and block copolymer.

Figure 3.3: *GPEC traces of (A) macroinitiator M1 (chlorine functional PMMA macroinitiator; M_n = 4200, PDI = 1.22) and DB1 (diblock copolymer of tBMA using M1 as macroinitiator; M_n = 2500, PDI = 1.30), (B) macroinitiator M3 (chlorine functional PMMA macroinitiator; M_n = 12800, PDI = 1.15) and DB3 (diblock copolymer of tBMA using M3 as Macroinitiator; M_n = 21500, PDI = 1.22) using heptane–THF gradient (2%/min) on a silica column.*

The sensitivity of GPEC compared to that of SEC is evident from the elution behavior of M5 and DB5 in SEC and GPEC respectively (Figure 3.2 and 3.4). In GPEC, the peaks from the block copolymer and the macroinitiator are well resolved. However, the block copolymer peak in GPEC has two distinct features. The first feature is that part of the peak for the diblock copolymer falls under the macroinitiator peak, which may indicate the presence of a small fraction of dead polymer chains. The second feature is the asymmetric nature of the peak due to the broad chemical composition distribution of the PtBMA in the block copolymer as demonstrated in Chapter 2. This shows that the block copolymerization was poorly controlled. Note that a low PDI (1.20) of the block copolymer is obtained by SEC analysis. The origin of the dead material can be due to the following two reasons. The first may be due to termination reactions during the block copolymerization. The second may be due to the presence of a small fraction of nonfunctional (without chlorine-end group) macroinitiator in the high molecular weight macroinitiator synthesis (from the macroinitiator step, See Scheme 1.1, Chapter 1).
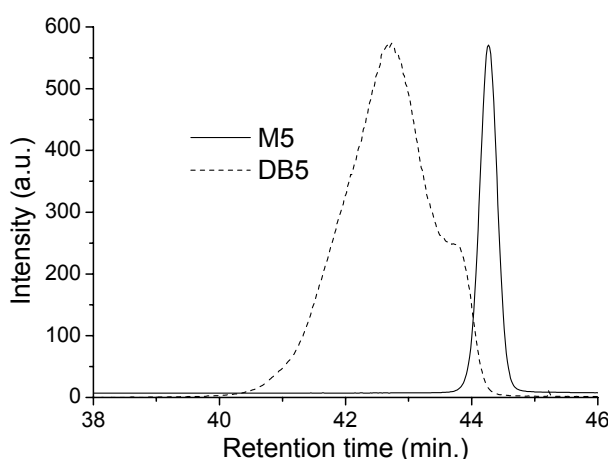
Figure 3.4: *GPEC traces of macroinitiator M5 (chlorine functional PMMA macroinitiator; M_n = 38600, PDI = 1.20) and DB5 (diblock copolymer of tBMA using M5 as macroinitiator; M_n = 45500, PDI = 1.28) using heptane–THF gradient (2%/min) on a silica column.*

To improve the control of polymerization and to understand the origin of the observed dead material in GPEC, polymerizations were also done under homogeneous catalyst conditions. Two approaches were considered to obtain homogeneous polymerization conditions. The first approach was to use an excess of polar solvent MEK, which increases the solubility of the CuBr/PMDETA

catalyst in the polymerization. The weight ratio of macroinitiator to solvent was increased from the earlier used ratio of 1:2 to 1:6. The result of this experiment is listed in Table 3.2 (Entry 8). The macroinitiator used was M7 (M_n = 60900) and the corresponding block copolymer was DB7-1. The SEC and GPEC results of M7 and DB7-1 are shown in Figure 3.5A and B respectively. Once again, SEC peaks of the macroinitiator and block copolymer are highly overlapping giving no information about the purity and the chemical composition of the block copolymer. In contrast to SEC analysis, GPEC analysis of the M7 and DB7-1 shows two well-separated peaks indicating the block copolymer formation. Moreover, the block copolymer peak DB7-1 is unimodal without any shoulder that is overlapping with the macroinitiator peak in contrast to the GPEC trace of block copolymer DB5 (Figure 3.4).
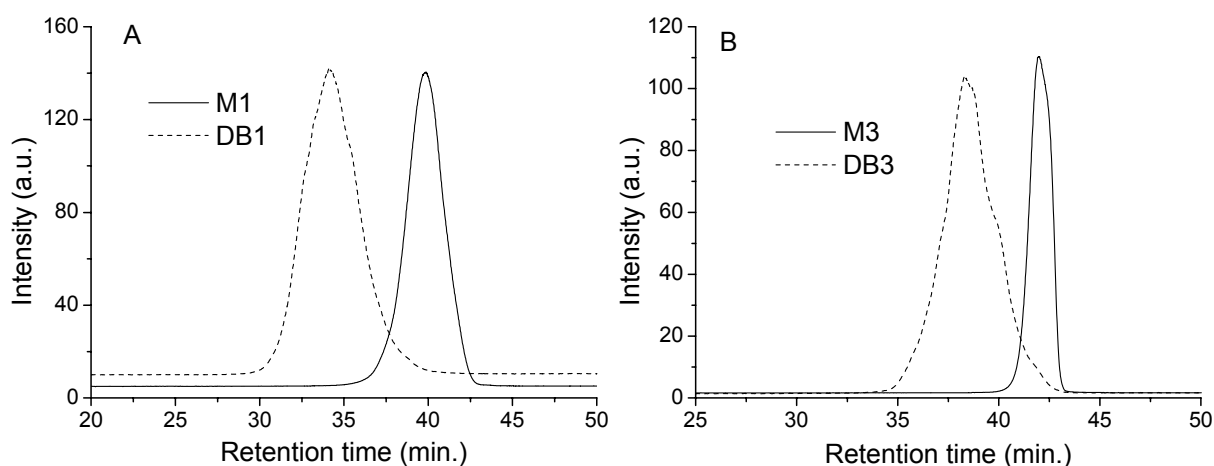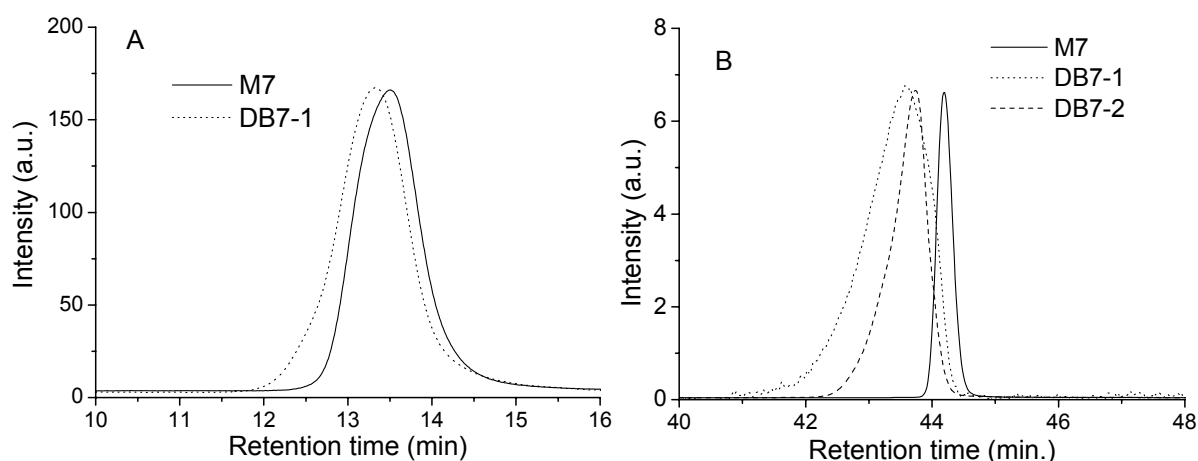

Figure 3.5: (A) *SEC traces of macroinitiator M7 (chlorine functional PMMA macroinitiator; M_n = 60900, PDI = 1.18) and DB7-1 (diblock copolymer of tBMA using M7 as macroinitiator; M_n = 69700, PDI = 1.32). [PMMA-Cl]$_0$ = [CuBr]$_0$ = [PMDETA]$_0$ = $1.95*10^{-3}$ mol/L; [tBMA]$_0$ = 0.481 mol/L and (B) GPEC traces of macroinitiator M7, DB7-1, and DM7-2 (diblock copolymer of tBMA using M7 as macroinitiator; M_n = 66700, PDI = 1.18 using heptane–THF gradient (2%/min) on a silica column.*

The improved control over the polymerization is attributed to the nearly homogeneous polymerization conditions obtained using an excess of MEK. The increased solubility of Cu^{II} species under homogeneous conditions effectively deactivates the growing polymer radicals and regulates the polymerization in a better fashion. Note that SEC analysis gives a low PDI of the block copolymer. The second approach of using a completely homogeneous catalyst, namely

CuBr/dNbpy, in the polymerization was also carried out with macroinitiator M7. The weight ratio of macroinitiator to solvent was 1:6 as in the case of the DB7-1. A three times excess of catalyst was used compared to the concentration of the macroinitiator to counterbalance the low activity of the dNbpy catalyst system. The activity of the ATRP catalyst system is related to its redox potential, which can be measured by cyclic voltametry. Matyjaszewski *et al.*[25] showed that the redox potential ($E_{1/2}$) of the CuBr/dNbpy complex ($E_{1/2}$ = −0.060 V) is higher than the redox potential ($E_{1/2}$ = − 0.075 V) of the CuBr/PMDETA complex reflecting the lower activity of the former catalyst complex. The result of this experiment is also listed in Table 3.2 (Entry 9). Longer reaction times (20 h) were required in the dNbpy system compared to the PMDETA catalyst system (10 h) indicating the lower activity of the dNbpy complex, even when using three times excess of the catalyst compared to macroinitiator. SEC was again not useful in the analysis of the resulting block copolymer (DB7-2). The result of the GPEC analysis of DB7-2 is also shown in Figure 3.5B. Here again, the block copolymer peak is unimodal and shifted clearly towards the lower retention time revealing the presence of the block copolymer structure. The absence of the shoulder further demonstrates the good control achieved in the polymerization. The difference in the activities of the dNbpy and PMDETA ligand is distinctively seen from the PDI of the resulting block copolymers. A lower PDI (1.18) was observed with dNbpy compared to the PMDETA (PDI = 1.32) system indicating the higher rate of deactivation with the dNbpy ligand. This difference clearly demonstrates that a lower number of monomers is inserted per activation-deactivation cycle in the case of the CuBr/dNbpy system. These differences are also reflected in the GPEC traces of the DB7-1 and DB7-2 (See Figure 5B). A broader peak was seen for DB7-1. It was shown in Chapter 2 that the broadness of the peak is related to the distribution of PtBMA block lengths. The results obtained in this Chapter indicate that homogeneous catalyst conditions are needed in the initiation of high molecular weight PMMA macroinitiators to obtain the corresponding high molecular weight block copolymers with pure block copolymer structure. This is due to the increased solubility of the Cu^{II} species (deactivator in ATRP) during the polymerization. Furthermore, the shoulder observed in the GPEC traces of DB5 and DB6 may originate from possible termination reactions occurring under the observed heterogeneous polymerization conditions (due to the low amount of polar solvent MEK in conjunction with the CuBr/PMDETA catalyst, which results in the limited solubility of the Cu^{II} species). This shoulder is not originating from the nonfunctional macroinitiator from the high molecular weight PMMA macroinitiator synthesis.

3.4 Conclusions

The results of the atom transfer radical polymerization of methyl methacrylate using the CuCl/*N,N,N,N′,N‴,N‴*-hexamethyltriethylenetetramine (HMTETA) catalyst system with 2,2,2–trichloroethanol (TCE) as initiator indicate that poly(methyl methacrylate) (PMMA) macroinitiators with well-defined molecular weight, low polydispersity index (PDI), and high end-group functionality can be obtained. PMMA macroinitiators successfully initiate block copolymerization of *tert*-butyl methacrylate (tBMA) resulting in poly(MMA-*b*-tBMA) diblock copolymers with a low PDI for a range of tBMA block lengths. Gradient polymer elution chromatography (GPEC) was used to confirm the block copolymer structure and was successfully used to demonstrate the effect of molecular weight of the macroinitiator, nature of catalyst system (heterogeneous *vs* homogeneous), and the amount of solvent on the degree of control achieved in the block copolymerization. In particular, the use of a homogeneous catalyst system, CuBr/4,4′-di-5-nonyl-2, 2′-bypyridine (dNbpy), and an excess of methyl ethyl ketone (MEK) as solvent lead to the synthesis of well-controlled high molecular weight diblock copolymers with a short second block length. This can be explained by the complete solubility of the Cu^{II} complex, the deactivating species in the ATRP mechanism due to use of dNbpy ligand and the polar solvent (MEK). The homogeneous catalyst condition results in dynamic activation/deactivation exchange reactions between the growing polymer chains and dormant polymer chains giving rise to well-controlled block copolymers. GPEC is a powerful complementary technique to SEC in the analysis of block copolymers, especially with a short second block length.

3.5 References

(1)   Kotani, Y.; Kato, M.; Kamigaito, M.; Sawamoto, M. *Macromolecules*, **1996**, 29, 6979.

(2)   Granel, C.; Dubois, Ph.; Jerôme, R.; Teyssie, Ph. *Macromolecules*, **1996**, 29, 8576.

(3)   Shipp, D. A.; Wang, J. L.; Matyjaszewski, K. *Macromolecules*, **1998**, 31, 8005.

(4)   Haddleton, D. M.; Duncalf, D. J.; Kukulj, D.; Radigue, A. P. *Macromolecules*, **1999**, 32, 4769.

(5)   Uegaki, H.; Kotani, Y.; Kamigaito, M.; Sawamoto, M. *Macromolecules*, **1998**, 31, 6756.

(6)   Moineau, G.; Minet, M.; Teyssie, Ph.; Jerôme R. *Macromolecules*, **1999**, 32, 8277.

(7)   Matyjaszewski, K.; Shipp, D. A.; Teyssie, Ph.; Jerôme, R. *Macromolecules*, **1999**, 32, 8277.

(8)   Beuermann, S.; Paquet, D. A., Jr.; Mc Minn, J. H.; Hutchinson, R. A. *Macromolecules* **1996**, 29, 4206.

(9)   Coleman, M. M.; Painter, P.C. J. *Macromol. Sci., Rev. Macromol. Chem.* **1978**, C16, 1975.

(10)   Staal, W. J.; Ph. D. thesis, Eindhoven University of Technology, Eindhoven, The Netherlands, **1996.**

(11)   Matyjaszewski, K.; Xia, J. *Chemical Reviews*, **2001**, 101, 2921.

(12)   Kamigaito, M.; Ando, T.; Sawamoto, M. *Chemical Reviews*, **2001**, 101, 3689.

(13)   Matyjaszewski, K.; Wang, J. L.; Grimaud, T.; Shipp, D. A. *Macromolecules*, 1**998**, 31, 1527.

(14)   Kroll, R.; Eschbaumer, C.; Schubert, U. S.; Buchmeister, M. R.; Wurst, K. *Macromol. Chem. Phys.* **2001**, 202, 645.

(15)   Destarac, M.; Matyjaszewski, K.; Boutevin, B. *Macromol. Chem. Phys*. **2000**, 201, 265.

(16)   Snijder, A. Ph.D. Thesis, Eindhoven University of Technology, Eindhoven, The Netherlands, **1996**.

(17)   Grimaud, T.; Matyjaszewski, K. *Macromolecules*, **1997**, 30, 2216.

(18)   Eisenberg, A.; Kim, J. S. *Introduction to Ionomers*, John Wiley & Sons, Inc., **1998**.

(19)   Matyjaszewski, K.; Nakagawa, Y.; Jasieczek, C. B. *Macromolecules*, **1998**, 31, 1535.

(20)   Destarac, M.; Matyjaszewski, K.; Silverman, E.; Ameduri, B.; Boutevin, B. *Macromolecules*, **2000**, 33, 4613.

(21)   Destarc, M.; Alric, J.; Boutevin, B. *Macromol. Rapid Commun*. **2000**, 21, 1337.

(22)   Pascual, S.; Coutin, B.; Tardi, M.; Polton, A.; Varion, J. P. *Macromolecules*, **1998**, 32, 1432.

(23)   Chambard, G.; Klumperman, B.; German, A. L. *Macromolecules*, **2000**, 33, 4417.

(24)   Benough, W. I.; Fairservice, W. H. *Trans. Faraday Soc.* **1965**, 61, 1206.

(25)   Qiu, J.; Matyjaszewski, K.; Thouin, L.; Amatore, C. *Macromol. Chem. Phys.* **2000**, 201, 1625.

Chapter 4

A Morphology Study on Well Defined Di- and Triblock Copolymers of MMA and t-BMA and their Acid and Ionic Counterparts by Small Angle X-ray Scattering

ABSTRACT: The synthesis, molecular and morphological characterization of potassium neutralized poly(methyl methacrylate) (PMMA)-based block ionomers were investigated. Poly(methyl methacrylate-*b*-potassium methacrylate) [P(MMA-*b*-K$^+$MA)] diblock and poly(potassium methacrylate-*b*-methyl methacrylate-*b*-potassium methacrylate) [P(K$^+$MA-*b*-MMA-*b*-K$^+$MA)] triblock ionic counterparts in a large range of molecular weights were prepared by selective hydrolysis and subsequent neutralization of the corresponding poly(methyl methacrylate-*b*-*tert*-butyl methacrylate) [P(MMA-*b*-tBMA)] and poly(*tert*-butyl methacrylate-*b*-methyl methacrylate-*b*-*tert*-butyl methacrylate) [P(tBMA-*b*-MMA-*b*-tBMA)] ester precursors. Small angle X-ray scattering (SAXS) and Fourier transform infrared (FTIR) spectroscopy were used to investigate the influence of polymer architecture (*AB*, *ABA*), composition of the nonionic/ionic blocks, and block copolymer chemical structure, i.e., from block ester, acid and ionic form, on the final morphology of these materials. The SAXS results indicate that a wide range of interdomain spacings (10–30 nm) can be achieved in the precursors and in the ionic counterparts by controlling the total degree of polymerization of the ester precursors. A non-equilibrium block copolymer structure was formed in acid and ionic copolymers due to the presence of strong interactions between the block components, which influences the thermodynamic and kinetic aspects of the microphase separation of the block copolymers. The FTIR results confirmed the presence of strong hydrogen bonding in acid and ionic (arising from the presence of unneutralized acid groups) block copolymers.

4.1 Introduction

Block copolymers and ionomers are two classes of microphase separated systems that were extensively studied during the past decades.[1-6] In block copolymers, microphase separation is driven by the thermodynamic immiscibility of the dissimilar (homo)polymer blocks where the covalent bond between the blocks prevents macrophase separation. Self-assembled, periodic structures with a size scale of 10–50 nm, such as body centered cubic packed (bcc) spheres, hexagonal close

packed (hcp) cylinders, alternating lamellae, and more complex phases, were theoretically predicted and experimentally observed.[7] The specific structure achieved with a particular system depends on the copolymer composition, molecular weight, copolymer architecture, and the magnitude of the repulsive interactions between the chemically dissimilar blocks as characterized by a temperature-dependent χ-interaction parameter.

The microstructure of the ionomers is less ordered than that of the block copolymers. Ionomers exhibit microphase separation of ion-rich aggregates as a result of electrostatic interactions between the ions and dipoles.[8,9] In this case, the characteristic size of the microphase is typically 2–5 nm, at least an order of magnitude smaller than that of the block copolymers. Aggregation of the ionic species depends on the dielectric constant of the matrix polymer, architecture of the polymer, ionic content, and the nature of the anion and the cation.[4] Several properties[4-6] such as modulus, glass transition temperature, viscosity, melt strength and fatigue can be influenced dramatically by incorporating ionic cross-links. A number of models[8,10-12] for the morphology of the ionomers and the microstructure of ionic aggregates have been proposed during the past 25 years, but to date no general consensus about the correct model has been reached. For a better understanding of the structure–morphology–property relationships of ionomers, materials with a more specific architecture, defined molecular weight, and a low polydispersity index (PDI) are required. Several research groups recently consolidated the characteristics of the block copolymer and ionomer micophase-separation into a single material by preparing block copolymer ionomers,[13-18] where in one of the blocks of the block copolymer contains ionic groups. Since the present chapter focuses on the morphological features of the block ionomers and precursors, the following sections will briefly describe the relevant results pertaining to these systems.

Block ionomers with a two-phase morphology

Eisenberg *et al.*[13,19] reported the first experimental study of the bulk morphology of *ABA* triblock ionomers with a long nonionic midblock of polystyrene (PS) and fully ionized relatively short ionic end blocks of poly(4-vinylpyridinium methyl iodide) (P4VPMI) by small angle X-ray scattering (SAXS). In this study, it was shown that these materials exhibit a two-phase morphology, and the ionic blocks, even at very short ionic block lengths, self-assemble into spherical microdomains dispersed in the nonionic matrix, i.e., in a manner very similar to that of nonionic block copolymers. The size of the ionic microdomains was found to be dependent on the ionic block length (P4VPMI) at a given PS block length. The polymer chains in the ionic blocks were highly extended in contrast to the PS chains (middle block), which have a coiled configuration,[14] as

shown by small angle neutron scattering (SANS). Wilkes *et al.*[15] reported a similar two-phase morphology for *AB* and *ABA* type methacrylic based block ionomers with a long 2-ethylhexyl methacrylate (EHMA, $T_g \approx -27$ °C) or n-hexyl methacrylate (n-HMA, $T_g \approx -10$ °C) block as a nonionic rubbery matrix phase (*B* block) and a short cesium methacrylate (CsMA) block as a domain forming ionic phase (*A* block). The ionomer block, poly(cesium methacrylate), was prepared by hydrolysis and subsequent neutralization of a precursor block of poly(*tert*-butyl methacrylate) (tBMA).

Block ionomers with a three-phase morphology

Weiss *et al.* [16,17] and other research groups[18] reported a three-phase morphology for block copolymer ionomers prepared by lightly sulfonating (random introduction of the ionic groups, 5-10 mol % of sulfonation level) the polystyrene end blocks of a poly(styrene-*b*-(ethylene-*co*-butylene)-*b*-styrene) (SEBS). The morphology of the block ionomer consisted of ionic microdomains of 3–4 nm, due to the ionic aggregation distributed within polystyrene microdomains of 20–30 nm that were dispersed in a rubbery poly(ethylene-*co*-butylene) continuous matrix. It is important to realize that the ionic groups are randomly distributed in the PS block, similar to a sulfonated polystyrene ionomer.

Morphological features of the two-phase ionomers

More systematic studies on the styrene/EHMA/n-HMA (*A* block) based *AB* and *ABA* block ionomers[20-22] with short ionic blocks of 4-vinylpyridinium methyl iodide/cesium methacrylate (*B* block), respectively, showed two important features in SAXS. The first feature is a peak at low q-values interpreted as an interparticle correlation factor (structure factor), while the second feature is a peak at higher q attributed to the form factor of the spherical domains. Only the structure factor feature was present in methacrylate ionomers. It was concluded that (1) the average characteristic Bragg distance (d_B) is more affected by the length of the ionic block compared to the length of the nonionic block at a given total degree of polymerization of the block ionomer, (2) the radius of the ionic microdomains is strongly dependent on the ionic block length and not much influenced by their chemical nature, architecture, the length of the nonionic blocks, and the sample preparation method, (3) the ionic domain radius is in the order of the fully chain extended length, and (4) the morphological features of the nonionic precursors are generally found to be similar to those of the corresponding ionic materials except for peak positions and relative peak widths. The important additional conclusions from the morphological study on the methacrylate block ionomers reported by Wilkes *et al.*[15] were (1) considerable reorganization (morphological changes) within the material

occurs with increasing polarity, i.e., from ester to an acid and to an ionomer form of the end blocks, (2) transmission electron microscopy (TEM) analysis of the block ionomers indicated the presence of ionic domains with a distorted cylindrical morphology with a short range order. However, detailed morphological features of the block precursors (esters and acids) and ionic counterparts, specifically with a large range of acid or ionic compositions, and molecular weight of the total block copolymer, were not investigated.

It is well known that methyl methacrylate (MMA) and methacrylic acid (MAA) segments show strong inter- and intramolecular hydrogen bonding[23-25] in the copolymer form, i.e., P(MMA-*co*-MAA), and in the homopolymer blends (PMMA/PMAA blends). All the blends are totally miscible over the entire composition at room temperature, whereas phase separation occurred at higher temperature indicating the presence of a lower critical solution temperature (LCST, T_{LCST} = 150 ^{o}C) phase behavior for these blends. Furthermore, FTIR spectroscopy, DSC, and high-resolution solid-state ^{13}C NMR spectroscopy experiments indicated that a higher extent of hydrogen bonding, a higher T_g and a better homogeneity was obtained in the random copolymers compared to the blends. These results were rationalized in terms of presence of a higher fraction of intermolecular hydrogen bonded carbonyl groups from PMMA in the random copolymer than in the corresponding blend. One important implication of this hydrogen bonding interaction between the MMA and MAA segments is that the morphology of the MMA and MAA acid diblock copolymers (precursors for diblock ionomers) may strongly depend on the acid content or composition of the acid (MAA) block, since the presence of hydrogen bonding may influence the thermodynamic and kinetic aspects of the microphase separation.

In this chapter, the results of the morphological investigation of PMMA based di- and triblock ionic counterparts with the ionic content in the ionomer range (< 15 mol %) and higher ionic contents are presented. Diblock poly(methyl methacrylate-*b*-potassium methacrylate) [P(MMA-*b*-K^{+}MA)] and triblock poly(potassium methacrylate-*b*-methyl methacrylate-*b*-potassium methacrylate) [P(K^{+}MA-*b*-MMA-*b*-K^{+}MA)] ionic counterparts in a large range of molecular weights were obtained by selective hydrolysis and subsequent neutralization of the corresponding poly(methyl methacrylate-*b*-*tert*-butyl methacrylate) [P(MMA-*b*-tBMA)] and poly(*tert*-butyl methacrylate-*b*-methyl methacrylate-*b*-*tert*-butyl methacrylate) [P(tBMA-*b*-MMA-*b*-tBMA)] precursors. Small angle X-ray scattering (SAXS) was used to investigate the morphology of these materials. A wide range of interdomain spacing (characteristic Bragg distance, d_B) is achieved in the precursors and in the ionic counterparts by controlling the total degree of polymerization of the

ester precursors. Fourier transform infrared (FTIR) spectroscopy was used to study the various molecular interactions present in the block acids and ionomers. Tri- and diblock ionic counterparts and the corresponding precursors (acids and esters) were synthesized with similar PtBMA block length and total degree of polymerization (with in the limitation of the atom transfer radical polymerization) to study the influence of molecular architecture on the morphology. The influence of polymer architecture (*AB*, *ABA*), the length or the composition of the nonionic and the ionic blocks, and block copolymer chemical structure, i.e., from block esters, acids and ionic counterparts, on the morphological features are presented.

4.2 Experimental Section

4.2.1 Materials

The synthesis of the di- and triblock ester precursors was described in detail in Chapter 2 and 3. Dichloromethane (DCM, 99%, Aldrich) and trifluoroacetic acid (TFA, 99%, Aldrich) were distilled freshly and stored under argon atmosphere. Tetrahydrofuran (THF, 99%, Aldrich), potassium hydrogen phthalate (KHP, 99%, primary standard, Aldrich) and potassium hydroxide (KOH) solutions in ethanol (0.1 and 0.5 mole/l, Merck) were used as received. However, KOH was standardized each time prior to neutralization of the acid block copolymers.

4.2.2 Analysis and Measurements

Determination of Molar Mass and Molar Mass Distribution. Size exclusion chromatography (SEC) measurements were carried out to determine the apparent molecular weights of the ester precursors. A detailed description of the SEC system was given in the experimental section of the Chapter 2. An overview of the materials studied is given in Table 4.1. (See section 4.2.3 for the nomenclature used to represent the samples.)

Spectroscopic Analysis. The chemical composition of the ester precursors was determined by FTIR spectroscopy. The detailed FTIR procedure and analysis of the data were described in Chapter 2. FTIR measurements of block acids and ionomers were performed on a BioRad FTS 6000 spectrometer equipped with a UMA500 microscope. Samples were prepared using diamond anvil cells with type IIA diamonds (High Pressure Diamond Optics, Inc.). FT-NMR spectra of P(MMA-*b*-MAA) block copolymers were recorded with a Varian 400 MHz spectrometer to monitor the selective hydrolysis of the ester block copolymers. The NMR spectra were recorded in

CDCl$_3$ or DMSO (depending on the acid content) at 25 ^{o}C. All chemical shifts are reported in ppm downfield from tetramethylsilane (TMS), used as an internal standard (δ = 0 ppm).

Small angle X-ray scattering (SAXS). SAXS experiments were performed on beamline BM26 at ESRF Grenoble, France. A 2D gas-filled wire frame detector with pixel array dimensions of 512 $\times$ 512 was used at this beam line. The exposure time for each measurement was 180 s. The wavelength (λ) of the X-rays was 1.0 Å and a sample-to-detector distance of 4 and 5.5 m were used for tri- and diblock copolymers respectively. Bulk polymers were used to study the morphology of the block copolymers. Lindemann capillaries were filled with 25-30 mg of the polymer sample and were sealed. The capillary was mounted in a custom designed aluminum holder and measurements were performed. The SAXS patterns were corrected for the detector response and then were masked in appropriate sections to avoid streak like parasitic scattering contributions from the capillary. The data was finally radially averaged along the azimuthal angle using the FIT2D program of Dr. Hammersley, ESRF. The characteristic Bragg spacing, d_B ($d_B = 2\pi/q$), was calculated by using the peak maximum of the scattering vector (q), where q = $4\pi(\sin\theta)/\lambda$ and 2θ is the scattering angle. The scattering angle was calibrated by using collagen of a rat-tail. The resulting d-values have an experimental accuracy of $\pm$ 0.01 Å.

Solid state NMR. Solid state NMR measurements were used to explore the microstructure and to gain insight in mobility differences. All solid state NMR experiments were performed on a Bruker DMX500 spectrometer operating at a ^{1}H- and ^{13}C-NMR frequency of 500.13 MHz and 125.13 MHz, respectively. A 4-mm magic-angle spinning (MAS) probehead was used with sample-rotation rates of 8 kHz to avoid overlapping of spinning side bands and other peaks. The radio-frequency power was adjusted to obtain a 5 µs 90-degree pulse both for ^{1}H and ^{13}C nuclei. The 38.56-ppm resonance of adamantane was used for external calibration of the ^{13}C chemical shift. Proton spin-lattice relaxation $T_{1\rho}(^1$H) was measured for each of the polymer components separately via cross-polarization (CP) to the ^{13}C nuclei. The typical number of scans (NS) was 256, relaxation delays in CP-derived experiments (D1) were 5 s, and the number of experiments per relaxation data set was 18.

4.2.3 Synthetic Procedures

Selective hydrolysis of di- and triblock ester precursors. The P(MMA-*b*-tBMA) block copolymers were selectively hydrolyzed to poly(methyl methacrylate-*b*-methacrylic acid)

[P(MMA-*b*-MAA)]. The diblock ester copolymer (M_n = 22 K/mole, PDI = 1.26; 3.0 g, 5.08 mmol *tert*-butyl ester) and DCM (in a weight ratio of 1:10) were added to a 100 ml three-neck round-bottom flask with a magnetic stirrer. The flask was sealed with a rubber septum and bubbled with argon for 30 minutes. Once the block copolymer was completely dissolved, the required amount of trifluoroacetic acid[26,27] (TFA; 2.9 g, 25 mmol, 5.0 equivalents to *tert*-butyl ester) was added to the flask. The mixture was left to stir at room temperature. Samples were taken at intermediate times to monitor the hydrolysis reaction. These samples were analyzed using ^{1}H-NMR spectroscopy. After the mixture was allowed to stir at room temperature for 5 h, the DCM and excess TFA were removed at room temperature with dry nitrogen gently flowing through the flask overnight. The resulting glassy polymer was dried for three days under vacuum at 40 ^{o}C to remove traces of TFA present in the polymer (boiling point = 72 ^{o}C at atmospheric pressure). The triblock esters were also hydrolyzed by a similar procedure. PMMA homopolymer was also hydrolyzed by TFA under same reaction conditions as a control experiment.

Neutralization of the acid block copolymers. The dried P(MMA-*b*-MAA) diblock copolymer (typically 2 g) was neutralized in THF (50 ml) with a standardized 0.1 M KOH solution. The end point of neutralization was noted by a change in color of the polymer solution from colorless to pink color, which is the typical color of the phenolphthalein indicator in the basic solution. At this point, a 3 % excess neutralizing agent was added to obtain complete neutralization. The solvent was removed using rotary evaporation and the resulting diblock ionomer was recovered. The ionomer was further vacuum dried at 80 ^{o}C for 72 h. A similar procedure was applied to the triblock acid copolymers.

Nomenclature. The nomenclature used for the samples can be best explained using an example. The designation TMT-12/80/12 refers to a triblock ester precursor with a PMMA middle block and PtBMA as outer block. The degree of polymerization of PMMA is 80 and that of PtBMA is 24 (sum of the lengths of two outer blocks, i.e., 12+12). h-TMT-12/80/12 and K$^+$-TMT-12/80/12 refer to the corresponding triblock acid and ionic counterpart respectively. A similar nomenclature is used for the diblock copolymers.

4.3 Results

An efficient synthetic procedure based on atom transfer radical polymerization (ATRP) was developed to prepare well-defined PMMA block ionomers. The synthetic strategy (See Scheme 1.1; Chapter 1) uses *tert*-butyl methacrylate (tBMA) as the precursor for the methacrylic acid to

overcome the acid group sensitivity of the ATRP catalyst system. Table 4.1 lists the molecular characteristics of the block copolymers investigated in this study. A series of diblock ionic counterparts and precursors were synthesized with similar ionic block lengths but different nonionic block lengths to study the effect of nonionic block length on the morphological features.

4.3.1 Molecular characterization

Selective hydrolysis of the PtBMA block to PMAA block. Selective cleavage of the *tert*-butyl ester groups in the presence of methyl esters (from the PMMA block) was achieved by treating the ester precursor block in dichloromethane with anhydrous TFA[26,27] at room temperature. The PMMA homopolymer was also treated with TFA under the same reaction conditions as a control experiment. ^{1}H-NMR and FTIR spectroscopy were used to monitor and confirm the hydrolysis reaction. Results of the ^{1}H-NMR analysis of the PMMA homopolymer control experiment at various reaction times indicated that no change in the concentration of the methyl ester ($-OCH_3$) group of PMMA (The ratio of the methylene protons from the backbone and methyl ester group was constant throughout the reaction).

Table 4.1: *Molecular characteristics of MMA/tBMA block ionomers*

Sample	Total M_n (PDI)[a]	PMMA block mol. wt (M_n)[a]	Mole fraction of tBMA from FTIR	Volume[b] fraction of PtBMA $(V_{f,PtBMA})$	PtBMA block mol. wt (M_n)[c]	DP of PtBMA
TMT-14/26/14	6000 (1.30)	2600	0.52	0.60	4000	28[d]
TMT-12/80/12	10700 (1.27)	8000	0.23	0.30	3400	24
TMT-15/160/15	19000 (1.25)	15900	0.16	0.25	4300	30
TM-26/42	12480 (1.30)	4200	0.38	0.50	3700	26
TM-28/60	13300 (1.30)	4200	0.32	0.43	4000	28
TM-41/76	17200 (1.28)	7600	0.35	0.45	5800	41
TM-34/115	19450 (1.23)	11500	0.23	0.33	4800	34
TM-42/132	22400 (1.26)	13200	0.24	0.34	6000	42
TM-50/168	24100 (1.18)	16800	0.23	0.33	7100	50
TM-41/550	61600 (1.23)	55000	0.07	0.10	5800	41

[a]from SEC analysis in THF using universal calibration for PMMA with PS standards. [b]calculated with ρ PMMA = 1.2 g/cm^3 and ρ PtBMA = 1.02 g/cm^3 for the ester precursors, taken as equal to volume fraction of poly(methacrylic acid) (PMAA) block in ionomers. [c]calculated using the mole fraction of PtBMA from FTIR and the known molecular weight of the PMMA block; $M_{PtBMA} = (M_{0,tBMA}*m_{tBMA})/(M_{0,MMA}*m_{MMA})*M_{PMMA}$, where M_{PtBMA} is molecular weight of the PtBMA block, m_{tBMA} is the mole fraction of the tBMA in the block copolymer, and $M_{0,tBMA}$ is the molecular weight of the tBMA monomer. [d]Cumulative degree of polymerization (DP) of the outerblocks for triblock copolymers.
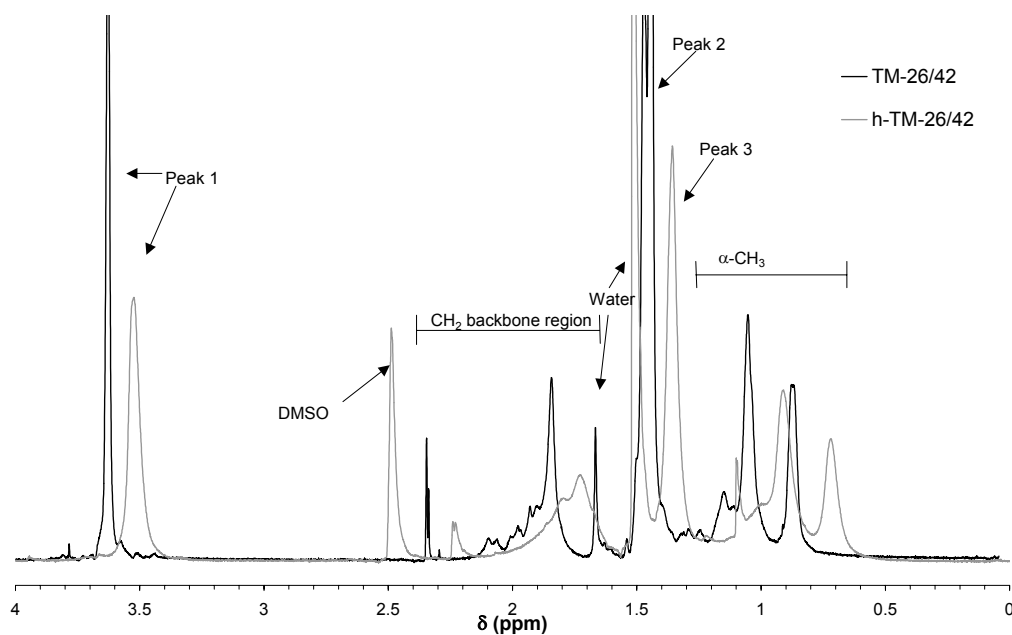
Figure 4.1: *^{1}H-NMR spectra of TM-26/42 and h-TM-26/42.*

The ^{1}H-NMR spectra of a P(MMA-*b*-tBMA) ester diblock and the corresponding P(MMA-*b*-MAA) acid copolymer (h-TM-26/42) are given in Figure 4.1. This figure is also representative for other compositions. The first effect of converting the tBMA ester groups into acid groups is a shift of all peaks to a lower chemical shift (δ) due to the acidic environment of the block copolymer (PMAA block).[26] Peak 1 in Figure 4.1 is present for both TM-26/42 (3.63 ppm) and h-TM-26/42 (3.53 ppm). This peak is assigned to the methyl ester (–OCH$_3$) group of MMA. The presence of this peak in the spectrum of h-TM-26/42 confirms that the ester group of MMA is left intact. Peak 2 (1.46 ppm) is only present for the TM-26/42 and is due to the *tert*-butyl group. Splitting of peak 2 is perhaps due to differences in chemical shift between chain-end (due to the halogen end group from the ATRP chemistry) and main-chain *tert*-butyl groups. The absence of this peak in the spectrum for h-TM-26/42 indicates that all ester groups of tBMA have been converted into acid groups. Peak 3 (1.36 ppm) is only present for the h-TM-26/42 and can be assigned to the *tert*-butyl trifluoroacetate product, which is formed as a side product during the hydrolysis.[26] This was also independently confirmed by performing ^{1}H-NMR analysis on a mixture of TFA and *tert*-butanol in CDCl$_3$. Peak 3 is present as a singlet ruling out the possibility that peak 3 is due to *tert*-butyl ester groups present because of incomplete hydrolysis. Water present in the CDCl$_3$ is seen at 1.62 ppm. It

has to be noted that in the case of high molecular weight ester block copolymers the hydrolysis reaction was incomplete even after a reaction time of 60 h. This observation will be later used in the morphology section.

FTIR spectroscopy was also used to study the hydrolysis reaction. The relevant regions of the FTIR spectra of the TM-26/42 and the h-TM-26/42 are shown in Figure 4.2. Figure 4.2A comprises the carbonyl (C=O) stretching region of the FTIR spectra. In TM-26/42, the C=O bands corresponding to methyl and *tert*-butyl ester groups of PMMA and PtBMA overlap at 1730 cm^{-1}. The new C=O shoulder band at 1700 cm^{-1} in the spectrum of h-TM-26/42 clearly shows the conversion of *tert*-butyl ester groups to acid groups upon hydrolysis. Figure 4.2B contains the C–H and O–H stretching regions of the FTIR spectra of TM-26/42 and h-TM-26/42. In both samples, the C–H stretch is seen around 3000 cm^{-1}. However, the high intensity of the C–H band in the h-TM-26/42 is due to the overlapping of the strong O–H band caused by the presence of the carboxylic acid groups. Furthermore, weaker superimposed bands in the 2700–2500 cm^{-1} region are due to the overtones and combinations of bands near 1420 and 1300 cm^{-1} (due to O–H bend and C–O stretch) enhanced by the Fermi resonance with the broad O–H stretch band.

Neutralization of acid blocks to ionomers. Acid block copolymers were neutralized in THF with a stochiometric amount of ethanolic KOH (0.1 N) to the corresponding block ionomers. FTIR spectroscopy was used to monitor the neutralization step. The FTIR spectra of the h-TM-26/42 acid and the corresponding block ionomer (K$^+$-TM-26/42) are shown in Figure 4.3. The main difference between the two spectra is the appearance of a new band at approximately 1570 cm^{-1} for the K$^+$-TM-26/42. This band is arising from the asymmetric C=O stretch of the carboxylate anion and is therefore indicative for the presence of neutralized acid groups. The presence of this band confirms that the neutralization process was successful. It is worthwhile to note that the carbonyl region (1750–1620 cm^{-1}) in the FTIR spectrum of the block ionomer is very broad, which suggests the presence of strongly interacting groups along the polymer backbone and possible incomplete neutralization. A 3 % excess neutralizing agent was also added after the end point of the titration to achieve 100 % neutralization but the FTIR analysis strongly indicates towards incomplete neutralization. Principal component analysis (PCA)[28] can be used to obtain the correct number of the spectral band components contributing to this complex broad band. However, no such attempt was made here due to the possible presence of several interacting groups in the region. For the same reason, FTIR results were not used to obtain quantitative information about the degree of

neutralization. This observation will be used further during the discussion of the morphological features of the block ionomers.
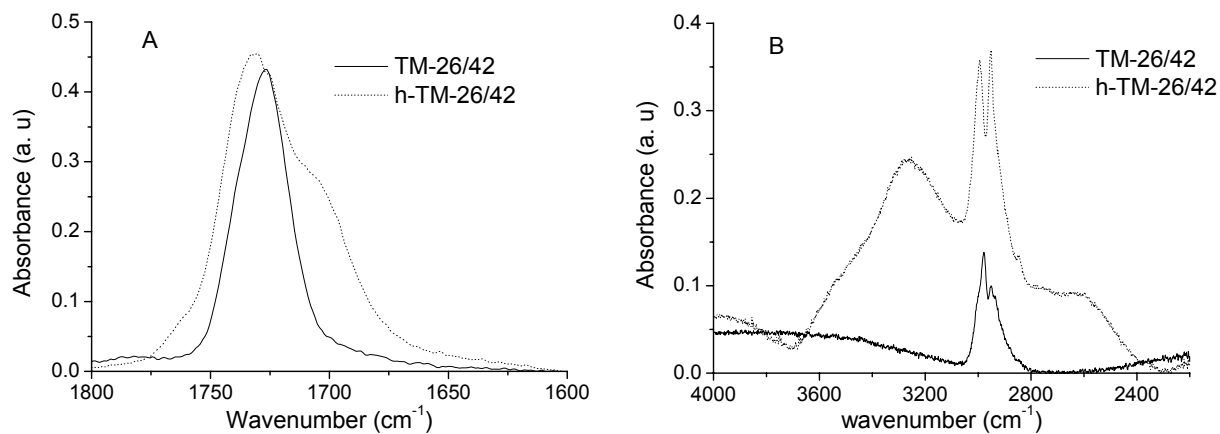
Figure 4.2: *FTIR spectra of TM-26/42 ester and h- TM-26/42 in the region of (A) 1800–1600 cm^{-1} and (B) 4000–2400 cm^{-1}.*
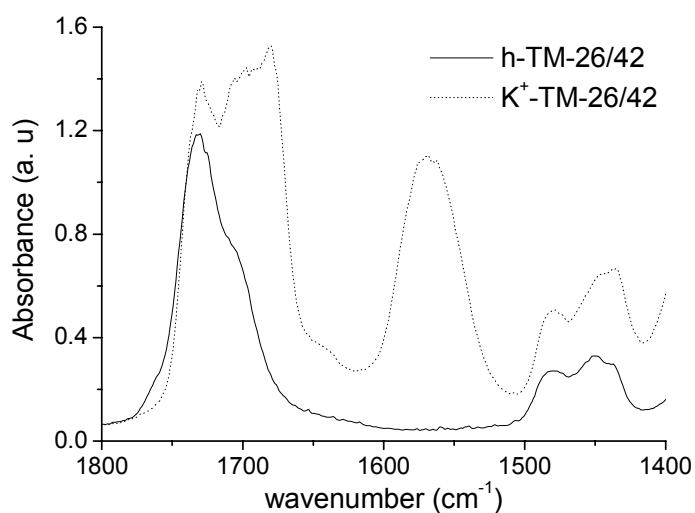
Figure 4.3: *FTIR spectra of TM-26/42 ester and K^{+}- TM-26/42 in the region of 1800 cm^{-1} to 1400 cm^{-1}.*

4.3.2 Morphological characterization

The morphology of the di- and triblock precursors and ionomers was investigated by SAXS. This section is divided into two parts. In the first part the morphological features of the precursors (esters and acids) and ionomers are presented. In the second part, the morphological features of the diblocks going from esters to acids respectively to ionic counterparts are presented.

4.3.2.1 Morphology of triblocks

Figure 4.4 shows typical SAXS data plotted as intensity I *vs.* scattering vector *(q)* of the ester precursor, acid precursor and the ionomer for the TMT-12/80/12 material. A distinct deviation from the asymptotic behavior of the decreasing scattering intensity at q $\sim$ 0.02–0.04 Å^{-1} is observed for the ester precursor, which implies microphase separation in the system, but it is not clearly developed. However, a more distinct single broad peak was observed for acid precursor (h-TMT-12/80/12, q_{max} = 0.037 Å^{-1}) and ionomer (K$^+$-TMT-12/80/12, q_{max} = 0.04 Å^{-1}), which indicates the absence of higher orders in these materials. Upon neutralization of the acid functionalities to ionic functionalities, there is a further increase in intensity and the SAXS peak shifts to a slightly larger q-value compared to the corresponding acid block copolymer. Furthermore, on neutralization the SAXS peak becomes broader (peak width at half height) compared to the acid precursor. The effects of the total block length or degree of polymerization ($N = N_A + N_B$) and the PMMA block length on the morphology of the precursors and ionomers was further investigated.
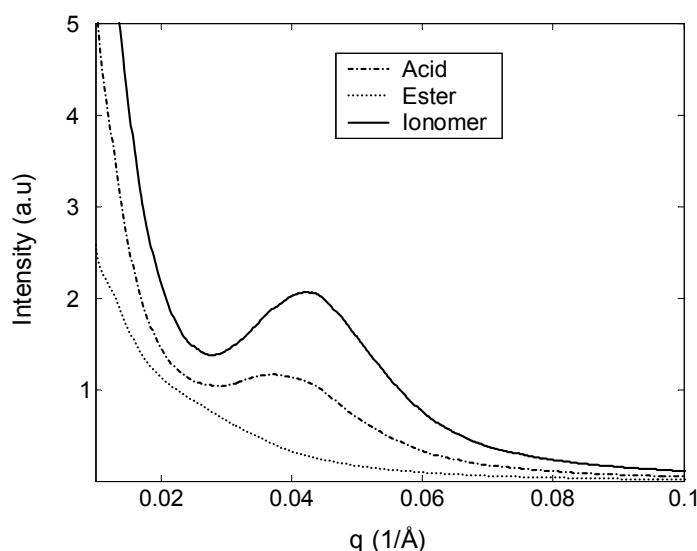
Figure 4.4: *SAXS profiles of TMT-12/80/12.*

Figure 4.5A and 4.5B show the SAXS data of the precursors and ionomers of TMT-15/160/15 and TMT-14/26/14 samples with different block lengths. Compared to the TMT-12/80/12 ester precursor (Figure 4.4) a distinct peak is seen in the TMT-15/160/15 ester and a weak shoulder peak is seen in the TMT-14/26/14 ester copolymer only after Lorentz correction (Lorentz[29-31] corrected plot, i.e., $I*q^2$ *vs.* q plot; not shown here; use of Lorenz corrected plots for this block copolymer is justified since the volume fraction predicts a lamellar morphology). This suggests that an increase in total N (overall block length) drives the microphase separation in the TMT-15/160/15 ester as expected by the theory of block copolymer phase separation. Similarly, the decrease in total N for the TMT-14/26/14 ester results only in a weak phase separation, which may indicate that a critical value of product χN is present in these systems for microphase separation.
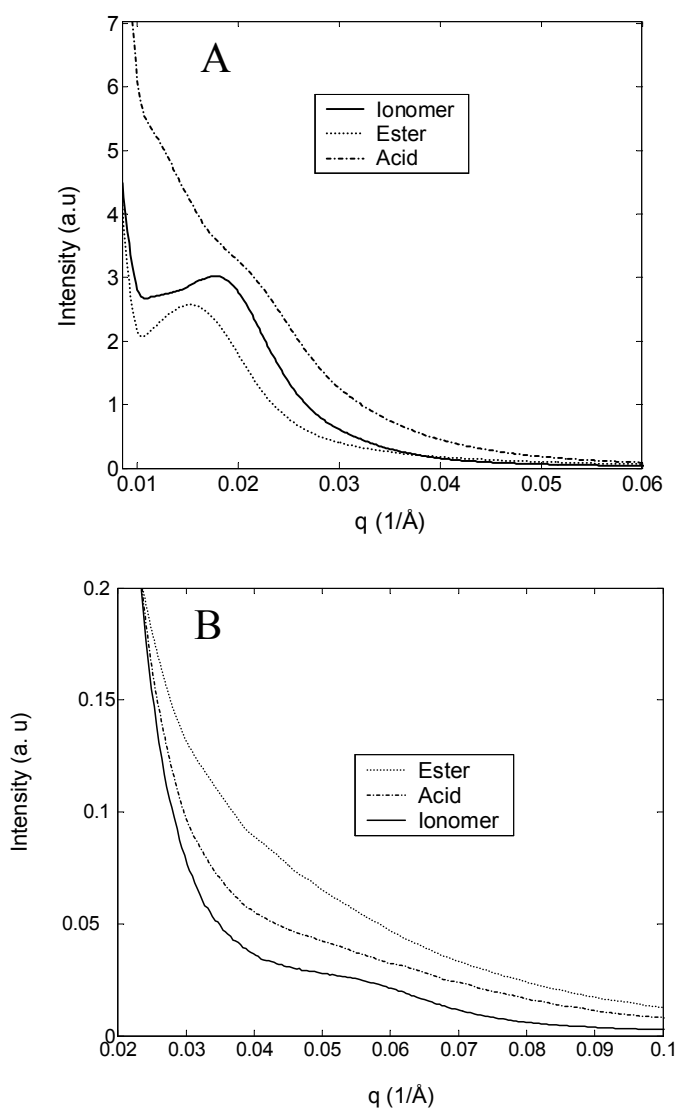
Figure 4.5: *SAXS profiles of (A) TMT-15/160/15 and (B) TMT-14/26/14.*

A similar trend is observed for the corresponding acid precursors (h-TMT-15/160/15 and h-TMT-14/26/14, Figure 4.5A and 4.5B). Upon neutralization a distinct peak is seen in the K^+-TMT-15/160/15 and K^+-TMT-14/26/14 block ionomers due to the increased immiscibility between the ionic and nonionic segments as observed in the K^+-TMT-12/80/12 ionomer. A similar trend of increased peak width at half height and peak shift in K^+-TMT-15/160/15 and K^+-TMT-14/26/14 ionomers is observed as in the case of K^+-TMT-12/80/12.

4.3.2.2 Morphology of diblocks

a. Morphology of ester precursors. Figure 4.6A, 4.6B and 4.6C show the SAXS profiles of the ester precursor, acid precursor and the ionic counterpart for the TM-28/60 ($V_{f, PtBMA}$ = 0.43), TM-50/168 ($V_{f, PtBMA}$ = 0.33), and TM-41/550 ($V_{f, PtBMA}$ = 0.1) samples, respectively. The ester precursors of all three samples show a single, strong and slightly asymmetric scattering peak, implying a clear microphase separation in these precursors. The presence of only one order also indicates the absence of a long-range periodicity in these materials. Furthermore, the position of the SAXS peak shifts to lower q-values as the total degree of polymerization (*N*) of the ester block increases indicating the influence of the total *N* on the periodicity of the sample.

b. Morphology of acid precursors. The SAXS profiles of the acid precursor for the TM-28/60, TM-50/168 and TM-41/550 samples are also shown in Figure 4.6. A clear and narrow single peak is present for the h-TM-41/550 diblock with a low acid content indicating microphase separation. A weak broad shoulder peak is distinctly seen in the h-TM-50/168 indicating that the extent of microphase separation is lower in this material compared to the corresponding ester TM-50/168 block copolymer. A very weak broad and single peak with very low intensity is seen in the h-TM-28/60 ($V_{f, PtBMA}$ = 0.43, Figure 4.6A). However, it was necessary to anneal (5 hours at 150 ℃) the sample to observe the microphase phase separation. In summary, compared to diblock esters microphase separation is suppressed in the acid block copolymers. This effect is more pronounced in the diblock acids with high acid contents. Furthermore, compared to the diblock esters, a broader peak width (peak width at half height) is seen in all the diblock acids, which may indicate the nonuniform size of the microphase separated domains in acids. The small but distinct shift of the scattering peak to a higher q-value in the acid blocks of h-TM-41/550 and h-TM-50/168 compared to the corresponding ester blocks may possibly be accounted for by a redistribution in packing density as the phase separation is influenced by the changes in the chemical structure of the block copolymer. A similar trend was trend was observed in the triblock TMT-15/160/15.
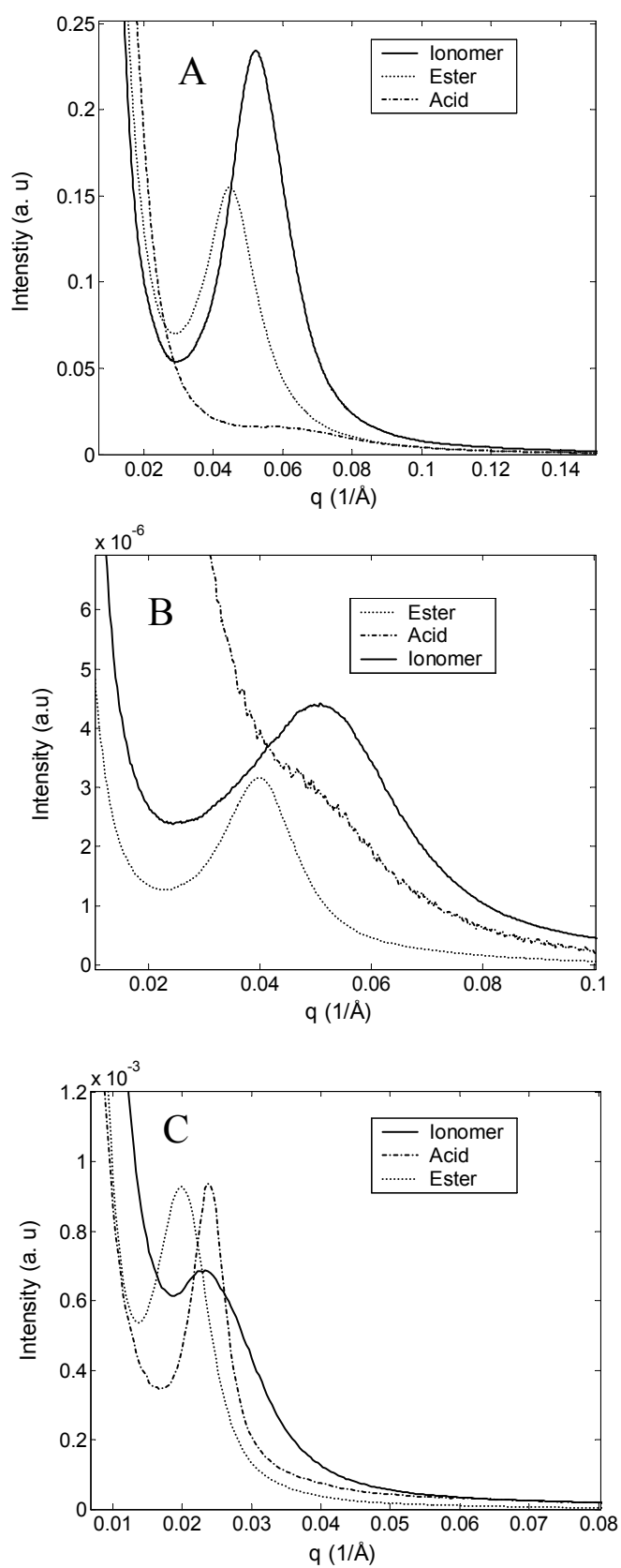
Figure 4.6: *SAXS profiles of (A) TM-28/60, (B) TM-50/168 and (C) TM-41/550.*

FTIR spectroscopy was used to study the molecular interactions between the MMA and MAA segments and further understand the acid content dependent morphology of the acid block copolymers. More specifically, the position of the carbonyl band (C=O) of esters and acids is very sensitive to these molecular interactions. FTIR spectra of h-TM-28/60, h-TM-50/168, and h-TM-41/550 block copolymers with three different acid levels are shown in Figure 4.7. A shoulder in the carbonyl band at 1700 cm^{-1} is indicative for the presence of the acid dimer[32]structure due to hydrogen bonding (HB) between two acid groups and is referred to as AA-HB (See Figure 4.8). It is evident from Figure 4.7 that the shoulder at 1700 cm^{-1} increases for higher acid contents, indicating the presence of more hydrogen bonding (AA-HB).
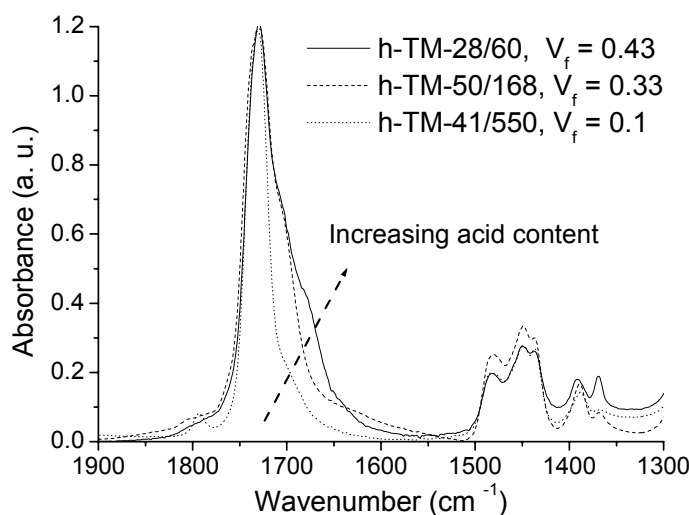
Figure 4.7: *FTIR spectra of diblock acid copolymers with three different acid contents.*

Furthermore, a new shoulder band is seen towards lower wavenumbers (1700–1640 cm^{-1}) for acid block copolymers with higher acid content. No such lower wavenumber band is seen in the poly((meth)acrylic acid)[32] homopolymer. This new band in the spectrum of h-TM-28/60 is due to the HB between the carbonyl group of methyl ester of MMA and the hydroxyl group of MAA. It is well known that the position of the carbonyl band[33] for the hydrogen bonded ester groups is lower than that of the free ester groups. This hydrogen bonding between the acid functionality (from PMAA block) and the ester functionality (from PMMA segment) is referred to as AE-HB (See Figure 4.8; note that Figure 4.8 also shows the other chemical structures present in the acid

copolymers). This is clearly seen as a broad shoulder peak in the region of 1680–1640 cm^{-1} for the highest acid content (h-TM-28/60) sample. P(MMA-*co*-MAA) random copolymers investigated in this thesis (See Chapter 5) also showed AE-HB in the 1680–1640 cm^{-1}. However, earlier studies[25,34] indicated that such AE-HB in the homopolymer blends (PMMA/PMAA) and in the copolymers of MMA/MAA was observed at 1705 cm^{-1} in the FTIR spectra.

$\upsilon_{HB(Dimer)}^{O-H} \approx 3000\,\text{cm}^{-1}$ $\upsilon_{HB(Dimer)}^{C=O} \approx 1700\,\text{cm}^{-1}$

$\upsilon_{F(MAA)}^{C=O} \approx 1680\,\text{cm}^{-1}$ $\upsilon_{F(MAA)}^{O-H} \approx 3300\,\text{cm}^{-1}$

AA-HB   AE-HB

$\upsilon_{F(MAA)}^{O-H} \approx 3450\,\text{cm}^{-1}$ $\upsilon_{F(MAA)}^{C=O} \approx 1750\,\text{cm}^{-1}$

$\upsilon_{F(MAA)}^{C=O} \approx 1730\,\text{cm}^{-1}$

"Free" MAA   "Free" MMA
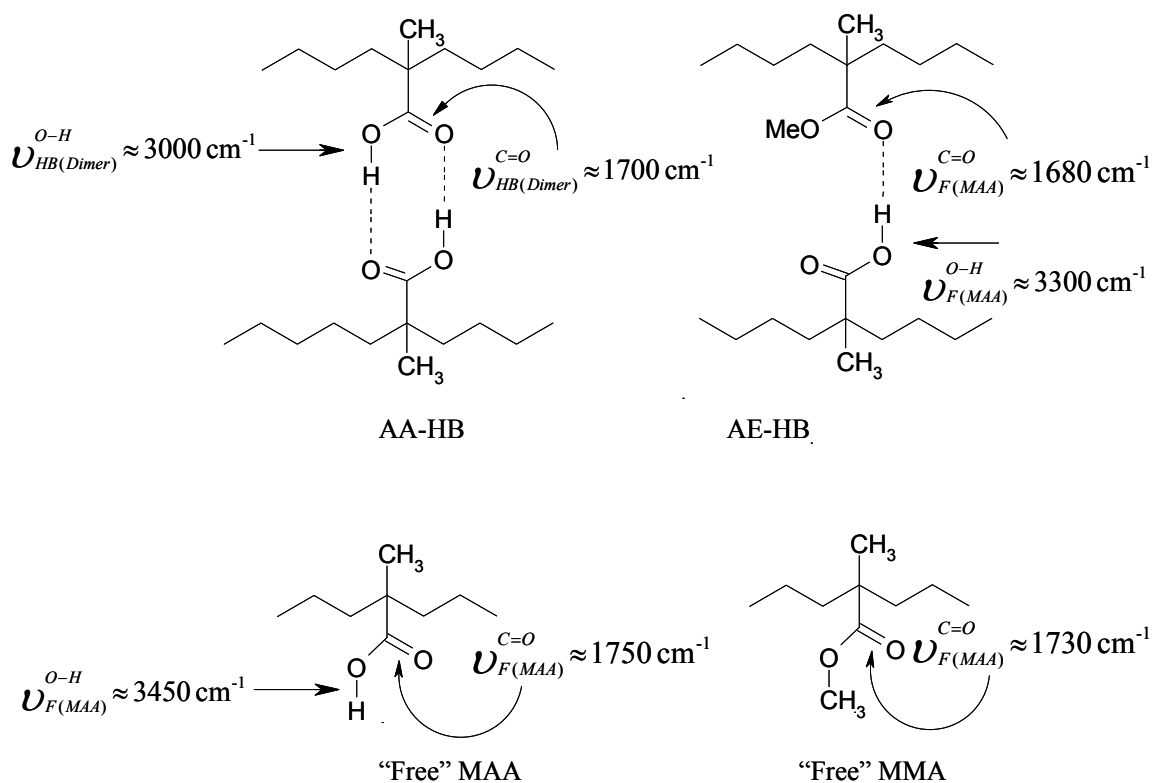
Figure 4.8: *Schematic showing AA- and AB-Hydrogen bonding of the carbonyl groups in the P(MMA-co-MAA) acid copolymer.*

c. Morphology of diblock ionic counterparts. SAXS profiles of the ionic counterparts K$^+$-TM-28/60, K$^+$-TM-50/168, and K$^+$-TM-41/550 are also shown in Figure 4.6. A distinct peak with strong intensity is seen in all diblock ionic counterparts independent of the ion content except for 4.6C. Upon neutralization, the SAXS peak becomes broader (peak width at half height) compared to the acid and ester precursor, as discussed in the triblock ionomer section. Furthermore, the q-value of the ionomer scattering peak is lower than the corresponding acid precursor, but higher than the corresponding ester precursor. This distinct trend observed among the q-values of precursors and

ionomer was not reported in the earlier studies of methacrylate ionomers (Mc Grath *et al.*[15]). Moreover, the trend observed in this study for the q-values of the precursors and ionomers is also opposite to the trend reported for the q-values of precursors and ionomers in block ionomers based on styrene (nonionic block) and 4-vinylpyridinium methyl iodide/cesium methacrylate (ionic block) segments.[13,19,20,21,22] In this case, the q-value for the ionomer is lower than the corresponding precursor. It is important to realize that no interaction is present between the ionic and nonionic blocks in styrene based ionomers.

4.3.2.3 Differential scanning calorimetry (DSC)

DSC was also used to identify the microphase separation and to determine the glass transition temperature (T_g) in diblock ionomers. The DSC measurements were performed in the temperature range of 30–150 ^oC and the results of the second heating runs of K^+-TM-50/168 and K^+-TM-41/550 are shown in Figure 4.9A and B respectively. It is evident from Figure 4.9A that a single broad T_g is observed in the former ionomer, however two T_g's are seen in the latter ionomer.

4.3.2.4 Solid state NMR: 1H spin-lattice relaxation experiments

An important tool for studying the microphase structure of heterogeneous polymers is ^{1}H-^{13}C cross-polarization magic-angle spinning (CPMAS) NMR. This technique offers the possibility to link the heterogeneity information of ^{1}H NMR to the high resolution of MAS ^{13}C NMR.[35-39] Recent examples of investigations of the microdomain structure of semicrystalline polymers, polymer blends, and block copolymers can be found in the literature.[36-38]

In the present study focus is on proton spin-lattice relaxation in the rotating frame ($T_{1\rho}$), associated with the behavior of the proton spins in the presence of a radio-frequency field. For a better chemical resolution ^{1}H $T_{1\rho}$ was measured via the ^{13}C NMR signals. The observed averaging of the $T_{1\rho}$ values of individual components in a copolymer by spin diffusion reflects the structure on the nanometer scale (See Discussion section). The ^{13}C CPMAS spectra of PMMA, PtBMA and the diblock TM-51/168 are shown in Figure 4.10A. The spectra are quite similar for the two homopolymers PMMA and PtBMA except the *tert*-butoxy group from PtBMA homopolymer, which shows two bands, i.e., at 28 ppm (from the methyl groups of the *tert*-butoxy group) and 80 ppm (from the quaternary carbon of the *tert*-butoxy group). Asterisks in the spectra indicate spinning side bands. By comparison with the *homopolymer* spectra, it is easy to assign the peaks in the *block-copolymer* spectrum. Separate proton $T_{1\rho}$ values were measured via the well-resolved

signals in the ^{13}C NMR spectra of PMMA, PtBMA and TM-51/168. The results are summarized in Figure 4.10B. The $T_{1\rho}(^1H)$ values of PMMA and PtBMA homopolymers of comparable molecular weights were 10 ms and 22 ms, respectively. These values are taken as the respective intrinsic $T_{1\rho}(^1H)$'s for the PMMA and the PtBMA in the block copolymer. From Figure 4.10B, it can be seen that spin diffusion causes complete averaging of the different intrinsic $T_{1\rho}(^1H)$ behavior of the PMMA and PtBMA components into common value of 17 ms for the block copolymer, as a whole. This result suggests, that there is no microphase separation for the block copolymer, which seems to contradict the SAXS results. This apparent paradox is explained in the discussion section.
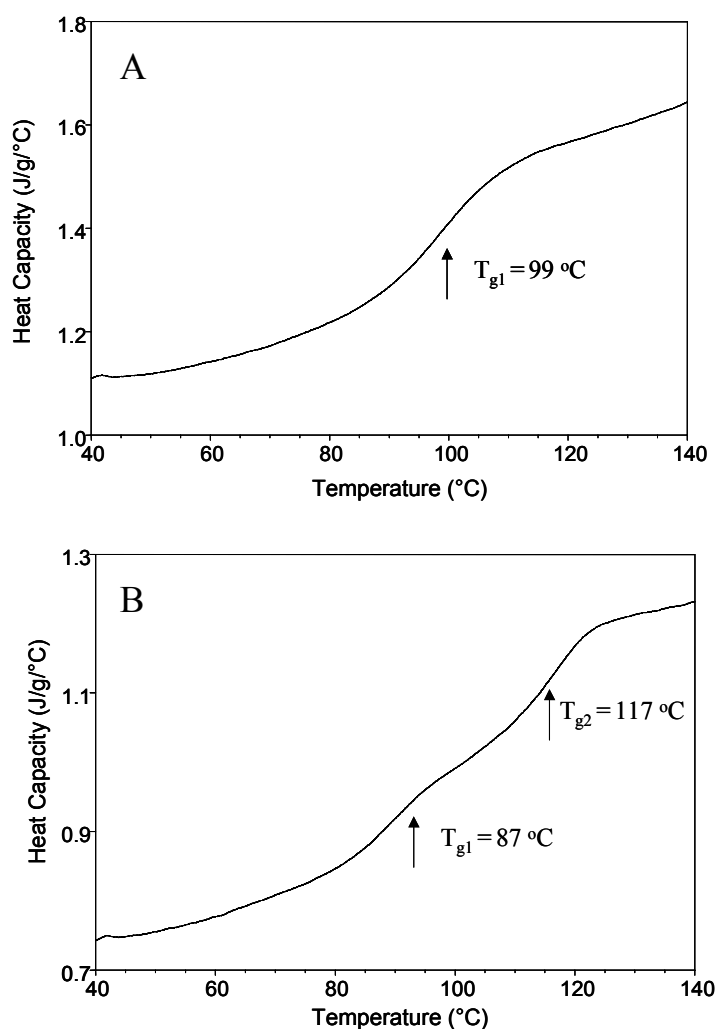
Figure 4.9: *DSC traces of (A) the TM-50/168 and (B) TM-41/550.*
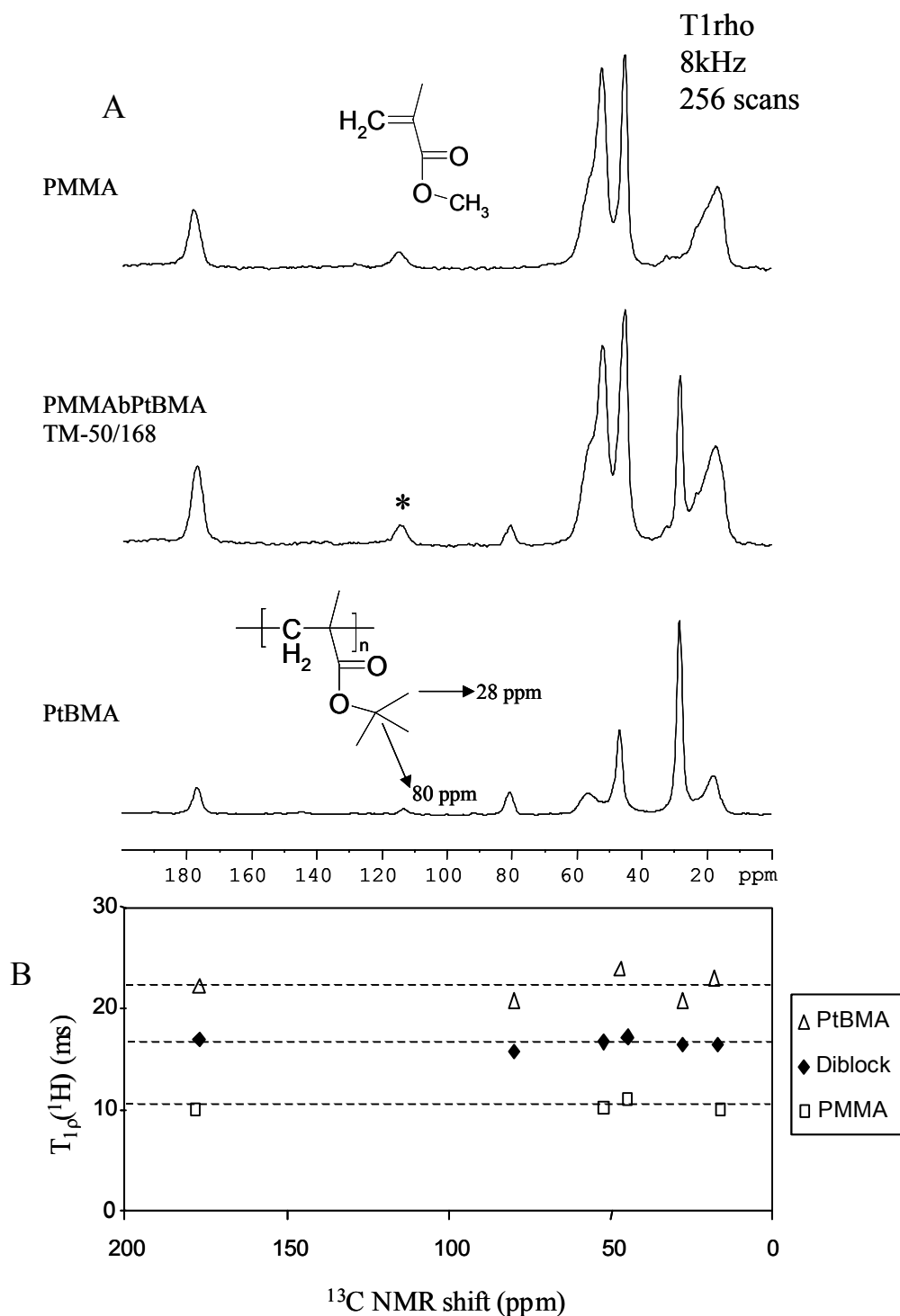
Figure 4.10: (A) *CPMAS 13C NMR spectra of (a) PMMA [CH3: 18 ppm, backbone: CH2: 41 ppm, backbone quaternary carbon: C: 46 ppm, OCH3 (methoxy): 52 ppm, C=O (ester carbonyl): 176 ppm], (b) PMMA-b-PtBMA [CH3: 18 ppm, CH3 (from tert-butyl group): 28 ppm, CH2 (backbone): 41 ppm, quaternary carbon (back bone): C: 46 ppm, OCH3 (methoxy): 52 ppm, quaternary carbon (tert-butyl group): C: 80 ppm, C=O (ester carbonyl): 176 ppm] and (c) PtBMA [CH3: 18 ppm, CH3 (from tert-butyl group): 28 ppm, CH2 (backbone): 41 ppm, quaternary carbon (back bone): C: 55 ppm, quaternary carbon (tert-butyl group): C: 80 ppm, C=O (ester carbonyl): 176 ppm]; side bands are indicated by asterisks and (B)* $T_{1\rho}(^1H)$ *values for the homopolymers and the block copolymer.*

4.4 Discussion

In ionomers, the architectural factors greatly influence the nature of ion aggregation in the system. As shown in the literature, multiplet or cluster formation has been observed in a number of systems in random ionomers for which the ion groups are randomly placed along the polymeric backbone.[4,9,11,40,41] In telechelic[42] systems, however, where the ionic groups are placed only at the chain ends, the multiplets aggregate in an ordered fashion to form supermultiplets and therefore the formation of clusters is unlikely. Hence, the morphology of the ionomers is significantly affected depending on the architectural features of the ionomers. In the diblock ester precursors investigated in this study, the degree of polymerization of the PtBMA block ($N_A \sim 30$ to 40) was kept constant and the degree of polymerization of PMMA (N_B) was varied systematically from as low as 60 to as high as 550. This variation gives us the opportunity to control the density of ionic aggregates or ionic domains in the PMMA matrix.

4.4.1 Morphology of triblocks

Microphase separation in block copolymers, *(A-B)$_n$*, is determined by three factors:[43,7] the overall degree of polymerisation, $N = N_A + N_B$, the architectural constraints characterized by *n* and the composition *f* (overall volume fraction of component *A* or *B*), and the *A-B* segment-segment interaction parameter χ (where χ is Flory– Huggins interaction parameter and a segment is usually defined as a repeat unit). The first two factors are regulated through the polymerization stoichiometry and influence the translational and configurational entropy, while the magnitude of (the largely enthalpic) χ is determined by the selection of the *A-B* monomer pairs. The high chemical structural similarity between the two monomers MMA and tBMA investigated in this study (two monomers differ only in side group and belong to the methacrylate family) should give a small χ value between the monomer segments. The absence of a clear scattering peak in the TMT-12/80/12 (see Figure 4.4) ester precursor may be due to a low degree of polymerization ($N = N_A + N_B = 24 + 80 = 104$, where *B* is the PMMA block and *A* is the PtBMA block, see Table 4.1), and the molecular architecture (*ABA,* triblock) of the copolymer. At the same composition *f* (overall volume fraction of the *A* component), the *ABA* triblock copolymer has two arms of block '*A*' compared to one arm of block '*A*' in an *AB* diblock copolymer. Furthermore, the length of block '*A*' in the triblock copolymer is reduced by half compared to the length of block '*A*' in the diblock copolymer. This may result in a higher interfacial energy ($F_{interf} = \gamma_0 * A_{interf}$) and lower configurational entropy

for the polymer chains in the triblock copolymer compared to the diblock copolymer. For the same χ value, the *ABA* triblock copolymer has to pay a higher entropic penalty to confine two *A* blocks into domains than to confine a single *A* block in the corresponding *AB* diblock. This may not be possible with the short mid block present in TMT-12/80/12, hence a clear microphase separation is absent in the TMT-12/80/12.

Upon hydrolysis, considerable reorganization of the domains takes place due to the presence of interactions between the methacrylic acid (MAA) segments and the MMA block segments. The increase in the scattering intensity in the acid precursor can be attributed to the enhancement of the scattering contrast upon hydrolysis. X-ray scattering is due to the contrast[44] provided by the difference in electron densities of the two phases present in the block copolymer. In the systems investigated here, the electron densities of PMMA, PtBMA, PMAA and PK$^+$MA are 0.195 e/Å^3, 0.337 e/Å^3, 0.381 e/Å^3, and 0.497 e/Å^3 respectively. In the calculation of these electron densities, the following polymer densities were used: 1.2 g/cm^3 for PMMA, 1.02 g/cm^3 for PtBMA, 1.18 g/cm^3 for PMAA[23], and 1.6 g/cm^3 for PK$^+$MA.[45] It is evident from the electron density values that the difference in the electron densities between PMMA and PtBMA, PMAA and PK$^+$MA increases. Hence, the contrast in the intensity of the peak increases as the chemical structure of the block copolymer changes from ester to acid to ionomer counterpart.

The scattering peak represents the periodic spacings between the regions of similar electron density in the material. The SAXS peak is interpreted as an interparticle correlation factor and as the higher order SAXS reflections are not observed it is difficult to assign a specific morphology for the scattering entities. The application of Bragg's law to the peak gives a characteristic Bragg distance (d_B). The spacing obtained from the position of the acid (h-TMT-12/80/12, Figure 4.4) peak is ~ 16.7 nm. The precision on d_B is of the order of 3 %. On neutralization of the acid functionalities to ionic functionalities, there is a significant increase in intensity and the SAXS peak shifts to a slightly larger q-value. A lower d_B of 14.8 nm is obtained for K$^+$-TMT-12/80/12 compared to the corresponding h-TMT-12/80/12 acid. The SAXS peak of the triblock ionomer K$^+$-TMT-12/80/12 (see Figure 4.4) has a higher intensity and larger peak width than the corresponding acid precursor. The larger peak width may be due to (1) the presence of intermolecular ionic interactions or multiplet formation within the PK$^+$MA phase, which influences the microphase separation of the block ionomer, and (2) the presence of a greater dispersity in either the distances between the scattering centers, their size and shape due to the strongly interacting ionic and nonionic blocks (arising due to the incomplete neutralization). The small but distinct shift of the

scattering peak to a higher q-value in the ionomer is due to the redistribution in packing density as the phase separation is further promoted by neutralization. Table 4.2 lists the d_{Bragg} values for all the three triblocks including the precursors and ionomers.

4.4.2 Morphology of diblocks

a. Ester precursors. Diblock esters with a wide range of molecular weights were synthesized to understand the structure–morphology relationships in these block copolymers. Comparing the SAXS profiles of diblock TM-28/60 (Figure 4.6A) and the triblock TMT-12/80/12 (Figure 4.4) one can see the effect of architecture on the microphase separation of the ester precursors. The TM-28/60 ester is better organized and microphase separated than the TMT-12/80/12 triblock ester at a comparable degree of polymerization of PtBMA. This may be due to the reduced length of PtBMA block in the triblock ester (reduced by half comparable to that in diblock copolymer, assuming symmetric nature of the polymerization from a difunctional PMMA macroinitiator) as discussed in the morphology section of the triblocks. The application of Bragg's law to the peak gives the characteristic domain distance, d_B, and these values are listed in Table 4.2 for all the diblocks. It can be seen that a wide range of d_B (11 nm to 32 nm) is obtained by varying the PMMA block length.

The effect of the total block length (N) or the molecular weight dependence on the characteristic Bragg spacing (d_B) of diblock esters is shown in Figure 4.11, where $\log(d_B)$ is plotted as a function of $\log N$. It is evident that d_B increases with N, and is proportional to N^{α}, and the power calculated from the slope of the straight line, $\alpha = 0.5 \pm 0.01$, is similar to that predicted for Gaussian coils. This dependence of interdomain spacing, d_B, on N is predicted for block copolymers in the Weak Segregation Limit[46] (WSL). However, it is important to know that the diblock ester copolymers investigated in this study differ not only in molecular weight but also in composition. This may not be an ideal way to investigate the influence of molecular weight on the domain spacing (d_B). The scaling of d_B on N in our ester precursors might indicate that these block copolymers can be classified as belonging to WSL, which is not much surprising due to the very similar monomer structure of MMA and tBMA. The mean field theory[47] of block copolymer phase separation predicts that for block copolymers in the WSL limit, the minimum of product $\chi*N$ is close to $(\chi*N)_{ODT}$, the order-disorder transition (ODT) for microphase separation. The value of $(\chi*N)_{ODT}$ is 10.5 for a symmetric diblock in WSL. With $N = 75$ for the TM-26/42 ($V_{f, PtBMA} = 0.5$, Refer to Table 4.2) sample, this leads to $\chi > 0.1$. This value is higher than the reported value of the

χ parameter (= 0.07 ± 0.02) between PMMA and poly(alkyl methacrylates)[48] and this may be due to the low molecular weight of the TM-26/42 (can be treated as oligomer) investigated in this study, where end groups can also influence the χ parameter. The reported literature value is obtained from the high molecular weight polymers (M_n = 20 kg/mole).

Table 4.2: *Characteristic Bragg spacing (d_{Bragg}) between the domains in MMA/tBMA block precursors and ionomers from SAXS analysis.*

Sample	d_{Bragg} between the domains[a] (nm)			Total DP of Block	Volume[b] fraction of PtBMA ($V_{f,PtBMA}$)
	Ester precursor TMT/TM	Acid precursor h-TMT/h-TM	Ionomer K^+-TM/T/K^+-TM		
TMT-14/26/14	10.8	10.2	10.5	54	0.60
TMT-12/80/12	NA[c]	16.6	14.8	104	0.30
TMT-15/160/15	35	NA	41	189	0.25
TM-26/42	11.0	NA	10.1	68	0.50
TM-28/60	14.0	NA	12.0	88	0.43
TM-41/76	14.0	NA	12.3	117	0.45
TM-34/115	14.8	11.4	13.6	149	0.33
TM-42/132	16.5	14.6	14.0	174	0.34
TM-50/168	15.7	11.6	12.3	218	0.33
TM-41/550	31.6	26.5	27.5	591	0.10

DP stands for total degree of polymerization [a] spacing corresponding to the position of the SAXS peak, d_{Bragg} = $2*\pi$ / q_{max}, where q_{max} is the scattering vector value at peak maximum. [b] calculated with ρ PMMA = 1.2 g/cm^3 and ρ PtBMA = 1.02 g/cm^3 for the ester precursors, taken as equal to volume fraction of poly(methacrylic acid) (PMAA) block in acids and poly(potassium methacrylate) block in ionomers. [c] identification of the peak maximum was not possible due to very broad weak peak.

b. Morphology of the acid precursors. The SAXS results showed that compared to the ester precursors, microphase separation in the corresponding acid precursors is a strong function of acid content and microphase separation is suppressed in the block acids with higher acid content. Upon hydrolysis of the *tert*-butyl groups, acid groups are introduced in the diblock copolymer. The FTIR results indicate that acid groups in the acid precursor exhibit two types of hydrogen bonding namely: AA-HB and AE-HB (See Figure 4.8), which suggests a strong interaction and possible segment miscibility between MMA and MAA segments via hydrogen bonding. Similar segment interactions were observed in the case of PMMA/PMAA homopolymer blends and completely miscible blends were obtained at all compositions. However, the results from this study indicate

that microphase separation is dependent on the amount of the acid content and correspondingly on the extent of the hydrogen bonding. It is worthwhile to recall that the amount of PtBMA in the ester block is assumed to be proportional to the amount of the PMAA and PK$^+$MA in the corresponding acid and ionomer blocks.
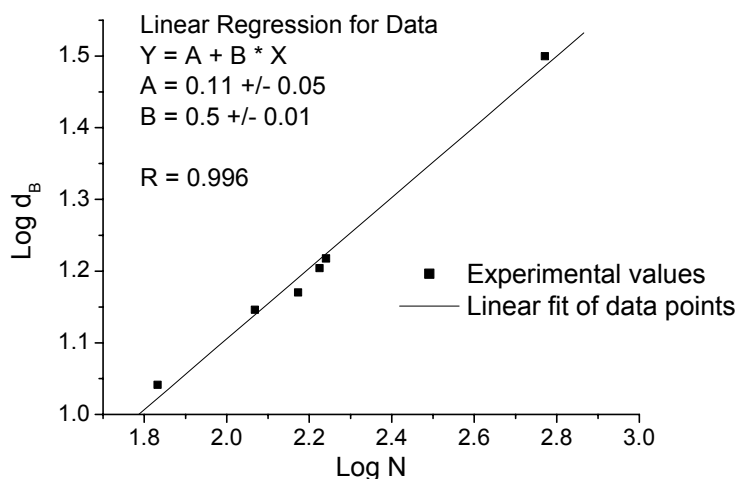
Figure 4.11: *Logarithmic plot of Bragg spacing (d$_B$) versus total degree of polymerization N.*

h-TM-26/42 with high acid content (high concentration of the acid groups compared to the ester groups) forms a extensive hydrogen bonding (both AA- and AE-HB), hence a miscible system (no SAXS peak) is obtained. However, h-TM-41/550 with low acid content (low concentration of the acid groups compared to the ester groups, i.e., dilution of the acid groups) forms a low number of hydrogen bonds and as a result an immiscible system (SAXS peak and microphase separation) is obtained (See Figure 4.7). It is important to note that the molecular weights (i.e., total degree of polymerization, *N*) of h-TM-26/42 and h-TM-41/550 are different, which may also influence the microphase separation of the block copolymer. In general, a high *N* favors microphase separation. In summary, the presence of hydrogen bonding in the block copolymers influences the thermodynamic and kinetic aspects of the microphase separation, hence a non-equilibrium morphology is present in these systems. The effect of annealing on microphase separation in the high acid content block copolymer, h-TM-41/76 (*V$_{f, PtBMA}$* = 0.45), is shown in Figure 4.12. It is quite evident that a weak phase separation is seen in the sample after annealing at 150 °C for 5 h. Note that the h-TM-41/76 block is stable till 200 ^{o}C (See section 7.4.1.1; Chapter 7),

hence thermal degradation during the annealing procedure is negligible. The development of the weak peak in Figure 4.12 after annealing may be due to the temperature sensitivity of the hydrogen bonds, which also changes the interaction parameter (χ) between the two segments. Hydrogen bonds are weakened at 150 °C (possible LCST behavior), which promotes the microphase separation of the block copolymer.[24,25] A similar macrophase separation was reported at high temperature in the blends of PMMA/PMAA.[25]
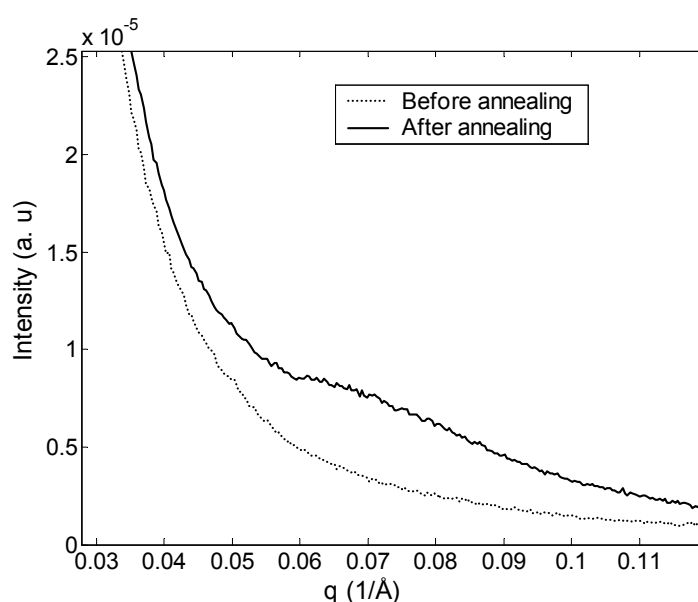
Figure 4.12: *SAXS profiles of diblock acid copolymer (h-TM-41/76) before and after annealing.*

c. Morphology of diblock ionic counterparts. Solution neutralization was used to prepare the block ionomers. It is well established that micellar and kinetically trapped structures are formed during the neutralization.[49] The following two factors determine the microphase separation and final morphology of the ionic counter parts. The degree of incompatibility or immiscibility between the ionic (PK$^+$MA) and nonionic (PMMA) blocks drives the microphase separation, whereas the ionic aggregates act as physical cross-links and influence the size and shape of the phase separated domains. The degree of incompatibility between the blocks is much larger for the ionomers than for the corresponding esters and acids favoring microphase separation. Conversion of the carboxylic acids to the corresponding salts upon neutralization destroys the hydrogen bonding capability of the carboxylic acid groups, which removes the large extent of favorable interactions. However, it is worth recalling that the FTIR spectrum of the block ionomer (Figure 4.3) also shows a complex

spectrum in the carbonyl region indicating the presence of strongly interacting functional groups arising due to the possible incomplete neutralization. The d_B (characteristic Bragg distance) for the ionomers is determined from the maximum of the SAXS peak and the values are given in Table 4.2. The d-spacings for the ionomers increase with increasing DP, similar to the esters and acids. A broad range in d_B (10 to 30 nm) could be obtained in this study by controlling the degree of polymerization of PMMA block indicating the possibility of achieving the variable ionic domain density in the PMMA matrix.

An attempt to give a qualitative explanation for the distinct shift of the SAXS peak maximum from the ester to acid to ionic form is made here. SAXS analysis indicates that the maximum in the scattering vector increases in the following order: $q_{ester} < q_{ionomer} < q_{acid}$ and corresponding domain spacing decreases in the following order: $d_{B,ester} > d_{B,ionomer} > d_{B,acid}$. As mentioned in the results section, the distinct trend observed in this study is opposite to the trend observed in the reported styrene based block ionomers.[19] The FTIR results on PMMA based acid block copolymers investigated in this study indicate the presence of strong interaction between the nonionic (PMMA) and the acid (PMAA) blocks. This implies that the polymer chains in the nonionic block may not have a true Gaussian conformation in the acids compared to the corresponding ester precursors. These strong interactions in the acid form lead to a large interfacial thickness and a diffuse interface is obtained. This may also influence the size, shape and curvature of the acid domains in the P(MMA-*b*-MAA) block copolymer. Hence, the domain spacing ($d_{B,acid}$) of the acid block copolymer is lower than the corresponding ester block ($d_{B,ester}$).

Upon neutralization of the acid block to the corresponding ionic block the increase in immiscibility between the ionic and nonionic blocks implies an increase of the χ parameter, hence, a stronger thermodynamic driving force[50] (super strong segregation and a sharp interface) for the microphase separation. Moreover, neutralization destroys the hydrogen bonding capability of the acid groups. Consequently, a high surface energy is present between the ionic and the nonionic phase and the system will tend to reach an equilibrium morphology by minimizing the total surface area between the two phases. Polymer chains (PK^+MA) in the ionic domains are relatively more stretched (to minimize the total surface area) compared to the polymer chains (PMAA) in the acid domains of the corresponding acid precursor P(MMA-*b*-MAA). This proceeds until the entropy cost of stretching the ionic chains is balanced by the surface energy gained through an increase in the radius of the ionic domains. Hence, the domain spacing ($d_{B,ionomer}$) of the ionomer block copolymer is higher than the corresponding acid precursor ($d_{B,acid}$). However, FTIR spectra of the

ionomer (Figure 4.3) also indicated the presence of strongly interacting functional groups, which could be due to the incomplete neutralization of the acid block precursor. The presence of large composition differences in the ionic block as a result of incomplete neutralization may lead to ionic domains with large distribution in size and shape. As a result a different packing density of the ionic domains is present in ionomers compared to the ester domains in the corresponding ester precursor. Consquently, a large distribution in interionic domain distances in the block ionomer is observed. The presence of a broader (large peak width at half height) peak in the SAXS profile of the ionomer (see Figure 4.6A, 4.6B, 4.6C) compared to the precursors (esters and acids) indicates towards a large polydispersity in the interionic domain distances and supports the above explanation.

To obtain more structural information of the ionomers the following procedure is applied: first, the domains were assumed to be spherical or cylindrical (depending on the volume fraction of the ionic block) and arranged on some regular lattice of unknown symmetry. This starting hypothesis is justified by the available experimental data on the block ionic precursors investigated in this study (the SAXS peak is assigned to the structure factor), reported data on similar block ionomers,[19,20,21,22] and by analogy with the known structure of ionomer precursors (esters and acids) at similar volume fraction of one of the components, e.g., spherical microdomains arranged on a body centered cubic lattice (for K^+-TM-41/550 diblock with $V_{f, PtBMA} = 0.1$) or cylindrical domains arranged on a hexagonal close packed lattice (for K^+-TM-50/168, $V_{f,PtBMA} = 0.33$). For the spherical and cylindrical morphologies, the continuous phase is assumed to be PMMA.[19] For all morphologies, complete phase separation and a negligible interphase thickness have been assumed, a reasonable assumption in view of the very high driving force for phase separation between ionic and nonionic segments. Knowing the position of the characteristic Bragg distance (d_B) and the volume fraction of the ionic microdomains (V_f), it is possible, by using simple crystallographic and geometric calculations, to compute the morphological parameters for different shapes of the scattering units arranged on different paracrystalline lattices. This is done for spherical domains (for K^+-TM-41/550) arranged on simple cubic (SC), body centered cubic (BCC), face centered cubic (FCC), and hexagonal close packed lattices; for cylindrical domains (for K^+-TM-50/168 and K^+-TM-34/115) arranged on a hexagonal close packed (HCPC) lattice. The parameter calculated for these morphologies is the radius, R, of the sphere or cylinder. For the case of spherical domains, all the lattices examined gave similar results. However, only the results of the body centered cubic (BCC, the most commonly observed cubic lattice for block copolymers) lattice for TM-41/550 ionomer were selected for further discussion.

Table 4.3 gives the different morphological parameters for the ionic counterparts. It must be kept in mind that the morphological parameters reported here are indirect and have been calculated on the basis of stoichiometry. They are thus extrapolation values for completely phase separated and perfectly shaped domains. In all the samples, the radius (R_{BCC} or R_{HCPC}) of the domains calculated is higher than the random coil end-to-end distance ($<r_0^2>^{1/2}$) of the corresponding poly(methacrylic acid) block, which is the domain-forming block. (PMAA is taken as an approximation for poly(potassium methacrylate), which may not be a correct approximation; $<r_0^2>^{1/2} = (C_\infty N l^2)^{1/2}$, where $C_\infty = 14.3$ for PMAA[51], $l = 0.154$ nm, and N is the number of C–C bonds).

Table 4.3: *Relevent morphological parameters, obtained assuming paracrystalline model, and from space-filling calculations for spherical domains on a body centered cubic and cylindrical domains on a hexagonal close packing for MMA/tBMA block ionoic counterparts*

Sample	d_{Bragg} Ionomer[a] (nm)	R_{BCC}[b] (nm)	R_{HCPC}[c] (nm)	$<r_0^2>^{1/2}$ of PMAA block	Fully extended length of PMAA block	Volume[b] fraction of PMAA ($V_{f,PMAA}$)
K⁺-TM-34/115	13.6	NA	4.7	4.8	8.5	0.33
K⁺-TM-42/132	14.0	NA	5.0	5.4	10.5	0.34
K⁺-TM-50/168	12.3	NA	4.2	5.8	12.5	0.33
K⁺-TM-41/550	27.5	9.2	NA	5.3	10.2	0.10

[a] Spacing corresponding to the position of the SAXS peak, $d_{Bragg} = 2*\pi / q_{max}$, where q_{max} is the scattering vector value at peak maximum. [b] Radius of the spherical ionic domain assuming body centre cubic lattice, $R_{BCC} = [4.40/q_{max}]*(V_{f,PMAA})^{1/3}$ $V_{f,PMAA}$ = volume fraction of the poly(methacrylic acid). [c] Radius of the cylindrical ionic ionic domain assuming hexagonal closed packing macro lattice

$$R_{HCPC} = a\left(\frac{\sqrt{3}}{2\pi}V_{f,PMAA}\right)^{1/2}$$ where a = distance between the centres of the adjacent cylinders.

The radius of the cylindrical domain forming ionic counterparts was lower than the extended chain length of the PMAA block (e.g., for TM-34/115 sample with N_A 34 units of the core forming block, the fully stretched planar zigzag length, obtained by multiplying the number of units of the core forming block by 0.25 nm, is 8.5 nm compared to the experimental R_{HCPC} of 4.7 nm). However, for the spherical domain forming block ionomer, i.e., K⁺-TM-41/550, with a R_{BCC} of 9.2 nm for which the fully stretched planar zigzag length is 10.2 nm. The fact that the radius of the spherical domain is close to or larger than the fully stretched zigzag length of the domain-forming

block was reported earlier.[22] Eisenberg *et al.*[19,21,22] explained this by the effect of ionic chain polydispersity on the final morphology. At a given polydispersity, it is possible that the longest chains extending all the way to the center of the microdomains with the shorter chains occupying the regions closer to the surface. Consequently, the longest chains would play an important role in determining the radius. Furthermore, they concluded that the method of preparation of the block ionomer also influenced the effect of ionic chain polydispersity on the sizes of the ionic microdomains. The PDI (1.20–1.25) of the block ionomer precursor copolymers (synthesized by ATRP) used in this work are relatively higher than the PDI (1.08−1.12) of the precursor copolymers (synthesized by anionic polymerization) reported by other research groups.[19,21,22] Moreover, hydrolysis of the PtBMA block to PMAA block was incomplete for this high molecular weight block, which may also play a role in determining the radius of the ionic microdomain.

4.4.3 DSC analysis

DSC results also indicate the microphase separation in the diblock ionomer. The presence of two T_g's in K^+-TM-41/550 indicates microphase separation. The ionic content of K^+-TM-50/168 is higher than of K^+-TM-41/550, which may lead to a higher value of the ionic block T_g, which is not observed in the measured temperature range. DSC measurements were not performed above 150 ^{o}C in order to avoid the possible thermal degradation of the samples.

4.4.4 Solid state NMR

Spin–lattice relaxation in the rotating frame $[T_{1\rho}(H)]$ are sensitive to the nanostructure of heterogeneous materials. This can be used as a convenient probe to determine the length scale of the separated minority phase at a level of a few nanometers. The single $T_{1\rho}(^1H)$ value observed for the diblock TM-51/168 can be explained in the following way. The protons in a polymer form a network of nuclear spins coupled by magnetic dipole interactions. In this coupled network, spin diffusion occurs, which tends to locally average the NMR properties of individual protons at a length scale depending on the specific ^1H NMR property under study. As a result of this spin diffusion, NMR cannot resolve individual NMR $T_{1\rho}$ values of components in a heterogeneous polymer, which are closer together than the spin-diffusion path length $L \sim [6DT_{1\rho}]^{1/2}$. Here, D denotes the (effective) spin-diffusion coefficient, which depends on the proton density in the polymer and the rotational mobility of the polymer chains. The higher the proton density, the

stronger the dipolar interactions and the faster proton spin diffusion. Spin diffusion is fast in crystalline or glassy polymer domains, and slow in rubbers with a low cross-link density. With a typical D value of ~1 nm^2/ms for spin diffusion in a polymer,[36] and the PMMA $T_{1\rho}(^1H)$ value of 10 ms, the spin diffusion path length is ca. 8 nm. A rough analysis of $T_{1\rho}(^1H)$ in terms of copolymer domains larger or smaller than $[6D\,T_{1\rho}(^1H)]^{1/2}$ usually assumes a sharp phase boundary. In reality, the case is complicated by the presence of more gradual density gradients. Indeed, the results of SAXS suggest that the ester block copolymers have a diffuse phase boundary. The $T_{1\rho}(^1H)$ averaging found for the block copolymer implies that spin diffusion at the $T_{1\rho}(^1H)$ time scale proceeds at a length scale comparable to, or larger than the PtBMA domain size.
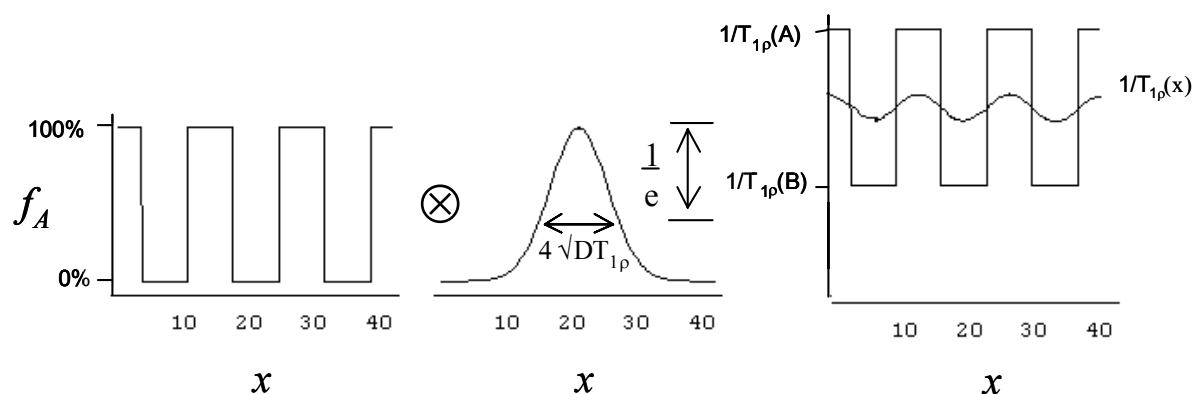
Figure 4.13: *Schematic illustration of the averaging effect on $T_{1\rho}(^1H)$ in a copolymer with sharp boundaries, and domain sizes of 14 nm by (one-dimensional) spin diffusion at a length scale $[2D\,T_{1\rho}(^1H)]^{1/2} \sim 4.5$ nm; (left) density of component A ($T_{1\rho}(A) < T_{1\rho}(B)$), (center) spin diffusion density function, (right) resulting averaging of $T_{1\rho}$.*

Figure 4.13 illustrates schematically, how one-dimensional spin diffusion at a length scale of $[2D\,T_{1\rho}(^1H)]^{1/2} \sim 4.5$ nm averages out $T_{1\rho}(^1H)$ relaxation differences in a copolymer with sharp boundaries, and domain sizes of 14 nm. This explains the apparent paradox between the common $T_{1\rho}$ value found for the PMMA and PtBMA component in the block-copolymer, and the phase separation indicated by the SAXS. Further experiments, probably above T_g, where $T_1(^1H)$ is shorter, are required to confirm the SAXS picture with solid state NMR.

4.5 Conclusions

The FTIR and NMR results of the hydrolysis of the poly(methyl methacrylate-*b-tert*-butyl methacrylate) [P(MMA-*b*-tBMA)] and poly(*tert*-butyl methacrylate-*b*-methyl methacrylate-*b-tert*-butyl methacrylate) [P(tBMA-*b*-MMA-*b*-tBMA)] ester precursors indicate the successful synthesis of poly(methyl methacrylate-*b*-potassium methacrylate) [P(MMA-*b*-K$^+$MA)] diblock and poly(potassium methacrylate-*b*-methyl methacrylate-*b*-potassium methacrylate) [P(K$^+$MA-*b*-MMA-*b*-K$^+$MA)] triblock ionic counterparts in a large range of molecular weights and compositions. The influence of polymer architecture (*AB*, *ABA*), the composition of the nonionic/ionic blocks, and block copolymer chemical structure, i.e., from block esters, acids and ionic counterparts on the final morphology of these materials was investigated by small angle X-ray scattering (SAXS).

A single peak was observed in di- and triblock precursors and the ionic counterparts indicating a clear microphase separation and absence of higher order structures. The SAXS results indicate that diblock ester precursors are better organized than the triblock ester precursors due to the differences in the block lengths in the two architectures. It was found that considerable reorganization of the block copolymer takes place as the chemical structure changes from an ester to an acid to an ionic form. The presence of strong interactions between the block components in acid and ionic (in ionic counterparts arising from the acid groups present due to possible incomplete neutralization) copolymers influences the thermodynamic and kinetic aspects of the microphase separation. The FTIR results confirmed the presence of strong hydrogen bonding in acid and ionomer block copolymers. Further, the SAXS results indicate that a wide range of interdomain spacing (characteristic Bragg distance, d_B, 10-30 nm) can be achieved in the precursors and in the ionic counterparts by controlling the total degree of polymerization of the block copolymer.

The SAXS analysis points out that interdomain spacing decreases in the following order: $d_{B, ester} > d_{B, ionomer} > d_{B, acid}$. This can be related to the formation of the phase separated domains in ionic counterparts and acids with large distribution in size and shape due to presence of large composition differences in the ionic block as a result of incomplete neutralization and presence of hydrogen bonding in acid block copolymers respectively. The relatively high polydispersity index (PDI = 1.2–1.25) of the block copolymer precursors may also contribute towards the observed shift in the interdomain spacing. As a result, a large distribution in inter domain distances are observed in the block ionomer and the acid precursor compared to the ester precursor.

4.6 References

(1)   Hadjichristidis, N.; Pispas, S.; Floudas, G. *Block Copolymers: Synthetic Strategies, Physical Properties, and Applications*, **2003**, Wiley-Interscience.

(2)   Hamley, I. W. *The Physics of Block Copolymers*, 24, **1998**, Oxford University Press.

(3)   Sperling, L. H., Ed. *Recent Advances in Polymer Blends, Grafts and Blocks*; **1974**, Plenum: New York.

(4)   Eisenberg A.; Kim, J. S. *Introduction to Ionomers*, **1998**, John Wiley & Sons, Inc.

(5)   Tant, M.R.; Mauritz, K, A.; Wilkes, G. L. Eds. *Ionomers: Synthesis, Structure, Properties and Applications*, **1997**, Blackie Academic and Professional: London.

(6)   Schlick, S. *Ionomers: Characterization, Theory, and Applications.* **1996,** Ed.; CRC Press: Boca Raton, FL.

(7)   Bates, F. S.; Fredrickson, G. H. *Annu. Rev. Phys. Chem.* **1990**, 40, 525.

(8)   Eisenberg, A. *Macromolecules*, **1970**, 3, 147.

(9)   MacKnight, W. J.; Taggart, T. P.; Stein, R. S. *J. Poly. Sci., Polym. Symp.* **1974**, 45, 113.

(10)   Marx, C. L.; Caulfield, D. F.; Cooper, S. L. *Macromolecules*, **1973**, 6,3.

(11)   Yarusso, D. J.; Cooper, S. L. *Macromolecules*, **1983**, 16, 1871.

(12)   Kumar, S.; Pineri, M. *J. Poly. Sci., Polym. Phys. Ed.* **1986**, 24,1767.

(13)   Gauthier, S.; Eisenberg, A. *Macromolecules*, **1987,** 20, 760.

(14)   Gouin, J. P.; Eisenberg, A.; Williams, C. E. *Macromolecules*, **1992**, 25, 1368.

(15)   Venkateshwaran, L. N.; York, G. A.; Deporter, C. D.; McGrath, J. E.; Wilkes, G. L. *Polymer*, **1992**, 33(11), 2277.

(16)   Weiss, R. A.; Sen, A.; Pottic, L. A.; Willis, C. L. *Polymer*, **1991**, 32, 1867.

(17)   Mani, S.; Weiss, R. A.; Williams, C. E.; Hahn, S. F. *Macromolecules*, **1999**, 32, 3663.

(18)   Storey, R. F.; Baugh, D. W. *Polymer*, **2000**, 41, 3205.

(19)   Gouin, J. P.; Williams, C. E.; Eisenberg, A. *Macromolecules*, **1989**, 22, 4573.

(20)   Gouin, J. P.; Bosse, F.; Nguyen, D.; Williams, C. E.; Eisenberg, A. *Macromolecules*, **1993**, 26, 7250.

(21)   Nguyen, D.; Varshney, S. K.; Williams, C. E.; Eisenberg, A. *Macromolecules*, **1994**, 27, 5086.

(22)   Nguyen, D.; Zhong, X. F.; Williams, C. E.; Eisenberg, A. *Macromolecules*, **1994**, 27, 5173.

(23)   Mansur, C. R. E.; Tavares, M. I. B.; Monteiro, E. E. C. *Journal of Applied Polymer Science*, **2000**, 75, 495.

(24)   Mansur, C. R. E.; Monteiro, E. E. C. *Journal of Applied Polymer Science*, **1998**, 68, 345.

(25)   Huang, C. F.; Chang, F. C. *Polymer*, **2003**, 44, 2965.

(26)   Ma, Q.; Wooley, K. L. *Journal of Applied Polymer Science*, **1998**, 68, 345.

(27)   Greene, T. W.; Wuts, P. G. M. *Protective Groups in Organic Synthesis*; John Wiley & Sons: New York, **1991**.

(28)   Malinowski, E. *J. Chemom.* **1987**, 1, 33.

(29)   Lu, X.; Steckle, W. P.; Weiss, R. A. *Macromolecules*, **1993**, 26, 5876.

(30)   Lu, X.; Steckle, W. P.; Weiss, R. A. *Macromolecules*, **1993**, 26, 6525.

(31)   Lu, X.; Steckle, W. P.; Hsiao, B.; Weiss, R. A. *Macromolecules*, **1995**, 28, 2831.

(32)   Dong, J; Ozaki, Y.; Nakashima, K.; *Macromolecules*, **1997**, 30, 1111.

(33)   Lin-Vien, D.; Colthup, N, B.; Fateley, W. G.; Grasselli, J. G. *The handbook of Infrared and Raman*

       Chracteristic Frequencies of Organic Molecules, **1991**, 117, Academic Press.

(34)   Kuo S. W.; Chang, F. C. *Macromolecules*, **2001**, 34, 4089.

(35)   Schimidt-Rohr, K.; Clauss, J.; Blumich, B.; Spiess, H. W. *Magn. Reson. Chem.*, **1990**, 28, S3.

(36)   Schimidt-Rohr, K.; Spiess, H. W. *In Multidimensional Solid State NMR and Polymers*; Academic Press: London, 1994.

(37)   Jack, K. S.; Wang, J.; Natansohn, A.; Register, R. A. *Macromolecules*, **1998**, 31, 3282.

(38)   Yu, H.; Natansohn, A.; Singh, M. A.; Torriani, I. *Macromolecules*, **2001**, 34, 1258.

(39)   Eckman, R. R.; Henrichs, P. M.; Peacock, A. J. *Macromolecules*, **1997**, 30, 2474.

(40)   Lee, D.; Register, R. A.; Yang, C.; Cooper, S. L. *Macromolecules*, **1988**, 21, 998.

(41)   Mauritz, J. J. *Macromol. Sci. Rev. Macromol. Chem. Phys.* **1988**, 28, 65.

(42)   Jerome, R.; Broze, G. *Rubb. Chem. Technol.*, **1985**, 58, 223.

(43)   Leibler, L. *Macromolecules*, **1980**, 13, 1602.

(44)   Glatter, O.; Kratky, O. *Small Angle X-ray Scattering*, **1982**, p. 228, Academic Press Inc. (London) LTD.

(45)   Moffitt, M.; Eisenberg, A. *Macromolecules*, **1997**, 30, 4363.

(46)   Leibler, L. *Macromolecules*, **1980**, 13, 1602.

(47)   Matsen, M. W.; Bates, F. S. *Macromolecules*, **1996**, 29, 1091.

(48)   Scherble, J.; Stark, B.; Stuhn, B.; Kressler, J.; Bidde. J.; Horing. S.; Schubert, D. W.; Simon, P.; Stamm, M. *Macromolecules*, **1999**, 32, 1859.

(49)   Moffitt, M.; Esenberg, A. *Macromolecules*, **1997**, 30, 4363.

(50)   Nyrkova, I. A.; Khokhlov, A. R.; Doi, M. *Macromolecules*, **1993**, 26, 3601.

(51)   Brandrup, J.; Immergut, E. H.; Grulke, E. A. *Polymer Hand Book*, VII 1, **1999**, John Wiley & Sons, Inc.

Chapter 5

PMMA Random and Telechelic Polyester Ionomers: Synthesis, Molecular and Morphological Characterization

ABSTRACT: The synthesis, molecular and morphological features of potassium neutralized poly(methyl methacrylate) (PMMA)-based ionomers containing 5, 10, and 15 mol % ion content and with different molecular weights were investigated. Fourier transform infrared spectroscopy (FTIR) was used for molecular characterization of the ionomers. Small angle X-ray scattering (SAXS) coupled with dynamic mechanical thermal analysis (DMTA) was used to elucidate the morphological features of the PMMA ionomers. Results obtained are compared with those reported for cesium- and sodium-neutralized PMMA ionomers and are discussed in terms of Eisenberg, Hird, and Moore (EHM model) multiplet-cluster model. A distinct SAXS peak with clear maximum was observed only at 10 and 15 mol % ion content. The SAXS results indicated formation and aggregation of multiplets, with a broad range of inter multiplet spacing centered around ~ 70 Å. However, a single glass transition temperature (T_g) was observed in the DMTA analysis implying that no cluster phase is formed in these ionomers. High dielectric constant of the PMMA matrix and presence of strong interactions between the ionic and nonionic groups (from the FTIR analysis) may suppress the formation and aggregation of the multiplets in the PMMA matrix, which reduce the electrostatic interactions of the ionic groups and hinder the cluster phase formation.

The synthesis, molecular and morphological features of the isophthalic acid based amorphous polyesters with 5.3 and 3.7 mol % acid content were studied. SAXS, FTIR and differential scanning calorimetry (DSC) were used to investigate the influence of molecular parameters such as acid content, counter ion, and degree of neutralization on the ionomer morphology. FTIR spectra measured at room and elevated temperatures indicated the influence of the counter ion on the ion aggregate formation. Zinc counterion forms mixture of tetra- and hexa-coordinated aggregates, where as potassium forms a single ionic aggregate. The results of the SAXS indicated the muliplet formation and an intermultiplet distance of ~ 35 Å were measured. The results of the SAXS and FTIR indicated the presence of a critical ion content above which a clear microphase separation was observed. The SAXS analysis also confirmed the presence of large distribution of the ionic aggregates in the zinc ionomer.

5.1 Introduction

It is now well established that the physical, mechanical, and viscoelastic properties of ionomers are strongly dependent on the morphology.[1-3] Several parameters such as the architecture of the backbone, flexibility of the backbone, dielectric constant of the polymer matrix, ionic content, degree of neutralization, chemical nature of the ionic groups, and the presence of plasticizers determine the observed morphology in the ionomer.[1,4] The architecture of the ionomer is one of the most important parameter that determines the morphology of the ionomer[1]. By controlling the location of the ionic functionality on the polymer chain ionomers with large variation in architecture such as random[1], telechelic[5], block,[1,6-8] segmented[9], and star[10-12] can be synthesized. Chapter 4 presented the salient morphological features of the poly(methyl methacrylate-*b*-potassium methacrylate) (PMMA-*b*-K⁺MA) and poly(potassium methacrylate-*b*-methyl methacrylate-*b*-potassium methacrylate) (PK⁺MA-*b*-PMMA-*b*-PK⁺MA) ionomers in a large range of molecular weights illustrating the effect of the architecture on the observed ionomer morphology. However, most commercial ionomers such as Surlyn® and Nafion® are random ionomers, in which ionic functionalities are randomly distributed along the polymer backbone. Several models[13-16] have been proposed to describe the morphology and the structure–property relationships of the random ionomers during the last 25 years. However, a general consensus on the correct model of ionomer structure and properties is lacking, though the model proposed by Eisenberg, Hird, and Moore (EHM model) is the most acceptable for random ionomers.[4]

In this chapter, the morphological features of two types of ionomers are investigated. Poly(methyl methacrylate) random ionomers and amorphous telechelic polyester ionomers based on isophthalic acid are selected because of their proven performance in the coatings applications. Compared to crystalline ionomers, amorphous ionomers are more suitable for studying the effect of ionic interactions on the morphology and on the structure-property relationships to avoid the complexities arising from crystalline domains. Since the present chapter focuses on the investigation of structure–morphology–property relationships of PMMA and polyester ionomers, the following section will briefly describe the relevant results pertaining to these systems.

PMMA ionomers

The morphological features and dynamic mechanical properties of poly(methyl methacrylate-*co*-sodium methacrylate) [P(MMA-*co*-Na⁺MA)) ionomers with 6, 12 and 24 mol % ion content were recently described.[17,18] PMMA based acid precursors were prepared by either hydrolysis of PMMA or by random copolymerization of methyl methacrylate and methacrylic acid.

PMMA ionomers with sodium (Na) as counter ion were prepared by solution neutralization of the acid precursors. Dynamic mechanical thermal analysis (DMTA) was used to study the morphology of these PMMA ionomers. DMTA results indicated the presence of two separate tan δ (mechanical loss) peaks.[17] The lower temperature peak is associated to the glass transition, T_{g1}, of the hydrocarbon-rich matrix phase and the higher temperature peak is a result of the glass transition, T_{g2}, of the ion-rich cluster phase. A decrease in the intensity of the matrix peak and an increase in intensity of the cluster peak were found with increasing ion content. Furthermore, the secondary (β)-transition peak, reflecting the local motion of the side groups of PMMA, was spread into two in the PMMA ionomer indicating the presence of two different environments corresponding presumably to the cluster phase and the matrix phase. However, no small angle X-ray scattering (SAXS) data were available on these clustered PMMA ionomer samples.

Contradictory to the P(MMA-*co*-Na$^+$MA) ionomers, a single T_g was found in the DMTA analysis of the poly(methylmethacrylate-*co*-cesium methacrylate) [P(MMA-*co*-Cs$^+$MA)] ionomers with an ion content of 10 mol %.[19] A gradual increase in T_g was found upon increasing the ion content. However, the absence of second dynamic mechanical peak in the tan δ curve as well as the absence of a second inflection point in the dynamic storage modulus curve suggested that the ion-rich cluster phase was absent in these ionomers. Moreover, no SAXS peak was observed for the cesium-neutralized ionomers.[20] Thus, it was concluded that the cesium (Cs) neutralized PMMA ionomer is unclustered. These discrepancies were attributed to the differences in the counter-ions, i.e., Cs and Na. The larger size of the Cs counterion hindered the clustering of the multiplets compared to the smaller Na counterion. Also, the possible effect of water absorption disrupting the clusters was mentioned. Cs ionomers were obtained by precipitation into water, followed by vacuum drying at 160 $^\circ$C for 2 days prior to molding, while Na ionomers were freeze-dried in benzene/methanol (90/10, v/v), followed by vacuum drying for one week. The amount of remaining water, if any, could be higher in the precipitated samples than in the freeze-dried samples.

Plasticization of the P(MMA-*co*-CsMA) ionomer induced multiplet formation.[21] Non-polar plasticizers such as dioctyl phthalate and 4-decylaniline induced multiplet formation resulting in a SAXS peak. It was concluded that plasticization reduces the matrix T_g strongly, which makes electrostatic forces relatively more important than the elastic forces of the polymer chains. As a result, the extent of association of ionic groups is increased due to the increased thermal mobility of the polymer chains, which also increases the electrostatic interaction between the ionic groups. The characteristic average Bragg distance (calculated from the SAXS peak) was between 50 to 70 Å, which is still too large for the PMMA ionomer to have a significant amount of the cluster phase.[21]

These studies suggest that morphological features of the ionomers with a high dielectric constant matrix such as PMMA depend strongly on the counter ion used for neutralization and the extent of plasticization.   Further studies are needed for a complete understanding of the structure–morphology–property relationships in the PMMA ionomer.

Polyester ionomers

Most studies on synthetic, structural, and physical properties on ionomers to date have been focused on addition-type polymers,[1] e.g., polyethylene, polystyrene, PMMA, and polyisobutylene, with a few cases in which the ionic functionalities are introduced via a condensation process.[22-25] The range of ion-containing structures can be substantially broadened with condensation-type synthetic techniques. Interesting examples of these structures can include polyesters, polyamides, polycarbonates, and polyimides. It is well known that polyesters as one of the important engineering polymers offer a broad range of physical properties such as combined heat and chemical resistance, dimensional stability, and mechanical strength. Several research groups investigated the structure–morphology–property relationships of polyester ionomers.[26-29] The ionic groups can be introduced through copolymerization or by post-polymerization modification of the polyesters. Sulfonated polyethylene terephthalate (PET) and polybutylene terephthalate (PBT)[23] ionomers were prepared by random copolymerization of an ionic functional comonomer, i.e., dimethyl 5-sodiosulfo-1,3-phenylene dicarboxylate (Na-SIP). Several characterization techniques, such as DSC, SAXS, DMTA and WAXS were used to study the crystallization and ionic aggregation of polyester ionomers. The nature of the ionic aggregation and microphase separation of ionic groups in semi-crystalline polymers may not be necessarily identical to that found in completely amorphous ion-containing polymers, especially at high crystallinity levels. Similarly, the crystallization process is also influenced by the presence of ionic groups. Small angle light scattering (SALS) and WAXS studies indicated that the crystallinity and crystallization rate decreases with increasing ion content and is completely eliminated at the highest sulfonation level.[23] The change from bulk crystallization to bulk ionomer formation occurred at 8-12 mol % of the SIP. However, similar to amorphous ionomers, crystalline ionomers showed a higher stiffness, T_g, and melt viscosity than their non-ionic homologues. Polyester ionomers are used as functional compatibilizers, adhesives and viscosity modifiers. Melt rheology studies on well-defined telechelic poly(ethylene isophthalate) (PEI) amorphous ionomers demonstrated that at lower temperatures (< 150 ^{o}C) the ionomers exhibited characteristic mechanical properties indicative of high molecular

weight polymers.[30] At higher temperatures (> 150 $^{\circ}$C), the ionic multiplets disassociated and the melt viscosity decreased, due to which processing is facilitated.

In this chapter, the results of the synthesis, molecular and morphological characterization of the P(MMA-*co*-K^{+}MAA) ionomers and isopthalic acid based polyester ionomers are presented. Carboxylated ionomers are selected because of their weaker associations and higher thermal stability than the sulfonated ionomers.

5.2 Experimental Section

5.2.1 Materials

Methyl methacrylate (MMA, 99%) and methacrylic acid (MAA, 99%) were passed through a column containing inhibitor remover (for removing hydroquinone and monomethyl ether hydroquinone) and stored at –15 $^{\circ}$C. 2,2′-Azobis(2,4-dimethyl valeronitrile) (V-65) (Wako) is stored at –15 $^{\circ}$C and used as received. *N,N*-dimethylformamide (DMF, 99.9%) and potassium hydroxide (KOH) solutions in ethanol (0.1 and 0.5 mol/l) were used as received. However, KOH was standardized each time prior to neutralization of the acid precursors. All chemicals were purchased from Aldrich, except DMF (Merck) and V-65. Isophthalic acid based low molecular weight polyester precursors were obtained from DSM Resins, Zwolle, The Netherlands. Polyesters were obtained with two different acid contents, i.e., 3.7 and 5.4 mol % of carboxylic acid units. The molecular weight of the polyesters was in the range of 3000-6000 g/mol.

5.2.2 Analysis and Measurements

Determination of Apparent Molar Mass and Molar Mass Distribution. Size exclusion chromatography (SEC) measurements were carried out to determine the molecular weights of the P(MMA-*co*-MAA) acid precursors. A Waters GPC equipped with a Waters 600 pump, a Waters 410 differential refractometer (40 °C), a Waters WISP 712 autoinjector (50 µL injection volume), a PL gel (5 µm particles) 50 × 7.5 mm guard column, and two PL gel mixed-D (5 µm particles) 300 × 7.5 mm columns (40 °C) were used. Data acquisition and processing were performed using the Waters Millennium 32 (v32) software. A mixture of tetrahydrofuran (THF, Biosolve, stabilized with butylated hydroxytoluene, BHT) and acetic acid (95:5 volume ratio) was used as eluent at a flow rate of 1.0 mL/min, dilute polymer solutions of 2 mg/mL were made, and 50 µL of this solution was injected for analysis. Calibration was done using polystyrene (PS) standards (Polymer Laboratories, 580–7.1 × 10^{6} g mol^{-1}) and molecular weights were calculated using the universal

calibration principle with Mark–Houwink parameters for PMMA[31] (PMMA: $K = 0.944 \times 10^{-4}$ dL g^{-1}, $a = 0.719$, PS: $K = 1.14 \times 10^{-4}$ dL g^{-1}, $a = 0.716$, THF as solvent and temperature = 25 ^{o}C).

Spectroscopic analysis. FTIR measurements of P(MMA-*co*-MAA) and polyester acid precursors and corresponding ionomers were performed on a BioRad FTS 6000 spectrometer equipped with a UMA500 microscope. Samples were prepared using diamond anvil cells with type IIA diamonds (High Pressure Diamond Optics, Inc.). One hundred scans at a resolution of 4 cm^{-1} were signal-averaged and the BioRad Merlin software was used to analyze the spectra.

Differential scanning calorimetry. DSC measurements were performed to study the glass transition temperature (T$_g$). A Perkin-Elmer Pyris1 DSC apparatus was utilized. Temperature calibration was performed with indium. Polymer samples of 2.5–3.5 mg mass were weighed with a precision balance and encapsulated in standard (crimped) aluminum pans of known mass. Empty pans with almost identical weights were used in the reference side and for the zero line run. A heating and cooling rate of 10 ^{o}C/min was used. The temperature range for polyester samples was 40–180 ^{o}C, while a temperature range of 40–150 ^{o}C was used for methacrylate samples. Bulk ionomer samples were used for DSC analysis.

Thermogravimetric analysis (TGA). The thermal stability of the polymer was measured using a Perkin-Elmer Pyris 6 TGA. Approximately 10 mg of polymer was heated from 40 ºC to 700 ºC with a heating rate of 10 ºC/min and under a N$_2$ flow of 20 ml/min. The results were analyzed using the Pyris 4.01 software.

Small angle X-ray scattering (SAXS). SAXS experiments on methacrylate ionomers were performed on beamline BM26 at the ESRF Grenoble, France. A 2D gas-filled wire frame detector with pixel array dimensions of 512 × 512 was used. The exposure time for each measurement was 180 s. SAXS experiments on polyester ionomers were measured on ID02 beamline at ESRF Grenoble, France. The detector used was an image intensifier coupled to a Frelon CCD camera. Pixel array dimensions were 1024 × 1024. The exposure time for each measurement was 3 s. The wavelength (λ) of the X-rays was 1.0 Å and the sample-to-detector distance was 1.5 m for both types of ionomers. Fully dried bulk polymers were used to study the morphology of the polyester ionomers. Lindemann capillaries were filled with 25–30 mg of the polymer sample and were sealed. The capillary was mounted in a custom designed aluminum holder. However, for methacrylate ionomers compression molded films were used. The SAXS patterns were corrected for the detector response and then were masked in appropriate sections to avoid streak like parasitic scattering contributions from the capillary. The data was finally radially averaged along the

azimuthal angle using the FIT2D program of Dr. Hammersley, ESRF. The characteristic Bragg spacing, d_B ($d_B = 2\pi/q$), was calculated by using the peak maximum of the scattering vector (q_{max}), where $q = 4\pi(\sin\theta)/\lambda$ and 2θ is the scattering angle. The scattering angle was calibrated by using collagen of a rat-tail. The resulting d values have an experimental accuracy of ± 0.01 Å.

Dynamic Mechanical Thermal Analysis (DMTA). Samples for DMTA were made using compression molding. Sufficient amounts of powder were put into a 0.2 mm thick mold (40 × 20 mm). The mold containing the powder was pre-heated in the press at 220 ºC and a pressure of 80 bar was applied for 25 min. The pressure was released several times during this step to allow for degassing. Finally, the mold was cooled down to room temperature (water cooling) under the same pressure. The compression-molded plates were cut into rectangular samples and these samples were measured on a DMA 2980 (TA Instruments). A temperature sweep with a heating rate of 4 ºC/min was performed during a dynamic test (tensile rectangular film mode) at a frequency of 1 Hz and with amplitude of 20 μm. For some of the measurements, a certain preload was applied.

5.2.3 Synthetic Procedures

Preparation of poly(methyl methacrylate-co-methacrylic acid). P(MMA-*co*-MAA) acid copolymers were prepared by solution polymerization of purified methyl methacrylate and methacrylic acid monomers using V-65 as the initiator under an argon atmosphere. HPLC grade DMF was used as the solvent and the reaction temperature was kept at 55 ºC. MMA (59.3 g, 0.593 moles), MAA (2.7 g, 0.031 moles) and DMF (126.4 g, 1.729 moles) were added to a dry 500 ml three-neck round-bottom flask. The flask was sealed with a rubber septum and bubbled with argon for 60 minutes. Next, the initiator V-65 (0.070 g, 0.28 mmole) was added to the flask. The flask was covered with aluminum foil to avoid exposure to light and bubbled with argon for 10 minutes. The flask was immersed in an oil bath at 55 ºC. Polymerization was stopped after 2 h, typically at 10–15 % conversion to restrict the composition drift during the polymerization. The polymer solution was poured in a 50:50 methanol/water mixture to precipitate the polymer. The P(MMA-*co*-MAA) copolymer was filtered off under vacuum and dried in an oven at 80 ºC under vacuum.

Acid value determination. The acid values of P(MMA-*co*-MAA) and polyester acid precursors were determined using a standardized 0.1 M ethanolic KOH solution. The polymer (typically 2 g) was dissolved in THF (50 ml) and a few drops of indicator solution (phenolphthalein, 2 mg/ml in ethanol) were added. The solution was titrated until the color of the solution changed from colorless to pink. The acid value of the polymer, AV (mg KOH/g polymer), was determined by

$$AV = \frac{V * N * M_{KOH}}{m} \qquad\qquad (5.1)$$

where V is the volume of KOH solution added (ml), N is the molarity of the KOH solution (mol/l), M_{KOH} is the molar mass of KOH (56.1 g/mol), and '*m*' is the mass of the polymer (g).

Neutralization of the acid precursors to corresponding ionomers. The dried P(MMA-*co*-MAA) acid precursors (typically 2 g) was neutralized in THF (50 ml) with a standardized 0.1 N ethanolic KOH solution. The end point of neutralization was noted by a color change of the polymer solution from colorless to pink, which is the typical color of the phenolphthalein indicator in the basic solution. At this point, a 3 % excess neutralizing agent was added to obtain complete neutralization. A few ml of ethanol was added to avoid precipitation of the ionomer during the neutralization. The resulting random ionomers were obtained by precipitation in excess *n*-heptane. The solvent was removed using rotary evaporation and the resulting ionomer was recovered. The ionomer was further vacuum dried at 80 ºC for 72 h. It is has to be noted that the 3 % excess neutralization was insufficient to have complete neutralization of the methacrylate random ionomers as indicated by the FTIR analysis, hence some free acid groups were present the ionomer. This point is later used in the results and discussion section.

Two phase solution neutralization for the polyester acid precursors. Polyester ionomers with sodium and zinc counterions were obtained by using a two-phase neutralization[32] procedure as described below. Typically, 10 g of polyester acid precursor was dissolved in a mixture of 90 g toluene and 10 g of isopropanol at room temperature. After complete dissolution, 6.5 g of the aqueous solution containing 1 g of zinc acetate (ZnAc) was added. The two-phase reaction mixture was mixed for 30 min. Then, approximately 45 g of solvent was distilled off and new solvent (toluene/isopropanol) was added to the viscous system to remove the excess of water. The mixture was allowed to homogenize at 80 ºC for 30 min after which the solvent was evaporated and the polymer was dried under vacuum at 80 ºC for 48 hrs. Potassium ionomers of polyesters were obtained from titration method. FTIR spectroscopy was used in the qualitative study of the neutralization procedure. FTIR results indicated that complete neutralization was observed with potassium and sodium counter ions, however some unneutralized acid groups were present with zinc counterion (See Figure 5.11 A).

Nomenclature. The nomenclature used for the samples can be best explained using an example. The designation RC5-1 refers to a random copolymer of MMA and MAA with 5 mol % acid

content. Similarly the designation RC5-1-K$^+$100 refers to the corresponding potassium neutralized ionomer with a degree of neutralization of 100 %. A similar nomenclature is used for polyester (PE) ionomers.

5.3 Molecular characterization of the PMMA ionomers

5.3.1 Synthesis of P(MMA-*co*-MAA) copolymers

The precursor materials for random ionomers, viz. P(MMA-*co*-MAA) random copolymers, were synthesized using FRP. Three different acid contents and two different molecular weights were targeted, viz. 5, 10 and 15 mol % of MAA. The acid values and the mol % MAA of the resulting random copolymers were determined using titration. The results of the synthesis of P(MMA-*co*-MAA) copolymers are given in Table 5.1.

Table 5.1: P(MMA-co-MAA) copolymers synthesized using FRP

Ex. No	[MAA][a] (mole %)	SEC analysis		Acid Value[b] (mg KOH/g)	MAA content[c] (mol %)
		M_n	PDI		
RC5-1	5	101,000	1.78	27.8	4.9
RC5-2	5	127,000	1.75	27.6	4.9
RC10-1	10	105,000	1.86	51.4	9.0
RC10-2	10	133,000	1.87	50.2	8.8
RC15-1	15	112,000	1.86	75.9	13.3
RC15-2	15	126,000	1.84	72.1	12.6

[a]*MAA content of the reaction mixture.* [b]*Average value of two measurements.* [c] [a]*MAA content of the copolymer; Determined from the acid value of the polymer.*

The acid contents determined from the acid value show a reasonable agreement with the theoretical acid content (from the feed ratio during the polymerization) especially at low acid contents (5 mol %). However, at high acid contents, (10 and 15 mol %) the values of the experimental acid content (from titration) are lower than the values of the theoretical acid content. This may be an indication that titration is not a suitable method to measure higher acid contents. Although, the end point of the titration was noted by the appearance of pink color (phenolphthalein color in the basic media), it seems that not all the acid groups are neutralized at the end point. However, it is important to note that all the accessible acid groups are neutralized at the end point. The details of the neutralization are further discussed in the molecular characterization section. One

another possible explanation for the differences in the measured and theoretical acid content is due to the higher reactivity of the MMA compared to MAA during the polymerization, as a result a different composition is obtained for the comonomer mixture (theoretical value) and the copolymer (experimental acid value) at given conversion. However, presence of free acid groups (from the FTIR analysis, See section 5.3.2) in the RC15-1-K$^+$100 rules out the latter explanation. High molecular weight polymers were synthesized, since the so far reported work on the methacrylate ionomers was done at similar molecular weights.[19,20] However, it is important to realize that the melt viscosity of these materials will be high, which may lead to some difficulties in processing of the ionomers.

5.3.2 Neutralization of P(MMA-*co*-MAA) copolymers

Solution neutralization was used to obtain P(MMA-*co*-K$^+$MA) random ionomers. The neutralization is monitored using FTIR spectroscopy. Figure 5.1 shows the FTIR spectra of RC5-1, RC10-1 and RC15-1 and the corresponding ionomers in the carbonyl region. It is evident from Figure 5.1A that the methyl ester of the MMA monomer shows a single broad carbonyl (C=O) band at 1730 cm^{-1}. However, a shoulder in the carbonyl band at 1700 cm^{-1} indicates the presence of the acid dimer structure due to the hydrogen bonding (HB) between two acid groups and is referred to as AA-HB and is represented in Figure 4.8 (See chapter 4).[33] It is evident from Figure 5.1A that the shoulder at 1700 cm^{-1} increases for higher acid contents, indicating the presence of more hydrogen bonding (AA-HB).

A new shoulder band is seen towards lower wave numbers (1700–1680 cm^{-1}) for acid copolymers with higher acid content (RC15-1, Figure 5.1A). Such lower wavenumber band is never seen in the poly((meth)acrylic acid) homopolymer.[33] This band in the FTIR spectrum of the RC15-1 with 15 mol % acid content may be due to the HB between the carbonyl group of methyl ester of MMA and the hydroxyl group of MAA, and is referred to as AE-HB (See Figure 4.8, chapter 4). It is well known that the position of the carbonyl band for the hydrogen bonded ester groups is lower than that of the free ester groups.[34] This is clearly observed as a broad shoulder peak in the region of 1700–1680 cm^{-1} for the highest acid content sample. However, earlier studies indicated that such AE-HB in the homopolymer blends (PMMA/PMAA) and in copolymers of MMA/MAA was observed at 1705 cm^{-1} in the FTIR spectra.[35]
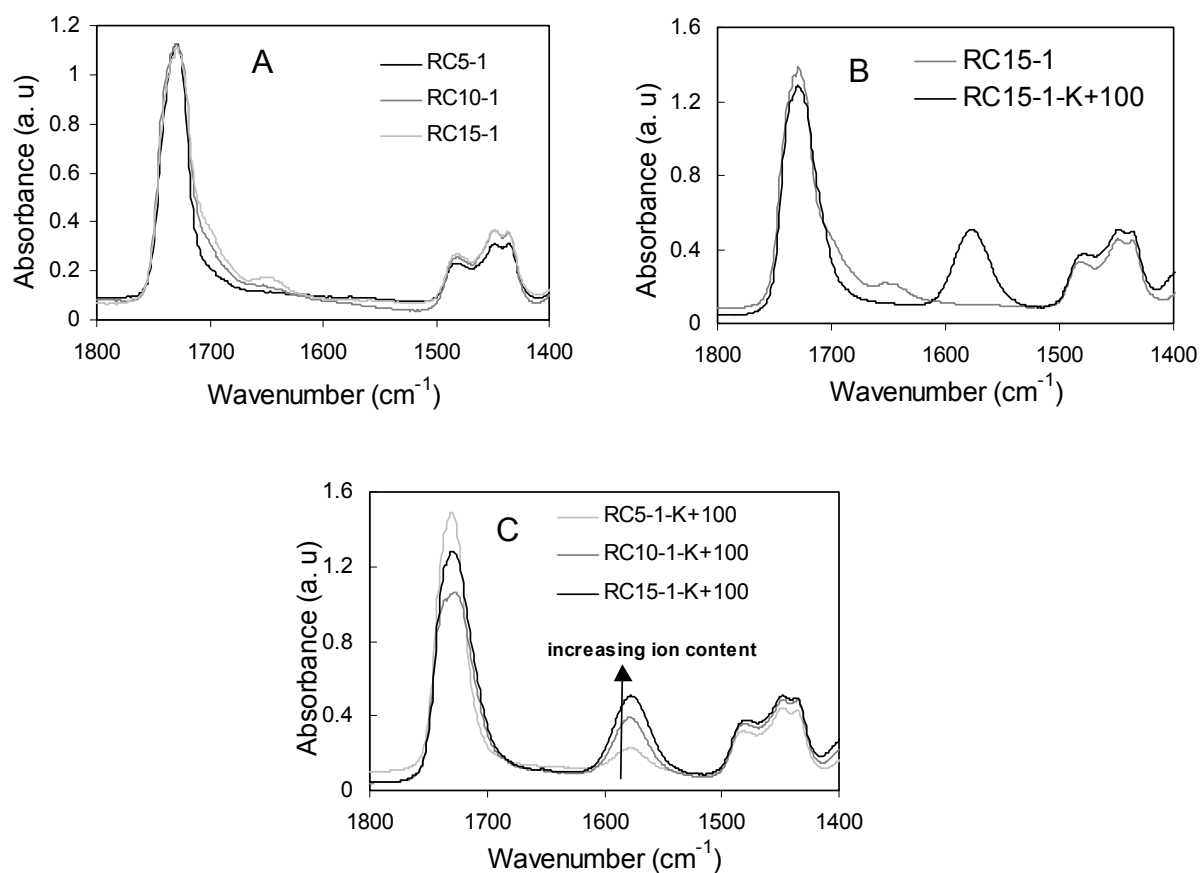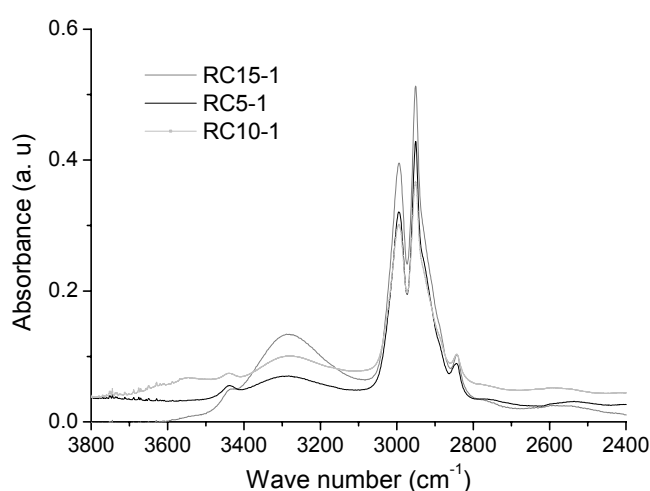
Figure 5.1: *FTIR spectra in the 1400–1800 cm^{-1} region for (A) P(MMA-co-MAA) copolymers with different acid content, (B) RC15-1 and RC15-1-K$^+$100, and (C) random ionomers with different ion content.*

Further evidence of the interaction between the acid and ester functionalities in the P(MMA-*co*-MAA) acid precursor is also shown in Figure 5.2, which shows the hydroxyl (O–H) stretching regions for the copolymer from 3800 to 2400 cm^{-1}. All the three acid copolymers show a major peak with a maximum near 3300 cm^{-1}, which is assigned to the hydroxyl (O–H) stretching of the AE-HB dimer (See Figure 4.8, Chapter 4) formed due to the hydrogen bonding between the carbonyl group of the MMA and the carboxyl acid group of MAA.[36] A small shoulder band with a maximum near 3450 cm^{-1} is assigned to the hydroxyl (O–H) stretching of the unassociated carboxylic acid groups[36] (See Figure 4.8). In addition, the hydroxyl (O–H) stretching of the AA-HB dimer shows a broad peak with a maximum near 3000 cm^{-1} and has a strong overlapping with the C–H stretch. It is important to note that the FTIR spectra of pure poly(methacrylic acid) in the 3600–2400 cm^{-1} region shows a major peak at 3000 cm^{-1} due to the AA-HB and the 3450 cm^{-1} band due to the free unassociated carboxylic acid units.[34,36] It is also clear from Figure 5.2 that as the acid

content increases the area of the band at 3300 cm^{-1} increases, suggesting the increase in AE-HB interaction. Principal component analysis[37] (PCA) can be used to obtain the correct number of the spectral band components contributing to a complex FTIR band and quantitative estimation of each type of HB present in the broad carbonyl or hydroxyl bands. Reliable peak fitting was not possible for the carbonyl band due to the large shoulder in the carbonyl region and for the hydroxyl band due to large overlapping of the C–H stretch band with AA-HB band respectively. Thus, no further attempt was made to obtain quantitative data.
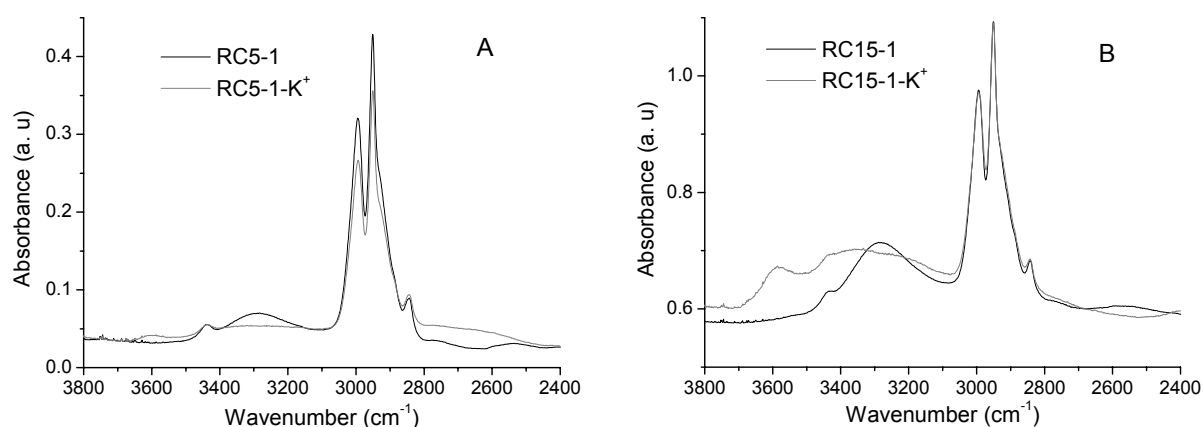

Figure 5.2: *FTIR spectra in the 3800–2400 cm^{-1} region for P(MMA-co-MAA) copolymers at different acid contents.*

The main difference between the RC1-15 and RC1-15-K^{+}100 ionomer (See Figure 5.1B) is the appearance of a new band at approximately 1570 cm^{-1}. This band is arising from the asymmetric C=O stretch of the carboxylate anion and is therefore indicative for the presence of neutralized acid groups.[38] The presence of this band confirms that the neutralization process was successful and that ionic groups are indeed present in the ionomers. It can be seen from Figure 5.1C that the relative height of this band increases with increasing ion content. Furthermore, the width of the carbonyl band in the ionomer is smaller than the width of the carbonyl band in the acid copolymer (see Figure 5.1B), suggesting that neutralization destroys the hydrogen bonding capacity of the acid groups.

Figure 5.3 shows the FTIR spectra of acids, i.e., RC5-1, RC15-1, and corresponding ionomers, i.e., RC5-1-K^{+}, RC15-1-K^{+} respectively in the 3800 to 2600 cm^{-1} region. It is evident

from this figure that the O–H stretch (with a maximum around 3300 cm^{-1}) did not completely disappear for the RC15-1-K$^+$ ionomer. This suggests that the degree of neutralization was not 100%. It is worthwhile to recall that the titration method indicated complete neutralization (appearance of pink color) for this ionomer. This may account for the lower acid values measured for the ionomers with an ion content of 10 and 15 mol %. This observation is further utilized in the morphology section of the chapter.

Figure 5.3: *FTIR spectra in the 3800–2400 cm^{-1} region for P(MMA-co-MAA) and ionomers with (A) 5 mol % ion conent and (B) 15 mol % ion content.*

5.3.3 Thermogravimetric (TGA) analysis of methacrylate random ionomers.

The thermal stability of the ionomers and their precursor materials was studied using TGA. The main purpose of this study is to determine the conditions that can be used for processing of these materials. The weight loss as a function of the temperature is compared for ionomer and the acid precursor under nitrogen atmosphere. The TGA traces of RC15-1 and the corresponding random ionomer are shown in Figure 5.4. These results are representative for other samples. The temperature at which the degradation starts is called the onset temperature (T$_{onset}$). Two steps of degradation can be observed for the acid copolymers. The first step starts at a temperature of about 160 ºC. This first step is related to the intermolecular reaction of acid groups to cyclic anhydrides.[39] The weight loss in this first step increases with increasing acid content. One step degradation can be seen for the random ionomers. This difference between acids and ionomers can be related to the higher reactivity of the acid groups compared to the ionic groups. The weight percentage left after 600 ºC was approximately zero for the acid, and nonzero for the ionomer. This nonzero value is

called as ash content, which increases with increasing ion content. The counterions (K^+) present in the ionomers form inorganic salts during the degradation, which are stable at high temperatures. The thermal stability for these materials follows the order: acid copolymer < random ionomer.
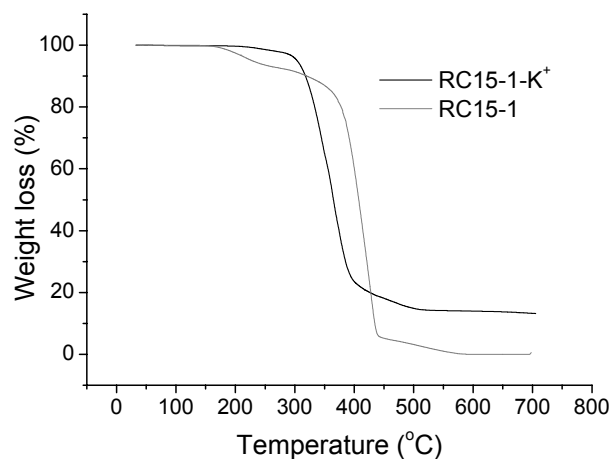
Figure 5.4: *TGA traces of RC15-1 and RC15-1-K^+ 100 recorded under nitrogen atmosphere.*

## 5.4 Morphological characterization of the PMMA ionomers

5.4.1 Results

Small angle X-ray scattering (SAXS), dynamic mechanical thermal analysis (DMTA), and differential scanning calorimetry (DSC) were used to understand the morphological features of the random ionomers.

5.4.1.1 SAXS analysis. SAXS measurements were performed on thin compression molded ionomer samples. The results of the SAXS study on the compression-molded samples of methacrylate random ionomers are shown in Figure 5.5. It is quite clear that broad SAXS peaks are (q = 0.05 to 0.3 $Å^{-1}$) observed for all the ionomers except for the 5 mol % acid content, for which no clear maximum is seen in the SAXS pattern. At a given molecular weight, the peaks become more pronounced as the ion content is increased. Generally, the width (width of the peak at half height) of the SAXS peak is related to the distribution of distances between scattering centers. It is evident that a large peak width is seen for all the ionomers irrespective of the ionic content.

The position of the peak maximum (q-value at the peak maximum) was determined only for the ionomers with an ion content of 10 and 15 mol %, and the broadness of the peak complicated an

accurate determination. Accurate q-values could only be determined for RC15-1-K$^+$100 and RC10-2-K$^+$100 (0.082 and 0.086 Å^{-1} respectively). The corresponding d-spacings are 77 and 73 Å. Another feature in the SAXS pattern is that the peaks become less pronounced as the molecular weight of the ionomers is increased, especially for the ion contents of 10 and 15 mol %. This indicates that the morphology for ionomers with higher M_n is less organized than the lower M_n. The increase in viscosity at higher M_n reduces the mobility of the chains to form regular multiplets with a strong correlation. Upon careful investigation of Figure 5.5, for the ionomers with $M_n \sim 100,000$ g/mol (Figure 5.5A) the peak maximum shifts to lower q-values (and higher d-spacings) as the ion content increases from 10 to 15 mol %. However, for higher M_n, (Figure 5.5B) a clear trend is not observed with increasing ionic content.
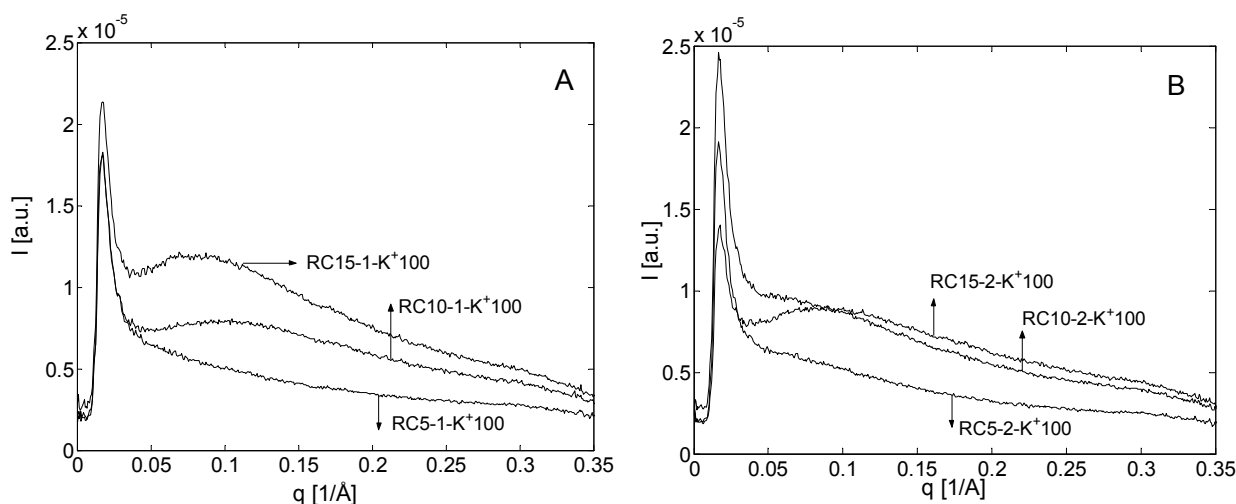
Figure 5.5: *SAXS profiles for methacrylate ionomers with different ion contents 5, 10, and 15 mol %) and comparable mo lecular weights (A) $M_n \sim 100$ K, (B) $M_n \sim 120$ K.*

5.4.1.2 Dynamic mechanical thermal analysis (DMTA).   DMTA analysis was performed on RC5-1, RC10-1, RC15-1, and the corresponding ionomers. DMTA is used to determine glass transition temperatures of the acid precursors and the ionomers. The storage modulus (G′) and the tangent of the phase lag (tan δ) as a function of temperature are given for these materials in Figure 5.6. All acids and ionomers show the characteristic dynamic mechanical response for glassy polymers. The storage modulus (Figure 5.6A) decreases gradually upon increasing temperature. A sharp decrease in the storage modulus can be observed at the glass transition temperature. At this temperature, the polymer chains become mobile and the polymer state changes from glassy to rubbery. A peak in tan δ close to the T_g can be observed in Figure 5.6B. The DMTA analysis

suggests that a second dynamic mechanical peak in the tan δ curve and a second inflection point in the dynamic storage modulus are absent in the ionomers. However, a small shoulder peak around 150 °C is seen for the RC15-1-K^{+} ionomer.
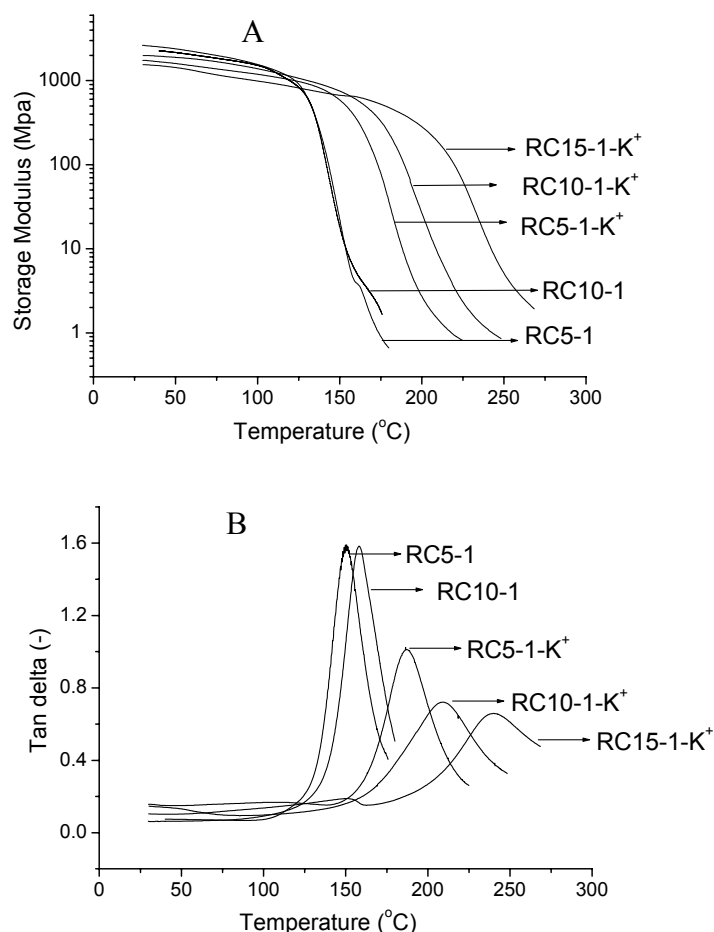
Figure 5.6: *Results of the DMTA experiments for the acids and ionomers; (A) the storage modulus and (B) loss tangent (tan δ) as function of temperature.*

Figure 5.6B suggests that the width of the loss tangent peak associated with the chain mobility increases with increasing ion content. It is important to recall that similar DMTA results were observed in the case of cesium-neutralized PMMA ionomers, which were not clustered.[19,20] After the T_g transition, the decrease in storage modulus levels off and the so-called rubber plateau is reached. In this rubber-elastic region, the rubber plateau modulus (G^0_N) is defined, which can be used to determine the network density[40]. This modulus is defined as the 'most elastic' storage modulus in this region, which is the storage modulus at the minimum of tan δ. However, in all the experiments this minimum is never reached prior to the degradation temperature. Therefore, no

rubber plateau modulus could be determined for these materials. The onset of the reduction in storage modulus is often regarded as a good measure for T_g. The T_g is determined as the temperature at which the tangent of the storage modulus at low temperature (glassy region) intersects the tangent at the maximum decay of the storage modulus.[41] The results of this analysis are given in Table 5.2.

Table 5.2: *Glass transition temperatures (T_g) for the PMMA ionomers and acid precursors measured by DMTA and DSC*

Sample Name	T_g values from DMTA		T_g values from DSC	
	Acid precursor	Ionomer	Acid precursor	Ionomer
RC5-1	126	153	112	144
RC10-1	127	172	111	NA
RC15-1	131	205	110	NA
RC5-2	NA	NA	113	146

5.4.1.3 Differential scanning calorimetry. DSC measurements were performed on all P(MMA-*co*-MAA) copolymers and the corresponding random ionomers. In the DSC experiments the second heating run was used for analysis. Therefore, final temperatures (200 ^{o}C) were chosen below the temperatures at which degradation starts in order to avoid degradation in the first run. The results are given in Table 5.2. The T_g-values of the acid copolymers with the lowest molecular weight are almost constant for all the acid contents. The glass transition temperatures of the ionomers could only be determined for ion contents of 5 mol %. A significant increase in T_g can be seen for the ionomers with an ion content of 5 mol % compared to the corresponding acids. This increase in T_g is caused by the presence of ionic cross-links in the ionomers. The DSC curves for RC5-1 and RC5-1-K$^+$ are shown in Figure 5.7. For 10 and 15 mol % ionomers, no clear T_g was observed within the limits of the DSC heating scan.
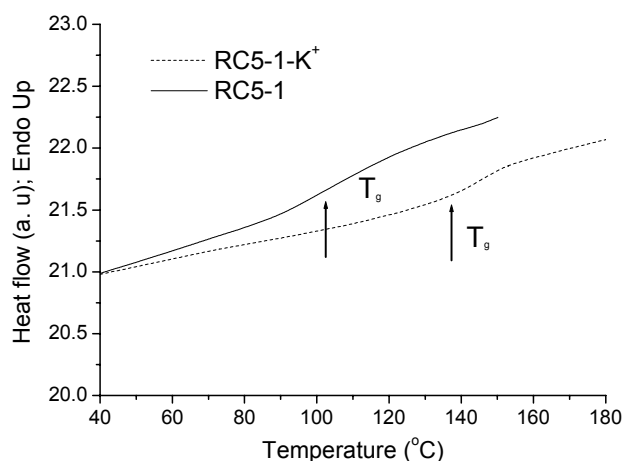
Figure 5.7: *DSC traces of RC5-1 and the corresponding ionomer (RC5-1-K$^+$).*

5.4.2 Discussion

5.4.2.1 SAXS analysis. For a large number of dry ionomers, a small-angle peak is seen in SAXS plot at a q value, which is characteristic for a distance between the scattering centers.[1] It is worthwhile to recall the important concepts of the Eisenberg-Hird-Moore (EHM) model, which is valid for most of the random ionomers, to understand and interpret the morphological features of the PMMA ionomers investigated in this study.[4] A brief summary of the model is given here. According to EHM model, several ion pairs aggregate due to the electrostatic interactions to form multiplets in the nonpolar matrix. The multiplet sizes are 6–8 Å (a few ion pairs). The formation of the multiplets depends on the competition between electrostatic interactions among ion pairs and the elastic forces of the chains to which the ionic groups are attached. A low dielectric constant and T_g of the host polymer favor the aggregation because of strong Coulombic interaction and weak elastic restriction. The sizes of the multiplets depend on the nature of the ionic groups, the dielectric constant of the matrix, the chain stiffness, and distance of the ion pair from the backbone. The mobility of the polymer chains immediately surrounding the multiplet is reduced relative to that of the bulk material and is referred to as restricted mobility layer. The size of the multiplet including the reduced mobility layer is close to 30 Å in diameter and is expected to be too small to manifest its own T_g. Thus a single multiplet will essentially act as a cross-link. With increasing ion content, the number of the multiplets increases leading to overlapping of the restricted mobility regions referred to as clusters. At a particular ion content, the sizes of the clusters exceed the threshold size

for independent phase behavior (50–100 Å), at which point they exhibit their own T_g. The ionomer shows two T_g's, one for the nonpolar matrix and the second one for the clusters.

It is now well established that the "ionic" SAXS peak arises primarily from the most prevalent intermultiplet distance within the clusters (see Figure 1.2, Chapter 1).[1,15] Most of this intermultiplet distances are intracluster spacings; however, some scattering may also be due to distances between multiplets in neighboring clusters, distances between isolated multiplets and those in nearby clusters, or distances between different single multiplets.[4] The SAXS results confirm the formation and presence of the multiplets. A possible explanation for the observed differences in the peak broadness and its distinct maximum at higher ion contents is given here. Multiplets are formed at low ion contents (5 mol %), but most likely their number is only small, so they are dispersed in the PMMA matrix with little correlation between them. The number of multiplets is higher for higher ion contents and the multiplets are distributed with a spatial correlation between them. Therefore, a clear scattering peak maximum with increased intensity can be observed for higher ion contents. The measured intensity in SAXS is proportional to the contrast between the nonpolar hydrocarbon PMMA matrix and polar multiplets ($\Delta\rho$), number of multiplets (N_m), and volume fraction of the multiplets (φ). An increase in ion content, in principle, increases all the above-mentioned factors to a different extent and, hence all factors contribute towards the observed increase in intensity.

Compared to the reported SAXS studies on cesium-neutralized PMMA ionomers, where no SAXS peak was observed, the potassium (K)-neutralized ionomers investigated in this study show a clear SAXS peak.[19,20] To explain the observed difference between the counterions, one should consider the mechanism of the multiplet formation, and the parameters influencing the multiplet formation. A number of factors govern the formation of multiplets in random ionomers, some of which are determined by the ionic species themselves and others by the nature of the host polymer. The most important ionic parameter that affects multiplet formation is the strength of the electrostatic interactions between the ion pairs.[4] The size of the ions and the partially covalent character of the ionic bond determine the electrostatic interaction between the ion pairs. If the electrostatic interactions between ion pairs are too weak to overcome the elastic forces of the chains to which they are attached, no multiplets will form. The characteristics of the host polymer such as low dielectric constant and low T_g tend to favor the ionic aggregation, while a high dielectric constant and/or high T_g tend to inhibit multiplet formation. It is important to note that the dielectric constant (ε) of PMMA ($\varepsilon_{PMMA} = 3$) is higher than of polystyrene ($\varepsilon_{PS} = 2.5$).[42] According to

Eisenberg's theory of multiplet formation, the total number of ion pairs in the multiplet (n_0) can be expressed as the ratio of the volume of the multiplet (V_m) to the volume of an ion pair (V_p), as in

$$n_0 = V_m / V_p \qquad\qquad (5.2)$$

As the radius of the metal ion increases, the volume of a multiplet (V_m) will be decreased.[4] The reason is as follows. In the range of low ion concentration, the ions are assumed to exist in the form of single ion pairs. The ease with which isolated ion pairs would form multiplets is a function of the inter-ion distance. The smaller the energy required to remove an ion pair from the multiplet and the fewer the ion pairs kept in the multiplet. Therefore, V_m will be smaller. Moreover, as the radius of the metal ion increases, the ion pair volume (V_p) increases, so that the average number of ion pairs involved in a multiplet (n_0) becomes smaller [Eq. (5.2)]. Consequently, the ability of the isolated ion pairs to form multiplets decreases, as the radius of the metal ion increases. Thus, the ionomer with cesium as the counter-ion (univalent radius = 169 pm; 1 picometer (pm) = 10^{-12} m) contains no multiplets or fewer than the ionomer with potassium as the counter-ion (univalent radius = 133 pm).[43] This may explain the presence of the SAXS peak in potassium-neutralized PMMA ionomer. It is important to note that the mechanical and viscoelastic properties of the unclustered ionomers are quite different from those of clustered ionomers.[19] Specifically, for the unclustered ionomers, the rubber modulus (above T_g of the matrix) will be lower than the clustered ionomers.

The characteristic d-spacings are 77 and 73 Å for RC10-1-K$^+$100 and RC15-1-K$^+$100. Thus, decreasing the size of the cation, i.e., using potassium as counterion instead of cesium results in the aggregate formation. Similar d-spacing values, i.e., 70–40 Å, were observed in the case of plasticized P(MMA-*co*-Cs$^+$MA) ionomers.[21] Moreover, the DMTA results also indicated the absence of second T_g, i.e., cluster T_g, the plasticized PMMA ionomer. This contradictory results, i.e., presence of SAXS peak and absence of the cluster T_g in the DMTA analysis can be explained by suggesting that the average d-spacing of ca. 70 Å is still too large for the PMMA ionomer to have a significant amount of the cluster phase.[21] Therefore, only a very small percentage of multiplets may exist in the cluster region, which may not show an independent T_g in the DMTA analysis. It is worthwhile to note that the observed d-spacings are substantially higher than the values (~23 Å) reported for clustered polystyrene based ionomers [P(S-*co*-MAA) and P(S-*co*-AA)] with ion contents of 5 and 10 mol %.[44,45]

In this section, an attempt is made, to explain the trend between the observed d-spacings and ion contents for a given M_n. In general, an increase in the ion content increases the number of ion

pairs; consequently, more multiplets will be formed leading to the decrease in the d-spacings. However, the 'low' molecular weight ionomer, i.e., RC1 with M_n = 100 K, shows the opposite behavior. In this case, the increase in the ionic content results in an increase in d-spacings. This observation is surprising and no such opposite relation is reported earlier for PMMA ionomers. The maximum in d-spacings is influenced by (a) ion content, (b) extent of multiplet formation and (c) average distance between the ionic groups along the polymer chain. As the ion content increases, more ion pairs are introduced in the matrix. The increase in number of ion pairs may lead to more multiplets with correlation between them or isolated multiplets or solvated ion pairs depending on the dielectric constant of matrix, T_g, and counterion. All of these forms may contribute towards the broadening of the SAXS peak and, concomitantly, the position of the peak maximum. In random ionomers there is a distribution of distances between the ionic groups along the polymer chain. Very short interionic group distances will probably result in both ion pairs being incorporated into the same multiplet, effectively forming a short loop of polymer chain emanating from the multiplet surface and this distance is called as "loopback" distance.[4] Thus, intergroup distances slightly longer than the "loopback" distance will be dominant in determining intermultiplet distances and will probably give rise to a most prevalent or preferred spacing. In the RC-1 ionomer with M_n = 100 K, as the ion content increases, the distribution of the ionic groups in the ionomer or acid groups in the corresponding acid precursor changes, which may lead to different "loopback" distance. Consequently, a different distribution of the d-spacings may occur at high ion/acid content. Furthermore, it is worthwhile to recall that the FTIR analysis (especially in the O–H region, i.e., 3600–2800 cm^{-1}) indicated incomplete neutralization. The unneutralized acid functionalities and polar methyl ester carbonyl have some significant interactions with the neutralized groups, which may influence the ion pair association, multiplet formation, and their phase separation from the PMMA matrix. This suggests that these favorable interactions also influence the maximum of the SAXS peak. Further experimental work is needed to confirm the abovementioned explanations.

5.4.2.2 DMTA analysis. A characteristic feature of the DMTA of the ionomers is the gradual increase in the glass transition temperature (T_g) and high modulus retention over a large temperature range as the ion content increases. Since the rate of the increase of the T_g of the ionomer with ion content was similar to that for many other ionomers, this is indicative of multiplet formation due to ionic interactions. The absence of a second peak in the tan δ curve as well as the absence of a second inflection point in the dynamic storage modulus curve may indicate that clusters are not present in these ionomers. Further, no rubber-like plateau modulus was observed

over the ion concentration range studied (0–10 %), suggesting that the multiplets dissociate above the T_g. In Figure 5.8, the T_g is plotted as a function of the ion content. The T_g increases linearly with ion content, with a rate of 6.3 $^{\circ}$C/(mol % ion content). This value is higher than the reported value [5.5 $^{\circ}$C/(mol % ion content)] for PMMA ionomers with sodium as counterion.[17] However, it is important to realize that in the latter case two T_g's were observed and the reported value is for the matrix T_g. In our case, a single T_g is seen, which may be resulting from a morphology intermediate between a fully clustered ionomer and an un-clustered ionomer. The fact that the width of the loss tangent peak increases with an increase in ion content may indicate that a wide range of the polymer mobilities are present in the ionomers with high ion content. This observation agrees with the SAXS results, which showed a wide range of intermultiplet distances. It is worthwhile to recall that the mobility of the polymer chains immediately surrounding the multiplet is reduced relative to the bulk material.[4]
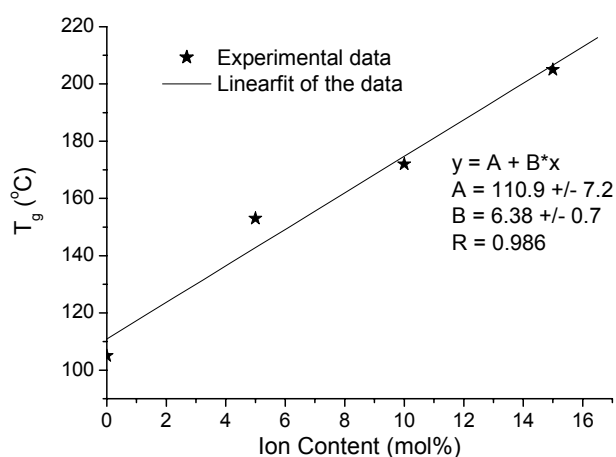
Figure 5.8: *Plot of Glass transition temperatures of PMMA ionomers v*s. ion content as measured by DMTA.

5.4.2.3 Model for the morphology of P(MMA-co-K^{+}MA) ionomers.

An attempt is made in this section to explain the experimental data on the ionomer morphology investigated in this study with existing models described in the literature. The observed morphological features are: (1) the presence of the SAXS ionic peak with a corresponding d-spacing of ~ 70 Å indicating the formation of the multiplets, and (2) the DMTA analysis indicates a single T_g for the ionomer suggesting the absence of clusters in these ionomers. Several models have been proposed to describe the random ionomers morphology over the last 25 years.[13-16] It is now well proved that the origin of the SAXS

peak is due to the intermultiplet scattering, hence only those models, which attribute the SAXS peak to intermultiplet interference will be discussed here.

The EHM model attributes the SAXS peak to intermultiplet interference. However, some scattering may also be due to distances between multiplets and isolated multiplets.[4] The SAXS peak can also be interpreted as distances between phase-separated ion-poor and ion-rich regions, i.e., inter-ion-rich domain distances (similar to block ionomer morphology). The ion-rich regions contain most of the aggregates of multiplets. Nonpolar matrix regions or ion-poor regions contain the isolated ion pairs. However, the observed d-spacings (~ 70 Å) are too small to be interpreted as inter-ion-rich domain distances. Hence we rule out this possibility for our systems. The EHM model predicts that a higher dielectric constant and high T_g hinder the multiplet formation and complete phase separation of the multiplets from the matrix. The absence of a cluster peak in the P(MMA-*co*-K$^+$MA) ionomer is due to the inability of the multiplets to form clusters. To understand this observation parameters that contribute towards the cluster formation have to be reviewed.

According to the EHM model the thickness of the region of restricted mobility surrounding each multiplet is mainly determined by the flexibility of the polymer backbone; the more flexible the chain, the thinner is the region of the restricted mobility.[4] The distance over which polymer segments experience an appreciable restriction in mobility is assumed to be of the order of the persistence length of the bulk polymer. The persistence length is a measure of the distance over which a local inflexibility in a polymer chain persists. This suggests that flexible-chain ionomers with a small value of the persistence length have only a thin region of restricted mobility surrounding each multiplet. The multiplets would thus have to be in very close proximity to one another to have an overlap of the surrounding restricted regions.[4] This would necessitate a large number of overlapping regions in order to form clusters with discernible properties. Thus, the onset of two-phase behavior in flexible ionomers should only occur at significantly higher ion contents than that in ionomers with stiffer chains. This was indeed observed experimentally in PMMA ionomers. The persistence length of the polymer chain in PMMA is ~ 7 Å, whereas for polystyrene it is ~ 10 Å.[4] It was found in PMMA ionomers that cluster formation and phase inversion (i.e., cluster phase with high T_g is more dominant than the matrix phase with low T_g) occur at higher ion contents than in styrene ionomers.[17] Furthermore, one of the key features of the EHM model is that approximately twice the persistence length between multiplets is required for a two-phase behavior (presence of sufficient amount of cluster formation) to be observed. At much larger intermultiplet distances, no overlap of restricted mobility regions occurs, thus resulting in only single observable T_g.[4] The current SAXS results on the P(MMA-*co*-K$^+$MA) indicate a d-spacing of ~ 70 Å, which is

approximately 10 times higher than the persistence length of the PMMA. Very less or no overlapping of the restricted mobility regions occurs in these systems. Consequently, no clusters are formed in the ionomers resulting in a single T_g as indicated by the DMTA analysis. Thus, with the available experimental data we may conclude that the EHM model describes the morphology of the PMMA ionomers investigated in this study. A simplified pictorial representation of the observed morphology is shown in Figure 5.9.
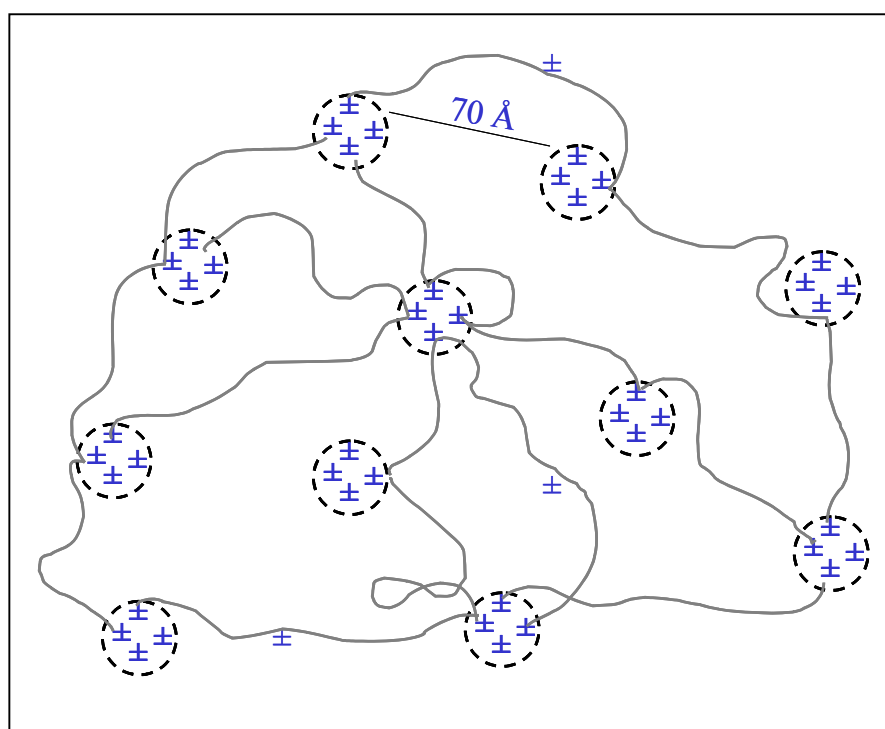
Figure 5.9: *Schematic representation of the observed morphology in the PMMA ionomers investigated in this study.*

The actual morphology could me more complicated. Only multiplets are shown in the Figure and the surrounding restricted mobility regions are not shown. It is important to realize that every single ion pair (±) is attached to a polymer segment. For simple representation, center multiplet is shown with all the polymer segemtents and other multiplets are shown only with one/two polymer chain segments. Further, uniform sizes of the multiplets with same number of ion pairs are considered. Considering the dimensions of polymer chains and those of multiplets and clusters, it seems reasonable that one polymer chain may be anchored to a relatively large number of different multiplets and probably even passes through numerous multiplets. The intermultiplet

region consists of nonionic chain material in the form of long nonionic segments, loops, and chain ends. In addition, this region may contain isolated ion pairs and isolated multiplets. The large increase in the T_g with increase in ion content is due to the restricted mobility of the polymer chain, which essentially passes through many multiplets. It is worthwhile to recall that the increase in T_g via ionic cross-linking is higher than the covalent cross-linking due to the differences in the local structure of the cross-linking point.[46,47]

5.5 Molecular characterization of the polyester ionomers

Low molecular weight isophthalic acid based polyester samples (See Scheme 5.1) were obtained from DSM. Table 5.3 summarizes the characteristics of the polyesters investigated in this study. These polyesters are amorphous in nature due to the asymmetry of the isophthalic acid monomer. The acid content of the polyesters was determined by a volumetric titration method and the resulting acid values are also summarized in Table 5.3. Two different acid contents, i.e., 3.7 and 5.3 mol %, are selected to study the influence of acid content on the ion aggregation and ionomer formation. Molecular weights of the polyesters decreases in the following order PE1 > PE2 > PE3.

Scheme 5.1: Chemical structure of the isophthalic acid based polyester.
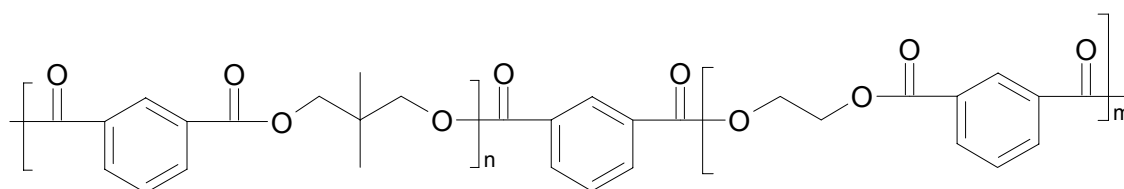
Table 5.3: *Summary of the amorphous polyesters investigated in this study*

Sample code	Acid content (mol %)	Molecular weight M_n (g/mol)	Glass transition Temperature, T_g (^{o}C)
PE1	5.3	6000	59
PE2	5.3	4800	58.5
PE3	3.7	3000	57.5

5.5.1 Neutralization of the acid precursors to ionomers

A two-phase solution neutralization method was used to obtain polyester ionomers. The neutralization process was monitored using FTIR spectroscopy. Figure 5.10A shows the FTIR spectra of PE1 and PE1-K$^+$100 in the carbonyl region. It is seen that a single broad carbonyl (C=O) band at 1730 cm^{-1} assigned to the ester derivative of the isophthalic acid is present in both PE1 and PE1-K$^+$100. Similarly, the bands at 1610 and 1588 cm^{-1} corresponds to the skeletal vibrations involving the C=C stretch of the aromatic rings. These skeletal bands frequently appear as doublets, depending on the nature of the ring substitution. A shoulder band at the 1700 cm^{-1} for PE1 acid precursor suggests the presence of acid dimers. Upon neutralization, the acid groups are converted to the corresponding salts, giving rise to a new band at 1570 cm^{-1} in PE1-K$^+$100. This band is assigned to the asymmetric stretch of the carboxylate anion (COO$^-$) confirming the formation of ionic groups. Furthermore, the shoulder band at 1700 cm^{-1} due to the acid dimer disappears upon neutralization. Figure 5.10B shows the FTIR spectra of the PE1 in the range of 1500–1640 cm^{-1} at different levels of neutralization. It is evident that as the degree of neutralization increases the intensity of the carboxylate asymmetric band increases suggesting the formation of more ionic groups. The peak shape changes from wide to narrow and the peak maximum shifts slightly to higher wavenumbers as the degree of neutralization increases. Moreover, the shoulder skeletal vibration band at 1588 cm^{-1} shifts to a higher wavenumber as the degree of neutralization increases. Similar trends were observed for PE2 and PE3. In earlier studies these observations were accounted to the formation of the multiplets and clusters.[4,13] Upon increasing neutralization, more and more carboxylate ionic groups are formed, which aggregate due to the electrostatic forces present between them. The number of ion pairs involved in aggregation will be increased gradually from dimer, to triplet, quartet, etc., and finally to a multiplet with increasing degree of neutralization. According to the basics of infrared spectroscopy, the frequency number of the absorption peak of a chemical group is proportional to the force constant and distance of the bond. Assuming that these relations can be roughly applied to the multiplet formation then the above mentioned changes in the FTIR spectra for various levels of degree of neutralization can be explained.

At low degrees of neutralization, the concentration of the carboxylate groups is not high enough so ion pairs form small aggregates like, dimers or triplets. The ionic cross-linking bonds involved in the small aggregates are fewer than those involved in the large ion pair aggregates.[48] The presence of a large number of ion pairs in the aggregates leads to a higher number of the ion

cross-linking bonds. As a result, a stronger force constant of the bond and lower distance between the ion pairs is observed. This leads to a higher frequency for large ion aggregates in the FTIR spectra. This means that the frequency for dimers, triplets, quartets, etc., would be gradually shifted to a higher value. Consequently, as the degree of neutralization increases, the concentration of the ionic groups increases, the dominant aggregation form changes from dimer, to triplet, to multiplet. The frequency will shift to higher values. At the same time, owing to the existence of different kinds of ion aggregation, peak overlap occurs and the peak shape changes from broader at low degree of neutralization to narrow at high degree of neutralization.
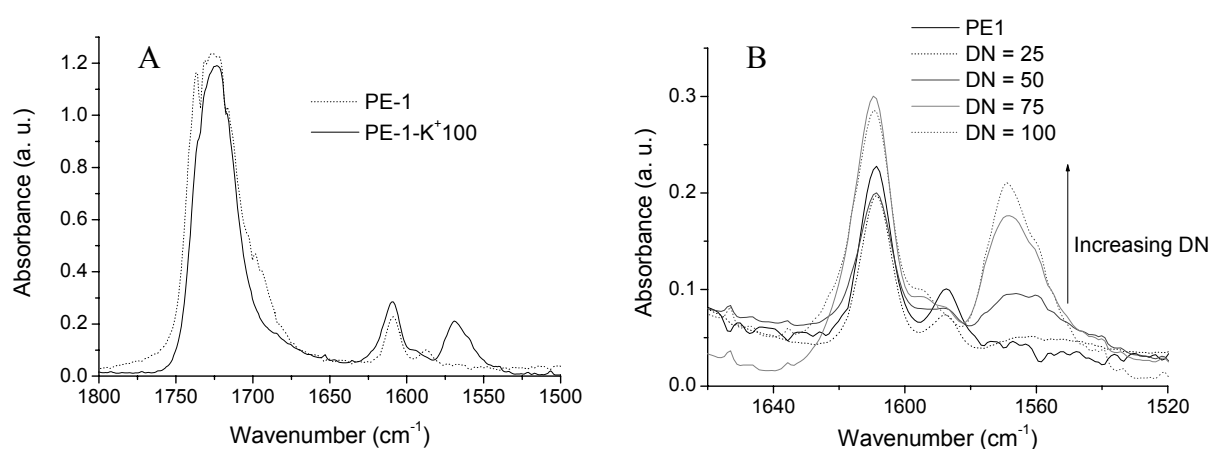

Figure 5.10: *(A) FTIR spectra of the PE1 and PE1-K$^+$100 in the 1500–1800 cm^{-1} range (B) FTIR spectra of the PE1 and corresponding ionomers at different levels of degree of neutralization (DN) in the 1520–1640 cm^{-1} range.*

It is well known that several properties of ionomers are dependent on the type of the counterion. Furthermore, ion aggregate formation and stability are also a strong function of the counterion. To understand the effect of counterion on the ion aggregation, PE1 was neutralized with three different counterions. Figure 5.11A shows the FTIR spectra in the 1660–1500 cm^{-1} region for the PE1 ionomer with K, Na (alkali metals) and Zn (transition metal) counterions. It is evident that K and Na show a similar asymmetric carboxylate band in the corresponding ionomer, indicating the presence of a similar ion aggregate structure. However, the Zn ionomer shows two broad distinct peaks compared to a single peak of the alkali metals. This implies that a different aggregate structure is present in the Zn ionomer. Presence of a weak shoulder peak at 1700 cm^{-1} (See Figure 5.11B) for Zn ionomer indicates incomplete neutralization.

Several research groups investigated the local environment around Zn(II) using FTIR[49-53] and extended X-ray absorption fine structure spectroscopy (EXAFS).[54-58] It has been revealed that the coordination structure around Zn is sensitive to changes in temperature, water absorption and pressure, but there still remain several controversies. The possible coordination structures present in zinc neutralized poly(ethylene-*co*-methacrylic acid) (PEMAA) ionomers are (a) tetrahedral structure of the tetra-coordinated zinc carboxylate multiplet which gives a singlet at 1585 cm^{-1} in the FTIR (shown schematically in a 2-dimensional representation in Figure 5.12C), (b) the hexa-coordinated zinc carboxylate multiplet (HCZnM) which gives a doublet at 1536 cm^{-1} and 1565 cm^{-1} in the FTIR (Figure 5.12D), and (c) hexa-coordinated zinc carboxylic acid salt (HCZnS) which also leads to a doublet at 1537 cm^{-1} and 1620 cm^{-1} in the FTIR (hybrid structure, i.e., coordination structure involves both free acid groups and neutralized groups, Figure 5.12E). It is important to realize that a mixture of the coordination structures is present in the zinc ionomers including some free acid groups (Figure 5.12A) and non-coordinated or isolated ionic groups.
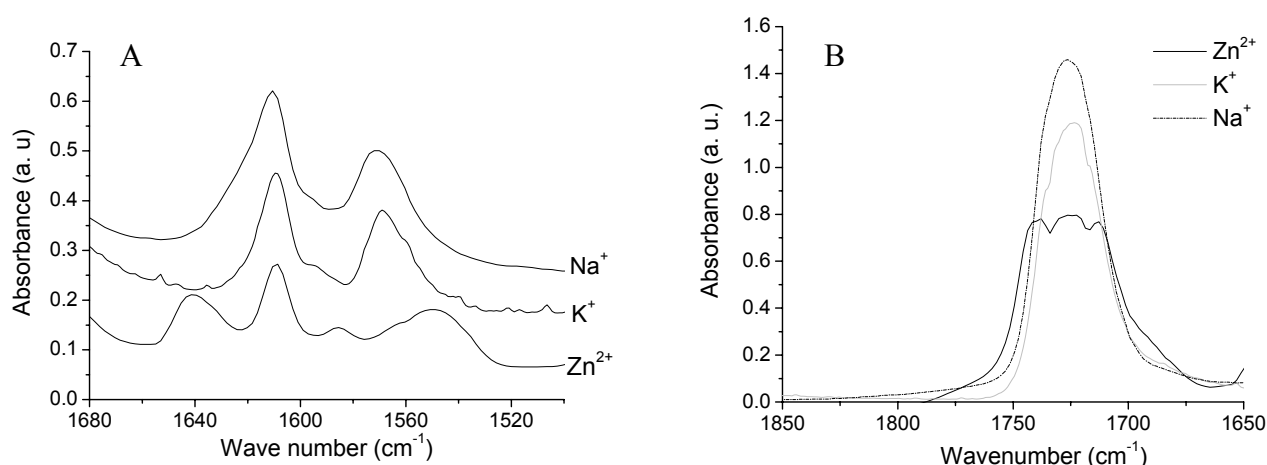
Figure 5.11: *FTIR spectra of PE1 ionomer with potassium, sodium and zinc counterion.*

The complete and accurate FTIR band assignments for the possible zinc coordination structures in the polyester ionomers is more complicated than for the PEMAA ionomer due to the presence of the skeletal vibrations of the aromatic ring bands, which strongly overlap with the zinc coordinated bands. Hence, only a partial assignment of the zinc spectra is presented here. The bands at 1548 and 1640 cm^{-1} are assigned to the hexa-coordinated zinc carboxylate multiplet (HCZnM) and hexa-coordinated zinc acid salt (HCZnS) respectively. However, the broad and asymmetric

nature of these bands indicates that other structures indeed might be present in the ionomer. It is well known that the aggregate structure of the zinc ionomer is sensitive to temperature. Hence, FTIR measurements were performed as a function of temperature in order to elucidate the possible structures present in the zinc ionomer.
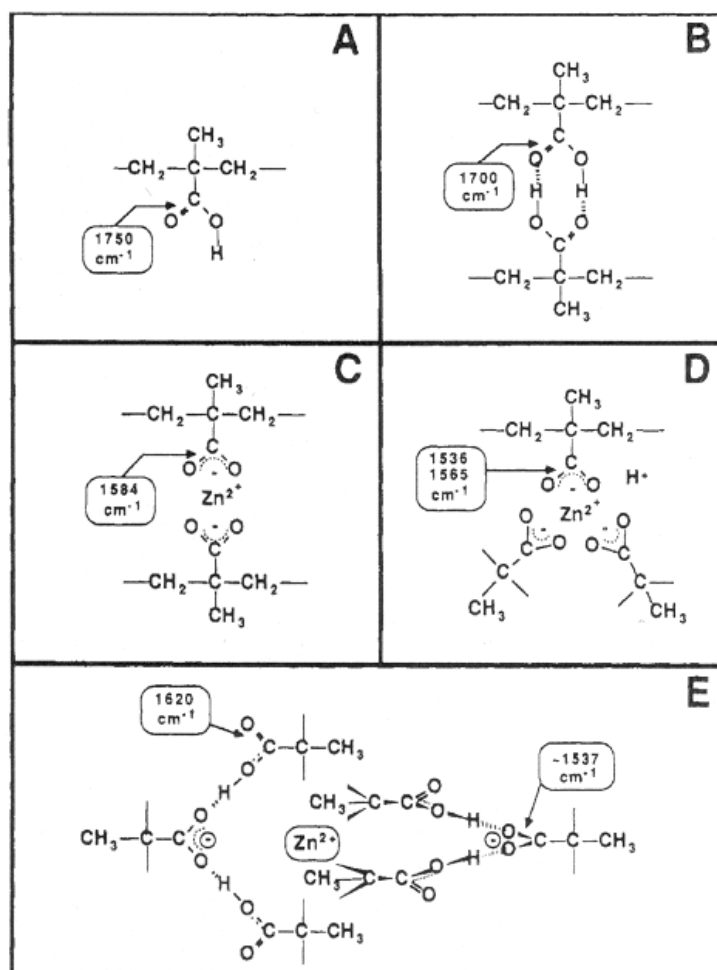
Figure 5.12: *Schematic representation of local structures in zinc ionomer: (A) carboxylic acid "monomer"; (B) carboxylic acid dimer; (C) tetra-coordinated zinc carboxylate; (D) hexa-coordinated zinc carboxylate; (E) zinc acid salt.*

Figure 5.13A and B show the FTIR spectra in the 1680–1500 cm^{-1} range for PE1 and the corresponding zinc ionomer recorded at various temperatures. As expected, the FTIR spectra of PE1 show only the bands from the skeletal vibrations of the aromatic rings, i.e., 1608 cm^{-1} and 1585 cm^{-1}, in the given region. Figure 5.13A indicates that the FTIR spectra of PE1 do not dramatically change upon increasing temperature except for some peak broadening at elevated temperatures.

However, notable changes are observed in the FTIR spectra of the zinc ionomer upon increasing the temperature. At 70 $^{\circ}$C two broad peaks are present with maxima centered around ~ 1547 cm^{-1} and ~ 1640 cm^{-1} due to the hexa-coordinated zinc complexes. Upon increasing the temperature up to 120 $^{\circ}$C, the intensity and width of the hexa-coordinated peaks increase indicating a reorganization of the coordination structures. The enhanced mobility of the polymer chains above the T_g may lead to the incorporation of neighboring isolated ion pairs in to the coordination structures. Upon further increasing the temperature from 120 $^{\circ}$C to 170 $^{\circ}$C, the intensity of the peaks at 1547 and 1640 cm^{-1} decreases and a new peak with maximum at 1566 cm^{-1} appears suggesting the formation of a different coordination structure. The simultaneous decrease in intensity of the hexa-coordinated peaks and increase of the intensity of the new peak at 1566 cm^{-1} may imply that the coordinated structures representing these bands are coupled.
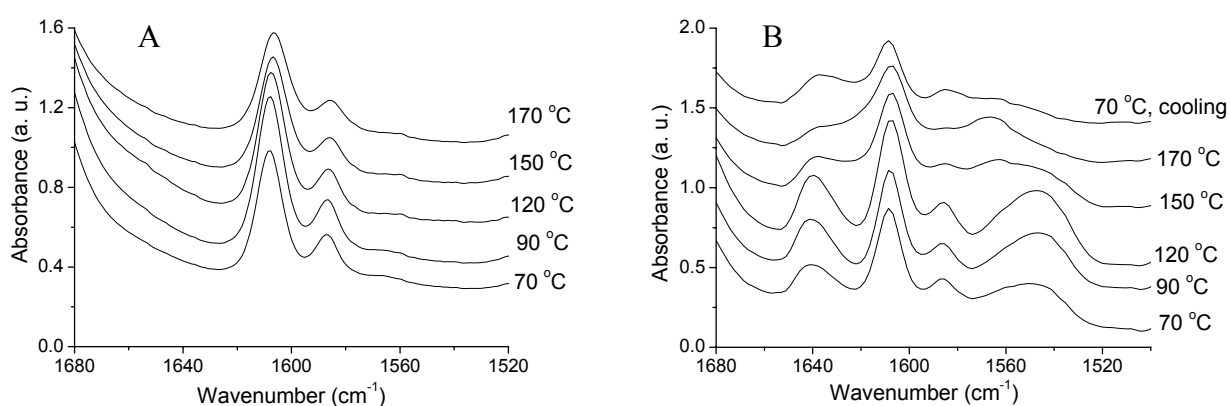
Figure 5.13: *FTIR spectra (A) PE1 and (B) PE1-Zn^{2+}100 at elevated temperatures.*

Similar FTIR studies performed on poly(ethylene-*co*-methacrylate) zinc ionomer showed that at elevated temperatures hexa-coordinated zinc complexes were converted to the corresponding tetra-coordinated (tetrahedral geometry) structures. With this information, the new peak at 1566 cm^{-1} is assigned to the tetra-coordinated zinc aggregates. Moreover, the FTIR spectrum of the ionomer upon cooling from 170 $^{\circ}$C to 70 $^{\circ}$C shows the presence of a mixed coordination structures with differences in the intensity of the peaks. For comparison purposes, FTIR measurements were also performed for the potassium ionomer at elevated temperatures. Figure 5.14 shows the FTIR spectra of the PE1-K^{+}100 ionomer. It is evident that no dramatic changes are seen in the FTIR spectra of the potassium ionomer except peak broadening at high temperatures. This indicates that the

potassium ion forms ionic aggregates that are more stable to temperature than the hexa- and tetracoordinated zinc aggregates.
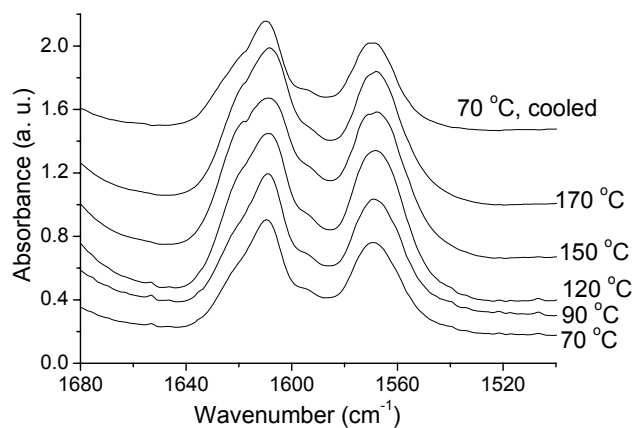

Figure 5.14: *FTIR spectra of the PE1-K$^+$100 at elevated temperatures.*

5.5.2 Thermal characterization of the polyester ionomers

The introduction of ionic groups influences several thermal properties such as the glass transition temperature and thermal stability of the ionomers. Differential scanning calorimetry (DSC) and thermogravimetric analysis (TGA) was used to investigate the thermal properties of the polyester ionomers.

5.5.2.1 Differential Scanning Calorimetry. The DSC profiles of the PE1-K$^+$ ionomers at different degrees of neutralization and the corresponding precursor (PE1) are shown in Figure 5.15 and the T_g's obtained from DSC are listed in Table 5.4. Similar DSC profiles were obtained for the PE2 and PE3 ionomers. A clear glass transition temperature (T_g) is observed for PE1 as expected for an amorphous polymer. The DSC data listed in Table 5.4 and Figure 5.15 indicate that the T_g increases gradually upon increasing the degree of neutralization. It is evident from Table 5.4 that the T_g reaches its maximum at a degree of neutralization of 75 %. Upon neutralization of the PE1 acid precursor, ionic aggregates are formed, which act as physical cross-links between the polymer chains. Hence, the mobility of the chains is reduced, which leads to an increase in T_g. Furthermore, for higher acid contents the T_g is higher, since more aggregates are formed. This is reflected in the T_g values of PE1-K$^+$100 and PE3-K$^+$100 respectively. The former ionomer with high acid content (5.3 mol %) has a higher T_g than the PE3-K$^+$100 ionomer with low acid content (3.7 mol %). The

T_g values from Table 5.4 for the K and Zn forms of the PE1 indicate that T_g is not influenced by the type of counter ion at similar degrees of neutralization (100 %).
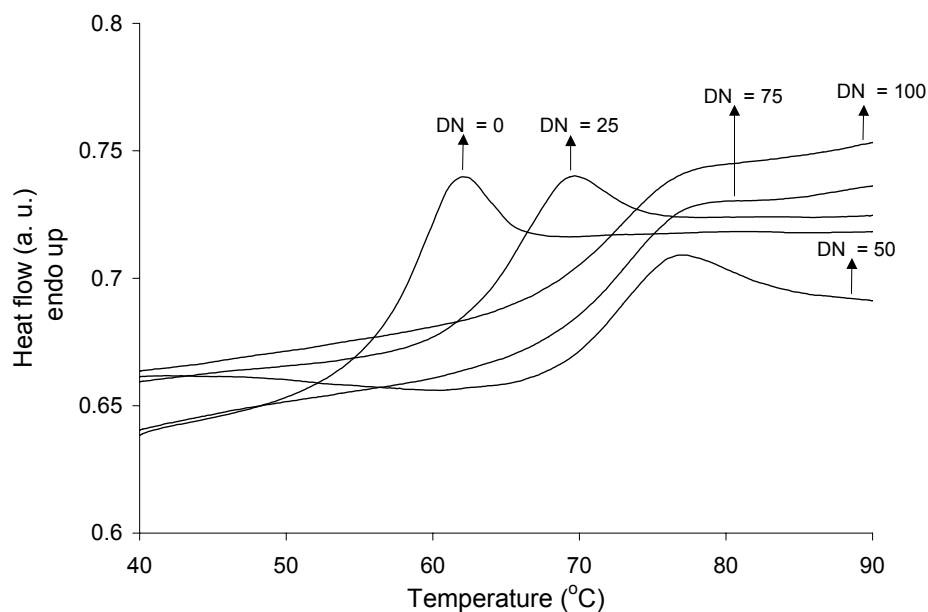
Figure 5.15: *DSC profiles of the PE1 and PE1-K$^+$ at different degrees of neutralization (DN).*

Table 5.4: *Summary of the DSC results of the polyester precursors and corresponding ionomers with K, Na and Zn counterion*

Sample name	Degree of neutralization (DN)	Glass transition temperature (T_g) ^{o}C		
		Potassium ionomer	Sodium Ionomer	Zinc Ionomer
PE1	0	59		
	25	65	64	
	50	68	67	
	75	70	70	65
	100	72	72	71
PE2	0	58.5		
	100	71		
PE3	0	57.5		
	100	64		

5.5.2.2 Thermogravimetric analysis (TGA)

The thermal stability of the polyester acid precursors and corresponding ionomers is determined under nitrogen atmosphere. TGA is only an indirect method to confirm the formation of ionic groups or aggregates. As explained earlier, upon neutralization ionic aggregates are formed which act as cross-links between the polymer chains. The thermal stability of the polymer may be influenced due to the presence of these ionic cross-links. The onset temperature of the degradation (T_{onset}) for the acid precursor and ionomer can reflect the effect of ionic cross-links on the thermal stability of acids and ionomers. All three base polyesters have a similar T_{onset} temperature (~ 225 ^{o}C) confirming the presence of similar backbone structure and similar end groups. Table 5.5 summarizes the data from the TGA analysis. Upon comparing the data from Table 5.5, it is clear that T_{onset} for all ionomers is higher than the corresponding acid precursors, indicating the formation of ionic cross-links. Furthermore, it is evident from Table 5.5 that T_{onset} for PE3-K$^+$100 is lower than T_{onset} for PE1 and PE2 ionomers, indicating the influence of ion content on the thermal stability of the ionomers. At high ion contents, more ionic aggregates are formed, which increase the number of cross-links between the polymer chains. This leads to a higher T_{onset} for higher ion content ionomer than the low ion content. A finite char yield is present for all the ionomers; however, no such char yield is present for acid precursors.

Table 5.5: *Summary of the TGA analysis of the polyesters and corresponding ionomers*

Sample code	T_{onset} (^{o} C)	Char yield at 700 ^{o} C (wt %)
PE1	230	0
PE1-K$^+$100	300	6
PE2	230	0
PE2-K$^+$100	295	5.5
PE3	225	0
PE3-K$^+$100	285	4.5

5.6 Morphological Characterization of Polyester Ionomers

Small angle X-ray scattering is extensively used to investigate the morphology of the ionomers.[1,15,16] The FTIR, DSC and TGA analysis indicated the formation of the ionic groups and association of the ionic groups possibly to ionic aggregates or multiplets. However, these are all indirect techniques to study the formation of the ionic aggregates. SAXS is a powerful technique to

understand the ion association and multiplet formation in the ionomers. Hence, SAXS was utilized to confirm the formation of the multiplets and moreover to investigate the influence of acid number and counterion on the ionomer morphology.

5.6.1 Effect of acid content

Figure 5.16 shows typical SAXS data plotted as scattered intensity I *vs.* q of the PE1, PE1-K^+100 and PE1-K^+75. No scattering peak is seen for the PE1 precursor indicating the homogeneity of the sample. A weak broad scattering peak (clearly deviating from the typical asymptotic decreasing intensity with q of the SAXS curve) is observed for PE1-K^+75 indicating a weak microphase separation. However, a broad single peak called as an *ionic peak* with a distinct maximum is present for PE1-K^+100 signifying a clear microphase separation in the sample. Furthermore, the intensity of the SAXS peak is higher in PE1-K^+100 than PE1-K^+75. It is evident from Figure 5.16 that an increase in degree of neutralization promotes the formation of multiplets. Similar results were observed and explained in the case of PMMA random ionomers (See section 5.4.2.1).
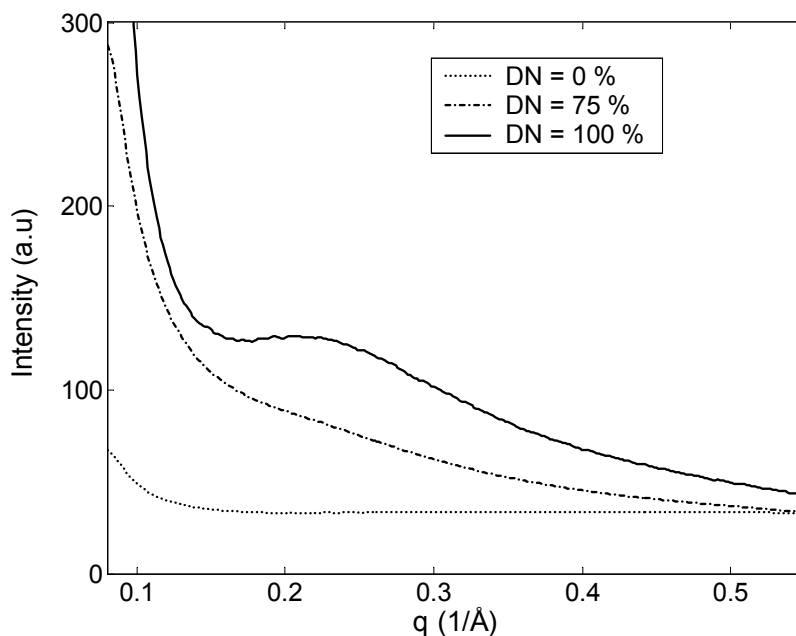
Figure 5.16: *SAXS profiles of PE1, PE1K^+75, and PE1K^+100.*

Figure 5.17 shows typical SAXS data plotted as scattered intensity I vs. q of the PE1-K$^+$100, PE2-K$^+$100 and PE3-K$^+$100 ionomers. Once again, a broad single peak with distinct maximum is present for both PE1-K$^+$100 and PE2-K$^+$100 ionomers with high ionic content suggesting the formation of the multiplets. However, a weak broad scattering peak (clearly deviating from the typical asymptotic nature of the SAXS curve) is observed for PE3-K$^+$100 indicating a weak microphase separation in the sample. PE3 with low ion content shows only a weak microphase separation due to the presence of a low number of multiplets. These results strongly suggest that critical ion content is present in these polyesters to form multiplets with a spatial correlation between them.
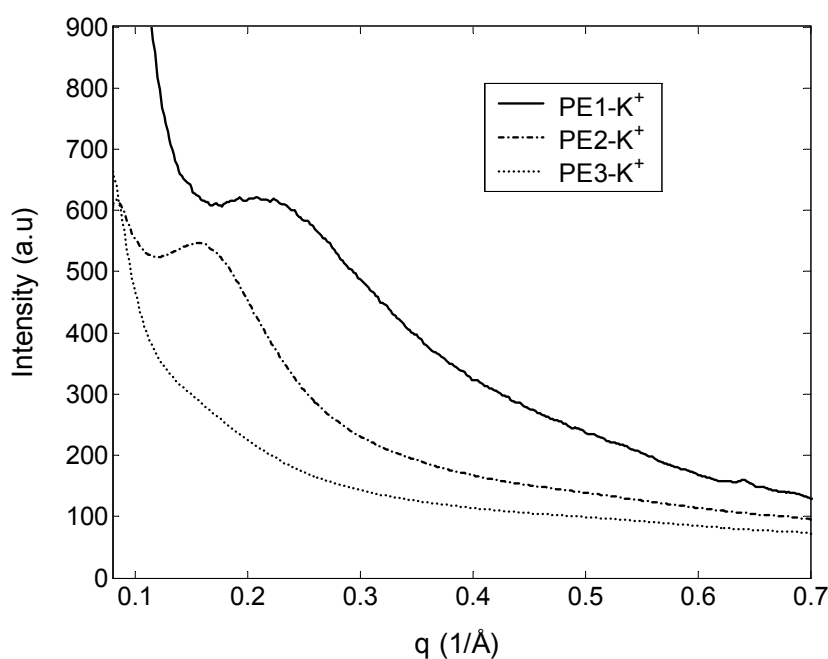
Figure 5.17: *SAXS profiles of PE1, PE2 and PE3; K$^+$ as counterion.*

5.6.2 Effect of counterion

The FTIR studies indicated that the ion association and aggregate formation is a strong function of the counter ion present in the ionomer. This effect is more visible in the ionomers with zinc as the counterion. The FTIR spectrum of the zinc neutralized ionomer showed the presence of various coordinated ionic aggregates such as tetra- and hexa-coordinated structures. This suggests that the multiplet formation and the corresponding SAXS profiles may be a strong function of the counterion used in the preparation of the ionomer. Figure 5.18 shows the SAXS data of the PE1-K$^+$100 and PE1-Zn^{2+}100 ionomers. For comparison, the PE1-K$^+$75 ionomer is also shown in Figure

5.18. Compared to the SAXS profile of the potassium ionomer, a very broad peak is seen for the zinc ionomer. Moreover, the peak covers the entire range similar to that of the SAXS profiles of the PMMA random ionomers (See Figure 5.5). This strongly suggests the presence of a large distribution in size and shape of the ionic multiplets. The SAXS results confirm the FTIR results. The large peak width of the zinc ionomer indicates the presence of large distribution in the intermultiplet distances. It is evident from the SAXS and FTIR results that zinc ionomers form multiplets with various coordination structures compared to the potassium ionomer. Similar SAXS results were obtained in polyethylene ionomers.[59] Bragg's law was applied to determine the characteristic d-spacings or intermultiplet distances for PE1-K$^+$100 and PE2-K$^+$100 ionomers. The corresponding d-spacings are ~ 32 Å for both ionomers. The d-spacings are half of the d-spacings (~ 70 Å) observed for the PMMA random ionomers.
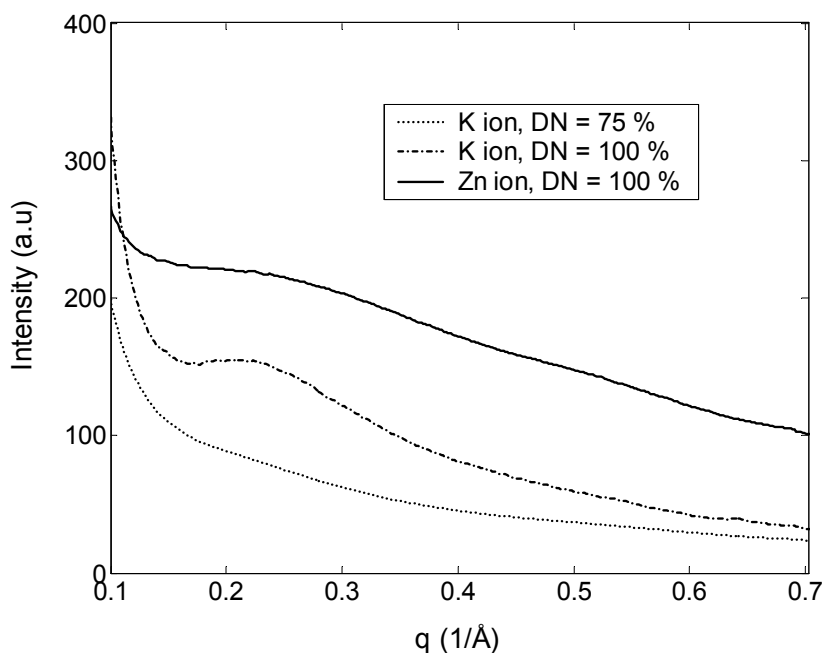
Figure 5.18: *SAXS profiles of PE1K$^+$100, PE1K$^+$75 and PE1Zn^{2+}100.*

5.7 Conclusions

Potassium neutralized poly(methyl methacrylate) (PMMA)-based ionomers containing 5, 10, and 15 mol % ion content and with different molecular weights were prepared by corresponding poly(methyl methacrylate-*co*-methacrylic acid) copolymers, which were synthesized by free radical polymerization of methyl methacrylate and methacrylic acid. Fourier transform infrared spectroscopy (FTIR) was used for molecular characterization of the ionomers and the results

indicate the presence of free acid groups in the ionomers specifically at at 10 and 15 mol % acid content. Small angle X-ray scattering (SAXS) coupled with dynamic mechanical thermal analysis (DMTA) was used to investigate the morphological features of the PMMA ionomers. A distinct SAXS peak with clear maximum was observed only at 10 and 15 mol % ion content. The SAXS results indicate formation and aggregation of multiplets, with a broad range of inter multiplet spacings centered around ~ 70 Å. However, a single glass transition temperature (T_g) was observed in the DMTA analysis implying that no cluster phase is formed in these ionomers. The results of the DMTA indicate that glassy modulus of the ionomers increases over a large temperature range and multiplets dissociate at high temperature. Furthermore, no rubbery modulus is observed in the ionomers. The results obtained are compared with those reported for cesium neutralized PMMA ionomers and are discussed in terms of the Eisenberg, Hird, and Moore (EHM model) multiplet-cluster model. The observed intermultiplet distances in the PMMA ionomers indicate that multiplets are too far apart to form a cluster phase. The high dielectric constant of the PMMA matrix and the presence of strong interactions between the ionic and nonionic groups (from the FTIR analysis) may hinder the formation and aggregation of the multiplets in the PMMA matrix, which may reduce the electrostatic interactions of the ionic groups and retard sufficient overlapping of the multiplets to form a cluster phase. Within the ion content range studied, the T_g increased at a rate of approximately 6 $^{\circ}$C/(mol %).

The synthesis, molecular and morphological characterization of the isophthalic acid based amorphous polyesters with 5.3 and 3.7 mol % acid content were studied to investigate the influence of molecular parameters such as acid content, counter ion, and degree of neutralization on the ionomer morphology. FTIR spectroscopy was used to identify possible coordination structures present in ionomers with zinc as counterion. FTIR spectra measured at room and elevated temperatures indicated the influence of the counter ion on the ion aggregate formation. Zinc counterion forms mixture of tetra- and hexa-coordinated structures, where as potassium forms a single ionic structure. The results of the DSC and the TGA gave an indirect proof for the formation of the ionic cross-links. The T_g of the ionomers increased compared to precursor due to the ionic cross-links. Further, the T_g increases with increasing degree of neutralization and reaches a saturation value at a degree of neutralization of 75 %. The thermal stability of the ionomer was higher than the corresponding precursor. The SAXS results confirmed the multiplet formation and an intermultiplet distance of ~ 35 Å were measured. The results of the SAXS and FTIR indicated the presence of a critical ion content above which a clear microphase separation was formed. The

presence of large distribution of the ionic aggregate sizes and distances in the zinc ionomer was also confirmed by the SAXS analysis.

5.8 References

(1)   Eisenberg A.; Kim, J. S. *Introduction to Ionomers*, John Wiley & Sons, Inc, **1998.**

(2)   Tant, M.R.; Mauritz, K, A.; Wilkes, G. L. Eds. *Ionomers: Synthesis, Structure, Properties and Applications*, Blackie Academic and Professional: London, **1997**.

(3)   Schlick, S. *Ionomers: Characterization, Theory, and Applications.* Ed.; CRC Press: Boca Raton, FL, **1996**.

(4)   Eisenberg, A.; Hird, B.; Moore, R. B. *Macromolecules*, **1990**, 23, 4098.

(5)   Jerome, R.; Broze, G. *Rubb. Chem. Technol.*, **1985**, 58, 223.

(6)   Gauthier, S.; Esenberg, A. *Macromolecules*, **1987**, 20, 760.

(7)   Venkateshwaran, L. N.; York, G. A.; Deporter, C. D.; McGrath, J. E.; Wilkes, G. L. *Polymer*, **1992**, 33, 11, 2277.

(8)   Weiss, R. A.; Sen, A.; Pottic, L. A.; Willis, C. L. *Polymer*, **1991**, 32, 1867.

(9)   Feng, D.; Venkateshwaran, L.; Wilkes, G. L.; Stark, J. E.; Leir. C. M. *J. Appl. Polym. Sci.* **1989**, *37,* 1549.

(10)   Mohajer, Y.; Tyagi, D.; Wilkes, G. L.; Storey, R. F.; Kennedy, J. P. *Polym. Bull.* **1982**, 8, 47.

(11)   Bagrodia, S.; Mohajer, Y.; Wilkes, G. L.; Storey, R. F.; Kennedy, J. P. *Polym. Bull.* **1983**, 9, 174.

(12)   Zheng, F.; Kennedy, J. P. *Journal of Polymer Science: Part A: Polymer Chemistry*, **2002**, 40, 3662.

(13)   Eisenberg, A. *Macromolecules*, **1970**, 3, 147.

(14)   Marx, C. L.; Caulfield, D. F.; Cooper, S. L. *Macromolecules*, **1973**, 6, 3.

(15)   Yarusso, D. J.; Cooper, S. L. *Macromolecules*, **1983**, 16, 1871.

(16)   Kumar, S.; Pineri, M. *J. Poly. Sci., Polym. Phys. Ed.* **1986**, 24, 1767.

(17)   Ma, X.; Sauer, J. A.; Hara, M. *Macromolecules*, **1995**, 28, 3963.

(18)   Ma, X.; Sauer, J. A.; Hara, M. *Macromolecules*, **1995**, 28, 5526.

(19)   Gronowski, A. A.; Jiang, M.; Yeager, H. L.; Wu, H.; Eisenberg, A. *Journal of Membrane Science*, **1993**, 82, 83.

(20)   Jiang, M.; Gronowski, A. A.; Yeager, H. L.; Wu. G.; Kim, J. S.; Eisenberg, A. *Macromolecules*, **1994**, 27, 6541.

(21)   Kim, J. P.; Eisenberg, A. *Polymer Journal*, **1999**, 31(3), 303.

(22)   Molnar, A.; Eisenberg, A. *Macromolecules*, **1992**, 25, 5774.

(23)   Gorda, K. R.; Peiffer, D. G. *Journal of Polymer Science: Part B: Polymer Physics*, **1992**, 30, 281.

(24)   Rao, B. R.; Datye, K. V. *Text. Chem. Color.* **1996**, 28, 17.

(25)   Ng, C. W. A.; Bellinger, M. A.; MaccKnight, W. J. *Polym. Mater. Sci. Eng.* **1993**, 69, 345.

(26)   Blanton, T. N.; Seyler, R. J. *In advances in X-Ray Analysis*; Gilfrich, J. V., Ed.; Plenum Press: New York, **1993**, 379.

(27)   Ng, A. C. W.; Lindway, J.; MacKnight, W. J. *Macromolecules*, **1994**, 27, 3027.

(28) Chen, L.; Yu, X. H.; Yang, C. Z.; Gu, Q. C.; Hu, T. D.; Xie, Y. N. *Journal of Polymer Science: Polymer Physics*, **1997**, 35, 799.

(29) Guo, X. Y.; Gu, L. X.; Feng, X. X. *Journal of Applied Polymer Science*, **2002**, 86, 3660.

(30) Kang, H.; Lin, Q.; Armentrout, R. S.; Long, T. E. *Macromolecules*, **2002**, 35, 8738 .

(31) Beuermann, S.; Paquet, D. A., Jr.; Mc Minn, J. H.; Hutchinson, R. A. *Macromolecules* **1996**, 29, 4206.

(32) Wouters, M. E. L. *Ph D Thesis*, Eindhoven University of Technology, **2000**.

(33) Dong, J; Ozaki, Y.; Nakashima, K.; *Macromolecules*, **1997**, *30*, 1111.

(34) Lin-Vien, D.; Colthup, N, B.; Fateley, W. G.; and Grasselli, J. G. *The handbook of Infrared and Raman Chracteristic Frequencies of Organic Molecules*, Academic Press, **1991**, 117.

(35) Huang, C. F.; Chang, F. C. *Polymer*, **2003**, 44, 2965.

(36) Jo, W. H.; Cruz, C. A.; Paul, D. R. *Journal of Polymer Science: Part B: Polymer Physics,* **1989**, 27, 1057.

(37) Malinowski, E. *J. Chemom.* 1, **1987**, 33.

(38) Han, K.; Williams, H. L. *Journal of Applied Polymer Science*, **1991**, 42, 1845.

(39) Guegan, P.; Cernohous, J.J.; Khandpur, A.K.; Hoye. T.R.; Macosko, C.W. *Macromolecules*, **1996**, *29*, 4605.

(40) Young, R. J. *Introduction to Polymers*, p. 232, Chapman and Hall Ltd., **1989.**

(41) van Melick, H. *Ph.D thesis*, Eindhoven University of Technology, **2002**.

(42) Brandrup, J.; Immergut, E. H.; Grulke, E. A. *Polymer Hand Book*, VII 1, **1999**, John Wiley & Sons, Inc.

(43) Huheey, J. E. *Inorganic Chemistry*, Harper & Row, New York, **1978**, p. 70.

(44) Fitzgerald, J. J.; Weiss, R. A. *J. Macromol. Sci., Rev. Macromol. Chem. Phys.* **1988**, C28, 99.

(45) Kim, J. S.; Wu, G.; Eisenberg, A. *Macromolecules*, **1994**, 27, 814.

(46) Jantas, R.; Szocik, H.; Michalek, M. *Poly. Bull,* **1998**, 41, 161.

(47) Sharaf, M. A.;Hassan, M. K. *Polymeric Materials: Science & Engineering,* **2003**, 89, 584.

(48) Han, K.; Williams, H. L. *Journal of Applied Polymer Science*, **1991**, 42, 1845.

(49) Coleman, M. M.; Lee, J. Y.; Painter, P. C. *Macromolecules*, **1990**, 23, 2339.

(50) Ishioka, T. *Polym. J.* **1993**, 25, 1147.

(51) Yano, S.; Nakamura, M.; Kutsumizu, S. *Chem. Commun.* **1999**, 1465.

(52) Kutsumizu, S.; Tadano, K.; Matsuda, Y.; Goto, M.; Tachino, H.; Hara, H.; Hirasawa, E.; Tagawa, H.; Muroga, Y.; Yano, S. *Macromolecules*, **2000**, 33, 9044.

(53) Kutsumizu, S.; Nakamura, M.; Yano, S. *Macromolecules*, **2001**, 34, 3033.

(54) Tsunashima, K.; Nishioji, H.; Hirasawa, E.; Yano, S. *Polymer*, **1992**, 33, 1809.

(55) Grady, B. P.; Floyd, J. A.; Genetti, W. B.; Vanhoorne, P.; Register, R. A. *Polymer*, **1999**, 40, 283.

(56) Welty, A.; Oooi, S.; Grady, B. P. *Macromolecules*, **1999**, 32, 2989.

(57) Farrell, K. Vl.; Grady, B. P. *Macromolecules*, **2000**, 33, 7122.

(58) Hashimoto, H.; Kutsumizu, S.; Tsunahima, K.; Yano, S. *Macromolecules*, **2001**, 34, 1515.

(59) Kutumizu , S.; Tagawas, H.; Muroga, Y.; Yano. S. Macromolecules, **2000**, 33, 3818.

Chapter 6

The Effect of Ionic cross-links on the Deformation behavior of PMMA

ABSTRACT: Simultaneous time resolved small angle X-ray scattering (SAXS) coupled with tensile testing was used to investigate the deformation behavior and craze initiation in poly(methyl methacrylate) (PMMA), poly(methyl methacrylate-*co*-methacrylic acid) copolymers and corresponding potassium ionomers. Craze initiation was suppressed in acid copolymers and ionomers compared to PMMA due to the presence of intermolecular interactions. The effective network density of ionomers is increased due to ionic cross-links, as a result crazing is supressed. A similar effect of an increase in network density due to the hydrogen bonding in acid copolymers, although to lesser extent, is responsible for the observed changes in the acid copolymers. It was also observed that ionomers with high molecular weight (M_n = 100 K), high acid content (10 mol %), and a high degree of neutralization (DN = 100) showed a lower strain at break due to the large number of the ionic cross-links and these samples broke prior to craze formation. However, PMMA ionomers with low molecular weight (M_n = 40 K) and low degree of neutralization (DN = 25, 75%) showed a good balance between increase in craze initiation stress and the maximum strain at break.

Uniaxial compression tests were used to study the intrinsic deformation behavior of the PMMAs synthesized by atom transfer radical polymerization (ATRP, low polydispersity index (PDI)) and free radical polymerization (FRP, high PDI). The glass transition temperature (T_g), yield stress and strain hardening modulus (G_r) for ATRP materials were higher than the FRP materials indicating the effect of the (PDI) on the intrinsic properties of the PMMA. This is due to the low molecular weight tail present in the FRP PMMA, which dilutes the effective network density of the polymer leading to a lower G_r value. Differential scanning calorimetry indicated the presence of a large distribution of thermal mobilities in FRP samples, which may result in a broad and lower T_g. The thermal mobility correction approach explains the differences in the G_r values of the FRP materials and the commercial PMMA (V052; measured at different temperatures).

6.1 Introduction

An important consideration for the use of polymers in engineering applications is an understanding of their response to mechanical loading, which includes both small-strain and large-strain properties, deformation mechanisms, and ultimate failure modes. It is well known that

amorphous glassy polymers exhibit two types of plastic deformation.[1,2] One is shear yielding, which occurs essentially at constant volume and leads to a permanent change in shape. Shear yielding can take place in either highly localized shear bands or diffuse shear deformation zones.[3] Another is crazing. Crazes are small crack-like defects and are connected by super-drawn fibrils. Crazes have due to these fibrils, unlike real cracks, some load-bearing capacity and when viewed on a microscopic level, they display large plastic deformations. The microscopic events that are likely to be involved in craze formation and nucleation is given below. First, plastic deformation starts at a local stress concentration. The non-linear nature of the yield process results in localization of deformation as the plastic strain increases. Since the material at some distance of the local deformation zone is relatively undeformed, the differences in volumetric strain induce a build-up of triaxial stresses. This leads to void formation and nucleation and, finally, crazes are formed in the deformation zone. Unlike shear yielding, crazing is a cavitational process, leading to an increase in volume. Which of these localization phenomena, i.e., shear yielding or crazing prevails is determined by the post-yield behavior, i.e., strain softening and strain hardening.[4,5]

The most striking example is the difference in macroscopic behavior between polystyrene (PS), poly(methyl methacrylate) (PMMA) and polycarbonate (PC). Figure 6.1A and B show the results of tensile and uniaxial compression tests for PS, PMMA and PC. PS and PMMA show brittle behavior, with fracture after only a few percent of strain, as can be seen in Figure 6.1A. PC, on the contrary, shows ductile behavior and deforms by shear yielding. PS exhibits substantial strain softening (See Figure 6.1B) and only a weak contribution of the strain hardening. Localizations of strain, induced during the initial stage of deformation, cannot be stabilized and evolve almost without limits. As a result, this extreme strain localization leads to the initiation of crazes and finally macroscopic failure. PC, on the other hand, exhibits only a moderate amount of strain softening and a stronger contribution of the strain hardening (Figure 6.1B). Localized plastic deformation zones, induced by strain softening, can be stabilized and transfer the deformation to other regions in the material. As a result, a larger volume participates in the deformation and shear yielding and stable necking are observed in a tensile test of PC (Figure 6.1A). However, addition of a notch induces craze initiation in PC.[4,6-8]

Two main strategies employed in increasing the toughness or changing the deformation mechanism from crazing to shear yielding of brittle amorphous polymers, like PMMA and PS, are (I) reducing the strain softening and/or (II) increasing the strain hardening as shown in Figure 6.2. Despite much research, the exact physical origin of the strain softening is not really clear.[9,10] Strain softening can be drastically reduced, or even eliminated, by mechanical pre-conditioning[4,8,11-18] or

pre-deformation and, similar to the yield stress, strain softening is sensitive to temperature, strain rate and pressure.[8,17-21] Furthermore, it is known that strain softening depends on the thermal and mechanical history and the testing conditions. Quenched samples exhibit less strain softening than slowly cooled specimens.[12,18,22,23]
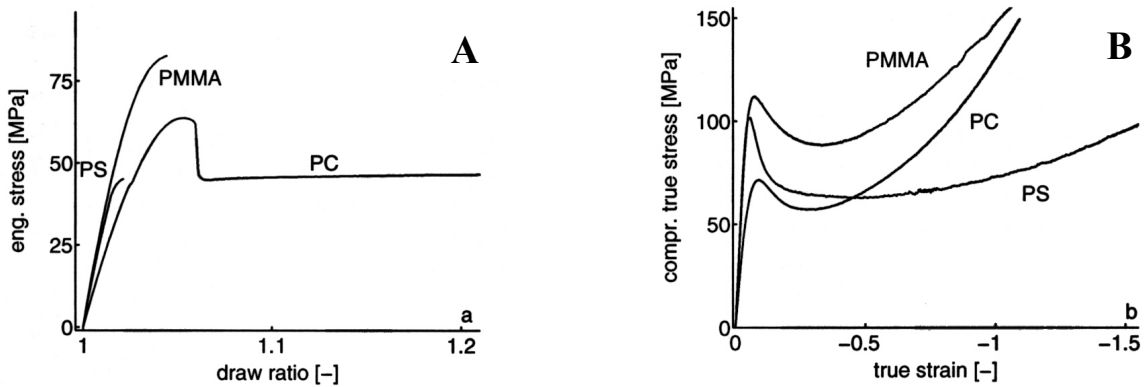
Figure 6.1: *Deformation behavior of PS, PMMA and PC in (A) tension and (B) compression tests.*
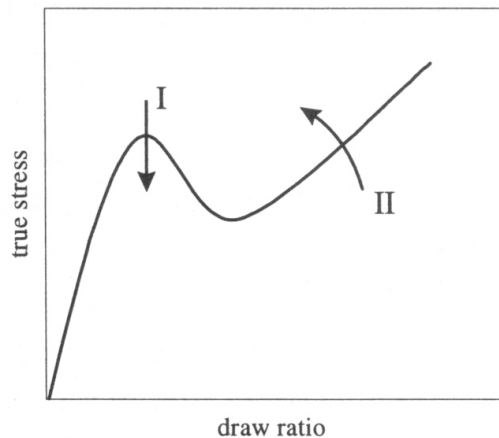
Figure 6.2: *Possible routes to improve material toughness by (I) reducing strain softening and (II) increasing strain hardneing.*

The strain hardening behavior of amorphous and semi-crystalline polymers is studied much more extensively. Strain hardening is regarded as a stress contribution of the entangled polymer network that can be enhanced by increasing the network density (ν).[1,2,6,8] Kramer *et al.*[1,2,6]

investigated changes in the deformation mechanism as a function of total network densities (sum of physical entanglements and covalent cross-links) for covalently cross-linked polymers. Crazing was the only observed deformation mechanism for polymers with $v < 4 \times 10^{25}$ chains/m^3. A combination of crazing and shear yielding occurred for polymers with $4 \times 10^{25} < v < 8 \times 10^{25}$ chains/m^3 and only shear yielding was observed when $v > 8 \times 10^{25}$ chains/m^3. It is important to note that PMMA appears to be an exception to this general rule, because the PMMA homopolymer exhibits only crazing, despite its v- value of 7.8×10^{25} chains/m^3. The apparent drawback of the covalent cross-linking of polymers is that the materials become intractable.

An interesting method to increase the network density is the introduction of cross-links based on ionic interactions. Recently, Hara and co-workers showed that the introduction of ionic cross-links in PS and PMMA resulted in a change in deformation mechanism from crazing to shear yielding.[24-27] These studies were performed on thin film samples under tension by using transmission electron microscopy (TEM). The observed changes in the deformation mechanism of thin films also resulted in improved mechanical properties such as tensile and fatigue of bulk samples of PS ionomers. However, no data are available on bulk samples of PMMA. Moreover, the observed changes in the deformation behavior were only attributed to the increase in the network density because of the additional ionic cross-links present in the ionomers. However, no information about the strain softening behavior of these ionomer samples is available. As explained earlier, strain softening is also an important factor that determines the toughness of the glassy amorphous polymers. To gain a more thorough understanding of how ionic cross-links (ionic aggregates) affect the complete deformation mechanisms of ionomers, it is important to understand the influence of introducing ionic cross-links on the strain softening behavior. Strain softening is dependent on the intermolecular interactions, which are strongly affected by the presence of ionic cross-links. This approach of investigating the intrinsic behavior may increase understanding of the effect of molecular structure on the macroscopic properties of the ionomers. Apart from these studies, as mentioned earlier PMMA is an exceptional glassy amorphous polymer since the macroscopic deformation shows only crazing although based on the network density it should show shear yielding during deformation. To understand this phenomenon and also to get an insight on the intrinsic behavior of the PMMA one has to investigate deformation of the PMMA homopolymers at different molecular weights and polydispersity indices (PDI).

This chapter presents the results of the mechanical properties of bulk specimens of the PMMA ionomers using time resolved small angle X-ray scattering (SAXS). Results on the

deformation behavior and craze initiation for PMMA, poly(methyl methacrylate-*co*-methacrylic acid) [P(MMA-*co*-MAA)] acid precursors and the corresponding potassium ionomers are presented. The effect of the ion content on the craze formation or craze initiation during the deformation is studied by coupling mechanical testing with SAXS. Furthermore, the results of the effect of molecular weight and PDI on the intrinsic deformation behavior of PMMA are also presented. Uniaxial compression tests were used to determine the intrinsic deformation behavior of PMMA. PMMA samples with similar molecular weight but different PDI were prepared by atom transfer radical polymerization (ATRP, low PDI) and conventional free radical polymerization (FRP, high PDI). This gives a unique opportunity to evaluate the ATRP chemistry with FRP chemistry. No such studies have been reported in the literature.
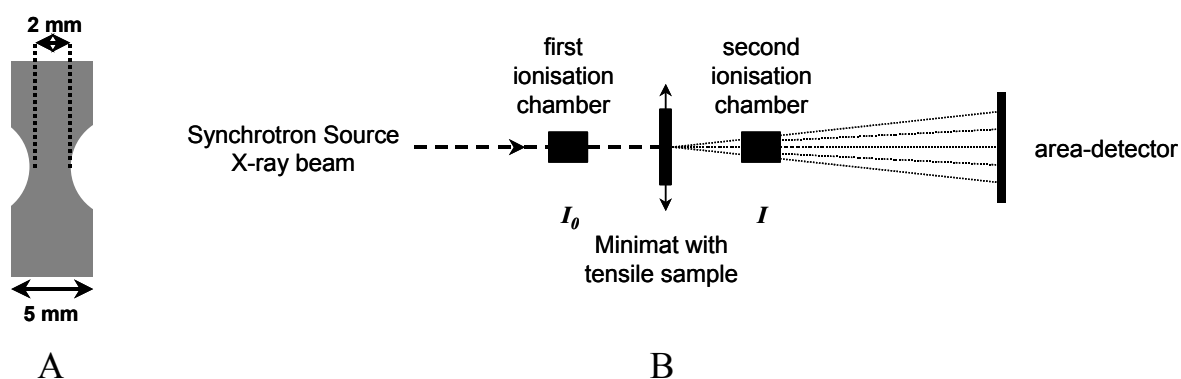
6.2 Experimental Section

6.2.1 Materials

PMMA homopolymers and precursor materials for random ionomers, viz. P(MMA-*co*-MAA) random copolymers, were synthesized using free radical polymerization at three different acid contents, viz. 5, 10 and 15 mol % of MAA. Potassium (K^+) ionomers were obtained by solution neutralization of the acid copolymers with a 0.1N ethanolic potassium hydroxide solution in tetrahydrofuran as solvent. The details of the synthesis, molecular and morphological characterization were described in Chapter 5. PMMA homopolymers with narrow PDI were prepared by using ATRP. This detailed synthesis was described in Chapter 3.

6.2.2 Analysis and Measurements

In-situ SAXS measurements and analysis of the data. Time-resolved SAXS (SAXS) using synchrotron radiation on beam line BM26 at the ESRF (European Synchrotron Radiation Facilities, Grenoble, France) coupled with tensile testing was used to study the microscopic deformation. A 2D gas-filled wire frame detector with pixel array dimensions of 512 × 512 was used. The wavelength (λ) of the X-rays was 1.0 Å and the sample-to-detector distance was 8 m. The test samples, as shown in Figure 6.3A, were stretched using a custom developed miniature tensile machine at a strain rate of 0.05 mm/min. A dog-bone shaped geometry is used in tensile measurements, to ensure that the developed strain due to the applied stress is located at the center of the sample. This will help in focusing the X-ray beam exactly in the local deformation zone. However, it is not possible to determine the actual strains with this geometry. A schematic of the

test set-up is shown in Figure 6.3B. The scattering angle was calibrated by using collagen of a rat-tail. The test samples were made using compression molded films of PMMA ionomers. Figure 6.4 shows the tensile testing machine used in the analysis.
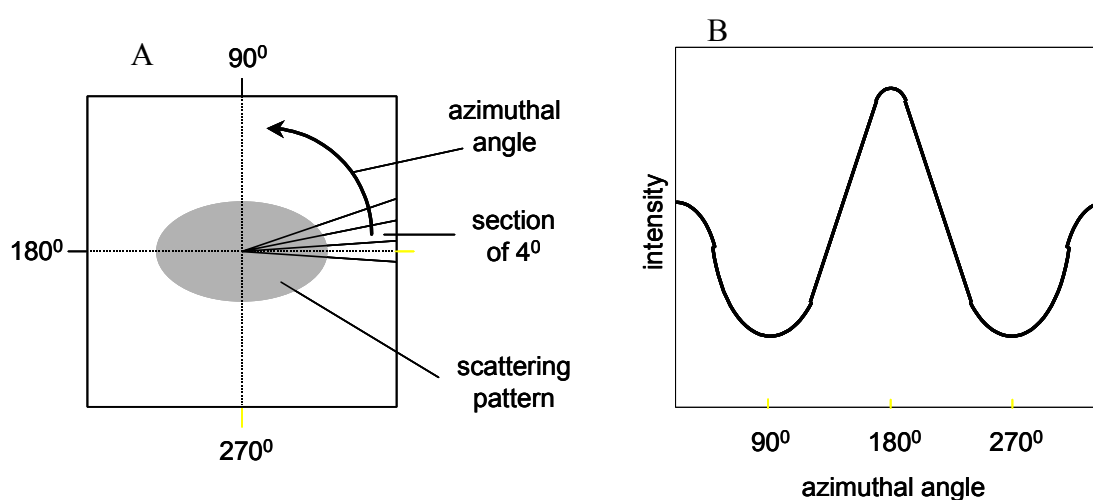

Figure 6.3: *Schematic representation of (A) tensile test bars used in the simultaneous SAXS-tensile experiments and (B) the experimental set-up at the ESRF.*
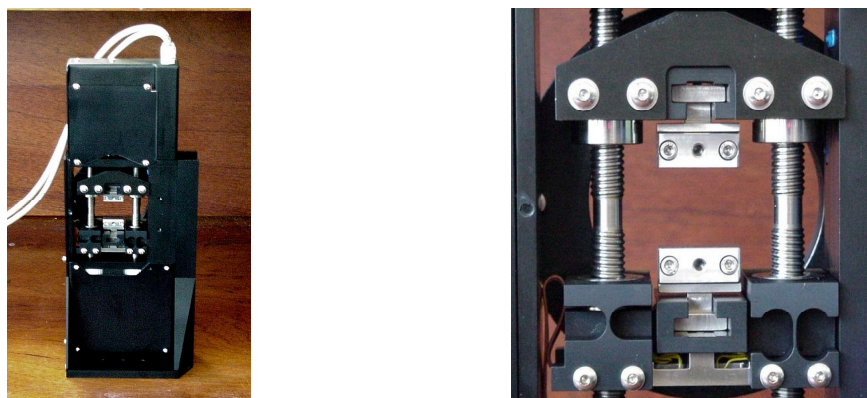
Figure 6.4: *Tensile testing machine used in the simultaneous SAXS-tensile experiments.*

Data analysis was carried out as described below. The raw X-ray data were first normalized by the simultaneously recorded beam intensity of the second ionization chamber in order to correct for sample thinning during deformation and the decreasing intensity of the X-ray source. Next, the data were divided by the detector response in order to correct for intrinsic errors in the intensity measurements of the detector used. Finally, the background scattering, which is mainly the result of air, is subtracted. From the resulting 2D scattering patterns, three-dimensional azimuthal plots were constructed to visualize the development of orientation and dilatation during tensile deformation.

Therefore, the 2D scattering patterns are first divided into 90 cake sections of 4 degrees each, which are, subsequently, integrated to determine the total intensity in each section, see Figure 6.5A. The distribution of the scattered intensity in the different directions relative to the tensile direction can be visualized by plotting the integrated intensity against the azimuthal angle, see Figure 6.5B. Intensities at 90° and 270° correspond to the tensile direction, whereas those at 180° are related to the perpendicular direction. A three-dimensional plot can be constructed by using the displacement or time as third axis, as shown in Figure 6.6.

Figure 6.5: *Schematic representation of X-ray data analysis: (A) division of the 2D scattering patterns in 4° sections and (B) the resulting azimuthal plot.*

Compression testing. Cylindrical bars ($\varnothing$ 3 mm $\times$ 75 mm) of PMMA were made using a mini-injection molding machine. The temperatures of the mold and the cylinder were 80 and 260 ºC respectively for polymers with low molecular weight ($M_n <$ 90 K) and 90 and 280 ºC for higher M_n. The nozzle of the cylinder was preheated before injection of the sample into the mold to guarantee a good flow. The bars were removed from the mold inside an oven at the same temperature as the mold. After all samples were processed, the oven was turned off and the bars were left to slowly cool down to room temperature in order to avoid non-uniform shrinkage. The bars were wrapped in thick aluminium foil and annealed 10 ºC above T_g (determined by DSC) for 2 hours. After annealing, the bars were quenched in cold water. This specific annealing procedure was performed to remove (a) residual stresses present during the cooling step of the molding, and (b) the possible ageing effects during the slow cooling process. The above-mentioned two factors strongly influence

the yield stress and hence the strain softening behavior. The bars were finally machined in to cylindrical samples ($\varnothing$ 3 × 3 mm).

Uniaxial compression tests were performed using a servo-hydraulic MTS 831.10 Elastomer Test System. Samples were compressed between two flat plates at a constant logarithmic strain rate of $3*10^{-3}$ s^{-1}. The friction between sample and plates was reduced by an empirically optimized method.[8] A thin PTFE tape was applied onto the sample and the surface between steel and tape was lubricated using a soap-water mixture. The relative displacement of the steel plates was recorded using an MTS 634.25F-25 extensiometer. The data were processed using the MTS Teststar IIs software.

Differential scanning calorimetry (DSC). DSC measurements were performed to measure the glass transition temperature (T_g). A Perkin-Elmer PYRIS1 DSC apparatus equipped with Pyris software was utilized. Temperature calibration was performed with indium. Polymer samples of 2.5–3.5 mg mass were weighed with a precision balance and encapsulated in standard (crimped) aluminum pans of known mass. Empty pans with almost identical weights were used in the reference side and for the zero line run. A heating and cooling rate of 10 $^{\circ}$C/min was used. The temperature range for PMMA samples was 40–180 $^{\circ}$C.

Nomenclature. The nomenclature used for the samples can be best explained using an example. The designation RC5-1 refers to a poly(methyl methacrylate-*co*-methacrylic acid) copolymer with 5 mol % acid content. RC5-1-K^+100 refers to the ionomer obtained after neutralization of the corresponding acid precursor to a degree of neutralization of 100 %. A similar nomenclature is used for all the acid precursors and the ionomers.

6.3 Results

6.3.1 Mode of deformation studied by in-situ SAXS

Table 6.1 summarizes the molecular characteristics of the PMMA homopolymer and poly(methyl methacrylate-*co*-methacrylic acid) [P(MMA-*co*-MAA)] acid precursors investigated in this study. Acid copolymers with 5, 10 and 15 mol % acid content were prepared to investigate the influence of acid content on the deformation modes. Furthermore, acid copolymers with two different molecular weights were also prepared to study the influence of molecular weight. It is worthwhile to recall that the viscosity will be higher for the high molecular weights, which might lead to difficulties in processing.

The detailed molecular and morphological characterization of the acid precursors and ionomers was presented in Chapter 5. Hence, only a brief summary is given here. SAXS results indicated the formation of multiplets in the ionomer with intermultiplet distances in the range of ~ 70 Å. However, the presence of a very broad SAXS peak suggested a very broad distribution of distances between the multiplets. The presence of such wide range of morphologies resulted in a single broad glass transition temperature in the DMTA analysis rather than two separated T_g's observed in the work of Hara[27] and coworkers. It was concluded from the SAXS and DMTA analysis that cluster formation is not present in the PMMA ionomers with potassium as counterion.

Table 6.1: *Results of the random copolymers and corresponding potassium (K) ionomer*

Sample Code	[MAA][a] (mole %)	Acid GPC		Acid Value[b] (mg KOH/g)	MAA content[c] (mol %)
		M_n (kg/mole)	PDI		
PMMA1	0	100	1.86	0	0
RC5-1	5	101	1.78	27.8	4.9
RC10-1	10	105	1.86	51.4	9.0
RC5-2	5	40	1.76	27.6	4.8
RC10-2	10	41	1.82	52	9.1
RC15-1	15	42	1.92	76	13.3

[a] *MAA content of the reaction mixture.* [b] *Average value of two measurements.* [c] *Determined from the acid value of the polymer.*
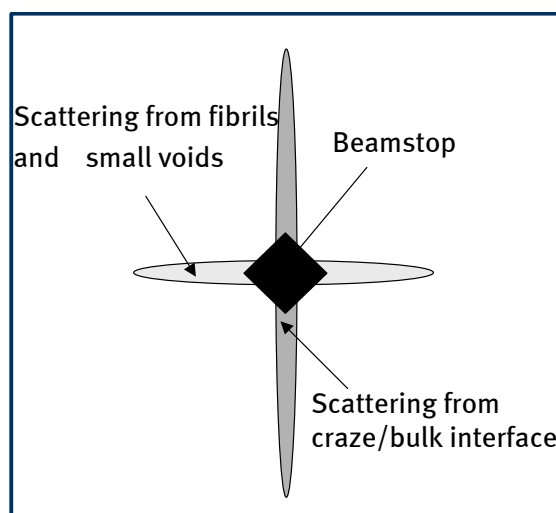
Tensile tests combined with in-situ SAXS can be used to see whether the introduction of ionic groups changes the deformation mechanism, similar to the reported TEM observations of Hara *et al.*[24-27] It was observed that the actual strain rate (clamp displacement divided by time) is slightly higher than the set value of 0.05 mm/min in tensile tests. The actual strain rate was about 0.055 mm/min and was constant during the entire tensile experiment. The azimuthal plots for PM1, RC5-1, RC5-1-K$^+$100 and RC5-2-K$^+$100 are shown in Figure 6.6.

The azimuthal plots of PMMA, the acid copolymer (RC1-5) and the ionomers (RC1-5-K$^+$100 and RC1-10-K$^+$100) differ in intensity and appearance of the peaks during the deformation. At the start of the experiments ($\Delta x = 0$ mm or time (t) = 0), hardly any scattering is observed. After a certain deformation, intense scattering peaks are developed in the tensile direction (at 90º and 270º). Very weak peaks develop perpendicular to the tensile direction (at 0º and 180º) upon further drawing. This cross-like pattern can be ascribed to the scattering of crazes[28] and is represented

schematically in Figure 6.7. The intense peaks in the tensile direction are the result of scattering and reflection caused by the electron density difference between the craze surface and the polymer matrix. The much weaker peaks perpendicular to the tensile direction can be attributed to the scattering of the craze fibrils. All samples broke at the end of the test. The main difference between PMMA and acid copolymer and ionomer is found in the displacement at which the crazing starts, denoted as $\Delta x_{crazing}$. These values are shown in Table 6.2. It is clear that that the acid copolymers and ionomer start to craze at larger clamp displacement than PMMA.
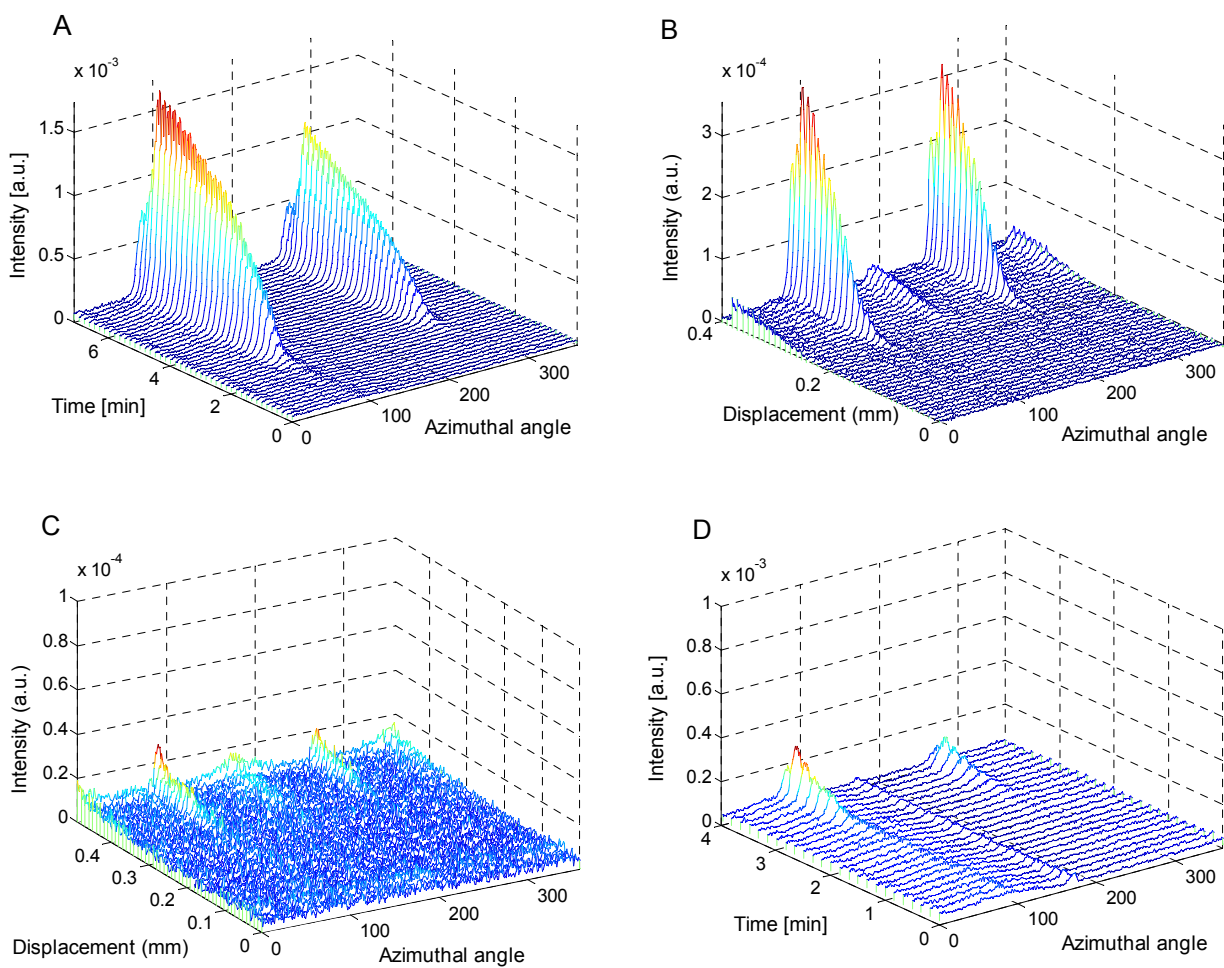
Figure 6.6: *SAXS data (azimuthal plot) for the in-situ deformation of compression molded films of (A) PMMA, (B) RC5-1 acid, (C) RC5-1-K⁺100 and (D) RC10-1-K⁺100. The displacement can be determined by multiplying the time with the actual strain rate, i.e., 0.055 mm/min.*

Figure 6.7: *Pictorial representation of the 2D SAXS pattern observed during the simultaneous SAXS and tensile testing of the samples.*

**Table 6.2:** *Results of tensile testing combined with in-situ SAXS*

Sample code	Acid content (mol %)	Degree of Neutralization (DN)	$\Delta x_{crazing}$[a] (mm)
PMMA	0	0	0.14
RC5-1	5	0	0.22
RC5-1-K^+100	5	100	0.30
RC10-1	10	0	0.21
RC10-1-K^+100	10	100	0.2
RC5-2	5	0	0.38
RC5-2-K^+75	5	75	0.52[b]
RC10-2	10	0	0.44
RC10-2-K^+75	10	75	0.35
RC15-1	15	0	0.55
RC15-1-K^+25	15	25	0.48[b]

[a] Clamp displacement where craze pattern appears in the azimuthal plot.
[b] Clamp displacement at which the sample broke, i.e., maximum displacement at break.

It is evident from Table 6.2 and Figure 6.6D that the high molecular weight fully neutralized RC10-1-K$^+$100 ionomer shows a lower value of $\Delta x_{crazing}$ than the corresponding acid precursor, i.e., RC10-1 with 10 mol % acid content. This indicates that at this high molecular weight and high ion content the sample breaks immediately after the formation of the crazes and are not suitable to study the influence of deformation behavior on the ion content. This point is further explained in the discussion section. Hence, no further experiments were performed on these molecular weights.
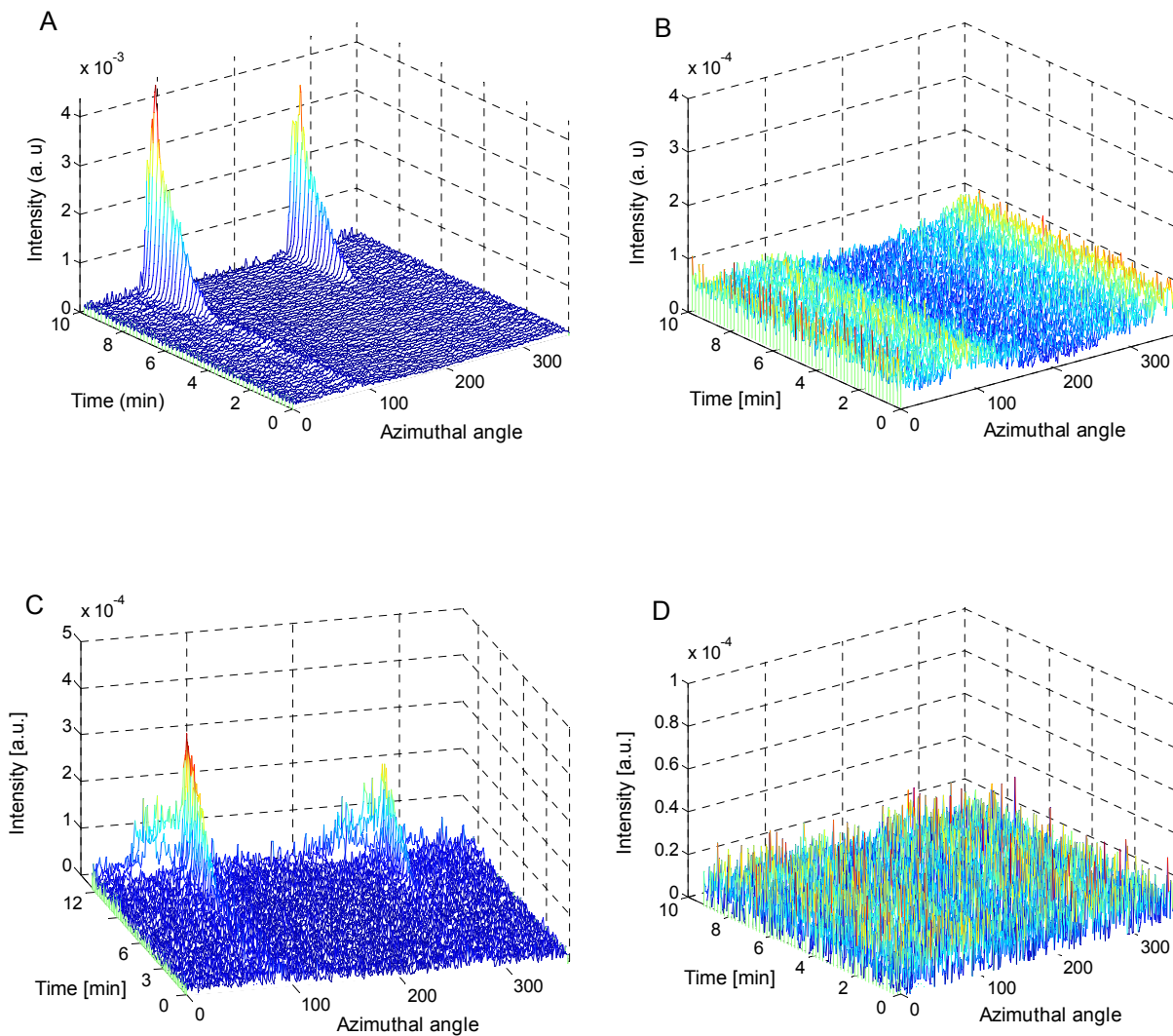
Figure 6.8: *SAXS data (azimuthal plot) for the in-situ deformation of compression molded films of (A) RC5-2 acid, (B) RC5-2-K$^+$100, (C) RC15-1 acid, and (D) RC15-1-K$^+$25. The displacement can be determined by multiplying the time with the actual strain rate, i.e., 0.055 mm/min.*

To circumvent the problem of sample breaking before craze formation, low molecular weight acid precursors were synthesized at 5, 10 and 15 mol % acid content. Moreover, these low molecular weight samples were only partially neutralized to avoid the high extent of ionic cross-linking. Figure 6.8 shows the azimuthal plots for the low molecular weight acid precursors with 5, 10, 15 mol % acid content and corresponding partially neutralized ionomers respectively. It is evident from Figure 6.8 and the data presented in Table 6.2 that craze formation is also suppressed in acids and ionomers of low molecular weights. By comparing the $\Delta x_{crazing}$ values of RC10-2-K^+75, RC5-2-K^+75 and RC15-1-K^+25 (See Table 6.2) it can be concluded that a low degree of neutralization is more favorable towards craze suppression with sufficient amount of strain at break.

6.3.2 Intrinsic deformation behavior of PMMA

The intrinsic deformation behavior of PMMA was studied using compression testing. Two polymerization methods were used to synthesize PMMA, viz. ATRP and FRP. The main difference between these methods can be found in the polydispersity index (PDI), which is low for ATRP (PDI < 1.37) and relatively high for FRP (PDI > 1.76). Therefore, the effect of the PDI on the deformation behavior can be studied. For each polymerization method, a large range of molecular weights was studied (50 kg/mol < M_n < 135 kg /mol) to see the effect of the molecular weight and PDI on the intrinsic properties of PMMA. A series of compression tests were performed on each PMMA in order to obtain reproducible results. The test samples made by injection molding were analyzed using GPC, which showed that the molecular weight is unaltered after processing for all materials. A commercial FRP grade (V052) was studied for comparison. The details of all materials are shown in Table 6.3. DSC was used to determine the T_g-values. Representative true stress-true strain curves for all materials are shown in Figure 6.9.

Table 6.3: *Results of compression testing on PMMA macroinitiatiors synthesized using ATRP and   FRP*

Sample code	GPC		T_g (DSC) (°C)	σ_y (MPa)	YD (MPa)	G_r (MPa)
	M_n (kg/mole)	PDI				
MI-ATRP-1	54	1.20	120	109	8.6	31
MI-ATRP-2	70	1.23	121	110	7.9	38
MI-ATRP-3	93	1.26	121	111	8.4	40
MI-ATRP-4	135	1.37	119	108	8.1	44
MI-FRP-1	50	1.76	114	105	9.2	33
V052	56	1.96	102	95	9.6	33
MI-FRP-3	103	2.13	109	101	8.6	34
MI-FRP-4	127	2.32	113	104	8.5	34
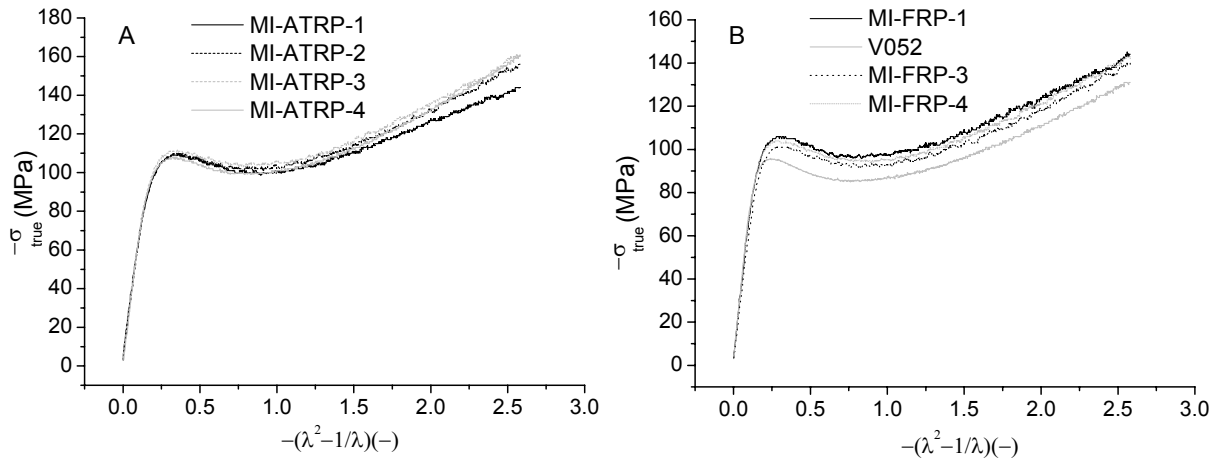
Figure 6.9: *Representative true stress-true strain curves for (A) PMMA synthesized using ATRP and (B) PMMA synthesized using FRP. λ = draw ratio.*

For each PMMA, the average values of the yield stress (σ_y), the yield drop (YD; the difference between the yield stress and strain softening minimum) and the strain hardening modulus (G_r) are determined. It is generally accepted that the true stress is proportional to $\lambda^2 - \lambda^{-1}$ (where λ is draw ratio) at large strains for rubber-elastic materials,[8] as can be seen in Equation 6.1.

$$\sigma_{true} = Y + G_r(\lambda^2 - 1/\lambda) \tag{6.1}$$

where Y is the rejuvenated yield stress. Figure 6.9 shows that all PMMA materials exhibit this neo-Hookean behavior at large strain. The strain hardening modulus is equal to the slope of the curve at large strains. The results of this analysis are given in Table 6.3. It is evident from Table 6.3 that the values of yield stress (σ_y), strain hardening modulus (G_r), and T_g are higher for the ATRP materials than for the FRP materials. The values of yield drop (YD) are comparable for both ATRP and FRP materials. Slightly higher values are observed for FRP materials, but the difference is small.

6.4 Discussion

6.4.1 Mode of deformation studied by in-situ SAXS

The results of the simultaneous SAXS and tensile testing experiments clearly indicate that crazing is suppressed for the acids and ionomers compared to PMMA most probably due to the presence of intermolecular interactions. For the acids, this can be related to hydrogen bonding

between acid groups and for ionomers to the presence of ionic cross-links or ionic aggregates. Chapter 5 described the detailed FTIR studies of the acid precursors indicating the presence of strong interactions among the polymer chains. The SAXS and DMTA results on the PMMA ionomers (from Chapter 5) confirmed the presence and formation of multiplets, which act as ionic cross-links. However, it is important to know that the increase in network density is higher for systems with covalent cross-links than ionic cross-links. The network density of linear polymers, ν_e, is simply the physical entanglement density and can be calculated using[6,7]

$$\nu_e = \rho N_A / M_e \tag{6.2}$$

Here, ρ is the density of the polymer (g/cm^3), N_A is the Avogadro number and M_e is the molecular weight between entanglements.

The network density relation in ionomers has to be modified for the presence of ionic aggregates and should be considered in addition to the physical entanglements. The effect on the network density can be similar to that of covalent cross-links, but the ionic cross-links are not as stable as covalent cross-links[7] and also differ in the functionality of the cross-link points. This is especially true for random ionomers, where polymer chains can interact in different aggregates. An effective network density (ν_{eff}) is defined, for ionomers as[7]

$$\nu_{eff} = \rho N_A (1/M_e + f*k/M_o) \tag{6.3}$$

Where f is the ion content (fraction) and M_0 is the repeat unit molecular weight of the ionomer. In this equation, k is a coefficient representing the effectiveness of ionic cross-links as compared to covalent cross-links (at temperatures far below T_g); therefore the range of k is $0 < k < 1$. It should be added that the k value reflects the effectiveness of ionic cross-links (due to the formation of multiplets in ionomers) according to their locations, i.e., whether they are in a matrix phase or in a cluster phase.[29] The k value of the latter should be higher.

With known values of ρ, M_o, and M_e, i.e., material constants for a base polymer, and ion content, f, of an ionomer, Hara and co-workers calculated the k values of sodium neutralized PMMA ionomer by comparing the ν values corresponding to the general craze–shear transitions (a transition from crazing only to crazing plus shear occurring at $\nu = 4 \times 10^{25}$ and a transition from crazing plus shear to shear only occurring at $\nu = 8 \times 10^{25}$).[6] They reported a k value of 0.46 for the

12.4 mol% sodium neutralized clustered PMMA ionomer.[7] Hence, it appears that ionic cross-linking would appear to be less than half as effective as covalent cross-linking. It is important to realize that this value of *k* cannot be directly applied to the potassium neutralized PMMA ionomers investigated in this study since the DMTA results indicated that no cluster phase is present in these systems (from Chapter 5). So the effective increase in network density will be lower than the reported sodium neutralized PMMA ionomers. No further attempts were made to calculate the effective network density from this method because of the large differences in the morphology of the potassium and sodium neutralized PMMA ionomers.

The increased network density due to the presence of interactions in ionomers and in acids leads to a higher craze initiation stress as compared with the yield stress.[7] As a result, craze formation is initiated at higher stresses in ionomers compared to PMMA homopolymers. This may indicate an increase in the fracture resistance of the ionomers and acids. In the high molecular weight and high ion content samples, the maximum strain at break is reduced due to the large number of the ionic cross-links and sample breaks prior to craze formation in the in-situ SAXS experiments. Hence, to achieve a good balance between the maximum strain at break and maximum $\Delta x_{crazing}$ a low molecular weight and a low degree of neutralization is needed. This indeed was observed in the low molecular weight ionomer samples. The SAXS results indicate that the craze initiation stress is increased for ionomers. However, it is important to recall that the glass transition temperature (T_g) of the ionomer is also increased due to the ionic cross-links, which leads to an increase in the yield stress measured at ambient temperature. Furthermore, the increase in yield stress may strongly influence the magnitude of strain softening in ionomer compared to PMMA homopolymer (See Figure 6.1). Thus, introduction of the ionic cross-links not only change the network density but also changes the yield stress and strain softening behavior in the ionomer. It is necessary to study the entire post-yield behavior to understand the deformation behavior of ionomers. This issue is addressed further in a separate section.

6.4.2 Intrinsic deformation behavior of PMMA. The results of the uniaxial testing of the PMMA samples synthesized by ATRP and FRP clearly show subtle differences in the intrinsic properties indicating the influence of polydispersity index (PDI) on the intrinsic properties. The observed values of the T_g are higher for the ATRP materials than FRP materials. Concomitantly, the values of yield stress are also higher for the ATRP materials. Since the number average molecular weight and microstructure are similar for the ATRP and FRP materials, the observed differences in

T_g can be attributed to the differences in the PDI. It is worthwhile to know that so far no reports are available about the microstructure such as tacticity differences in the PMMA synthesized by ATRP and FRP.

It is well known that the presence of a low molecular weight fraction in high PDI polymers, i.e., in FRP materials, may act as a plasticizing agents, which reduce the T_g. Moreover, DSC trace of the FRP PMMA shows a broader T_g transition compared to the ATRP PMMA confirming the presence of a large distribution of the segmental mobility in FRP PMMA (See Figure 6.10). It is important to know that although end groups are different in both types of PMMAs its influence on T_g is negligible at the molecular weights investigated in this study. Figure 6.11 displays the yield stress for all materials as a function of the T_g and a linear relation between the yield stress and T_g (R = 0.9924) of the PMMA is observed independent of the polymerization method used. It is worthwhile to note that the T_g of the commercial PMMA, i.e., V052, is much lower than other samples due to the possible presence of additives.
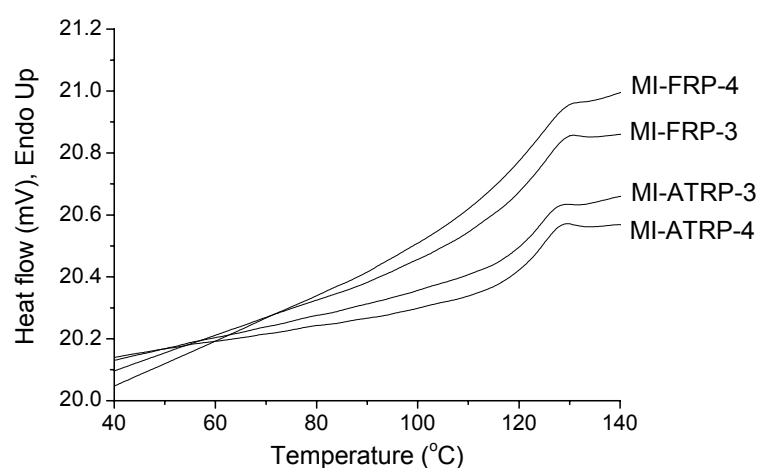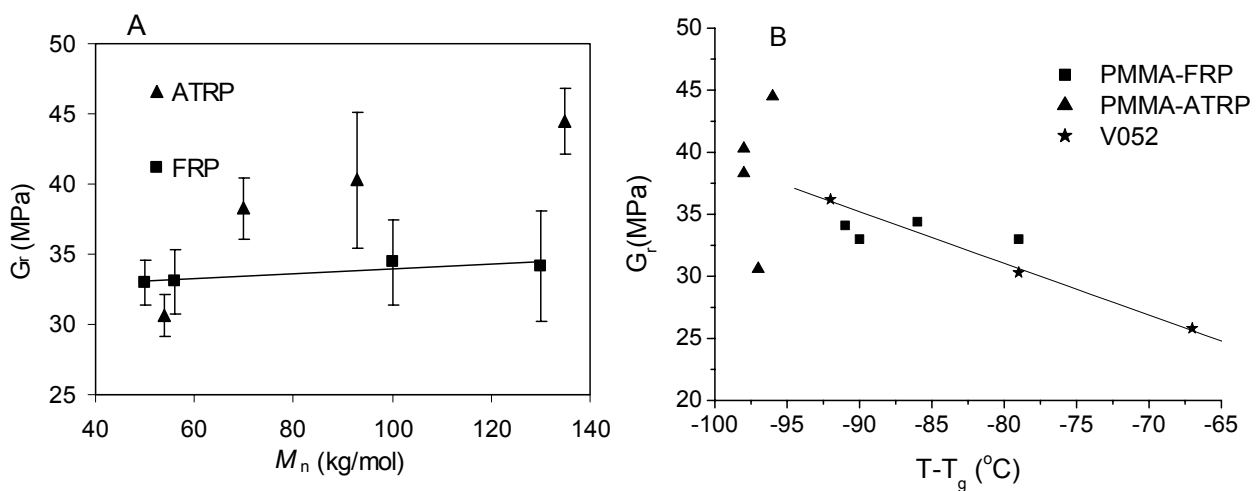

Figure 6.10: *DSC traces of the PMMA's synthesized by free radical polymerization (FRP) and atom transfer radical polymerization (ATRP).*

The strain hardening modulus (G_r) is given as a function of the molecular weight for both ATRP and FRP in Figure 6.12A. The modulus is comparable for ATRP and FRP materials for low molecular weights ($M_n \sim 50,000$). The modulus is consistently higher for ATRP compared to FRP for higher molecular weights. For glassy polymers, a critical molecular weight (typically 4 or 5 times M_e) exists below which the sample breaks during the compression test. The value of M_e for PMMA is 9,200, so we are close to this critical molecular weight for the low molecular weight

samples. This may explain why there is hardly any difference between ATRP and FRP materials with low M_n. Another difference between ATRP and FRP materials is that the modulus increases with increasing M_n for ATRP materials, whereas the modulus is almost constant over the whole range of molecular weights for FRP materials.
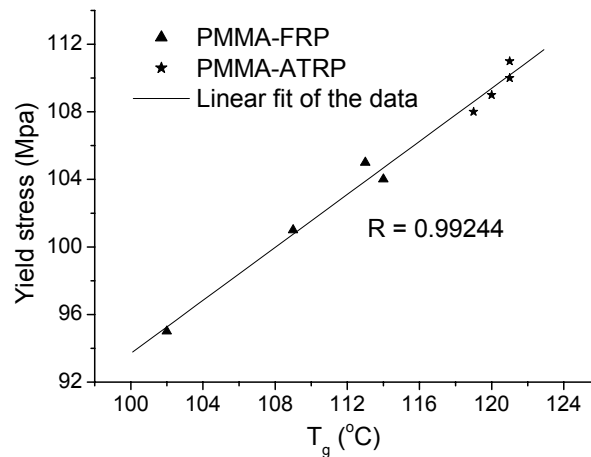
Figure 6.11: *Yield stress as a function of glass transition temperature (T_g) for PMMA's synthesized by free radical polymerization (FRP) and atom transfer radical polymerization (ATRP).*

Figure 6.12: (A) Strain hardening modulus (G_r) as a function of the molecular weight (the error bars are determined for a 95 % accuracy interval) and (B) *Strain hardening modulus as a function of (T-T_g) for PMMA's synthesized by free radical polymerization (FRP) and atom transfer radical polymerization (ATRP).*

An attempt is made here to explain the observed trends in the strain hardening modulus of the PMMA polymers synthesized by FRP and ATRP. It is well established that strain hardening modulus of glassy amorphous polymers is mainly determined by two variables, i.e., the network density and thermal mobility of the polymer chains. Van Melick recently studied the strain hardening behavior of PS/PPO blends and explained the trends observed in the strain hardening modulus using the above two variables.[4] At a given number average molecular weight, the effective network density for a linear polymer is dependent on the average number of entanglements per chain and strength of entanglement (which is same for ATRP and FRP PMMA's). For FRP materials with high PDI, the average number of entanglements per chain remains same upon increasing molecular weight due to the presence of large distribution in the molecular weights. The average number of entanglements remains same because low molecular weight tail present in the high PDI PMMA may dilute the effect from the high molecular weight tail. Thus, effective network density remains same for FRP PMMA's upon increasing molecular weight, which leads to a constant strain hardening modulus. However, for ATRP materials at a given molecular weight, the average number of entanglements per chain increases due to low PDI. Consequently, the effective network density is increased and a higher strain hardening modulus is measured. Thus, the observed differences in the strain hardening modulus of ATRP and FRP can be attributed to the differences in the PDI.

To validate above discussed reasoning, the strain hardening modulus (measured at T = 23 ºC) is also plotted as a function of the temperature difference with the material's glass transition temperature (T-T_g) in Figure 6.12B. In this manner, a correction is made for differences in chain mobility between the materials. For comparison, the results of compression tests on V052 at different temperatures are also included. It is evident that the G_r values of the FRP materials and V052 (at different temperatures) show a linear behavior indicating that the thermal mobility correction approach explains the differences between the G_r values of these materials. Thus, we may conclude that differences in the G_r modulus between the FRP and V052 is due to the differences in the thermal mobility of the polymer chains. However, it is also clear that the thermal mobility correction approach could not explain the trends observed in the G_r for ATRP materials.

## 6.4.3 Intrinsic deformation behavior of PMMA ionomers

As mentioned in the earlier sections, it is necessary to study the post-yield behavior via uniaxial compression testing to understand the complete deformation behavior of ionomers. However, processing of the PMMA ionomers turned out to be quite challenging due to high

viscosity (even at 5 mol % ions), high thermal stability of the ionic aggregates and the overlapping of the flow temperature (temperature needed to form uniform polymer melt with sufficient flow) and degradation temperature. It was not possible to perform uniaxial compression tests on ionomers.

Indentation techniques on thin polymer films are a possible method to study reproducible craze initiation, formation and to determine the craze initiation stress. On going numerical indentation work on polymer thin samples in the group of Govaert *et. al*[30] indicates that use of a cone shaped indenter with flat tip generates load stress vs displacement curves, which are sensitive to strain hardening modulus and yield stress or thermal history. Such sensitivity was not found while using a spherical indenter. Figure 6.13 A and B shows the simulated indentation plots as a function of strain hardening and yield stress respectively. The point where the indentation curve deviates from linearity is related to the yield point in the deformation and is sensitive to thermal history of the sample. Similarly the slope of the indentation curve at large displacements is sensitive to the strain hardening modulus. Thus, indentation method is quite suitable method, especially when it is difficult to make samples via injection molding, to investigate the effect of ionic cross-links on the post-yield behavior of the PMMA ionomers. Further experiments utilizing the thin films of PMMA ionomers (used in SAXS experiments) are needed to confirm the SAXS results.
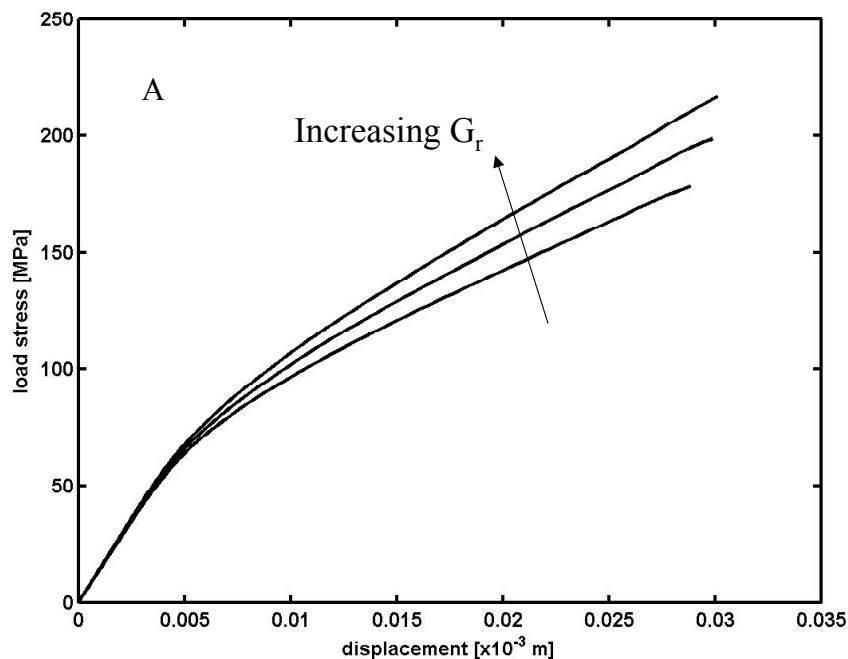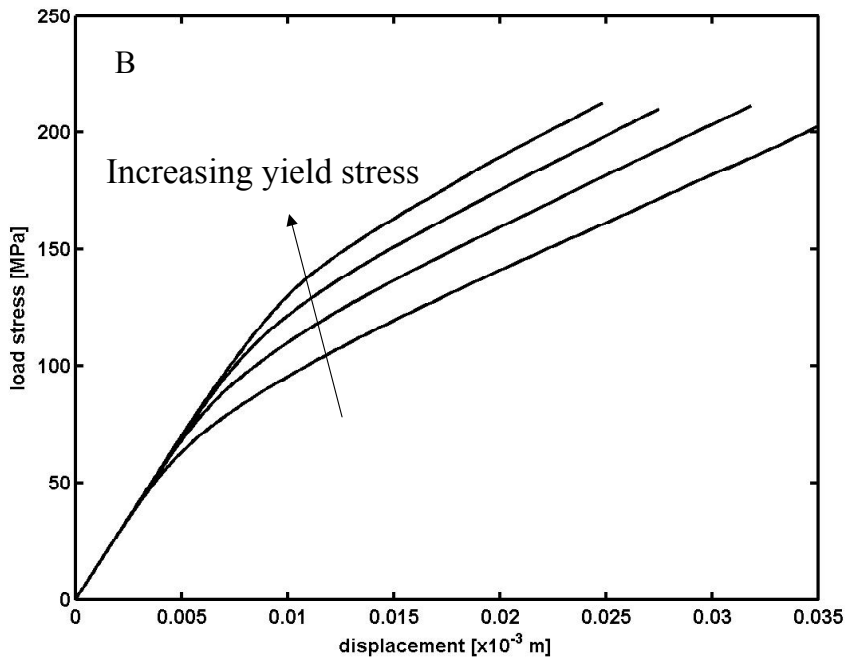
Figure 6.13: *Influence of (A) strain hardening and (B) yield stress on the simulated indentation curves.*

6.5 Conclusions

The results of the simultaneous time resolved small angle X-ray scattering (SAXS) and tensile testing on poly(methyl methacrylate) (PMMA), poly(methyl methacrylate-*co*-methacrylic acid) copolymers and the corresponding potassium ionomers clearly indicate that craze initiation or formation was suppressed in acid copolymers and ionomers compared to PMMA due to the presence of intermolecular interactions. These results are consistent with the reported results of the deformation changes of PMMA ionomers using transmission electron microscopy. Formation of the ionic aggregates, which act as ionic cross-links in ionomers is responsible for these changes: the effective network density and craze initiation stress are increased upon introduction of ionic cross-links. Similar effect of increase in network density due to the hydrogen bonding in acid copolymers, although to lesser extent, is responsible for changes in acid copolymers. This may indicate an increase in the fracture resistance of the ionomers and acids. The in-situ SAXS results on PMMA ionomers with high molecular weight and high acid content indicate that the maximum strain at break is reduced due to the large number of the ionic cross-links and these samples break prior to craze formation. PMMA ionomers with low molecular weight and a low degree of neutralization

are necessary to have a good balance between increase in craze initiation stress and the maximum strain at break. Further experiments, involving indentation techniques are needed to understand the influence of ionic cross-links on complete post-yield behavior PMMA ionomers.

The results of the uniaxial compression tests on PMMAs synthesized by atom transfer radical polymerization (ATRP) and free radical polymerization (FRP) show that the values of the glass transition temperature (T_g), yield stress and strain hardening modulus (G_r) for ATRP materials are higher than the FRP materials. The effective network density is diluted for FRP PMMA because of the low molecular weight tail arising from the high polydispersity index of the sample, hence a lower G_r value is measured. The presence of a large distribution of thermal mobilities in FRP samples results in broad T_g and hence a lower value is measured. The thermal mobility correction approach explains the differences in the G_r values of the FRP materials and the commercial samples (V052 measured at different temperatures). This study demonstrates the importance of controlling molecular parameters such as PDI and M_n, and their influence on intrinsic properties such as G_r of the polymers.

6.6 References

(1)   Kramer, E.J.; Berger, L. L. *Adv. Polym. Sci.* **1990**, 91/92, 1.

(2)   Kramer, E. J. *Adv. Polym. Sci.* **1983**, 52/53, 1.

(3)   Bowden, P. B. *In   The Physics of Glassy Polymers*; Haward, R. N., Ed.; **1973**, Applied Science Publishers: London.

(4)   van Melick, H. G. H.; Govaert, L. E.; Meijer, H. E. H. *Polymer*, **2003**, 44, 2493.

(5)   van Melick, H. G. H.; Govaert, L. E.; Meijer, H. E. H. *Polymer*, **2003**, 44, 3579.

(6)   Henkee, S. S.; Kramer, E. J. *Journal of Polymer Science*, **1984**, 22, 721.

(7)   Ma, X.; Sauer, J. A.; Hara, M. *Macromolecules*, **1995**, 28, 5526.

(8)   van Melick, H. G. H. *Ph.D Thesis*, Eidhoven University of Technology, The Netherlands, **2002**.

(9)   Hutchinson, J. M. *Prog. Pol. Sci.*, **1995**, 20, 703.

(10)   Struik, L. C. E. *Physical Aging in Amorphous Polymers and other Materials*, **1978**, Elsevier, Amsterdam.

(11)   Tervoort, T. A.; Govaert, L. E. *J. Rheol.*, **2000**, 44, 1263.

(12)   Hasan, O. A.; Boyce, M. C. *Polymer*, **1993**, 34, 5085.

(13)   Aboulfaray, M.; G'Sell, C.; Mangelinck, D.; McKenna, G. B. *J. Non-Cryst. Solids*, **1994**, 615, p172,.

(14)   G'Sell, C. *Plastic Deformation of Glassy Polymers: Constitutive Equations and Macromolecular Mechanisms.* In: H. J. Queens, et. al., Eds., Strength of Metals and Alloys, **1986**, Pergamon Press, Oxford.

(15)   Govaert, L. E.; Timmermans, P. H. M.; Brekelmans, W. A. M. *J. Eng. Mat. Tech.* **2000**, 122, 177.

(16)   Govaert, L . E.; Melick, H. G. H. van.; Meijer, H. E. H. *Polymer*, **2001**, 42, 1271.

(17)   G'Sell, C.; Hiver, J. M.; Dahouin, A.; Souahi, A. *J. Mat. Sci.* **1992**, 27, 5031.

(18)   van Melick, H. G. H.; Govaert, L. E.; Rasss, B.; Nauta, W. J.; Meijer, H. E. H. *Polymer*, **2003**, 44, 1171.

(19)   Spitzig, W. A.; Richmond, O. *Poly. Eng. Sci.* **1979**, 19, 1129.

(20)   Arruda, E. M.; Boyce, M. C.; Jayachandran, R. *Poly. Eng. Sci.* **1994**, 34, 716.

(21)   Zaraoulis, J. S.; Boyce, M. C. *Polymer*, **1997**, 38, 1303.

(22)   Cross, A.; Haward, R. N.; Mills, N. J. *Polymer*, **1979**, 20, 288.

(23)   Haward, R. N. *Colloid & Polymer Sci*. **1980**, 258, 643.

(24)   Hara, M.; Sauer, J. A. J. *Macromol. Sci., Rev. Macromol. Chem. Phys.* **1994**, C34, 325

(25)   Hara, M.; Jar, P. *Macromolecules*, **1988**, 21, 3187.

(26)   Sauer, J. A.; Hara, M. *Adv. Polym. Sci.* **1990**, 91/92, 69.

(27)   Ma, X.; Sauer, J. A.; Hara, M. *Macromolecules*, **1995**, 28, 5526.

(28)   Butler, M. F.; Donald, A. M.; Ryan, A. J.; *Polymer*, **1997**, 39, 781.

(29)   Eisenberg, A.; Hird, B.; Moore, R. B. *Macromolecules*, **1990**, 23, 4098.

(30)   Engels, T.A.P.; Pelletier, C. P.; Govaert, L.E. *On going work in* Dept. of Mechanical Engineering, Eindhoven University of Technology.

Chapter 7

Effect of Temperature on the Microstructure of Ionomers: Feasibility of Thermoreversible Cross-links

ABSTRACT: The influence of temperature on the stability of ion aggregates was investigated for telechelic polyester ionomers and poly(methyl methacrylate) (PMMA)-based diblock ionomers using small angle X-ray scattering (SAXS). The SAXS results of polyester ionomers indicated the presence of order-disorder transition (T_i) for the potassium neutralized polyester ionomer with 5.7 mol %. This is understood as arising from an increase in elastic forces of the polymer chains due to the increase in the temperature, which destabilizes the ionic aggregate structure and thereby promotes the dissociation of the ionic aggregates. Rheology experiments were also used to confirm the SAXS results in the case of polyester ionomers. Dynamic viscosity experiments confirmed the presence of the ion dissociation temperature. Furthermore, these measurements indicated that viscosity and storage modulus of the polyester ionomers were higher than for the precursors and were a strong function of ion content, counterion and degree of neutralization.

Poly(methyl methacrylate-*b*-potassium methacrylate) [P(MMA-*b*-K$^+$MA)] diblock ionomers with similar ionic P(K$^+$MA) block lengths and different nonionic block (PMMA) lengths were obtained from solution neutralization of the corresponding acid diblock precursors. SAXS results of the K$^+$-TM-41/550 diblock ionomer with long PMMA (with 550 units of MMA) block and short PK$^+$MA (with 41 units of K$^+$MA) block and K$^+$-TM-42/132 (with 132 units of MMA and 42 units of K$^+$MA) indicated that the thermal stability of the ionic aggregate in the block ionomer is a strong function of block copolymer composition. The observed results were discussed in terms of the solution properties of the block ionomers. The K$^+$-TM-41/550 block ionomer forms ionic aggregates with low aggregate number (N_{AN}) due to the long nonionic block. As a result weak ionic aggregate is formed, which dissociates at high temperatures.

7.1 Introduction

The physical and mechanical properties of multiphase polymer systems are strongly dependent on their morphology. Block copolymers and ionomers are two classes of microphase-separated systems that have been extensively studied.[1-6] It is now well established that the physical, mechanical, and viscoelastic properties of ionomers are strongly dependent on the morphology.[4-6]

Several parameters such as the architecture of the backbone, flexibility of the backbone, dielectric constant of the polymer matrix, ionic content, degree of neutralization, chemical nature of the ionic groups, and the presence of plasticizers determine the observed morphology in the ionomer.[4,7] The influence of above-mentioned parameters on the ionomer morphology was systematically investigated in this research. Chapter 4 presented the morphological features of the poly(methyl methacrylate-*b*-potassium methacrylate) [P(MMA-*b*-K$^+$MA)] and poly(potassium methacrylate-*b*-methyl methacrylate-*b*-potassium methacrylate) [P(K$^+$MA-*b*-MMA-*b*-K$^+$MA)] di- and triblock ionomers in a large range of molecular weights. The morphological features of the PMMA random and telechelic polyester ionomers were described in Chapter 5. The results indicate that block ionomers form ionic domains, with an ionic domain spacing of 10–30 nm (See Chapter 4). However, random/telechelic ionomers form ionic multiplets with an intermultiplet spacing of 3–7 nm (See Chapter 5).

Eisenberg's theory predicts that a critical temperature for dissociation of the ionic aggregates exists at which the elastic forces exceed the magnitude of the electrostatic interactions.[7] The thermal sensitivity of the ionic cross-links in contradiction to covalent cross-links can in principle be used to develop new resins with thermoreversible cross-link properties (see Chapter 1). However, a critical temperature for dissociation of the ionic aggregates, i.e., an order–disorder transition (T_i), as predicted by Eisenberg, was not observed experimentally for random ionomers[8,9] before the polymer degraded. Several parameters such as chemical structure of the ionomer backbone, architecture of the ionomer, ionic content, degree of neutralization, counterion and the presence of plasticizers determine the stability of the ionic aggregate. It is still a challenging task to optimize the aforementioned parameters in order to observe T_i in the case of ionomers.

It is well known that viscoelastic properties of ionomers such as melt viscosity are higher than their nonionic precursors[4-6] due to the formation of ionic aggregates. Furthermore, the presence of ionic aggregates effectively retards the translational mobility of the polymer chains. Hence, the parameters affecting the structure and stability of the ionic aggregates should also influence the melt rheology of the ionomer, which is a very important factor during the processing. Therefore, a complete understanding of the effect of the above-mentioned parameters on the ionic aggregation and the viscosity is necessary to develop materials with thermoreversible cross-links and with optimum processing conditions respectively.

Since the present chapter focuses on the influence of temperature on the order-disorder transition of the ionic aggregate (T_i) of the ionomers, the following section will briefly describe the relevant results pertaining to these systems. Several research groups recently consolidated the

characteristics of a block copolymer and ionomer microphase separation into a single material by preparing block copolymer ionomers,[10-15] in which one of the blocks of the block copolymer contains ionic groups. Weiss *et al.*[14,16] reported the microphase transitions of a block copolymer ionomer prepared by lightly sulfonating the polystyrene (PS) blocks of diblock and triblock copolymers of PS and poly(ethylene-*alt*-butylene) (PEB) or poly(ethylene-*alt*-propylene) (PEP). The microstructure was analyzed by SAXS and dynamic mechanical thermal analysis. These block ionomers showed two different levels of microphase separation, one due to self-assembly of the block copolymer structure (20−30 nm) and another one due to ionic aggregation (3−5 nm) within the microdomains formed by the polystyrene block. It is important to realize that ionic groups are randomly distributed in the PS block of the PEB/PEP block ionomer (similar to the sulfonated polystyrene ionomer), whereas ionic groups are sequentially present in the block ionomers investigated in Chapter 4, which show a two-phase morphology. A thermally induced order−disorder transition of the ionic aggregates (T_i) was observed for first time in sodium and zinc salt derivatives of the block ionomers. In addition to the elastic force of the ionomer chain opposing the ionic structure, a tendency for the two blocks to mix at elevated temperatures favors the destabilization of the ionic aggregation within the polystyrene microdomain. As a result, the net force opposing the aggregate structure exceeds the strength of the ionic interactions leading to the possibility of observing T_i prior to chemical degradation in the block copolymer ionomer. It was found that the ionic dissociation temperature (T_i) is a function of the degree of neutralization, ion aggregate size, and type of counterion.

Melt rheology studies on well-defined telechelic poly(ethylene isophthalate) (PEI) amorphous ionomers demonstrated that at lower temperatures (< 150 $^{\circ}$C) the ionomers exhibited characteristic mechanical properties indicative of high molecular weight polymers.[17,18] At higher temperatures (> 150 $^{\circ}$C), the ionic multiplets disassociated and the melt viscosity decreased. These experiments prove the existence of the order-disorder temperature (T_i) in telechelic ionomers, and also indicate that SAXS and rheometry are two important techniques to be used in identifying T_i and investigating the thermoreversible nature of the ionic cross-links.

In this study, telechelic polyester ionomers and PMMA-based diblock ionomers were used. Solution neutralization was used to prepare the ionomers, since this method is cleaner (minimizes the introduction of impurities from neutralization step) and avoids any possible thermal degradation usually involved with melt neutralization. It is therefore important to understand the mechanism of neutralization and formation of ionomers, especially in the case of block ionomers, and their microstructure parameters. It is also worthwhile to recall the structural similarities present between

the reported polystyrene ionomers and poly(methyl methacrylate) block ionomers investigated in this study. Several groups investigated the formation of micelles and the micellar characteristics (in solvents such as tetrahydrofuran, dioxane, and dimethyl formamide) of the block ionomers with non-ionic polystyrene (PS, with degree of polymerization of N_A) block attached to an ionic block (with degree of polymerization of N_B) consisting of poly(cesium acrylate) (PCsA),[19] poly(cesium methacrylate) (PCsMA), or poly(quaternized 4-vinylpyridine).[20] Solution characterization techniques such as SEC,[21,22] dynamic light scattering (DLS), static light scattering (SLS), and viscometry[21,23] and bulk characterization techniques, such as SAXS,[20,24] and transmission electron microscopy (TEM),[21] were used to establish the relationships between the block ionomer structure and composition of the block copolymers.

It is now well understood that diblock copolymers like PS-*b*-PMAA/PAA are soluble in tetrahydrofuran (THF)/dioxane and are present in single-chain form in these solutions, but when they are neutralized, the corresponding ionomers form micelles[19,23,25] in solution. For a low percentage neutralization, the micelles and single chains are in a dynamic equilibrium allowing exchange between them, whereas for a high percent neutralization the solvent is expelled from the micelle as the degree of neutralization increases, and the core becomes increasingly viscous and compact. At this point, the high viscosity of the core prevents the facile movement of single chains to and from the micelle, hence the dynamic equilibrium is slow and kinetically trapped structures are formed.[26] Although the movement of small molecules to and from the micelle cores will allow further neutralization, the aggregate can no longer adjust to these chemical changes, and the aggregate structure is effectively frozen in. It is important to note that the simultaneous presence of micelles and single chains in solution may probably be due to the polydispersity of the ionic end blocks; the single chains being the chains with very short ionic blocks while the micelles contain the chains with the longer ionic blocks. The scaling relations observed for the ionic core radius (R_{core}) and aggregate number (N_{AN}) are from this frozen state, which are actually "snapshots" of earlier thermodynamic states.

Comprehensive scaling laws for N_{AN}, i.e., the number of chains per micelle, and R_{core} as a function of the ionic block length (N_B) and nonionic block length (N_A) were established from the solution techniques.[23] It was found[25,26] that N_{AN} and R_{core} increased with the insoluble block length and decreased with the soluble block lengths ($N_{AN} \sim N_B{}^{\alpha} N_A{}^{-\beta}$, $R_{core} \sim N_B{}^{\kappa} N_A{}^{-\gamma}$ where α, β, κ, and γ are scaling exponents, whose values lie between 0 and 1) as predicted by theory[27,28] and corroborated by experimental evidence[29] in a wide range of systems. The values of the exponents vary from system to system, depending on the chemical nature of the blocks, the type of solvent,

and the relative block lengths. It is now well-established[20,21,24] from SAXS and TEM that these block ionomers in the solid state show a two-phase structure. The microstructure consists of spherical ionic domains (from the ionic blocks) embedded in a polystyrene matrix similar to that of the micellar morphology in a solution. Isolated micelles and some aggregates of micelles (formed in the process of sample preparation as a result of solvent evaporation) were observed in the solid state. A comparison of the aggregation numbers obtained in the solid state by SAXS with those determined in solution by SEC showed a satisfactory agreement (within a factor of less than 2) between the two methods except for the block ionomers with short ionic segments (N_A). These results imply that the morphology and the corresponding scaling laws for N_{AN} and R_{core} observed in the solution state of the block ionomers can be extrapolated to the solid state morphology of these materials with small error. Thus, literature results demonstrate that the R_{core} and N_{AN} in the solid state can be controlled by the block ionomer composition. This gives a simple and unique way to control and vary the strength of the ionic domains in block ionomers, which results in the possibility of observing and controlling the ion dissociation temperature (T_i) in the block ionomers.

This chapter presents the results of the influence of temperature on the microstructure of the telechelic ionomers and poly(methyl methacrylate-*b*-potassium methacrylate) [P(MMA-*b*-K$^+$MA)] diblock ionomers. SAXS was used to study the morphology of block and telechelic ionomers as a function of temperature. Rheological measurements were also performed on polyester ionomers with different ion content (5.7 and 3.5 mol %), molecular weight, and counter ion to confirm the SAXS results. PMMA diblocks with different molecular weights and different compositions were selected to study the influence of block length and composition on the ionomer structure. The results of the SAXS and rheological measurements on the stability of the ionic aggregates are presented.

7.2 Experimental Section

7.2.1 Materials

The details of the polyester ionomer synthesis were discussed in Chapter 5. Three grades of polyesters were obtained with two different acid contents, i.e., 3.7 and 5.4 mol % of carboxylic acid units. Polyester ionomers with sodium and zinc counterions were obtained by using a two-phase neutralization[30] procedure as described in Chapter 5. PMMA block ionomers were prepared by atom transfer radical polymerization and the details of the synthesis and morphology were described in Chapter 4.

Nomenclature. The designation PE1 refers to the polyester sample 1. PE1-K$^+$100 refers to potassium neutralized polyester ionomer of sample 1 with a degree of neutralization of 100. The designation TM-41/550 refers to a diblock ester precursor with a PtBMA block consisting of 41 monomer units connected to a PMMA block consisting of 550 monomer units. K$^+$-TM-41/550 refers to the corresponding diblock ionomer. Since the methacrylate diblock ionomers used in this study show a two-phase morphology, the notation used for ionic dissociation temperature (T_i) for ionomer block copolymers is equivalent to the order–disorder transition temperature (T_{ODT}) for the corresponding ester precursor.

7.2.2 Analysis and Measurements

Thermogravimetric analysis (TGA). The thermal stability of the polymer was measured using a Perkin-Elmer Pyris 6 TGA. Approximately 10 mg of polymer was heated from 40 ºC to 700 ºC with a heating rate of 10 ºC/min and under a N_2 flow of 20 ml/min. The results were analyzed using the Pyris 4.01 software. These data were used to select the higher temperature limit for the time resolved SAXS measurements of the block ionomers.

Small angle X-ray scattering (SAXS). SAXS experiments were performed at ESRF Grenoble, France. The details of the experimental setup were described in Chapter 4 (PMMA block ionomers) and Chapter 5 (Polyester ionomers). The wavelength (λ) of the X-rays was 1.0 Å. The sample-to-detector distance was 1.5 m for polyester and 5.5 m for block ionomers. A Linkam hot stage was used to control the temperature. Time resolved SAXS measurements were performed from 40 ºC to ~ 220 ºC with a heating rate of 10 ºC/min. An exposure time of 24 s was used for each measurement. Sample was cooled from the elevated temperature to the room temperature by a fast cooling rate, i.e., 100 ºC/min.

Rheological measurements. Dynamic viscoelastic measurements were conducted on Paar Physica UDS200 rheometer with 12.5mm parallel plate fixtures, under a flowing nitrogen atmosphere. The linear viscoelastic regime was determined by strain amplitude sweep (ASWP) experiments with an oscillatory frequency of 10 s^{-1}. From the ASWP measurements, the proper strain was chosen for the temperature scan. The strain was chosen based on the linear viscoelastic region and the torque. Temperatures of the ASWP experiments were 200, 150, 100 and 50 °C. The temperature scan was performed from 50 °C up to 200 °C with a heating rate of 10 ºC/min (linear). The strain was linearly increased during the measurement (based on amplitude sweep experiments).

7.3 Telechelic Polyester Ionomers

7.3.1 Results and Discussion

7.3.1.1 Influence of temperature on the ionic aggregates of the polyester ionomers: Small angle X-ray scattering. Time resolved small angle X-ray scattering (SAXS) was used to study the influence of temperature on the stability of the ionic aggregates or multiplets. The SAXS results from Chapter 5 revealed that potassium ionomers (PE2-K$^+$100 and PE1-K$^+$100) showed a distinct peak indicating a clear microphase separation. Therefore, the PE2-K$^+$100 sample was considered to perform the SAXS studies. The sample was heated from 40 ^{o}C to 200 ^{o}C at a heating rate of 10 ^{o}C/min and during the heating SAXS-data were taken at constant time intervals. This allows us to investigate the thermal stability of the ionic aggregates during the heating step.

Figure 7.1A shows the direct 2D-SAXS images of the PE2-K$^+$100 sample at four different temperatures, i.e., 40 ^{o}C, 75 ^{o}C, 200 ^{o}C and 25 ^{o}C respectively (clockwise direction). The first three images are from the heating run and the last image is from the cooled sample after completion of the heating run. Notable changes are observed in the SAXS profile of the ionomer on increasing the temperature. It is evident that the SAXS data image at 40 ^{o}C shows a single distinct ring referred to as *ionic ring* due to the ionic multiplets. The *ionic peaks* shown in the Figure 7.1B are obtained after integration of such 2D SAXS patterns. The SAXS image at 75 ^{o}C shows that the ionic ring becomes sharper compared to the image at 40 ^{o}C. It is worthwhile to recall that the T$_g$ of this ionomer is 72 ^{o}C. The enhanced chain mobility of the polymer chains above the T$_g$ of the ionomer allows more ionic groups to diffuse into the aggregates, leading to the formation of the more uniform multiplets in the ionomer matrix. Upon further increasing the temperature to 200 ^{o}C the intensity of the ionic ring decreases drastically and only a very weak ionic peak is observed upon close inspection of the 2D-image and I vs q plot. The decrease in intensity around 200 ^{o}C may indicate that most of the ionic multiplets are dissociated. At high temperatures the magnitude of the elastic forces of the polymer chains are increased, which destabilizes the electrostatic forces present between the multiplets and, as a result, the multiplets are dissociated at high temperatures as predicted by Eisenberg's theory of ionomer morphology.[7] This leads to a decrease in the intensity and broadening of the ionic ring. Thus, an order-disorder transition was observed for the PE2-K$^+$100. We rule out any possible thermal degradation or side reactions during the heating since the maximum temperature (200 ^{o}C) used in the SAXS experiments is 30 ^{o}C below the onset temperature for thermal degradation (T$_{onset}$ = 230 ^{o}C from TGA analysis, see section 5.5.2.2 in Chapter 5).

A

T = 40 ºC below T$_g$

T = 75 ºC above T$_g$

T = 180 ºC, in melt

T = 25ºC, cooling

B
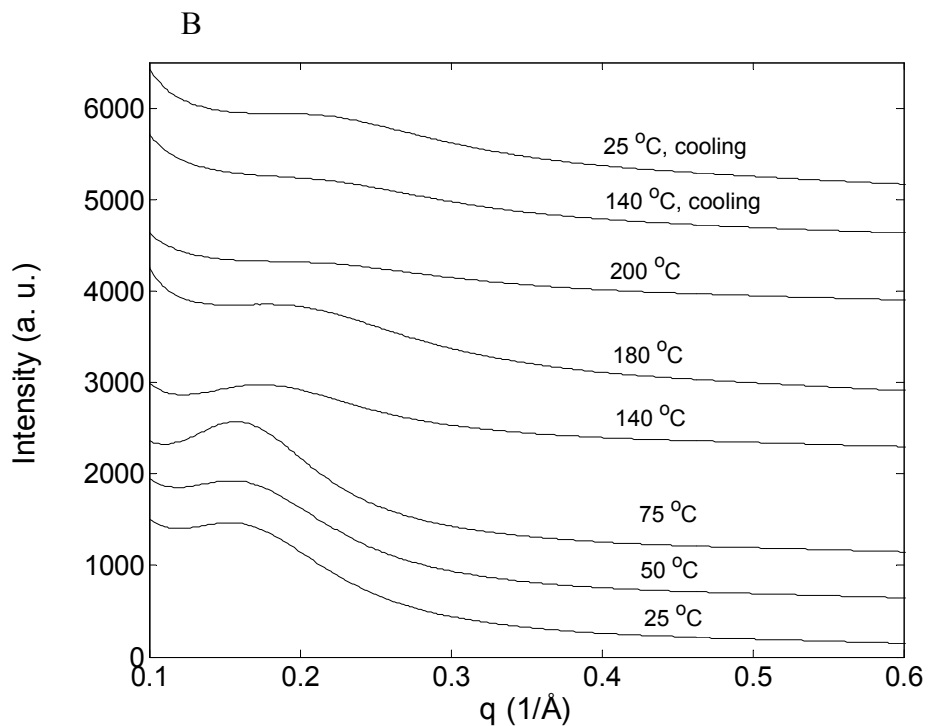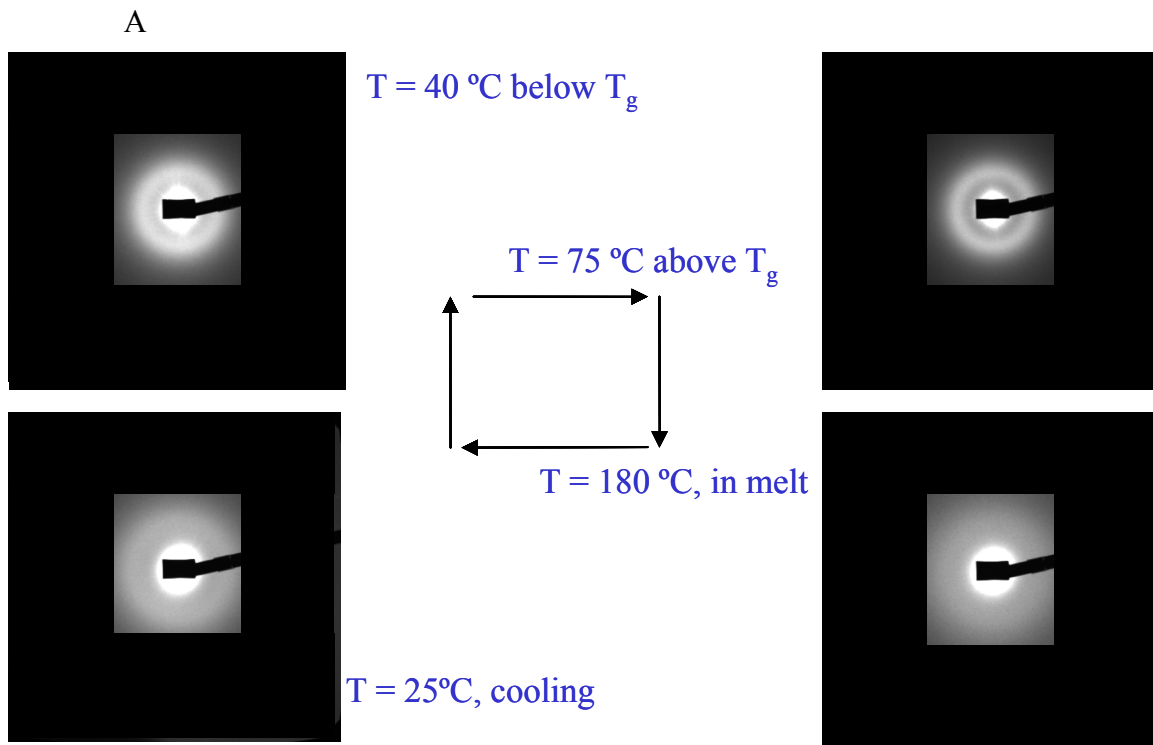
Figure 7.1: *(A) Time resolved 2D-SAXS images (B) Time resolved I vs. q plots of PE2-K$^+$100 at selected temperatures, i.e., 40 ^{o}C, 75 ^{o}C, 200 ^{o}C and 25 ^{o}C (cooling) respectively in clockwise direction.*

7.3.1.2 Melt Rheology. Figure 7.2A and 7.2B show the log-log plots of the complex viscosity *vs.* strain (amplitude sweep measurements) for the PE1 and the PE1-K$^+$100 ionomer measured at 90, 120, 150 and 180 ^{o}C temperatures respectively. It is evident from Figure 7.2 that the precursor and ionomer respond differently to the strain or deformation as a result of the differences in the chemical structure of the polymer melts. Viscosity remains constant for the PE1 during the entire strain region at all temperatures. However, the ionomer shows a nonlinear viscoelastic flow behavior at high strains and at high temperatures.
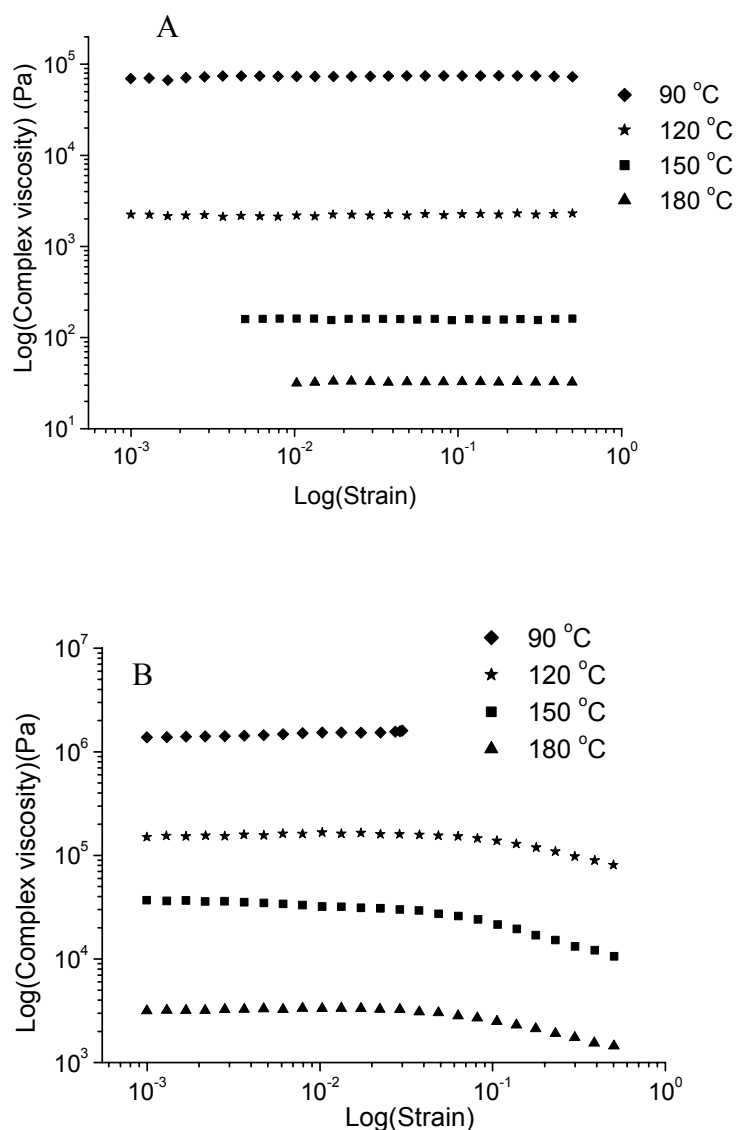
Figure 7.2: *Plots of the complex viscosity vs. strain for (A) the polyester precursor PE1 and (B) for corresponding potassium ionomer measured at 90, 120, 150 ^{o}C, and 180 ^{o}C respectively.*

Figure 7.3A shows the complex viscosity *vs.* temperature plots for the precursors PE1, PE2 and the three ionomers with potassium as counterion. It is evident that the precursor materials PE1 and PE2 have lower viscosities compared to corresponding ionomers in the entire temperature region indicating the influence of ionic cross-links on the viscosity. The ionic groups aggregate into nanometer-size domains within the nonpolar matrix and act as transient cross-links, strongly influencing ionomer melt flow behavior.[31] Ionomers typically have viscosities and storage modulus orders of magnitude greater than those of comparable nonionic polymers. Several parameters such as architecture, ion content, degree of neutralization, and counterion influence the ion aggregation, which also influence the rheological properties of the ionomers. Furthermore, the flow temperature (temperature at which a large drop in the viscosity occurs and is also the T_g of the polymer) is lower for precursors than the ionomers. It is worthwhile to recall that T_g of the ionomer is higher than the precursor (see section 5.5.2.1 in Chapter 5), which leads to a higher flow temperature in the ionomer. A sharp decrease in viscosity of the precursors is seen in Figure 7.3A, which is a typical flow behavior of low molecular weight polymers. However, for all the three ionomers, the decrease in viscosity with temperature is lower than that of precursors.

It can be seen from Figure 7.3A that the viscosity of PE3-K$^+$100 (with 3.7 mol % ion content) is lower than the PE1-K$^+$100 and PE2-K$^+$100 (with 5.3 mol % ion content) in the entire temperature region investigated, implying that the increase in viscosity is proportional to the number of neutralized acid groups. Moreover, a slight drop in the viscosity of the PE1-K$^+$100 at 160 ^{o}C, suggests the influence of temperature on the ionic cross-links; i.e., the weakening or dissociation of the ionic aggregates with temperature. These results confirm the time resolved SAXS results, which indicated the presence of the order-disorder transition (T_i) in the ionomers. The difference in temperature from SAXS and rheometry are due to the differences in the two measurements, i.e., SAXS is a static experiment, whereas rheological measurements were done in a dynamic state. A similar drop of the viscosity occurs at 130 ^{o}C for the PE2-K$^+$100 ionomer. The difference between the viscosities of the PE1-K$^+$100 and PE2-K$^+$100 ionomers (see Figure 7.3A) is maybe due to the differences in the molecular weights of the base polyester.

Figure 7.3B shows the plots of storage modulus (G′) and loss modulus (G″) *vs.* temperature for the PE1 and the corresponding potassium ionomer. It is evident that immediately after the flow temperature (72 ^{o}C) G′ of the PE1 is lower than the G″ indicating characteristics of typical low molecular polymer melt. However, G′ of the corresponding ionomer (PE1-K$^+$100) was higher than the G″, even after onset flow temperature (80 ^{o}C, see Figure 7.3A) implying the presence of

characteristics of a physically cross-linked polymer melt. A distinct crossover point between G′ and G″ occurs at the temperature of 160 ^{o}C, which suggests a decrease in the elastic component of the ionic cross-link network due to the dissociation of the ionic aggregates. The effect of temperature on the ionic aggregates, especially their aggregation behavior during heating and cooling was also studied with rheology measurements. The results of the viscosity and storage/loss modulus measurements during consecutive heating and cooling scans are shown in Figure 7.4A and B respectively for PE2-K^{+}100. It is evident that reproducible viscosity and modulus values were measured during heating and cooling scans suggesting that ion aggregation is quite stable to temperature changes and is truely thermoversible.
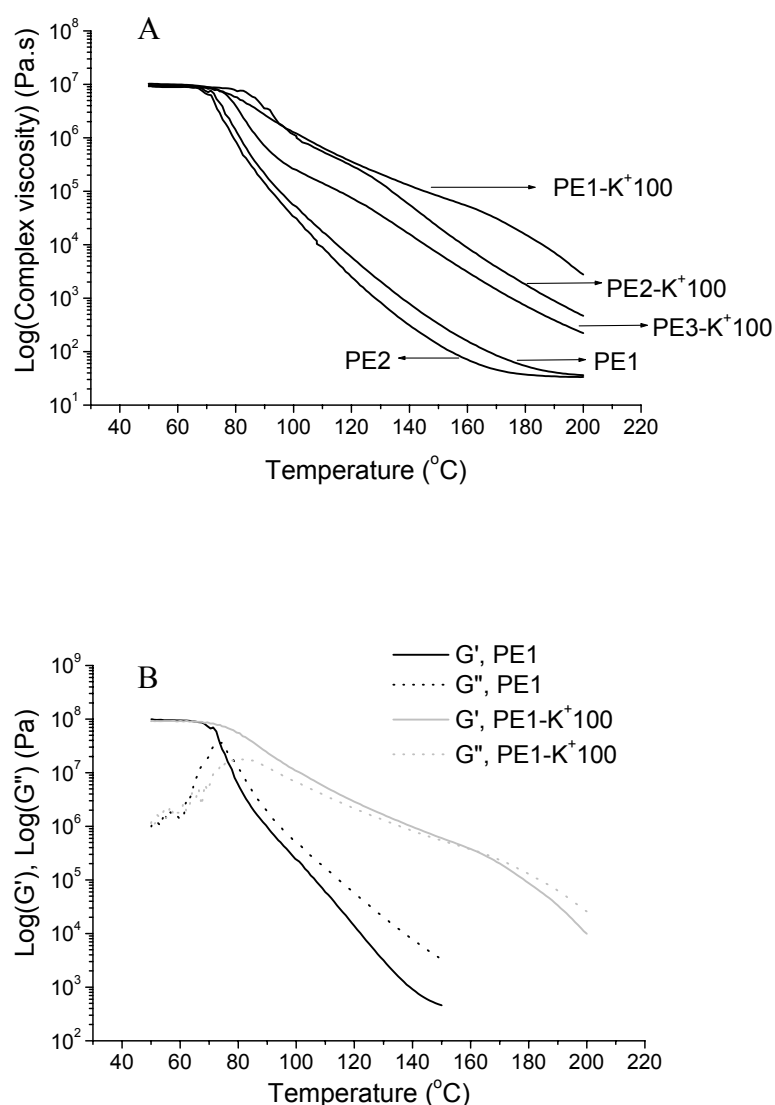
Figure 7.3: *(A) Plot of the complex viscosity vs. temperature for the polyester precursors and ionomers. (B) Plot of the storage modulus (G′) and loss modulus (G″) as a function of temperature for PE1 and PE1-K^{+}100.*
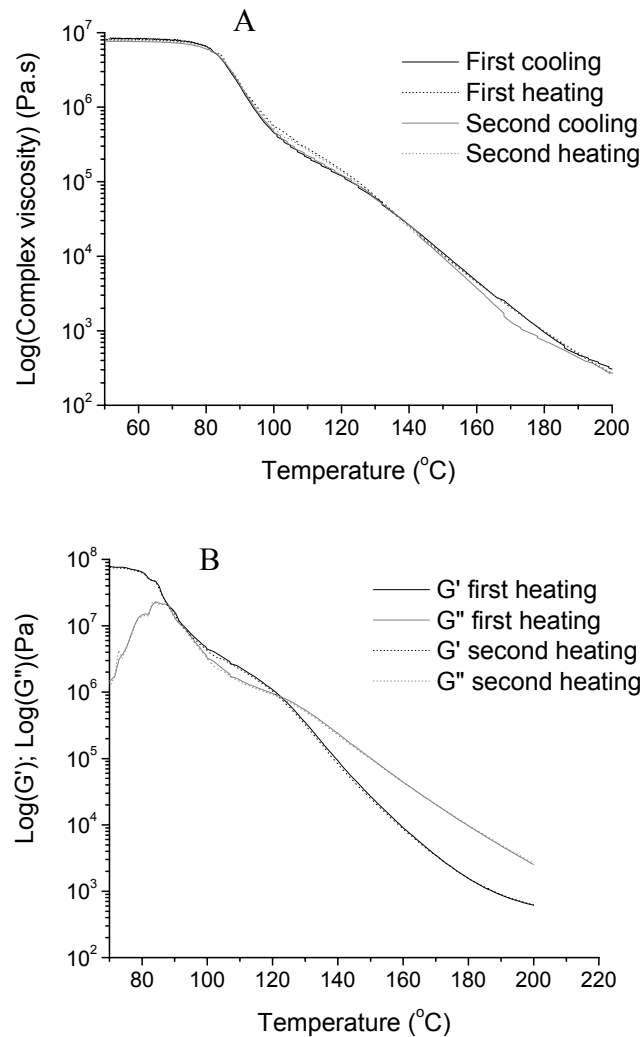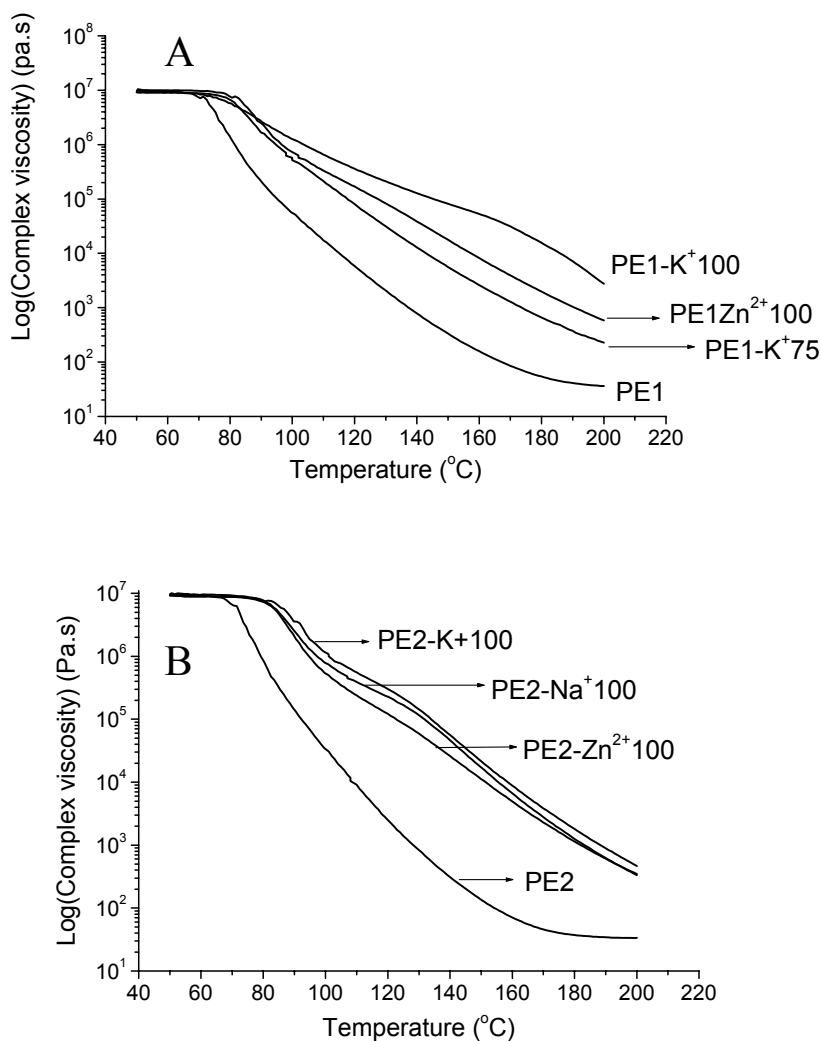
Figure 7.4: *(A) Plot of the complex viscosity vs. temperature of consecutive heating and cooling scans for PE2-K$^+$100 and (B) Plots of the strorage modulus (G') and loss modulus (G'') vs. temperature of consecutive heating scans for PE2-K$^+$100.*

Effect of degree of neutralization (DN) and counterion. Figure 7.5A shows the plot of complex viscosity *vs.* temperature for the PE1 and corresponding ionomers with a degree of neutralization of 75 and 100 %. For comparison PE1 neutralized with zinc counterion is also shown in this plot. All the ionomers indicated a higher onset of flow temperature compared to the PE1 precursor. It is evident that the viscosity of the PE1-K$^+$75 is lower than the viscosity of the PE1-K$^+$100 indicating the influence of the DN on the viscosity. At low DN, fewer ionic groups are present in the polymer matrix hence a lower number of aggregates are formed resulting in low viscosities. The drop seen in the viscosity of the PE1-K$^+$100 at 160 ^{o}C, which is attributed to the dissociation of the ionic cross-

links, is not observed in the PE1-K$^+$75 ionomer, due to the lower number of aggregates a complete ionic network is not formed in the PE1-K$^+$75. These results confirm the SAXS results (from Chapter 5), which indicated the presence of a critical ionic content above which a distinct ionic peak is seen in the ionomers. Further, the viscosity of the PE1-Zn^{2+}100 is lower than the corresponding potassium ionomer (PE1-K$^+$100).

Figure 7.5: *Plots of the complex viscosity vs. temperature for (A) the polyester precursor PE1 and corresponding potassium neutralized ionomers with degree of neutralization of 75 and 100 %, (B) the polyester precursor PE2 and corresponding ionomers with potassium, sodium and zinc as counterions.*

Figure 7.5B shows the viscosity *vs.* temperature plots for the PE2 precursor and corresponding ionomers with potassium, sodium (Na) and zinc (Zn) counterions. Once again, it is evident that the viscosity of the Zn ionomer is lower than that of K and Na ionomers. The results of

the FTIR and SAXS from the Chapter 5 established that formation of the ionic aggregates is a strong function of the type of the counterion present in the ionomer due to the differences in the coordination numbers of the counterions. Zinc forms different coordination structures such as tetra- and hexa-coordinated structures and zinc acid salt structures (see Figure 5.12, Chapter 5), which may have different contribution towards increase in viscosity. Further, the high temperature FTIR studies indicate that not all the ionic groups in the zinc ionomer are aggregated and stability of the zinc aggregates are lower compared to K or Na ionomers. It is worthwhile to know that zinc carboxylate bonds are less ionic than the K and Na-carboxylate one, which results in weaker dipole-dipole interactions or ionic interactions.

7.4 PMMA block ionomers

7.4.1 Results

Table 7.1 lists the molecular characteristics of the diblock ester precursors and ionomers investigated in this study. Two block ionomers and precursors with a similar ionic block length but different nonionic block length were selected to investigate the influence of block copolymer composition on the ionomer morphology, which may also show the effect of temperature on the ionic aggregates. It is important to know the thermal stability of the polymers prior to thermal stability of the ion aggregate studies.

Table 7.1: *Physical characteristics of MMA/tBMA diblock precursors and ionomers*

Sample	Total M_n (PDI)[a]	PMMA block MW; (M_n)[a]	Volume[b] fraction of PtBMA $(V_{f,PtBMA})$	PtBMA block MW; (M_n)[c]	T_{onset} (°C)	q_{max} (Å^{-1})
TM-41/550	61600 (1.23)	55000	0.1	5800	220	0.02
K$^+$-TM-41/550	61600 (1.23)	55000	0.1	4300	200	0.032
TM-42/132	22400 (1.26)	13200	0.3	6000	220	0.038
K$^+$-TM-42/132	22400 (1.26)	13200	0.3	6000	220	0.045

[a] from SEC analysis in THF using universal calibration for PMMA with PS standards. [b] Calculated with ρ_{PMMA} = 1.2 g/cm^3 and ρ_{PtBMA} = 1.02 g/cm^3 for the ester precursors, taken as equal to volume fraction of poly(potassium methacrylate) (PK$^+$MA) block in ionomers. [c] calculated using the mole fraction of PtBMA from FTIR and absolute molecular weight of the PMMA from SEC.

7.4.1.1 TGA analysis of the block ionomers. The TGA traces of the block ionomer K$^+$-TM-41/550 and corresponding precursors are shown in Figure 7.6. The weight loss as a function of

temperature is compared for block ionomer and the precursor materials, viz. ester and acid, under nitrogen atmosphere. These results are representative for other samples. It can be seen that all materials degrade by a two-step mechanism. The temperature at which the degradation starts is called the onset temperature (T_{onset}). T_{onset} for the block copolymers (ionomer and precursor) is lower than for PMMA ($T_{onset} \sim$ 240 °C, not shown in Figure 7.6). For ester diblock copolymers ($T_{onset} \sim$ 220–230 °C), the *tert*-butyl ester groups are transformed to acid groups and cyclic anhydrides at temperatures between 220–250 °C.[32] The acids ($T_{onset} \sim$ 190 °C) and ionomers ($T_{onset} \sim$ 220 °C) start to degrade at lower temperatures, which can be related to the formation of cyclic anhydrides (for ionomers possibly arising from the unneutralized acid groups) by an intramolecular dehydration mechanism.[32] The rate of degradation in the first step (i.e., the slope of this step) is lower for the acids and ionomers than for esters. The functional groups such as cyclic anhydrides formed at the start of degradation for acids and ionomers induce cross-linking of the polymer matrix and may increase the rigidity of the polymer chains, thereby decrease the rate of degradation. The weight percentage left after 600 °C was approximately zero for all materials, except the ionomers. This so-called ash content increases with increasing ion content and is originating from the inorganic salts formed during the degradation by the potassium counter ions (K^+) present in the ionomers. The TGA results indicate that temperature limit for heating experiments in SAXS is 220 °C to avoid the thermal degradation of the ionomers.
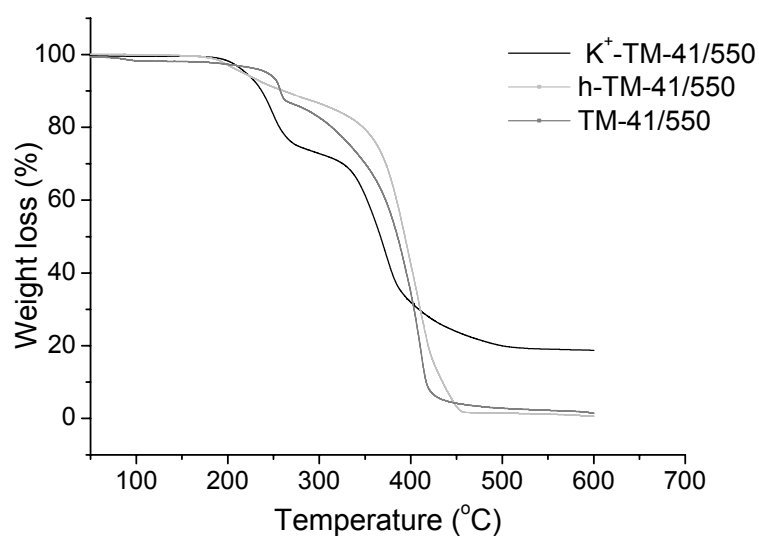
Figure 7.6: *TGA traces for the K^+-TM-41/550 ionomer, ester and acid precursors.*

### 7.4.1.2 Time resolved SAXS analysis

Block ionomer with low ionic content and precursor. Figure 7.7A & B show the SAXS profiles at selected temperatures of the ester precursor (TM-41/550) and ionomer (K^+-TM-41/550) from 40–200 ^oC using a heating rate of 10 ^oC/min. For both materials, a single SAXS peak ($q_{max} = 0.032$ Å^{-1} for the K^+-TM-41/550 and $q_{max} = 0.02$ Å^{-1} for the TM-41/550) is observed at room temperature implying a clear microphase separation.
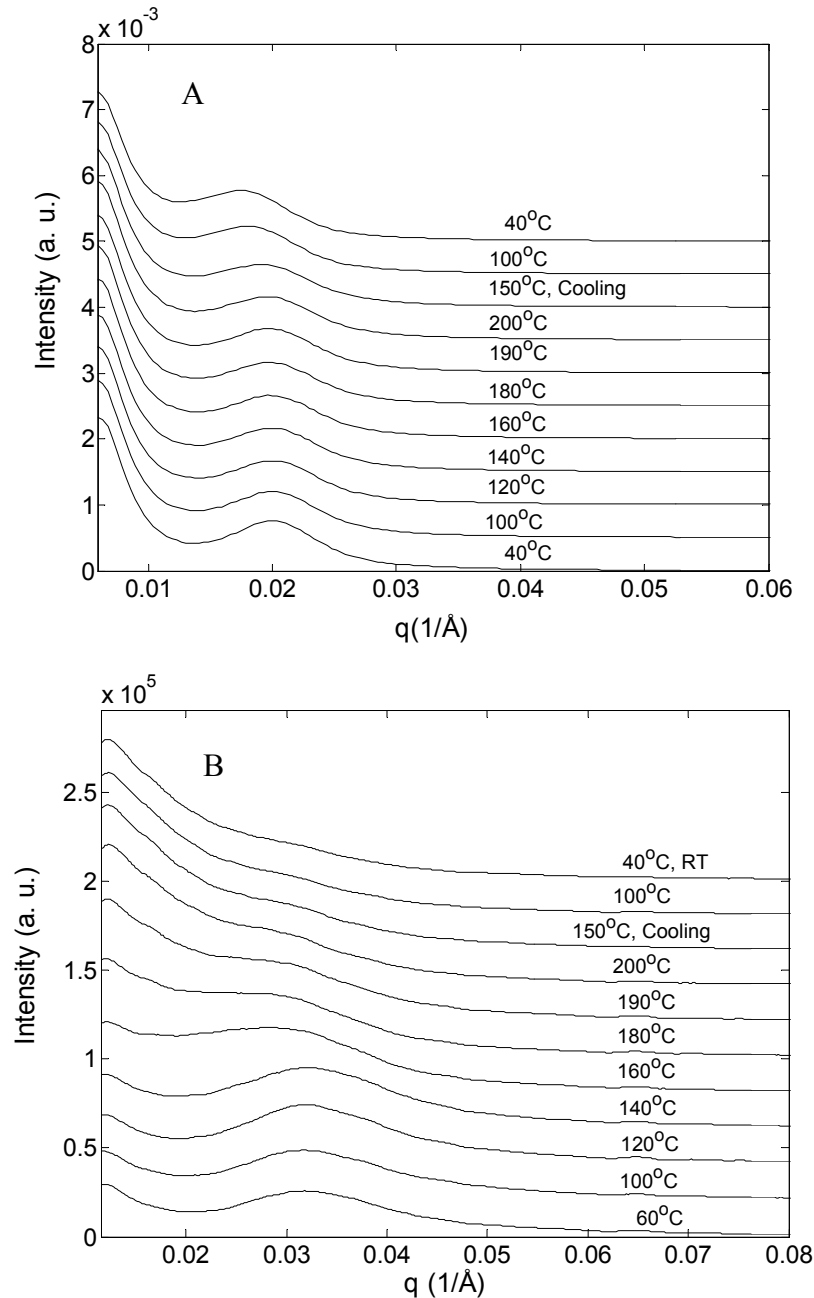
Figure 7.7: *SAXS profiles for the block microstructure of bulk sample of (A) TM-41/550 ester copolymer and (B) K^+-TM-41/550 ionomer block copolymer obtained while heating from 40 ^oC to 200 ^oC at 10 ^oC/min. A few SAXS profiles obtained during cooling are also shown.*

For the block copolymer ester, there is no change in the SAXS profile or in the intensity on increasing the temperature except that the peak maximum slightly shifted to lower q-values. However, notable changes are observed in the SAXS profile of the block copolymer ionomer on increasing the temperature. The SAXS patterns of K^{+}-41/550 in Figure 7.7B may be divided into three regions: (1) the first region (T < 140 °C) in which the intensity of the SAXS peak increases, (2) the second region (140 °C < T < 200 °C) in which the intensity of the SAXS peak decreases and the peak maximum shifts to lower q-values; however, it has to be noted that the intensity increases at low q values in this region, and (3) the third region (the cooling cycle, i.e., 200 °C < T < 40 °C) in which no change in the intensity or the peak position.

Block ionomer with high acid content and precursor. Figures 7.8 A & B show the SAXS profiles at selected temperatures of the ester (TM-42/132) and ionomer (K^{+}-TM-42/132) in the temperature region of 40–220 °C using a heating rate of 10 °C/min. A broad single SAXS peak (q_{max} = 0.045 Å^{-1} for the ionomer and q_{max} = 0.038 Å^{-1} for the ester precursor) is observed at room temperature for both materials implying a clear microphase separation. The temperature dependencies of the SAXS profiles of the ester and the ionomer are notably different. For the block copolymer ester, there is neither change in the SAXS profile nor in the intensity on increasing the temperature. However, significant changes are observed in the SAXS profiles of the K^{+}-TM-42/132 ionomer. The SAXS patterns of K^{+}-42/132 in Figure 7.8B may be divided into three regions: (1) the first region (T < 160 °C) in which a relatively small increase in the intensity of the SAXS peak is seen, (2) the second region (160 °C < T < 200 °C) in which a significant increase in the intensity of the SAXS peak is observed, and (3) the third region (220 °C < T < 40 °C) in which the intensity decreases. Note that there is no significant change in the position of the peak maximum (q_{max}) throughout the heating and cooling cycle. These observations clearly demonstrate the influence of the block composition on the thermal stability of the ionic aggregates in the block copolymer.
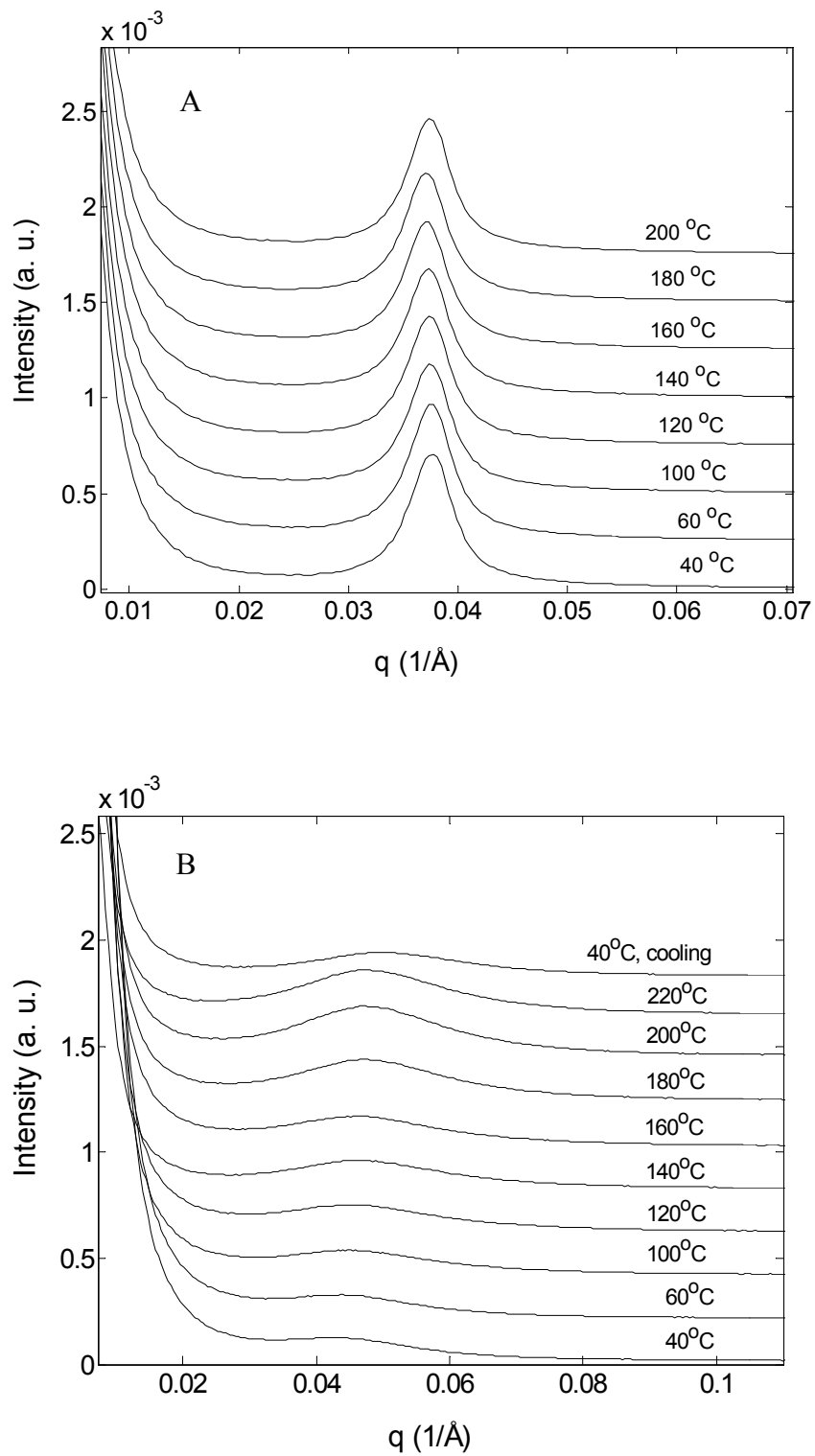
Figure 7.8: *SAXS profiles for the block microstructure of bulk sample of (A) TM-42/132 ester copolymer and (B) K⁺-TM-42/132 ionomer block copolymer while heating from 40 °C to 200 °C at 10 °C/min. A few SAXS profiles obtained during cooling are also shown.*

7.4.2 Discussion

Time resolved SAXS analysis. The scaling relations described in the introduction section indicate that at an identical temperature and solvent composition, micellization is very much a function of the overall copolymer composition. Thus, for a given length of the soluble block (in this case PMMA block), micellization was only observed above a certain "threshold" length of the insoluble segment or ionic block (in this case PK$^+$MA block). However, the value of this threshold length depends on the length of the soluble block, i.e., the longer the soluble block length, the higher the "threshold" length of the insoluble block for micellization. The two block ionomers investigated have a similar ionic block length (PtBMA, the precursor block for poly(potassium methacrylate) but a different nonionic block length. From the composition of the block ionomers, it can be anticipated that the K$^+$-TM-41/550 ionomer with a long nonionic block (N_A = 550, PMMA block) should have a lower aggregation number than the K$^+$-TM-42/132 block ionomer with a short nonionic block. The stability of the ionic aggregate is a strong function of the aggregation number. Thus, it is possible to control the stability and the strength of the ionic aggregate via control of the block copolymer composition. However, it is important to realize that the results observed in this study are only applicable to ionomers obtained via solution neutralization. Melt neutralization may lead to a different ion aggregate structure.

7.4.2.1 Diblock ester precursors. The SAXS results of the ester precursors indicate that the microstructure of these block copolymers is insensitive to the changes in the temperature. However, a slight reorganization of the domains during heating (due to the thermal expansion) leads to change in the overall domain spacing. These results may suggest that the order-disorder transition (T$_{ODT}$) temperature is higher than the degradation temperature of the ester copolymer.

7.4.2.2 Block ionomers with low ionic content. The SAXS results on the block ionomers indicate significant changes in the microstructure of the ionomers on increasing temperature. The increase in intensity in the first region of K$^+$-TM-41/550 ionomer (T < 140 °C) may be due to enhanced chain mobility above the T$_g$ of the block that allows more ionic groups to diffuse into the aggregates. It is worthwhile to recall that the ionic aggregates are kinetically trapped (aggregate structure is frozen during the solution neutralization and solvent evaporation). Upon heating reorganization takes place leading to a possible stable aggregate structure. The reorganization is more feasible in K$^+$-TM-41/550 ionomer because of the long nonionic block length (N_A = 550), which leads to increase in the "threshold" length of the ionic block length for micellization. Hence, not all the neutralized

chains are incorporated into the ionic aggregates. The measured intensity in SAXS is proportional to the contrast between the nonpolar hydrocarbon PMMA matrix and polar multiplets ($\Delta\rho$), number of multiplets (N_m), and volume fraction of the multiplets (φ). An increase in temperature may in principle increase all the above-mentioned factors to different extents. The decrease in intensity above 140 ^{o}C, i.e., in the second region (140 ^{o}C < T < 200 ^{o}C), suggests that some ionic aggregates are dissociated at these high temperatures. A similar decrease in intensity and broadening of the ionomer peak was observed for polyester ionomers investigated in this study and polystyrene based sulfonated ionomers (SPS).[16,33] As the temperature increases, an increased mobility of the chains gives rise to higher elastic forces that may promote dissociation of the ionic aggregates.

The increasing intensity at small angles in the same temperature range may indicate a change in the conformation or the radius of gyration (R_g) of the block ionomer during the heating cycle. This increase in intensity is in parallel with the decrease in intensity of the SAXS peak, which suggests that these two processes are coupled. It is well established that the slope of the plot (ln I *vs.* q^2; where I is intensity and q is scattering vector) at the low angles of the scattering curve can be used to calculate the R_g of the polymer chains, however, fitting a linear curve to the low angle intensity data did not lead to a good fit, hence the quantitative data about the changes in the R_g were not calculated. Upon cooling from 200 ^{o}C to 40 ^{o}C, i.e., in the third region, no further changes in the SAXS profile are seen. Since the ionomer is cooled rapidly from elevated temperatures to below T_g, insufficient time may be available for the ionic aggregation to completely reform.

7.4.2.3 Block ionomer with high ionic content. The SAXS results indicate relatively small changes in the K^+-TM-42/132 ionomer compared to K^+-TM-41/550. The shorter length of the PMMA block in the K^+-TM-42/132 compared to the K^+-TM-41/550 influences the ionic aggregation during the neutralization. The "threshold" length of the insoluble block (ionic block) for micellization of the K^+-TM-42/132 ionomer is lower and the aggregation number (N_{AN}, $N_{AN} \sim N_A^{-\beta}$ at the same N_B) is higher than the K^+-TM-41/550 ionomer. This may imply that the ionic aggregate in the K^+-TM-42/132 ionomer is more stable and stronger ionic interactions are present in the aggregate. It is important to realize that apart from decreasing the total degree of polymerization (*N*) of the K^+-TM-42/132 ionomer, the volume fraction of the ionic block ($V_{f, PtBMA} = 0.3$) is also changed and is higher than in the K^+-TM-41/550 ionomer ($V_{f, PtBMA} = 0.1$). As a result, a higher T_g (since the volume fraction of the higher T_g ionic block i.e., PK^+MA is high) and a different morphology (from the symmetric block copolymer phase diagram in the strong segregation limit

one expects a cylindrical morphology) are expected in the K$^+$-TM-42/132 block copolymer. These differences may very well result in a different morphology development as a function of temperature.

A higher temperature (T > 160 ^{o}C) is needed for the reorganization of the ionic domains, which suggests a higher T$_g$ for K$^+$-TM-42/132. The increase in intensity may be due to enhanced chain mobility above the T$_g$ of the block that allows more ionic groups to diffuse into the aggregates. The most significant increase in intensity occurs at 200 ^{o}C, and a further increase in the temperature (220 ^{o}C) results in a decrease in intensity. The decrease in intensity at 220 ^{o}C may indicate that some ionic aggregates are dissociated at this high temperature, but this is insignificant compared to the aggregate dissociation in the K$^+$-TM-41/550 ionomer.

7.5 Conclusions

The influence of temperature on the stability of ion aggregate for telechelic polyester ionomers and poly(methyl methacrylate) (PMMA)-based diblock ionomers is studied using time resolved small angle X-ray scatteing (SAXS). The SAXS results of polyester ionomers indicate the presence of order-disorder transition (T$_i$) for the potassium neutralized polyester ionomer with 5.7 mol %. This is understood as arising from an increase in elastic forces of the polymer chains due to the increase in the temperature, which destabilizes the ionic aggregate structure and thereby promotes the dissociation of the ionic aggregates. The results of the dynamic viscosity experiments of the potassium neutralized polyester ionomers confirmed the dissociation of the ionic aggregates at high temperature. Furthermore, the results of the viscosity and storage/loss modulus measurements during consecutive heating and cooling scans performed on the same polyester ionomer clearly demonstrate that ion aggregation is quite stable to temperature changes and is truely thermoversible. The viscosity of the polyester ionomers increases with increase in ion content and degree of neutralization due to increase in number of ionic groups. This results in the increase in number of ionic cross-links leading to increase in storage modulus. The viscosity of the polyester ionomers with zinc counter ion is lower compared to ionomers with potassium counterion due to the weaker ionic aggregates formed in the zinc ionomer. Furthermore, the dissociation of the ionic cross-links at high temperatures demonstrates the feasibility of obtaining thermoreversible cross-links via ionic cross-links.

The SAXS results of the K$^+$-TM-41/550 diblock ionomer with a long PMMA (with 550 units of MMA) and short PK$^+$MA (with 30 units of K$^+$MA) block and K$^+$-TM-42/132 demonstrate

that the thermal stability of the ionic aggregate in the block ionomer is a strong function of block copolymer composition. This can be understood from the mechanism of block ionomer formation via solution neutralization. The K^+-TM-41/550 block ionomer forms an ionic aggregate with a low aggregate number (N_{AN}) due to the long nonionic block compared to the K^+-TM-42/132 with a short nonionic block. As a result, a weak ionic aggregate is formed, which dissociates at high temperatures due to the increase in the elastic forces of the polymer chains at high temperatures. These results reveal the potential of the solution neutralization method in controlling the molecular characteristics of the ionic aggregates in the block copolymers.

7.6 References

(1)   Hadjichristidis, N.; Pispas, S.; Floudas, G. *Block Copolymers: Synthetic Strategies, Physical Properties, and Applications*, **2003**, Wiley-Interscience.

(2)   Hamley, I. W. *The Physics of Block Copolymers*, 24, **1998**, Oxford University Press.

(3)   Sperling, L. H. Ed. *Recent Advances in Polymer Blends, Grafts and Blocks*; **1974**, Plenum: New York.

(4)   Eisenberg A.; Kim, J. S. *Introduction to Ionomers*, **1998**, John Wiley & Sons, Inc.

(5)   Tant, M.R.; Mauritz, K, A.; Wilkes, G. L. Eds. *Ionomers: Synthesis, Structure, Properties and Applications*, **1997**, Blackie Academic and Professional: London.

(6)   Schlick, S. *Ionomers: Characterization, Theory, and Applications.* Ed. **1996**, CRC Press: Boca Raton, FL.

(7)   Eisenberg, A.; Hird, B.; Moore, R. B. *Macromolecules*, **1990**, 23, 4098.

(8)   Yarusso, D. J.; Cooper, S. L. *Polymer*, **1985**, 26, 371.

(9)   Galambos, A. F.; Stockton, W. B.; Loberstein, J. T.; Sen, A.; Weiss, R. A.; Russell, T. P. *Macromolecules*, **1987**, 20, 3094.

(10)   Gauthier, S.; Esenberg, A. *Macromolecules*, **1987**, 20,760.

(11)   Gouin, J. P.; Eisenberg, A.; Williams, C. E. *Macromolecules*, **1992**, 25, 1368.

(12)   Venkateshwaran, L. N.; York, G. A.; Deporter, C. D.; McGrath, J. E.; Wilkes, G. L. *Polymer*, **1992**, 33, 2277.

(13)   Weiss, R. A.; Sen, A.; Pottic, L. A.; Willis, C. L. *Polymer*, **1991**, 32, 1867.

(14)   Mani, S.; Weiss, R. A.; Williams, C. E.; Hahn, S. F. *Macromolecules*, **1999**, 32, 3663.

(15)   Storey, R. F.; Baugh, D. W. *Polymer*, **2000**, 41, 3205.

(16)   Lu, X.; Steckle, W. P.; Hsiao, B.; Weiss, R. A. *Macromolecules*, **1995**, 28, 2831.

(17)   Kang, H.; Armentrout, R. S.; Wang, J. L.; Long, T. E. *In Functional Condensation Polymers*, Carraher, C. C., Jr., Swift, G. G., Eds. Kluwer Academic: Dordrecht, **2002**; p 249.

(18)   Kang, H.; Lin, Q.; Armentrout, R. S.; Long, T. E. *Macromolecules*, **2002**, 35, 8738.

(19)   Nguyen, D.; Williams, C. E.; Eisenberg, A. *Macromolecules*, **1994**, 27, 5090.

(20)   Nguyen, D.; Zhong, X. F.; Williams, C. E.; Eisenberg, A. *Macromolecules*, **1994**, 27, 5173.

(21)   Desjardins, A.; Eisenberg, A. *Macromolecules*, **1991**, 24, 5779.

(22)   Zhong, X. F.; Varshney, S. K.; Eisenberg, A. *Macromolecules*, **1992**, 25, 7160.

(23)   Desjardins, A.; van de Ven, T. G. M.; Eisenberg, A. *Macromolecules*, **1992**, 25, 2412.

(24)   Nguyen, D.; Varshney, S. K.; Williams, C. E.; Eisenberg, A. *Macromolecules*, **1994**, 27, 5086.

(25)   Khougaz, K.; Zhong, X. F.; Eisenberg, A. *Macromolecules*, **1996**, 29, 3937.

(26)   Moffitt, M.; Esenberg, A. *Macromolecules*, **1997**, 30, 4363.

(27)   Whitmore, M. D.; Noolandi, J. *Macromolecules*, **1985**, 18, 657.

(28)   Nagarajan, R.; Ganesh, K. *J. Chem. Phys.* **1989**, 90, 5843.

(29)   Zhang, L.; Barlow, R. J.; Eisenberg, A. *Macromolecules*, **1995**, 28, 6055.

(30)   Wouters, M. E. L. *Ph.D Thesis*, Eindhoven University of Technology, **2000**.

(31)   Register, R. A.; Prud'homme, R. K. In Ionomers: *Synthesis, Structure, Properteis and Applications*, Tant, M.
R.; Mauritz, K, A.; Wilkes, G. L., Eds. *Ionomers: Synthesis, Structure, Properties and Applications*, **1997,**
Blackie Academic and Professional: London.

(32)   Guegan, P.; Cernohous, J.J.; Khandpur, A.K.; Hoye. T.R.; Macosko, C.W. *Macromolecules*, **1996**, *29*, 4605.

(33)   Weiss, R. A.; Lefelar, J. A. *Polymer*, **1986**, 27, 3.

Samenvatting

Ionomeren zijn polymeren die tot 15 mol procent polaire (ionogene) groepen bevatten aan de apolaire keten. Ionogene groepen worden geïntroduceerd door neutralisatie van in het polymeer aanwezige zure groepen. Het verschil in polariteit tussen de polaire (ionogene) groepen en de apolaire polymeerketen leidt tot micro-fasescheiding waarbij aggregatie optreedt van, de door toevoeging van zouten, neutrale polaire groepen tot zogenaamde ionogene multiplets met een karakteristieke dimensie van enkele nanometers. Deze ionogene aggregaten fungeren als fysische knooppunten (cross-links) en verbeteren verschillende eigenschappen, zoals modulus, hardheid, viscositeit en smeltsterkte. De temperatuurgevoeligheid van de ionogene knooppunten in vergelijking met de normale covalente knooppunten kan bijvoorbeeld gebruikt worden om nieuwe materialen te ontwikkelen met thermoreversibele vernettingseigenschappen omdat bij verhoogde temperatuur dissociatie optreedt van de ionogene multiplets. De toepassing van ionomeren als coatings op spuitgietartikelen via directe co-injectie was het uitgangspunt van dit proefschrift. Het beoogde voordeel van het gebruik van ionomeren is dat een aparte coatingsstap van het artikel na spuitgieten kan worden overgeslagen met als bijkomende voordelen het voorkomen van emissie van oplosmiddelen en een laag energieverbruik.

Het doel van het onderzoek is het bepalen van de relaties tussen structuur, morfologie en eigenschappen van ionomeren. De focus van het onderzoek lag daarom op de gecontroleerde synthese alsmede de morfologische karakterisering en het thermoreversibele karakter van ionogene knooppunten door variatie van a) de architectuur van het polymeer (blok vs. random vs. telecheel ionomeren), b) het molecuulgewicht, c) het inbouwpercentage ionogene groepen en d) het type tegen-ion. Als uitgangspolymeren werd gekozen voor poly(methylmethacrylaat) (PMMA) en polyester, veel gebruikte polymeren in de wereld van coatings. PMMA ionomeren met goed gedefinieerde architecturen werden gemaakt via 'gecontroleerde' en vrije radicaalpolymerisatie (FRP)-technieken.

Voor praktische en economische redenen werd een efficiënte procedure voor de bereiding van goed gedefinieerde PMMA blokcopolymeren ontwikkeld op basis van de zogenaamde "Atom Transfer Radical Polymerization (ATRP)", gebruik makend van makkelijk beschikbare en verwijderbare metaalkatalysatoren en initiatoren. Hierbij werd *tert*-butyl methacrylaat (tBMA) gebruikt vanwege de gevoeligheid van de ATRP katalysatoren voor zuurgroepen. Di- en triblok ester copolymeren van MMA and tBMA werden gemaakt met goed gedefinieerd molecuulgewicht en

polydispersiteitsindex (PDI) en met varierende tBMA samenstellingen. Het gebruik van "Normal Phase Gradient Polymer Elution Chromatography (NP-GPEC)" bleek, net zoals de veel gebruikte "Size Exclusion Chromatography (SEC)", een krachtige analysetechniek om de blokstructuren aan te tonen en de invloed van de reactiecondities op de blokcopolymeerstructuur te bestuderen. Trifluoro-azijnzuur werd gebruikt voor de selectieve hydrolyse van PtBMA naar de methacrylzure variant en Kalium hydroxide voor de neutralisatie van de zuurgroepen. Proton NMR (^{1}H-NMR) en FTIR spectroscopie toonden de aanwezigheid van zure en ionogene groepen aan.

De succesvolle synthese gaf een goede basis voor verder onderzoek naar de morfologie van PMMA blokcopolymeren. Kleine-hoek Röntgenverstrooiing (SAXS) toonde de volgende resultaten. Een singuliere piek werd waargenomen in het geval van di- and triblok uitgangsmaterialen (precursors) en de ionogene afgeleiden, duidend op éénduidige fasescheiding op micro-schaal en de afwezigheid van een hogere orde structurele organisatie. Verder toonden de SAXS experimenten aan dat de afstand tussen de domeinen kan worden gestuurd door middel van de polymerisatiegraad. Deze metingen lieten tevens zien dat de thermische stabiliteit van de ionogene aggregaten sterk afhankelijk is van de samenstelling. Een blokionomeer met een lang niet-ionogeen blok vormt bij een constante lengte van het ionogene blok een ionogeen aggregaat met een lager aggregatiegetal dan een blokionomeer met een kort niet-ionogeen blok. Het resultaat hiervan is een zwakker ionogeen aggregaat, dat zich reorganiseert bij hoge temperaturen. Deze resultaten laten zien dat de karakteristieken van de ionogene aggregaten in potentie gecontroleerd en gevarieerd kunnen worden.

PMMA 'random' ionomeren werden gebruikt om de invloed van de ionogene knooppunten, die fungeren als extra knooppunten en de vernettingsgraad verhogen, op de mechanische eigenschappen van PMMA te bestuderen, gegeven het feit dat de toename van de vernettingsgraad effectiever is voor 'random' ionomeren dan voor blokionomeren. PMMA 'random' ionomeren met Kalium als tegen-ion werden gesynthetiseerd via copolymerisatie van methylmethacrylaat en methacrylzuur met een variërend zuurgetal, gevolgd door neutralisatie van de zuurcopolymeren. SAXS en dynamisch mechanische metingen bevestigden de vorming van ionogene multiplets met een grote verscheidenheid aan afstanden tussen de multiplets; een bewijs van de grote invloed van de moleculaire architectuur op de morfologie van ionomeren. In het proefschrift worden deze resultaten besproken op basis van het Eisenberg, Hird en Moore (EHM) multiplet-cluster model.

Simultane in-situ SAXS metingen en trekproeven aan dunne films van PMMA en corresponderende Kalium ionomeren toonden aan dat de vorming van micro-scheurtjes (crazes) werd onderdrukt in deze ionomeren in vergelijking met puur PMMA, door de toename van de effectieve vernettingsgraad en de craze-initiatie spanning, hoewel de maximale verstrekbaarheid werd verlaagd. Dit zou kunnen leiden tot een toename van de slagvastheid. Het molecuulgewicht en de mate van neutralisatie van de zure uitgangsmaterialen zijn twee belangrijke factoren, die de balans bepalen tussen eigenschappen en verwerkbaarheid. De resultaten van compressieproeven aan puur PMMA met een lage (via ATRP) en hoge (via FRP) PDI lieten zien dat bij eenzelfde molecuulgewicht de 'strain-hardenings' modulus (G_r) hoger is voor de materialen met een lage PDI. Dit kan verklaard worden door verdunning van de effectieve netwerkdichtheid door materiaal met een laag molecuulgewicht dat aanwezig is in de PMMA met hoge PDI. Dit laat de grote invloed zien van de controle over de polydispersiteit en het molecuulgewicht op intrinsieke eigenschappen van polymeren, zoals G_r. Het laat tevens zien dat het gebruik van ionogene knooppunten in combinatie met een lage PDI een interessante benadering is om de mechanische eigenschappen van glasachtige polymeren te verbeteren zonder dat het ten koste gaat van de verwerkbaarheid.

Telechele polyester ionomeren met een hoge thermische stabiliteit van de hoofdketen en een lage sterkte van het ionogene aggregaat werden gebruikt om het thermoreversibele karakter van ionogene knooppunten aan te tonen. De resultaten verkregen met SAXS en FTIR spectroscopie toonden een kritisch ion-gehalte aan waarboven duidelijke fasescheiding optreedt. Hoge temperatuur FTIR en reologie-metingen lieten zien dat de thermische stabiliteit van de ionogene aggregaten en de viscositeit sterk afhankelijk zijn van het gebruikte tegen-ion. De SAXS en dynamische viscositeitmetingen lieten ook zien dat er een order-disorder temperatuur (T_i) bestaat voor de ionogene multiplets. Alle gezamenlijke resultaten laten zien dat polyester ionomeren potentieel gebruikt kunnen worden als basismaterialen voor spuitgietbare coatings. Meer onderzoek is nodig naar polyesters met een hoger molecuulgewicht dan de in dit onderzoek gebruikte materialen, om goede mechanische eigenschappen te verkrijgen met behoud van het thermoreversibele karakter. De in dit proefschrift gehanteerde benadering heeft geleid tot een beter begrip van de relaties tussen architectuur, morfologie en eigenschappen van ionomeren.

List of Publications

1. Karanam, S.; Goossens, J. G. P.; Klumperman, L.; Lemstra, P. J. *Macromolecules*, **2003**, 36, 3051.
   "Controlled Synthesis and Characterization of Low Molecular Weight Model MMA/*tert*-Butyl Methacrylate Triblock Copolymers via ATRP"

2. Karanam, S.; Goossens, J. G. P.; Klumperman, L.; Lemstra, P. J. *Macromolecules*, **2003**, In press.
   "Controlled Synthesis and Characterization of High Molecular Weight MMA/*tert*-Butyl Methacrylate diblock Copolymers via ATRP"

3. Karanam, S.; Goossens, J. G. P.; Lemstra, P. J. *Polym. Prepr. (Am. Chem. Soc., Div. Poly. Chem.)*, **2003**, 44(1), 807.
   "Controlled Synthesis and Morphological Characterization of Methacrylate Ionomers via ATRP"

4. Karanam, S.; Goossens, J. G. P.; Lemstra, P. J. *Preprints, DYFP of Polymers*, **2003**, 285, Cambridge, UK.
   "Influence of Ionic cross-links on the Deformation behavior of PMMA"

5. Karanam, S.; Goossens, J. G. P.; Bailly, C.; Nies, E. L. F. *manuscript under preparation.*
   "A Morphology Study on Well Defined Di- and Triblock Copolymers of MMA and t-BMA and their Acid and Ionic Counterparts by Small Angle X-ray Scattering"

6. Karanam, S.; Mee, M. A. J. V.; Goossens, J. G. P.; Govaert, L. E. *manuscript under preparation.*
   "Synthesis, Morphology and Mechanical Properties of PMMA Random Ionomers"

7. Karanam, S.; Wouters, M. E. L.; Goossens, J. G. P.; Bailly, C. *manuscript under preparation.*
   "Synthesis, Morphology and Rheological Properties of Polyester Telechelic Ionomers"

8. Karanam, S.; Goossens, J. G. P.; Bailly, C. *manuscript under preparation.*
   "A Small Angle X-ray Scattering Study on the Effect of Temperature on the Microstructure of block Ionomers"

9. Karanam, S.; Goossens, J. G. P.; Govaert, L. E. *manuscript under preparation.*
   "Influence of Polydispersity Index on the Network density and Strain Hardening Modulus of PMMA"

10. Karanam, S.; Bas, S.; Venkatesh, R.; Klumperman, L. *manuscipt under preparation.*
    "Identification of chain-end groups via MALDI-TOF in PMMA synthesized by ATRP"

Acknowledgements

Before ending this thesis I would like to express my heartiest thanks to all the people who have directly or indirectly contributed to this work in every possible way.

First, I would like to thank my first promotor prof.dr. P.J. Lemstra for giving me the opportunity to come to Eindhoven (Netherlands), the city of Philips, and accomplish my Ph.D. in his group. His support and trust resulted in its realization. My special thanks to him for motivating me to do the crucial rheology experiments and for introducing me the "Chain of Knowledge" approach. Bedankt Piet!

Secondly, I would like to thank my supervisor dr. Han Goossens for his interest and scientific input in the project. I am grateful to you for giving freedom to work, introducing me to the right people during the project, and for providing continuous encouragement and support.

Next, I want to express my gratitude to dr. Bert Klumperman for his valuable inputs in the chemistry aspects of the research, which resulted in a successful collaboration and rich scientific output. I look forward to work with you more in the future. I am grateful to prof.dr. Christian Bailly for being my second promotor, taking interest and giving important remarks about this thesis. I am thankful to prof.dr. Robert Jerome for his kind acceptance to be in my reading committee, despite his busy schedule and providing critical comments to improve this thesis. I am also thankful to prof.dr. Erik Nies for his valuable comments in the morphology part of the research.

Mechanical property studies in all aspects were always enriched by your expertise – dr. Leon Govaert. Thank you for your interest and guidance. I would like to thank dr. Peter Magusin for his help and interest in the solid state NMR experiments. I would also like to thank industrial partners (DSM, Akzo-Nobel, and Hartman) and EET (Economy, Ecology and Technology, Dutch environmental agency) for financial support and the FINIMOL team members from university, Auke Snijder, Dana Ionescu and Bert Keestra for their inputs and support during the project.

My sincere thanks to dr. Sanjay Rastogi for his help and enthusiasm towards my research, especially for allowing me to work in ID02 beam line for SAXS measurements. Thank you for the social and moral support. I am grateful to Mr. Wieb Kingma for helping me with chromatographic measurements and also for his willingness to talk with me in Dutch. I enjoyed working with you. I am also thankful to Mr. Otto for his interest and help in spectroscopic measurements.

I would like to thank dr. Mariëlle from TNO Eindhoven for helping me with rheology measurements, especially under the time constraints. Without your help the final chapter may not have materialized in time. I am thankful to dr. Irene Hovens from TNO Eindhoven for DMTA measurements and Sjef Garenveld from mechanical engineering for his help in making samples for mechanical properties. I also extend my thanks to dr. Joachim Loos for AFM measurements.

Naar Grenoble! Merci to all the people who contributed to the success of my measurements at the European Synchrotron Radiation Facility, Grenoble, France. I am thankful to the scientific group at Dubble beamline, especially, dr. Wim brass, dr. Sven, and dr. Igor for their assistance during the experiments. Thank

Curriculum Vitae

The author of this thesis was born in Anantapur, India on 6th November 1972. After completing Bachelors in Chemistry, he studied Chemistry at the Indian Institute of Technology, Chennai, India. In 1996 he obtained the Master of Science (M.Sc.) degree in Chemistry. Further, he accomplished a Master of Technology (M.Tech.) from the Indian Institute of Technology, New Delhi, India with a specialization in Polymer Science and Technology in 1997. After successful completion of the Masters, he started his carrier in polymer industry and worked till October 1998 as a Research Officer in the Polymers and Paints laboratory at the ICI India Research & Technology Center, Mumbai, India.

He started Ph.D. in November 1998 at the Eindhoven University of Technology, Eindhoven, The Netherlands in the group of prof.dr. P.J. Lemstra. The project was financially supported by the industries DSM, Akzo Nobel, Hartman and Dutch environmental agency E.E.T. During the first two years of the Ph.D. the author has successfully completed four modules of the course 'Registered Polymer Technologist' ('Register Polymeerkundige', RPK) organized by the 'National Graduate School of Polymer Science and Technology' ('Polymeertechnologie Nederland', PTN). From 1st November 2003, the author will join GE Plastics Research in Bergen op Zoom, The Netherlands as a product developer in the Crystalline Technology Business.